Aleksei Kuznetsov
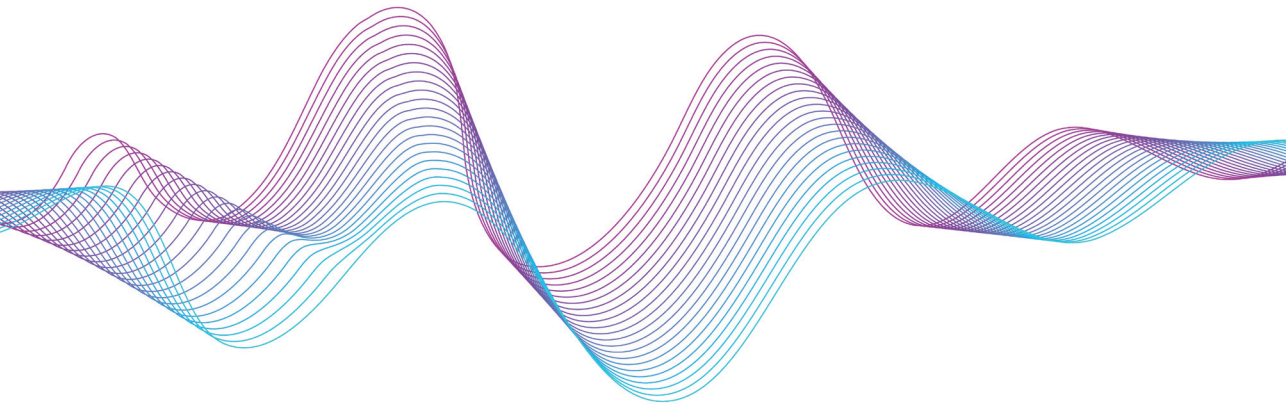
HYBRID ANAPOLE STATES AS A PLATFORM FOR NOVEL OPTICAL DEVICES

Doctoral Thesis

RIGA TECHNICAL UNIVERSITY

Faculty of Computer Science, Information Technology and Energy
Institute of Photonics, Electronics and Telecommunications

Aleksei Kuznetsov

Doctoral Student of the Study Programme "Telecommunications"

HYBRID ANAPOLE STATES AS A PLATFORM FOR NOVEL OPTICAL DEVICES
Doctoral Thesis

Scientific supervisor
Professor Dr. sc. ing. Vjačeslavs Bobrovs

RTU Press

Riga 2024

Kuznetsov, A. Hybrid Anapole States as a Platform for
Novel Optical Devices. Doctoral Thesis.
Riga: RTU Press, 2024. 153 pp.

Published in accordance with the decision of the Promotion Council
"P- 08" of 24. May 2024,
Minutes No. 31.

NATIONAL DEVELOPMENT PLAN 2020 | EUROPEAN UNION European Social Fund

INVESTING IN YOUR FUTURE

DOCTORAL THESIS PROPOSED TO RIGA TECHNICAL UNIVERSITY FOR THE PROMOTION TO THE SCIENTIFIC DEGREE OF DOCTOR OF SCIENCE

To be granted the scientific degree of Doctor of Science (Ph. D.), the present Doctoral Thesis has been submitted for defence at the open meeting of RTU Promotion Council on 6 September 2024 at the Faculty of Computer Science, Information Technology and Energy (FCSITE) of Riga Technical University (RTU), 12 Azenes Str., Room 201.

OFFICIAL REVIEWERS

Professor, Ph.D. Andrey Miroshnichenko
UNSW Canberra, Australia

Researcher, Ph.D. Inga Brice
University of Latvia, Latvia

Professor, Ph.D. Sandis Spolītis
Riga Technical University

DECLARATION OF ACADEMIC INTEGRITY

I hereby declare that the Doctoral Thesis submitted for review to Riga Technical University for promotion to the scientific degree of Doctor of Science (Ph. D.) is my own. I confirm that this Doctoral Thesis has not been submitted to any other university for promotion to a scientific degree.

Aleksei Kuznetsov ……………………………. (signature)

Date: ………………………

The Doctoral Thesis has been prepared as a thematically united collection of scientific publications. It comprises 12 scientific articles and publications in conference proceedings proceeding indexed in SCOPUS and WoS databases. Publications are written in English and are published in SCOPUS, WoS, databases, their total volume/number of pages is 95 pages.

CONTENTS

LIST OF ABBREVIATIONS

A
a-Si – Hydrogenated Amorphous Silicon
C
CMOS – Complementary Metal–Oxide–Semiconductor
D
DM – Dipolar Channel Scattering Maxima
E
ED – Electric Dipole
EQ – Electric Quadrupole
F
FDTD – Finite Difference Time Domain Method
FEM – Finite Element Method
H
HA – Hybrid Anapole
M
MD – Magnetic Dipole
MQ – Magnetic Quadrupole
P
PD – Positional Disorder
PML – Perfectly Matched Layer
Q
QNM – Quasinormal Mode
Quasi-BIC – Quasi-Bound States in Continuum
S
SCS – Scattering Cross-Section
SEM – Scanning Electron Microscope

LIST OF SYMBOLS

δ – Kronecker delta;

n – unit vector;

r – position, m;

i – imaginary unit;

λ – wavelength, m;

c – speed of light in vacuum, m/s;

k_0 – wave number, 1/m;

k_d – wave number in the environment, 1/m;

j_n - n-order spherical Bessel function;

p – electric dipole moment, C/m^2;

m – magnetic dipole moment, $A \cdot m^2$;

Q^e– electric quadrupole moment, $C \cdot m^2$;

Q^m – magnetic quadrupole moment, $A \cdot m^3$;

σ_{sca} – scattering cross-section, m^2;

σ_{eff} – effective scattering cross-section, m^2;

C_{sca}^p – scattering cross-section of electric dipole, m^2;

C_{sca}^m – scattering cross-section of magnetic dipole, m^2;

C_{sca}^{Qe} – scattering cross-section of electric quadrupole, m^2;

C_{sca}^{Qm} – scattering cross-section of magnetic quadrupole, m^2;

$n(\lambda)$ – real part of the refractive index;

$k(\lambda)$ – imaginary part of the refractive index;

n_{env} – refractive index of environment;

n_{sub} – refractive index of substrate;

ε_0 – dielectric constant of vacuum;

ε_d – dielectric constant of the environment;

S_L – lattice unit cell area, m^2;

D – lattice constant, m;

s – distance between the walls of metaatoms, m;

J_ω - induced electric current density, A/m^2;

E_{inc} – amplitude of the electric field of the incident wave, V/m;

E_0 – electric field of a normally incident plane wave, V/m;

H – height of the cylinder/cone, m;

R_{cyl} – radius of the cylinders, m;

R_{top} – top radius of the cone, m;

R_{bottom} – bottom radius of the cone, m;

T – transmission coefficient;

t – electric field transmission coefficients;

R – reflection coefficient;

r – electric field reflection coefficient;

A – absorption coefficient;

I_{noise} – power obtained (noise) by the spectrometer without any incident light, W/m^2;

$I_{substrate}$ – power obtained by the spectrometer when the light is incident on the substrate, W/m^2;

$I_{metasurface}$ – power obtained by the spectrometer when the light is incident on the metasurface with substrate, W/m^2.

1. OVERVIEW

1.1. Introduction

In recent years, all-dielectric nanophotonics have begun to develop at a rapid pace [1]–[6]. The popularity of research into high refractive index subwavelength structures is due to the ability to control light at the nanoscale without thermal loss, unlike plasmonic structures [7]–[9]. By carefully tuning the geometry of nanoscatterers and the dispersion of materials, it is possible to excite both electrical and magnetic resonances [9]–[12]. For example, using a combination of resonances makes it possible to obtain the Kerker effects [13]–[19]. Such single particles are called metaatoms, and their structure is called a metasurface [20]–[22]. With the help of such structures, it is possible to obtain effects that were previously inaccessible with the help of "conventional" materials, for example, artificial magnetism [23]–[25], non-radiative sources [26]–[28], supercavity modes and bound states in the continuum (BIC) [29]–[32], efficient generation of second and third harmonics [33]–[35], sensors [36], [37] or spin-orbit transformation [38], [39].

An intriguing direction in dielectric nanophotonics has become the existence of the so-called non-radiative anapole regime, which was first shown in [40]. The **anapole state** arises due to the destructive interference of the electric and toroidal dipole moments, which causes the particle in the anapole regime to become "invisible" but simultaneously non-trivial fields inside [18], [41]–[47]. Based on the anapole, it has already been proposed to obtain enhanced generation of the second and third harmonics [34], [35], giant photothermal nonlinearities [48], and "dark" lasers [49]. More recently, the next step in anapole electrodynamics, the **hybrid anapole** (HA) regime, has been proposed. This regime represents the simultaneous destructive interference of all dominant multipole moments with their toroidal analogues up to the magnetic quadrupole moment. Hybrid anapoles were first discussed in [50], and only recently hybrid anapoles emerged in dielectric nanocylinders, which has theoretically shown and experimentally demonstrated in [51]. It was shown that hybrid anapole states are superior to conventional anapoles in both scattering suppression and electromagnetic energy storage. Today, hybrid anapole is gaining popularity and becoming a promising area for research [52]–[55].

As part of this Doctoral Thesis, previously unstudied metasurfaces consisting of silicon particles in a hybrid anapole state were investigated. It was shown analytically and numerically that ultra-weak interaction with the environment naturally leads to unit transmittance without optical phase change. The optical properties of these structures were studied, including their interaction with the environment, how the parameters of the metasurface can be adjusted to preserve its optical properties. Additionally, a method for controlling the optical signal passing through such a structure was demonstrated. For the first time, an anapole state was obtained for particles in the shape of a truncated cone, and the dependence of the anapole state on the conicity was studied. This finding significantly simplifies and reduces the cost of producing new-generation photonic structures.

1.2. Rationale

Directional Huygens sources are of greatest interest in the development of metasurfaces with the ability to control light on the nanoscale. Due to the possibility of simultaneous overlap of electrical and magnetic resonances with different parities, it becomes possible to vary the optical phase of the transmitted radiation with unit transmission [21], [56]–[58]. As a result of the research, a number of applications have already been proposed, such as ultra-thin metalenses [59]–[61], dynamic transmission control [62], anomalous refraction [56], [63], [64], beam steering [65], holograms [66]–[70] and broadband Huygens' elements [71].

Huygens' metasurfaces must overcome fundamental constraints typically described by the coupling of structural elements [56], [72] to achieve complete control over light manipulation. Meta-atoms in an array interact with each other even at a distance of the order of a wavelength. This significantly complicates the design process, including the design of optical phase changes on individual structural elements. A number of works in metaoptics help solve this problem, for example, through careful optimization of the supercell [73]. This allows the situation to be improved, but the issue of optical phase mapping on individual meta-atoms remained open. All elements of metasurfaces must be carefully adjusted in their position in the structure to minimize interaction. In structures, special attention must be paid to the lattice period, substrate materials, and manufacturing errors - these are all degrees of freedom that interfere with the production of structures. For the reasons stated above, the effectiveness of such devices can be fundamentally limited [72].

For the structures described, highly symmetrical particles with simple geometries, such as spheres, cubes or cylinders, are usually used as meta-atoms, each of which supports a limited set of multipole interactions depending on size, material and aspect ratio, therefore often as auxiliary elements for the configuration of the multipole composition use complications, for example, multilayer structures [74]–[78].

Unfortunately, modern methods for producing dielectric metasurfaces have a number of disadvantages. It is challenging to obtain a metasurface with ideal cylinders; most cylinders have a slight lateral slope [79]–[81], leading to significant property deviations.

This Doctoral Thesis proposes a new concept to create transparent metasurfaces using silicon metasurfaces in a hybrid anapole state. The properties of metasurfaces based on hybrid anapole were studied in detail. The multiresonant nature of the hybrid anapole allows the transmitted optical phase to be varied over a wide spectral and geometric range. Most importantly, unlike Huygens's sources, the coupling between particles is practically negligible. Thus, the hybrid anapole particle approaches the ideal of a "true" meta-atom. This capability has been demonstrated, ultra-compact silicon arrays have been developed with particle wall spacing equal to 1/8 of the incident wavelength in the visible, and disordered metasurfaces have been studied that exhibit behavior identical to their periodic counterparts. The effect of the substrate was studied, and transmission window conservation was demonstrated when metasurfaces were applied to a wide range of dielectric materials, potentially facilitating their integration into a chip. As a proof-of-concept application, it was demonstrated that it was possible to modulate the optical phase of an ultrafast Gaussian pulse transmitted with unit

efficiency through a highly disordered metasurface deposited on a glass substrate based solely on the optical response of the periodic array. Finally, the influence of conicity on the properties of a hybrid anapole is shown, and for the first time, a hybrid anapole state has been obtained in silicon meta-atoms in the form of truncated cones, which greatly facilitates, simplifies and reduces the cost of fabrication such structures.

1.3. The aim and theses of the Doctoral Thesis

Summarizing the facts mentioned above about the directions of development of novel optical devices for a wide range of applications based on nanostructured elements, the following **aim of the Doctoral Thesis is proposed:**

To study new optical effects caused by interaction of high-index weakly absorbing nanoparticles and metasurfaces in a hybrid anapole state with light and to develop models of nanostructural elements for subsequent creation of qualitatively new photonic devices.

To achieve the stated aim, the following theses were proposed:

1. The hybrid anapole state enables design of ultra-dense silicon metasurfaces without strict adherence to the arrangement order of nanoparticles on the diverse substrates, achieving nearly perfect transmission and zero optical phase shift of transmitted radiation.
2. Silicon metasurfaces in the hybrid anapole state can control the phase of optical signals transmitted through the structure under continuous and ultrafast femtosecond pulse irradiation regimes.
3. The hybrid anapole state can be achieved in silicon truncated cone nanoscatterers with symmetry breaking along the main axis.

1.4. The tasks of the Doctoral Thesis

To achieve the set goal of the dissertation and to prove the proposed theses, it is necessary to perform the following **tasks:**

1. To demonstrate nearly perfect transmission and zero optical phase shift of radiation passing through silicon metasurfaces consisting of cylindrical metaatoms in a hybrid anapole state utilizing numerical methods alongside experimental measurements.
2. To investigate the interaction between silicon metasurfaces in a hybrid anapole state and diverse substrates characterized by varying refractive indices, and to show the absence of interaction of such metasurfaces with the surrounding environment.
3. To explore the influence of the distance between particles in a hybrid anapole state on metasurface optical properties and to demonstrate the absence of interaction among metaatoms during the design of ultra-dense metasurfaces.
4. To study the influence of the disorder of metasurface elements on the optical properties of the structure in a hybrid anapole state, and to show the possibility of maintaining transparency of the structure without strict adherence to the arrangement order of nanoparticles on the substrate.

5. To develop a method for controlling the phase of optical radiation passing through silicon metasurfaces composed of cylindrical metaatoms in a hybrid anapole state by changing the geometric parameters of metaatoms in a continuous irradiation regime.

6. To show the possibility of modulation using ultrafast femtosecond pulses passing through a metasurface in a hybrid anapole state by changing the geometric parameters of nanoscatterers with the possibility of a chaotic arrangement of metaatoms.

7. To study the influence of the conicity of silicon nanoparticles on the resulting optical properties of nanoscatterers in a hybrid anapole state.

1.5.   Research methods

To perform the tasks outlined in the Doctoral Thesis and to analyze the problems, mathematical calculations, numerical simulations, and experimental measurements were used. Numerical simulations were implemented in COMSOL Multiphysics, Ansys Lumerical, MATLAB, Wolfram Mathematica.

Scientific experiments described in the Doctoral Thesis and their results were carried out and discussed at:

- o Nanophotonics research laboratory (NANO-Photon Lab.) at Institute of Photonics, Electronics and Telecommunications (IPET) of Riga Technical University (RTU), Riga, Latvia.
- o Dynamics of Nanostructures' Laboratory at Tel Aviv University (TAU), Tel Aviv, Israel.
- o Advanced Optics and Photonics Laboratory, Nottingham Trent University, Nottingham, UK.
- o School of Optics and Photonics, Beijing Institute of Technology, Beijing, China.
- o QuasiLab, ITMO University, Saint Petersburg, Russia.
- o University of Graz, Graz, Austria.

1.6.   Publications and approbation

The results of the author's doctoral thesis are presented in **12 scientific articles and conference proceeding** indexed in SCOPUS and WoS databases:

1. **Kuznetsov, A.V.,** Canós Valero, A., Tarkhov, M., Bobrovs, V., Redka, D. and Shalin, A.S., "*Transparent hybrid anapole metasurfaces with negligible electromagnetic coupling for phase engineering*," Nanophotonics, Vol. 10, no. 17, pp. 4385-4398, 18 October **2021**.

2. **Kuznetsov, A.V.,** Canós Valero, A., Shamkhi, H.K., Terekhov P., Ni X., Bobrovs V., Rybin M.V., Shalin A.S., "*Special scattering regimes for conical all-dielectric nanoparticles*, " Scientific Reports, Vol. 12, p. 21904, 30 November **2022**.

3. **Kuznetsov, A.V.,** Canos Valero, A., Shalin, A.S. "*Optical properties of a metasurface based on silicon nanocylinders in a hybrid anapole state*," Proceedings of the 5th International conference on metamaterials and nanophotonics «METANANO 2020», Vol. 2300, No. 1, p. 020075, online, December **2020**.

4. **Kuznetsov, A.V.,** Canos Valero, A., "*Non-Huygens transparent metasurfaces based on the novel Hybrid anapole state*," Proceedings of the 6th International conference on metamaterials and nanophotonics «METANANO 2021», Vol. 2015, No. 1, p. 012079, online, November **2021**.

5. **Kuznetsov, A.V.,** Canos Valero, A., Terekhov, P. D., Shamkhi, H. K., "*Various multipole combinations for conical Si particles*," Proceedings of the 6th International conference on metamaterials and nanophotonics «METANANO 2021», Vol. 2015, No. 1, p. 012080, online, November **2021**.

6. Shalin, A.S., **Kuznetsov, A.V.,** Bobrovs, V., Valero, A.C., "*Novel Hybrid anapole state and non-Huygens' transparent metasurfaces*," Proceedings of the 4th International Smart NanoMaterials Conference 2021: Advances, Innovation and Applications «SNAIA 2021», Vol. 2172, No. 1, p. 012001, Paris, France, February **2022**.

7. Terekhov, P.D., **Kuznetsov, A.V.,** Canos Valero, A., Shamkhi, H.K., Ni X., Bobrovs V., Rybin M.V., Shalin A.S., "*Various Scattering Regimes of Truncated Cone Particles*," Proceedings of the CLEO: Applications and Technology 2023, San Jose, USA, 7-12 May **2023**.

8. **Kuznetsov, A.V.,** Bobrovs, V., "*Existence of the Hybrid Anapole for Si Conical Nanoparticles*," Proceedings of 12th International Conference on Computer Science Online Conference «CSOC 2023», Lecture Notes in Networks and Systems, Vol. 772, pp 397 – 401, online, 3-5 April **2023**.

9. **Kuznetsov, A.V.,** Bobrovs, V., "*Superscattering Regime for Si Conical Nanoparticles for the Different Directions of Excitation*," Proceedings of 12th International Conference on Computer Science Online Conference «CSOC 2023», Lecture Notes in Networks and Systems, Vol. 723, pp. 254 – 258, online, 3-5 April **2023**.

10. Babich N., **Kuznetsov, A.,** Bobrovs V., Kislov D., "*Optomechanical Manipulation of Nanoparticles in Hybrid Anapole State*," Proceedings of 12th International Conference on Computer Science Online Conference «CSOC 2023», Lecture Notes in Networks and Systems, Vol. 723, pp. 237 – 243, online, 3-5 April **2023**.

11. **Kuznetsov, A.V.,** Bobrovs, V., "*Transverse Kerker Effects in All-Dielectric Conical Nanoparticles,*" Proceedings of the 7th Computational Methods in Systems and Software 2023 (CoMeSySo2023) conference, Vol 909, pp. 278 – 281, online, **2024**.

12. **Kuznetsov, A.V.,** Bobrovs, V., "*Generalized Kerker Effects in All-Dielectric Conical Nanoparticles*," Proceedings of the 7th Computational Methods in Systems and Software 2023 (CoMeSySo2023) conference, Vol 909, pp. 283 – 287, online, **2024**.

Results of the Doctoral Thesis have been presented at the **15 international conferences**:

1. **Kuznetsov, A.V.,** Canos Valero, A., Shalin, A.S. "*Investigation of the optical properties of a metasurface based on silicon nanocylinders in a hybrid anapole state*," 3th School on Advanced Light-Emitting and Optical Materials «SLALOM 2020», Saint Petersburg, Russia, 29 - 30 June **2020**.

2. **Kuznetsov, A.V.,** Canos Valero, A., Shalin, A.S. "*Optical properties of a metasurface based on silicon nanocylinders in a hybrid anapole state*," 5th International conference on metamaterials and nanophotonics «METANANO 2020», online, December **2020**.

3. **Kuznetsov, A.V.,** Canos Valero, Terekhov, P. D., A., Shalin, A.S. "*Study of the optical properties of a metasurface based on silicon nanocylinders in a hybrid anapole state*," International scientific conference of students, graduate students and young scientists «Lomonosov-2020», online, 10 - 27 November **2020**.

4. **Kuznetsov, A.V.,** Canos Valero, A., Terekhov, P.D., Shamkhi H.K., Shalin, A.S., "*Investigation of various multipole combinations of silicone conical nano-scatterers*," 4th School on Advanced Light-Emitting and Optical Materials «SLALOM 2021», online, 28 - 30 June **2021**.

5. **Kuznetsov, A.V.,** Canos Valero, A., Terekhov, P.D., Shamkhi H.K., Shalin, A.S., "*Investigation of various multipole combinations of silicone conical nano-scatterers*," Summer School on Photonics of 2D materials «METANANO SCHOOL 2021», Saint Petersburg, Russia, 19 – 23 July **2021**.

6. **Kuznetsov, A.V.,** Canos Valero, A., "*Non-Huygens transparent metasurfaces based on the novel Hybrid anapole state*," 6th International conference on metamaterials and nanophotonics «METANANO 2021», online, November **2021**.

7. **Kuznetsov, A.V.,** Canos Valero, A., Terekhov, P. D., Shamkhi, H. K., "*Various multipole combinations for conical Si particles*," 6th International conference on metamaterials and nanophotonics «METANANO 2021», online, November **2021**.

8. Shalin, A.S., **Kuznetsov, A.V.,** Bobrovs, V., Valero, A.C., "*Novel Hybrid anapole state and non-Huygens' transparent metasurfaces*," 4th International Smart NanoMaterials Conference 2021: Advances, Innovation and Applications «SNAIA 2021», Paris, France, February **2022**.

9. Terekhov, P.D., **Kuznetsov, A.V.,** Canos Valero, A., Shamkhi, H.K., Ni X., Bobrovs V., Rybin M.V., Shalin A.S., "*Various Scattering Regimes of Truncated Cone Particles*," CLEO: Applications and Technology 2023, San Jose, USA, 7-12 May **2023**.

10. **Kuznetsov, A.V.,** Bobrovs, V., Shalin, A.S., "*Quasi-BIC on a Hybrid anapole regime in silicon metasurfaces*," The 9th International Conference on Antennas and Electromagnetic Systems «AES 2023», Torremolinos, Spain, 5-8 June **2023**.

11. **Kuznetsov, A.V.,** Bobrovs, V., "*Existence of the Hybrid Anapole for Si Conical Nanoparticles*," 12th International Conference on Computer Science Online Conference «CSOC 2023», Lecture Notes in Networks and Systems, online, 3-5 April **2023**.

12. **Kuznetsov, A.V.,** Bobrovs, V., "*Superscattering Regime for Si Conical Nanoparticles for the Different Directions of Excitation*," 12th International Conference on Computer Science Online Conference «CSOC 2023», online, 3-5 April **2023**.

13. Babich N., **Kuznetsov, A.,** Bobrovs V., Kislov D., "*Optomechanical Manipulation of Nanoparticles in Hybrid Anapole State*," 12th International Conference on Computer Science Online Conference «CSOC 2023», online, 3-5 April **2023**.

14. **Kuznetsov, A.V.,** Bobrovs, V., "*Transverse Kerker Effects in All-Dielectric Conical Nanoparticles*," 7th Computational Methods in Systems and Software 2023 (CoMeSySo2023) conference, online, **2024**.

15. **Kuznetsov, A.V.,** Bobrovs, V., "*Generalized Kerker Effects in All-Dielectric Conical Nanoparticles*," 7th Computational Methods in Systems and Software 2023 (CoMeSySo2023) conference, online, **2024**.

1.7.   Structure of the Doctoral Thesis

The dissertation is prepared as a thematically unified set of publications based on the developed theoretical models of novel optical devices for a wide range of applications.

CHAPTER 1: OVERVIEW. This chapter describes the scope of the Doctoral Thesis. In this chapter, the main research hypotheses and the importance of the novelty of research related to the silicon metasurface in hybrid anapole are formulated. This chapter also presents a brief description of the dissertation's structure. The list of publications and presentations at international conferences is also displayed in this chapter.

CHAPTER 2: METHODOLOGY. This chapter describes the basic methods and tools used for modeling and explaining the effects that occur during the interaction of radiation with metasurfaces in a hybrid anapole state. Three main stages are outlined.

2.1. Methods for numerical modeling of nanostructures. This chapter describes in detail the methods for numerical calculation the optical properties of subwavelength particles and identifies the software that uses the described methods.

2.2. Multipole decomposition. This chapter describes the main method for analyzing the physics of processes occurring in nanoscatterers and metasurfaces based on them.

2.3. Experimental measurements. This chapter describes the experiment conducted to verify the data obtained numerically.

CHAPTER 3: MAIN RESULTS. This chapter represents publications which reflect the main results obtained during the research and application of the optical properties of metasurfaces in hybrid anapole state. The results of the Doctoral Thesis were published in **12** publications indexed in the Scopus and WoS databases, including **2** articles in highly rated international scientific journals; the total Impact Factor is **13.3** (5-year Journal Impact Factor) with a total of **43** (13/03/2024) citations in journals indexed in Scopus.

CHAPTER 4: FINAL REMARKS. This chapter represents the main conclusions and discussion of the challenges and their solutions regarding theoretical and practical applications of the metasurfaces in hybrid anapole state.

2. METHODOLOGY

The chapter provides the main methods for studying the optical properties of the structures described in the Doctoral Thesis.

Currently, the main tool for studying the optical properties of nanostructures are numerical methods (e.g., finite element methods, discrete dipole approximation, finite difference methods, etc.). These methods primarily involve solving Maxwell's partial differential equations [82] and calculating of electric and magnetic fields at each point in the system. They take into account all geometric and material characteristics of the structure under consideration, such as shape of particles, their size, spatial position, structure of the incident beam, etc. These methods are implemented in commercial scientific software products (COMSOL Multiphysics, Ansys Lumerical, CST, etc.) and have been rigorously tested by the global scientific community. The results of their application are widely presented in the literature.

However, although numerical methods have proven excellent in engineering calculations, they cannot compete with analytical approaches when it is necessary to understand the physics of a phenomenon and, most importantly, to determine the range of parameters in which unusual new phenomena can be observed. Therefore, in addition to the aforementioned numerical methods, this dissertation employs multipole decomposition, which is convenient for studying anapole states of various orders [83].

The method of multipole decomposition of the reflection and transmittance coefficients of the metasurface will also be used, allowing for a qualitative analysis of the optical response of the system [10].

In addition to multipole analysis, the method of searching for eigenmodes in the COMSOL Multiphysics optical module was also used. This method is based on solving Maxwell's equations for electromagnetic fields in structures. It involves using the wave equation and boundary conditions to determine the propagation of electromagnetic waves in optical systems. The method relies on the numerical solution of the full Maxwell equations, including those for electric and magnetic fields. To find eigenmodes, one must solve the eigenvalue problem, which depends on the type of structure. Solving these equations allows for determining the characteristics of the eigenmodes, such as frequency and field distribution.

Thus, the method encompasses the physical principles of wave optics and mathematical techniques for the numerical solution of Maxwell's equations, enabling the study and optimization of electromagnetic fields in optical structures.

The primary material for nanoscatterers was the dispersion of the refractive index, measured experimentally, and chosen as a high-index dielectric material for particles and metasurfaces in the Doctoral Thesis (unless otherwise indicated) (Fig. 2.1).
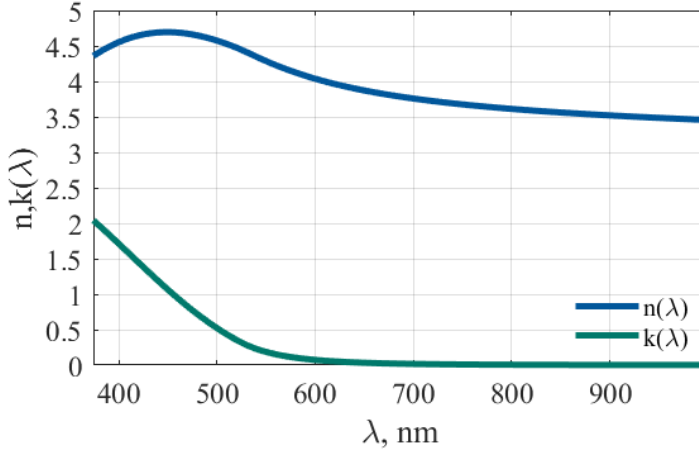
Fig. 2.1. Real (n) and imaginary (k) parts of the experimentally measured refractive index of hydrogenated amorphous silicon (a-Si) as a function of wavelength.

2.1. Methods for numerical modeling of nanostructures.

Two software packages were used as the main tools for numerical calculations: COMSOL Multiphysics, which uses the finite element method (FEM), and Ansys Lumerical, which uses the finite difference time domain (FDTD) method. In the FEM method, the software package solves differential equations by dividing the entire working area of the model into a finite number of elements. The values of the functions at the nodes are initially unknown and are determined as the solution to the problem. The FDTD method is based on finite difference sampling of Maxwell's equations and covers a wide range of frequencies, making it an excellent tool for various time-domain optical calculations. The multipole composition of single particles and metasurfaces was analyzed using scripts written in the aforementioned software packages. The eigenmodes of single particles, as well as their radiation patterns, were studied using the built-in capabilities of COMSOL Multiphysics.

Finite Element Method

To simulate the optical properties of dielectric nanoscatterers and metasurfaces based on them, the COMSOL Multiphysics software package using FEM was used [84]. FEM is a numerical method used to solve equations that describe the behavior of physical systems. In the context of optical phenomena, FEM can model the propagation of light through various media and structures.

FEM is based on approximating the solution of differential equations using the variational method. Optical problems in the COMSOL Multiphysics Optical Module use Maxwell's equations to describe electromagnetic fields in a medium. These equations describe the propagation of light and its interaction with materials. Within the FEM framework, Maxwell's

equations are approximated in finite elements, allowing for numerical solutions for complex structures.

The process of creating a model of a silicon metasurface on a glass substrate in a plane wave field in COMSOL Multiphysics involves the following. It is necessary to define the entire geometry, indicating its materials; for example, hydrogenated amorphous silicon on a glass substrate with a refractive index (n_{sub} = 1.5) was used as particles, and the environment was air (n_{env} = 1). Then, the "physics" in which the solution will take place is selected. In this case, the wavelength domain was selected, where it is possible to set boundary conditions, such as periodic ones, to simulate an infinite metasurface. A plane wave with polarization along the x axis was chosen as the incident radiation. A perfectly matched layer (PML) is an artificial absorbing layer for wave equations commonly used to truncate computational regions in numerical methods to simulate problems with open boundaries. Then it is needed to specify the grid and set the necessary parameters for calculations. After calculations, it is possible to analyze the results obtained, for example, to study the distribution of fields and energy or to calculate the transmission and optical phase of the radiation passed through the structure. A possible configuration of the model with a grid drawing is shown in Fig. 2.2.
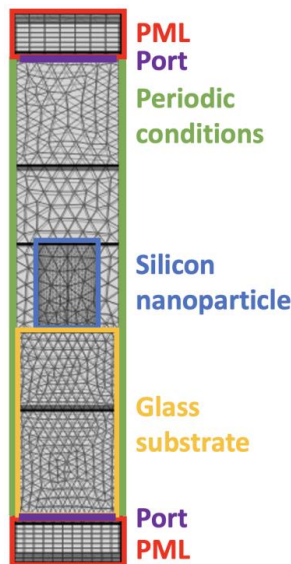

Fig. 2.2. Possible model configuration in COMSOL Multiphysics for simulation a silicon metasurface in a hybrid anapole state.

The advantages of FEM in optical modeling include its versatility for complex geometries, the ability to account for inhomogeneous materials, and the detailed description of the electric field distribution in space. COMSOL Multiphysics provides the flexibility to configure different boundary conditions and material properties, making it a powerful tool for optical modeling.

Despite many advantages, the FEM method also has certain disadvantages. For some large-scale and complex problems, the FEM method can be computationally expensive and time-

consuming, and using the FEM method effectively requires careful mesh tuning and optimization, which can be a labor-intensive process.

The finite element method in the COMSOL Multiphysics provides a powerful tool for modeling and analyzing optical phenomena. It is important to consider both the advantages and disadvantages of this method when selecting the appropriate tool for a particular optical application.

The main part of the Doctoral Thesis was calculated in COMSOL Multiphysics. Still, due to some limitations, part of the calculations was done using the FDTD method, described in the next subsection.

Finite Difference Time Domain method

This subsection examines the Finite Difference Time Domain FDTD method in the context of optical modeling using Ansys Lumerical software [85]. The FDTD method is a numerical approach widely used to simulate the propagation of electromagnetic waves in space and time.

This method is a discretization of electromagnetic fields in three-dimensional space and a discretization of time, which makes it possible to simulate their evolution in space and time. Applied to optical modeling, the FDTD method allows solving Maxwell's equations for electromagnetic fields in three dimensions and in ultrashort time intervals.

In the FDTD method, after numerically simulating the evolution of fields in space and time, the Fourier transform can be applied to the results to obtain the spectral characteristics of the field. This is especially useful for analyzing the frequency components of electromagnetic waves, which can be important, for example, when studying the interaction of light with optical structures. The Fourier transform can also be used to create spectral sources, scattering analysis, and other optical modeling tasks.

The process for creating a model in Ansys Lumerical is similar to that described for COMSOL Multiphysics. In the same way, geometry is added, materials are specified, a source and monitor are added to calculate the necessary parameters, and boundary conditions are specified. The main difference is the method, as mentioned earlier, the FDTD method is used here, so it becomes possible to set the shape of the incident pulse and quickly calculate the time dynamics of processes. A possible configuration of the model with a grid drawing is shown in Fig. 2.3.
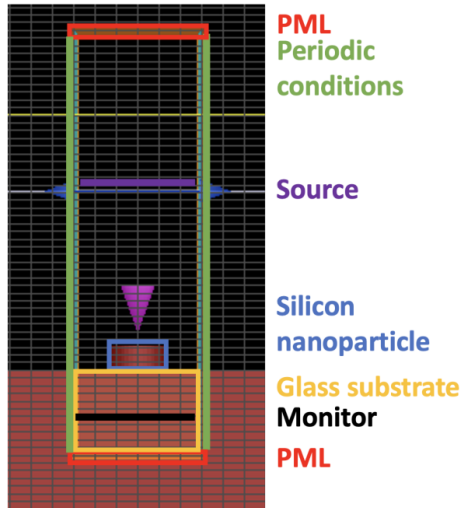
Fig. 2.3. Possible model configuration in Ansys Lumerical for simulation a silicon metasurface in a hybrid anapole state.

The advantages of the FDTD method include its versatility and ability to model a wide range of optical phenomena, including diffraction, interference, and the interaction of light with nanostructures. It also provides ease of integration with different types of materials and geometries.

The disadvantages of the FDTD method are, in particular, the requirement of large computational resources when modeling three-dimensional structures of high complexity. Also, the method may have limitations when modeling waves with lengths comparable to the grid dimensions.

The fundamental feature of the FDTD method is that it provides a simulation of the evolution of electromagnetic fields in space and time, which makes it a powerful tool for studying optical processes and the interaction of light with various structures. In this Doctoral Thesis, this method was used to simulate the time dynamics of pulses passed through the structure.

2.2.   Multipole decomposition

One of the most important tools for analyzing the optical properties of a scattering structure is multipole decomposition[86–89]. Using multipole decomposition, it becomes possible to characterize the interaction of electromagnetic radiation with a nanoscatterer.

Multipole decomposition is important in any scientific field where the interaction of electromagnetic radiation with material systems is studied. For example, in particle physics, multipole moments of nuclei provide information about the distribution of charges inside the nucleus. In chemistry, the polarizability of a molecule determines its properties, and in electrical engineering, multipole expansion is used to estimate the radiation of antennas, and this list can be continued for a very long time. In the region under study, using the multipole scattering

cross-section, it is possible to describe the interaction of silicon nanoresonators with a plane wave polarized along the x axis.

Multipoles are characterized according to their order: dipoles, quadrupoles, octupoles, etc. For each order there are electric and magnetic multipole moments. Each of the multipole moments is uniquely associated with the corresponding multipole field.

There are several approaches that can be classified depending on the types of multipoles. For example, Mie theory operates with spherical (cylindrical) multipoles, which are coefficients of field expansion in vector spherical (cylindrical) harmonics [12], [90], [91]. Another approach involves Cartesian multipoles obtained using the Taylor series of the scalar Green's function written in the far-field approximation.

In this Doctoral Thesis, recently obtained Cartesian representations of the first few spherical multipoles outside the long-wave approximation were used, the so-called exact multipoles.

Exact multipole expansion

This subsection discusses new exact expressions for the multipole expansion of electric charge and current proposed by Rasoul Alaee, Carsten Rockstuhl, I. Fernandez-Corbaton in work [92]. This work provides a simple path to update analytical and numerical models currently using the long-wavelength approximation. After revision of the model, the multipoles become accurate, and the expressions that are presented in this section were used for numerical calculations in the Doctoral Thesis for single particles and metasurfaces based on them.

In fact, exact expressions exist and can be found in standard textbooks, e.g. [93] without magnetizing current in it, or a new formulation was recently obtained in [94]. However, they are still not often used in the literature due to their complexity, because the formulas contain differential operators such as rotor, or vector spherical harmonics. Instead, in nanophotonics the long-wavelength approximation is very often used, which greatly simplifies the mentioned expressions. Their integrands contain algebraic functions of coordinate vectors and current density, reminiscent of expressions for multipole moments obtained in electro- and magnetostatics. It is worth noting that the long-wavelength approximation cannot be used for particles larger than the wavelength because the deviation for multipole moments will significantly affect the result (Fig. 2.4.).
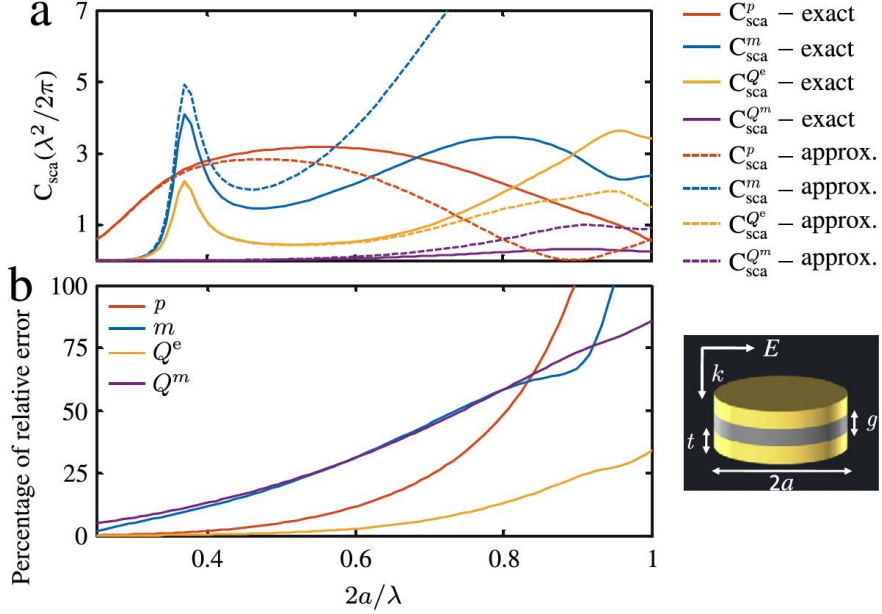
Fig. 2.4. (a) Contribution of each multipole moment to the scattering cross-section calculated with the approximate expressions and calculated with the exact expressions for a coupled nanopatch with given geometrical parameters as a function of the wavelength. (b) Relative error between the multipole moments calculated with the approximate expression and calculated with the exact expression [83].

It is also worth noting that multipole moments, like any other quantity in physics, have an identical physical meaning, regardless of their basis (Cartesian or spherical) or what approaches (scattered fields or induced currents) were used to extract them. Changing the basis will not change the physical meaning of multipole moments.

Thus, there is a need for precise expressions that are valid for any wavelength and particle size. Such expressions are presented up to the quadrupole order.

This multipole decomposition is shown in Eqs. (2.1.) - (2.4.) can be used for any particle shape:

$$p_\alpha = -\frac{1}{i\omega}\left\{\int d^3\mathbf{r} J_\alpha^\omega j_0(kr) + \frac{k^2}{2}\int d^3\mathbf{r}\left[3(\mathbf{r}\cdot\mathbf{J}_\omega)r_\alpha - r^2 J_\alpha^\omega\right]\frac{j_2(kr)}{(kr)^2}\right\}, \quad (2.1.)$$

$$m_\alpha = \frac{3}{2}\int d^3\mathbf{r}(\mathbf{r}\times\mathbf{J}_\omega)_\alpha \frac{j_1(kr)}{kr}, \quad (2.2.)$$

$$Q_{\alpha\beta}^e = -\frac{3}{i\omega}\{\int d^3\mathbf{r}\left[3(r_\beta J_\alpha^\omega + r_\alpha J_\beta^\omega) - 2(\mathbf{r}\cdot\mathbf{J}_\omega)\delta_{\alpha\beta}\right]\frac{j_1(kr)}{kr} +$$
$$+2k^2\int d^3\mathbf{r}\left[5r_\alpha r_\beta(\mathbf{r}\cdot\mathbf{J}_\omega) - (r_\alpha J_\beta + r_\beta J_\alpha)r^2 + r^2(\mathbf{r}\cdot\mathbf{J}_\omega)\delta_{\alpha\beta}\right]\frac{j_3(kr)}{(kr)^3}\}, \quad (2.3.)$$

$$Q_{\alpha\beta}^m = 15\int d^3\mathbf{r}\left\{r_\alpha(\mathbf{r}\times\mathbf{J}_\omega)_\beta + r_\beta(\mathbf{r}\times\mathbf{J}_\omega)_\alpha\right\}\frac{j_2(kr)}{(kr)^2}, \quad (2.4.)$$

21

where α, β = x, y, z;

k – wave number, 1/m;

c – speed of light in vacuum, m/s;

p – electric dipole moment, C/m^2;

m – magnetic dipole moment, A·m^2;

Q^e– electric quadrupole moment, C·m^2;

Q^m – magnetic quadrupole moment, A·m^3;

r – position, m;

J$_\omega$ - induced electric current density, A/m^2;

j$_n$ - n-order spherical Bessel function;

In these formulas, toroidal moments are already included as the second term in the electric multipole moments [74, 95, 96].

Using multipole moments, it is easy to obtain the total scattering cross-section as the sum of the scattering contributions of each of the multipoles according to the Eq.(2.5.):

$$\sigma_{sca} = C_{sca}^{p} + C_{sca}^{m} + C_{sca}^{Q^e} + C_{sca}^{Q^m} + \cdots =$$

$$= \frac{k^4}{6\pi\varepsilon_0^2 \left| \mathbf{E}_{inc} \right|^2} \left[\sum_\alpha \left(\left| p_\alpha \right|^2 + \left| \frac{m_\alpha}{c} \right|^2 \right) + \frac{1}{120} \sum_{\alpha\beta} \left(\left| kQ_{\alpha\beta}^e \right|^2 + \left| \frac{kQ_{\alpha\beta}^m}{c} \right|^2 \right) + \cdots \right], \quad (2.5.)$$

where |E$_{inc}$| - amplitude of the electric field of the incident wave, V/m;

ε$_0$ – dielectric constant of vacuum;

It is also worth emphasizing the connection between the exact induced multipole moments and the radiated electric field, which is expressed using the Eq (2.6.):

$$\mathbf{E} = \frac{k^2}{4\pi\varepsilon_0} \frac{e^{ikr}}{r} \left\{ \mathbf{n} \times (\mathbf{p} \times \mathbf{n}) + \frac{1}{c}(\mathbf{m} \times \mathbf{n}) - \frac{ik}{6}\mathbf{n} \times (\mathbf{Q}^e \times \mathbf{n}) - \frac{ik}{6c}(\mathbf{Q}^m \times \mathbf{n}) \right\}, \quad (2.6.)$$

where n - unit vector.

Multipole analysis of metasurfaces

High-index metasurfaces have been actively studied in recent years due to their promising optical properties[20], [37], [97]–[101]. The method of multipole decomposition of electromagnetic fields emitted by local current sources or scattered by nanoparticle structures is a powerful tool for studying their electromagnetic properties [77], [102], [103].

This subsection presents an efficient semi-analytical method for analyzing Cartesian multipole contributions to the transmission and reflection spectra of planar metasurfaces consisting of identical nanoparticles, which was first presented by the authors P.D. Terekhov, V.E. Babicheva, K.V. Baryshnikova, A.S. Shalin, A. Karabchevsky, and A.B. Evlyukhin in work [10] (Fig. 2.5).
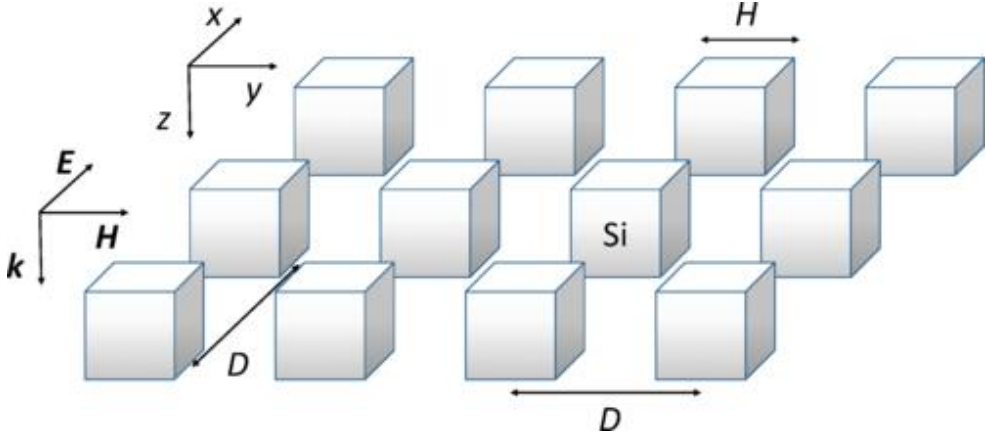
Fig. 2.5. Artistic representation of the considered silicon metasurface composed of nanocubes (infinite nanostructure illuminated with the linearly polarized plane wave) [10].

Amplitude reflection coefficients r and transmission coefficients t in the case of x-polarization can be obtained using the expressions (2.7.) - (2.8.), where p, m, Q, M – multipole moments, which are calculated using the formulas presented in the previous subsection Eqs. (2.1.) - (2.4.):

$$r = \frac{ik_d}{E_0 2S_L \varepsilon_0 \varepsilon_d} \left(p_x - \frac{1}{\upsilon_d} m_y + \frac{ik_d}{6} Q_{xz} - \frac{ik_d}{2\upsilon_d} M_{yz} - \frac{k_d^2}{6} O_{xzz} \right), \qquad (2.7.)$$

$$t = 1 + \frac{ik_d}{E_0 2S_L \varepsilon_0 \varepsilon_d} \left(p_x + \frac{1}{\upsilon_d} m_y - \frac{ik_d}{6} Q_{xz} - \frac{ik_d}{2\upsilon_d} M_{yz} - \frac{k_d^2}{6} O_{xzz} \right), \qquad (2.8.)$$

in the case of y-polarization, could be obtained the Eqs. (2.9.) - (2.10.):

$$r = \frac{ik_d}{E_0 2S_L \varepsilon_0 \varepsilon_d} \left(p_y + \frac{1}{\upsilon_d} m_y + \frac{ik_d}{6} Q_{yz} + \frac{ik_d}{2\upsilon_d} M_{xz} - \frac{k_d^2}{6} O_{yzz} \right), \qquad (2.9.)$$

$$t = 1 + \frac{ik_d}{E_0 2S_L \varepsilon_0 \varepsilon_d} \left(p_y - \frac{1}{\upsilon_d} m_x - \frac{ik_d}{6} Q_{yz} + \frac{ik_d}{2\upsilon_d} M_{xz} - \frac{k_d^2}{6} O_{yzz} \right), \qquad (2.10.)$$

where $k_d = k_0 \sqrt{\varepsilon_d}$ - wave number in the environment (k_0 - wave number in vacuum);

S_L - lattice unit cell area ($S_L = D^2$ for a square lattice, where D - lattice constant), m^2;

ε_0 - dielectric constant of vacuum;

ε_d - dielectric constant of the environment;

E_0 - electric field of a normally incident plane wave at the location of the multipole moments, V/m;

r - electric field reflection coefficient;

t – electric field transmission coefficients.

Reflection and transmittance coefficients are calculated using the Eqs. (2.11.) - (2.12.):

$$R = |r|^2 \,, \tag{2.11.}$$

$$T = |t|^2 . \tag{2.12.}$$

where R – reflection coefficient;

T – transmission coefficient.

Then the absorption coefficient A could be obtained from the following Eq. (2.13.):

$$A = 1 - R - T, \tag{2.13.}$$

where A – absorption coefficient.

In this subsection, a technique was presented that allows for multipole analysis of the transmission and reflection spectra of metasurfaces consisting of periodically arranged nanoparticles. It was shown how analytical multipole expansions of the field reflectance and transmittance coefficients of nanoparticle arrays can be obtained from single particle scattering.

After studying the multipole response in the gratings, this information can be used to optimize the optical properties of the gratings. For example, optimization can be performed by adjusting the overlap of different multipole resonances with their spectral positions determined by the particle geometry and lattice periods. Multipole decomposition of array fields and analysis of transmission and reflection spectra provide us with a more accurate and efficient tool for theoretical optimization of nanoparticle arrays. The second advantage is the ability to use the multipole response of single nanoparticles to evaluate the optical properties of arrays composed of them.

2.3.   Experimental measurements

There were two sets of samples. The first set of samples was fabricated by Advanced Optics and Photonics Laboratory from Nottingham Trent University, Nottingham, UK, represented by prof. Mohsen Rahmani. The second set of samples was fabricated by School of Optics and Photonics from Beijing Institute of Technology, Beijing, China, represented by prof. Huang Lingling.

To verify the numerical results obtained, experimental samples of metasurfaces with different lattice parameters and different radii of metaatoms were used. The experimentally measured refractive index dispersion of hydrogenated amorphous silicon was used as a material for numerical calculations Fig. 2.6.
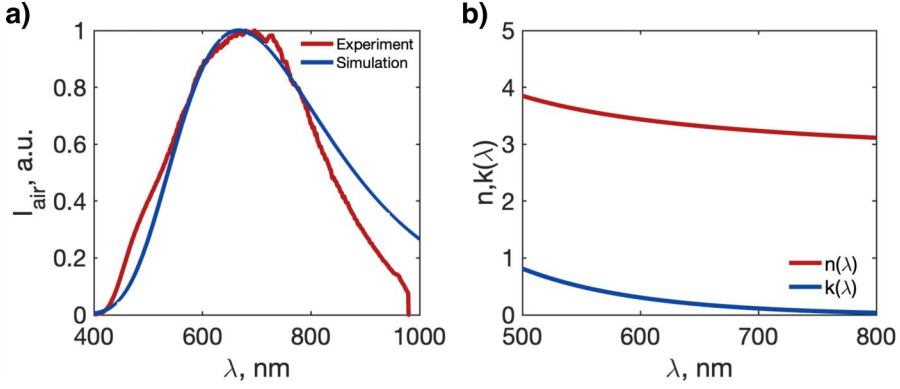
Fig. 2.6. (a) Intensity of incident radiation in free space versus wavelength. (b) Real (n) and imaginary (k) parts of the experimentally measured refractive index of amorphous hydrogenated silicon (a-Si) as a function of wavelength.

The effective scattering cross-section in this Doctoral Thesis was determined by the Eq. (2.14.):

$$\sigma_{eff} = \frac{\sigma_{sca}}{\pi R^2},$$ (2.14.)

where σ_{eff} – effective scattering cross-section, m^2;

σ_{sca} – scattering cross-section, m^2;

R_{cyl} – radius of the cylinders, m.

The arrangement of metasurface samples is shown in Fig. 2.7. The series was manufactured separately and consisted of 18 metasurfaces (6 different geometric configurations under 3 different manufacturing regimes) with more detailed parameters selected, consistent with theoretical calculations. And one additional sample on which a thin film of silicon is deposited with the same height as the height of the metaatoms.
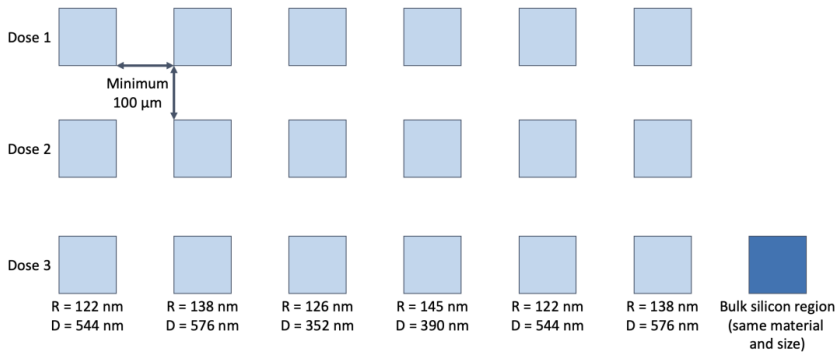

Fig. 2.7. Pattern on sample. Layout of samples with different geometric parameters of meta-atoms, periods, and different manufacturing regimes.

The geometric parameters with numbers of samples of the metasurfaces are shown in Table 2.1.

<div align="right">Table 2.1.</div>

<div align="center">Parameters of metasurfaces</div>

Sample number	Radius of cylinder, nm	Period of metasurface, nm
1	138	576
2	122	544
3	145	390
4	126	352
5	138	576
6	122	549

Transmission spectra of these metasurfaces were measured in the range of 400 - 1000 μm, the light source was a halogen lamp, and the detector was an OceanInsight QEpro spectrometer. The light was focused onto the metasurface and collected after it, using identical 40x lenses. The diameter of the focusing area was about 15 μm; the spectrum was taken from the center of the structure. The light incidence is normal, the light is unpolarized. Experimental transmission of the metasurface is calculated by spectrometer software using the Eq. (2.15.):

$$T = \frac{I_{metasurface} - I_{noise}}{I_{substrate} - I_{noise}},$$ (2.15.)

where I_{noise} – power obtained (noise) by the spectrometer without any incident light, W/m^2;

$I_{substrate}$ – power obtained by the spectrometer when the light is incident on the substrate, W/m^2;

$I_{metasurface}$ – power obtained by the spectrometer when the light is incident on the metasurface with substrate, W/m^2.

The experimentally measured refractive index dispersion of hydrogenated amorphous silicon (a-Si) of the second set of samples was used as a material for numerical calculations Fig. Fig. 2.8.
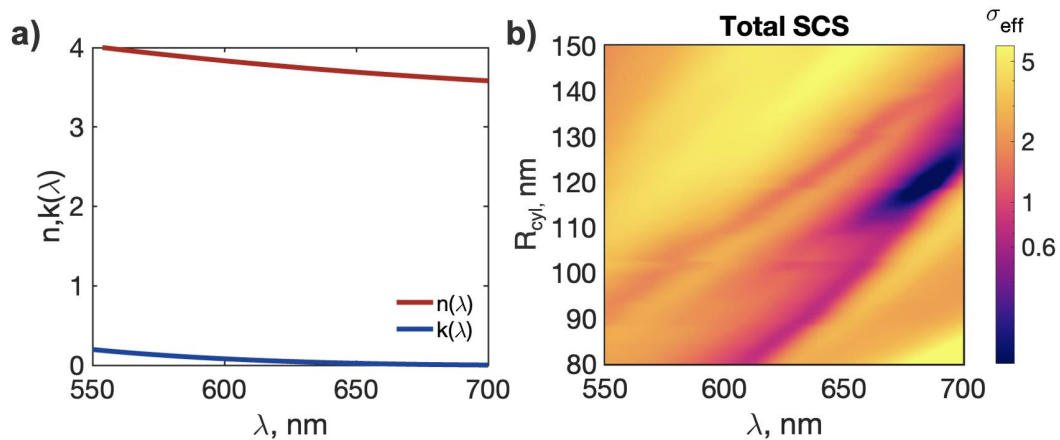
Fig. 2.8. a) Real (n) and imaginary (k) parts of the experimentally measured refractive index of amorphous hydrogenated silicon (a-Si) as a function of wavelength. b) Numerically calculated evolution of the hybrid anapole for single nanoparticle as a function of radius and wavelength.

As for the previous set, the Fig. 2.8.(b) shows a distinct hybrid anapole scattering dip for a single cylindrical particle with different radii.

3. MAIN RESULTS

This Doctoral Thesis proposes a new concept to create transparent metasurfaces using silicon metasurfaces in a hybrid anapole state. The properties of metasurfaces based on the hybrid anapole were studied in detail. The multiresonant nature of the hybrid anapole allows for variation of the transmitted optical phase over a wide spectral and geometric range. Importantly, unlike Huygens' sources, the coupling between particles is practically negligible. Thus, the hybrid anapole particle approaches the ideal of a 'true' meta-atom. This capability has been demonstrated through the development of ultra-compact silicon arrays with particle wall spacing equal to 1/8 of the incident wavelength in the visible spectrum, and disordered metasurfaces have been studied that exhibit behavior identical to their periodic counterparts. The effect of the substrate was studied, and conservation of the transmission window was demonstrated when metasurfaces were applied to a wide range of dielectric materials, potentially facilitating their integration into chips. As a proof-of-concept application, it was demonstrated that it was possible to modulate the optical phase of an ultrafast Gaussian pulse transmitted with unit efficiency through a highly disordered metasurface deposited on a glass substrate, based solely on the optical response of the periodic array. Finally, the influence of cones on the properties of a hybrid anapole is shown, and for the first time, a hybrid anapole state has been obtained in silicon meta-atoms in the form of truncated cones, greatly facilitating, simplifying, and reducing the cost of creating such structures.

The detailed results are presented in [PAPER 1], [PAPER 3], [PAPER 4], [PAPER 6], [PAPER 8], [PAPER 10] in **SUPLEMENTS**.

The main result of this scientific papers is the theoretical description, numerical simulation and experimental confirmation of the optical properties of silicon metasurfaces consisting of cylinders in a hybrid anapole state.

This doctoral thesis discovered that the recently identified non-scattering hybrid anapole regime can also be achieved in conical nanoparticles, in addition to elliptical and cylindrical ones. It is shown how adjusting geometric parameters enables the manipulation of anapole regimes for different multipoles, thereby achieving a hybrid anapole regime. This doctoral thesis represents a step forward in nanophotonics, allowing for the exploration of more complex shapes and fine-tuning of effects achievable with individual nano-scatterers. This research significantly reduces the cost of developing photonic devices and opens new avenues for practical applications in next-generation photonics. The findings of this doctoral thesis have potential applications in various research fields, such as creating diverse dielectric nanoantennas in the form of resonator chains compared to chains of spheres or cylinders. They also pave the way for metasurfaces capable of achieving optical effects that were previously unattainable.

The detailed results are presented in [PAPER 2], [PAPER 5], [PAPER 7], [PAPER 9], [PAPER 11], [PAPER 12] in **SUPLEMENTS**.

The main contribution of this paper is the theoretical description and numerical simulation of the hybrid anapole state in truncated silicon nanocones.

Unfortunately, at this moment, the materials that were measured have not yet been published, so this subsection demonstrates the obtained results.

First, it was necessary to demonstrate the existence of a hybrid anapole regime in single silicon nanoparticles for experimentally measured refractive index dispersion showed in Fig. 2.6.

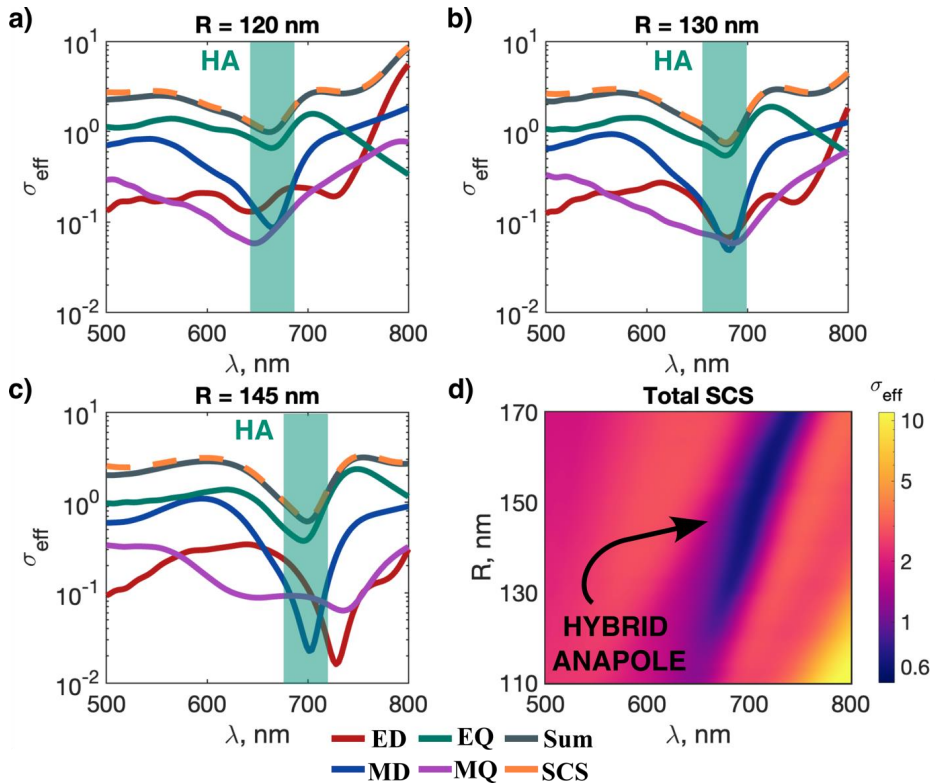Fig. 3.1. shows the results of numerical simulation.

Fig. 3.1. Numerically calculated evolution of the hybrid anapole for single nanoparticle as a function of radius and wavelength. (a–c): Multipole decompositions of the SCS (semilogarithmic scale) for selected radius R_{cyl}. In all calculations, the height of the nanoparticle was kept constant (H = 370 nm). (d) Total SCS as a function of radius and wavelength.

The Fig. 3.1.(a-c) shows the numerically calculated multipole decomposition of a single cylinder-shaped nanoscatterer for different radii for the experimentally measured refractive index. The hybrid anapole scattering dip changes with different geometric parameters but is still present for the parameters shown. The Fig. 3.1.(d) demonstrates at what geometric parameters an anapole dip will occur in such a silicon particle.

The height H of the resulting cylinders was H = 370 nm. Fig. 3.2. shows Scanning electron microscope (SEM) images of the metasurfaces.
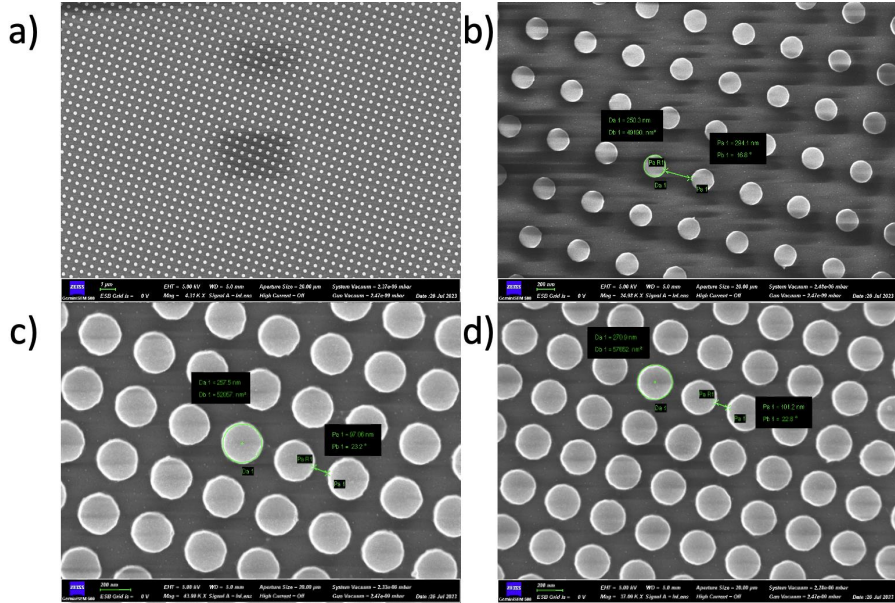
Fig. 3.2. Example SEM image of a metasurface. (a) General view of the metasurface with a distance between the walls of metaatoms s = 300 nm. (b) Metasurface with a distance between metaatoms s = 300 nm and radius R_{cyl} = 125 nm. (c) s = 100 nm and R_{cyl} = 130 nm. (d) s = 100 nm and R_{cyl} = 135 nm.

Transmission spectra of these metasurfaces were measured in the range of 400 - 1000 µm (Fig. 3.3).
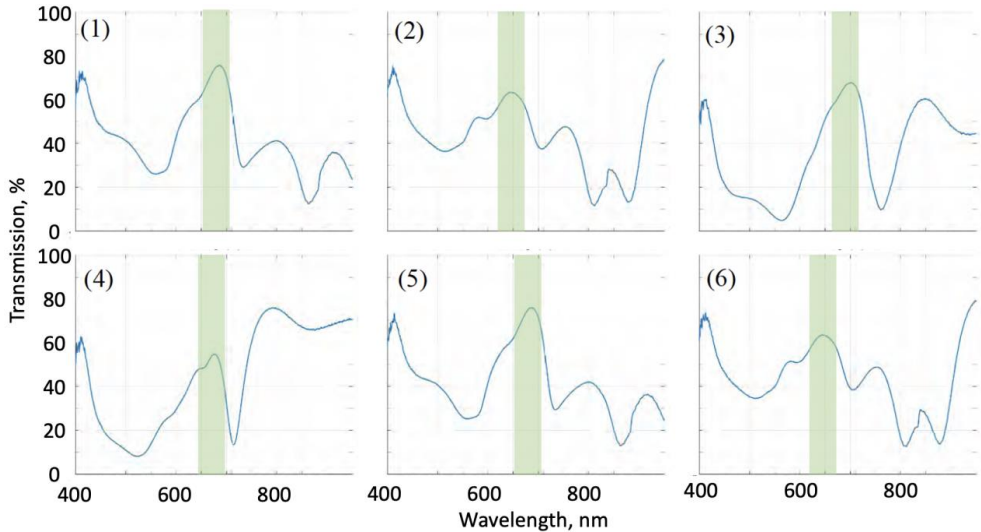

Fig. 3.3. Measured transmittance spectra for silicon metasurfaces in the hybrid anapole regime for metasurfaces with different periods s and radii R_{cyl}. The numbering corresponds to Table 2.1.

In the spectral response, a feature is visible in the range of 650 - 700 nm, corresponding to the hybrid-anapole state (maximum transmission, corresponding to the minimum of scattering). A comparison of conventional metasurfaces and superdense ones shows that the hybrid anapole peak of transmission almost does not change its spectral position.

To prove that this is indeed a hybrid anapole state, the Fig. 3.4. shows a multipole decomposition.
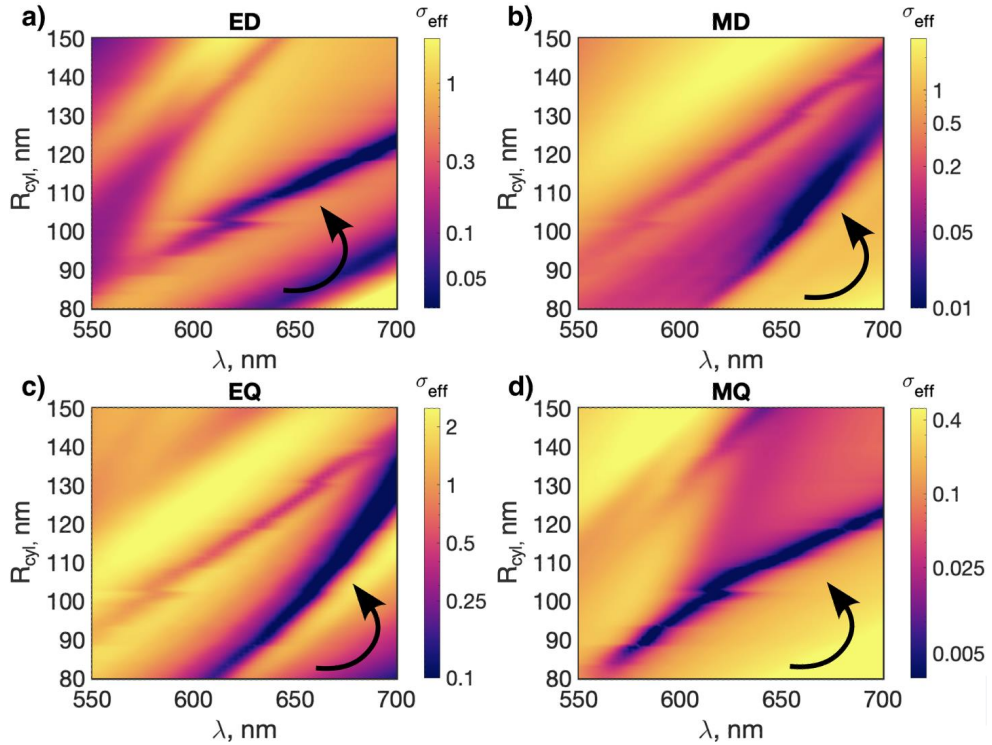
Fig. 3.4. Evolution of the SCS of each multipole (in log scale) (a) ED, (b) MD, (c) EQ, (d) MQ, as a function of wavelength and radii. The arrow indicates the anapole state of each of the multipoles.

The Fig. 3.4. shows anapole lines, which intersect in parameter space in a certain region, which is called the hybrid anapole state.

Using such particles, metasurfaces with two different radii and three different configurations were experimentally obtained: usual, dense and disordered (Fig. 3.5.).

Fig. 3.5. Measured transmittance spectra for silicon metasurfaces in the hybrid anapole regime for metasurfaces with different periods s, and structure without strict adherence to the arrangement order of nanoparticles for radius (a-c) R_{cyl} = 122 nm and (d-g) R_{cyl} = 138 nm.
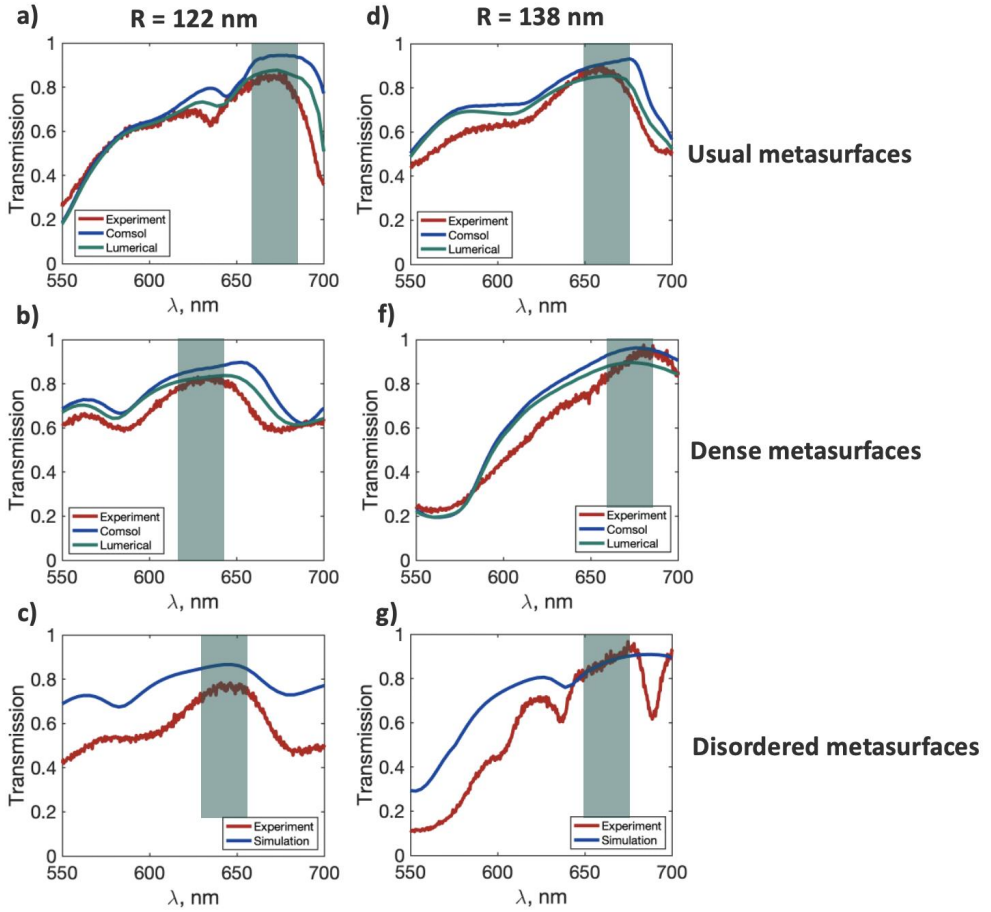
The main result of this part of the Doctoral Thesis is that the experimental results were compared with numerical simulations of metasurfaces for the current refractive index and radii. The numerical and experimental curves are quite similar. Transmission has a maximum, which indicates a hybrid anapole state in these metasurfaces.

The results obtained in the Doctoral Thesis were used:
- LZP project "*Dynamics of non-scattering states in nanophotonic (DNSSN)*" No. lzp-2021/1-0048
- LZP project "*Novel non-Hermitian singularities in all-dielectric nanostructures (NEO-NATE)*" No. lzp-2022/1-0553

4. FINAL REMARKS

In this final chapter, the main achievements of the presented Doctoral Thesis are discussed in **Section 4.1,** the main conclusions are discussed in **Section 4.2,** and **Section 4.3** gives a perspective for future research.

4.1. Main achievements of the Doctoral Thesis

The main achievements of the presented Doctoral Thesis can be summarized as follows:

1. A model of a metasurface has been developed, comprising silicon cylindrical meta-atoms that sustain a hybrid anapole state at a specific wavelength. It has been demonstrated that such a metasurface is transparent and does not alter the optical phase of the radiation passing through it at the anapole wavelength.

2. The practical implementation of metasurfaces will inevitably require the presence of a substrate. It can play an important role in the optical response and introduces magnetoelectric coupling. In sharp contrast to conventional resonances, hybrid anapole is extremely stable when applied to a substrate. In the studied nanocylinder with hybrid anapole state (in contrast to conventional anapoles or Huygens' sources), complete transmission is achieved due to the overlap of the resonant Mie and Fabry-Perot modes. The former can be associated with standing waves arising between the side walls of the resonator cavity, and the latter are mainly formed by standing waves between the upper and lower walls. Consequently, variations in the reflectivity of the substrate affect mainly the amplitude of the Fabry-Perot modes, while the Mie modes remain almost unchanged. However, in the presence of a significant contrast between the particle and the substrate, the hybrid anapole state changes insignificantly. However, as the refractive index of the substrate approaches the refractive index of the nanoparticle (the disappearance of the contrast and, accordingly, the leakage of the Fabry-Perot mode into the substrate), the hybrid anapole state gradually transforms into a conventional electric dipole anapole, still retaining a strong decrease in scattering.

   To study this phenomenon, it was obtained transmission, reflection, and absorption in the hybrid anapole state for a metasurface deposited on a series of hypothetical substrates with refractive indices varying in the range from 1 to 2. For numerical simulations, it was used the experimentally obtained refractive index dispersion for amorphous silicon.

   A gradual narrowing of the bandwidth is found, mainly due to the redshift of high-order Bloch modes. It is important to note that the total transmittance of the metasurface itself remains close to 100% in the vicinity of the hybrid anapole wavelength, even for a refractive index of 2.

   Unlike the case of a single particle, in the case of a metasurface the Mie and Fabry-Perot modes are coupled. As noted above, when the contrast decreases, the Fabry-Perot mode leaks into the substrate, and the hybrid anapole degenerates into

a regular anapole. In the presence of significant contrast, the hybrid anapole state-induced passband is very resistant to changes in the refractive index of the substrate. These results clearly show that the metasurface can be directly deposited on ordinary glass (SiO_2) or another substrate without additional design steps and provide full transmittance as well as optical phase control.

As a result, the contrast between the refractive indices of the elements of the metasurface and the substrate is maintained, the hybrid anapole metasurface is insensitive to various substrate materials, which greatly simplifies the experimental implementation of the proposed structures.

A unique advantage of the hybrid anapole metasurfaces studied in this Doctoral Thesis compared to traditional Huygens' metasurfaces is the stability of their characteristics to changes in the arrangement of particles, due to the fact that in the hybrid anapole state the individual elements of the hybrid anapole metasurface (metaatoms) practically do not interact with each other. In this case, the effective multipoles of meta-atoms on the substrate are almost identical to the multipoles of an isolated particle. This means that even at very small distances, they are not affected by the scattered fields of neighbors, unlike a conventional nanoantenna, for example, in the Kerker effect, the optical response of which is highly dependent on the presence and location of neighbors.

3. It was demonstrated that hybrid anapole retains its properties even at very small distances (down to 6% of the diameter of individual meta-atoms) between the elements of the metasurface. Successful suppression of reflection has been achieved for such closely packed metasurfaces. Importantly, the optical phase of the transmitted field also remains virtually unchanged. Besides its academic significance, this result sets the stage for implementing ultra-small pixels compared to what has been achieved on other platforms thus far, which is crucial, for instance, for holographic applications.

4. It was demonstrated that, unlike traditional periodic Huygens' metasurfaces, hybrid anapole metasurfaces are practically insensitive to disordering of meta-atoms. This was shown through a series of numerical calculations. It was found that the hybrid anapole state exhibits remarkable resistance to significant deviations from an ideal periodic lattice precisely because it is largely unaffected by its neighbors, rendering their arrangement insignificant. Additionally, it's worth noting that the proposed metasurface exhibits high field concentrations within the meta-atoms, characteristic of anapole regimes. Therefore, disordered hybrid anapole metasurfaces represent a fundamentally new and flexible platform for enhancing the interaction of light and matter at the nanoscale. This property of hybrid anapole metasurfaces presents a unique opportunity for their utilization in nonlinear optics, such as the generation of multiple harmonics.

It's noteworthy that such metasurfaces can be produced quite simply without the need for complex optimization methods or careful arrangement of meta-atoms. This is particularly crucial in the manufacturing of large metasurfaces, as maintaining

strict periodicity of meta-atoms on a large scale poses significant challenges. The complexity increases as the size of the metasurface grows, ultimately imposing a technological upper limit on its size. In contrast, hybrid anapole metasurfaces are not bound by such restrictions and can have practically unlimited dimensions.

5. A new mechanism was introduced to achieve 100% transmission and control the optical phase of the transmitted wave, based on the physics of a non-radiating state - a hybrid anapole. With future practical implementation in mind, the radius of the cylinder was chosen as the parameter to control the optical phase of the radiation. This choice was made because changing the radius of meta-atoms can be relatively easily realized using well-established fabrication techniques, such as electron beam lithography followed by reactive ion etching.

Using numerical methods, a "map" was created that related the specific transferred optical phase to the geometric parameter of the meta-atom. Such a map allows us to select a meta-atom that produces a specific optical phase, while maintaining complete transparency of the metasurface. The transmittance and optical phase were calculated for a hybrid anapole metasurface with small distances between metaatoms for various radii and wavelengths. Thanks to the map, it is possible to set the operating wavelength and observe a well-defined optical phase change for a set of radii within the hybrid anapole transparency window.

Thus, a method was demonstrated to control the optical phase of radiation transmitted through the structure by varying the radii of meta-atoms. In the studied case, the optical phase change primarily occurs due to an increase in the contribution of the electric quadrupole moment, which is significantly minimized by the electric quadrupole anapole. With the assistance of 2D maps, it becomes possible to select a specific optical phase delay for hybrid anapole nanocylinders of a given radius while maintaining complete transparency of the structure.

6. The possibility of modulating the optical phase of an ultrafast Gaussian pulse in transmission mode using a disordered hybrid anapole array on the surface of a glass substrate was investigated. Strong disorder in the plane was chosen to illustrate the system's independence from the arrangement of particles. Subsequently, a time-domain finite-difference time-domain (FDTD) simulation of the incoming x-polarized Gaussian pulse with a duration of 600 fs was conducted. The nanoparticle radius values ranged from 125 to 135 nm to fall within the range covered by hybrid anapole states.

As expected from previous calculations, the optical phases transferred by periodic and disordered metasurfaces were almost identical. Transmission remained above 85%, as confirmed by full-time profiles. Alternatively, although generally less practical, the device can also be wavelength-controlled. It was demonstrated that the interaction of Mie and Fabry-Perot modes enables additional optical phase modulation of the beam. An ultrafast optical phase modulator based on a disordered hybrid anapole array was numerically implemented. The results suggest the

possibility of flexible design of meta-atoms without the need for time-consuming optimization steps.

7. The influence of sample non-ideality on effects in dielectric nanoscatterers was investigated, and a quantitative study was conducted on the influence of taper $(1 - R_{top}/R_{bottom})$ on the resulting optical properties of the nanocavity. Specifically, the impact of the cone shape on the hybrid anapole regime in single nanoparticles and metasurfaces based on them was meticulously examined. It was found that the hybrid anapole state in cylinders is disrupted when changes are made to the shape due to alterations in the particle's symmetry. In such cases, previously closed channels open, leading to additional interactions between the resonator modes. Furthermore, the feasibility of achieving a hybrid anapole regime in conical particles was demonstrated for the first time, offering new opportunities for the design of photonic devices with more precise tuning of optical properties, thanks to the additional degree of freedom provided by the truncated cone radius

4.2.   Main conclusions

1. It has been demonstrated that metasurfaces in the hybrid anapole state exhibit nearly perfect transmittance and do not induce alterations in the optical phase or amplitude of transmitted radiation at the wavelength corresponding to the hybrid anapole state.

2. As a result of parametric modelling, changing the dielectric properties of the substrate (with the refractive index varying in the range of 1 to 2), transmission spectra, and maps of the spatial distribution of electromagnetic fields inside and outside the metaatom were calculated. It was demonstrated that in the presence of a contrast between the significant refractive index of the particle and the substrate, the hybrid anapole state remains extremely stable. However, as the refractive index of the substrate approaches that of the nanoantenna, leakage of the Fabry-Perot mode into the substrate was observed, causing the hybrid anapole to gradually transition into an electric dipole anapole.

3. It is shown that the same effect makes it possible to create metasurfaces in the hybrid anapole state with a very dense packing of metaatoms (the distance between the walls is up to 6% of the diameter of individual metaatoms). Metaatoms in the hybrid anapole state do not interact with each other.

4. The transmission spectra of metasurfaces were calculated for both perfectly ordered arrangements of metaatoms and disordered configurations. Upon comparing the obtained spectra and optical phase curves of the transmitted field, it is demonstrated that hybrid anapole metasurfaces are insensitive to disordering of metaatoms. Metaatoms in the hybrid anapole state are not influenced by their neighbours.

5. A method has been developed to control the amplitude and optical phase of the field passing through the metasurface in the hybrid anapole state. Through parametric numerical modelling (varying the radii of the nanocylinders), electromagnetic fields passing through the metasurface in the hybrid anapole state were analysed. A map

was then constructed linking the transmitted optical phase with the geometric parameter of the metaatom. This map allows for the selection of the geometric parameter that produces a desired optical phase while maintaining complete transparency of the metasurface.

6. A numerical simulation of an ultrafast optical phase modulator, utilizing a disordered array in a hybrid anapole state, was conducted with pulse duration of approximately 600 fs. Through alterations in the shape of the meta-atoms, control over the pulse passing through the structure was achieved. The results suggest the capability to flexibly design metadevices without the need for time-consuming optimization steps, achieving exceptionally high resolution.

7. The effect of changing the conicity on the resonances responsible for the hybrid anapole regime was demonstrated. Adjustment of the conicity effectively disrupts the fundamental symmetry of the particles and opens previously inaccessible channels, resulting in additional interactions between cavity modes. Understanding this effect may become crucial for future applications that leverage the unique properties of the hybrid anapole, such as metasurface engineering and sensing.

   Moreover, beyond the already established configurations of cylinders and ellipsoids in the hybrid anapole regime, the potential for achieving the hybrid anapole state in nanocones has been explored. Nanocones offer a simpler and easier to manufacture platform for implementing multipole interference effects. It was demonstrated that the hybrid anapole regime is sustained in nanocones, even with changes of up to 30% in the upper radius, albeit with a slight frequency shift of the resonance. Consequently, the library of all-dielectric nanostructures supporting the hybrid anapole regime has been expanded.

4.3. Further outlook

Metasurfaces in the hybrid anapole state offer a promising platform for various photonic effects and applications, owing to their unique properties. Current research can be expanded in the following directions:

- o Exploration of new photonic effects based on anapole metasurfaces, such as the attainment of high-quality quasi-bound states in the continuum using hybrid anapoles. This could serve as a promising platform for developing ultrasensitive sensors of a new generation.

- o Development of a model for a controllable optical structure comprising silicon metasurfaces in a hybrid anapole state, 2D materials, and substrates. Each element would interact with the others, enabling the creation of a selectively transparent structure for controlling optical radiation passing through it.

- o Investigation of optical forces acting on non-scattering single silicon particles in the hybrid anapole regime when irradiated with various forms of beams.

ACKNOWLEDGMENT

BIBLIOGRAPHY

1. Kivshar, Y.: All-dielectric meta-optics and non-linear nanophotonics. Natl Sci Rev. 5, 144–158 (2018). https://doi.org/10.1093/nsr/nwy017
2. Krasnok, A.E., Miroshnichenko, A.E., Belov, P.A., Kivshar, Y.S.: All-dielectric optical nanoantennas. Opt Express. 20, 20599 (2012). https://doi.org/10.1364/OE.20.020599
3. Koshelev, K., Kivshar, Y.: Dielectric Resonant Metaphotonics. ACS Photonics. 8, 102–112 (2021). https://doi.org/10.1021/acsphotonics.0c01315
4. Krasnok, A.E., Miroshnichenko, A.E., Belov, P.A., Kivshar, Y.S.: All-dielectric optical nanoantennas. Opt Express. 20, 20599 (2012). https://doi.org/10.1364/oe.20.020599
5. Yan, J., Liu, X., Ma, C., Huang, Y., Yang, G.: All-dielectric materials and related nanophotonic applications, (2020)
6. Yan, J., Liu, X., Ma, C., Huang, Y., Yang, G.: All-dielectric materials and related nanophotonic applications. Materials Science and Engineering R: Reports. 141, 100563 (2020). https://doi.org/10.1016/j.mser.2020.100563
7. Wang, J., Du, J.: Plasmonic and Dielectric Metasurfaces: Design, Fabrication and Applications. Applied Sciences. 6, 239 (2016). https://doi.org/10.3390/app6090239
8. Bosio, N., Šípová-Jungová, H., Länk, N.O., Antosiewicz, T.J., Verre, R., Käll, M.: Plasmonic versus All-Dielectric Nanoantennas for Refractometric Sensing: A Direct Comparison. ACS Photonics. 6, 1556–1564 (2019). https://doi.org/10.1021/acsphotonics.9b00434
9. Lalanne, P., Yan, W., Vynck, K., Sauvan, C., Hugonin, J.P.: Light Interaction with Photonic and Plasmonic Resonances. Laser Photon Rev. 12, 1–38 (2018). https://doi.org/10.1002/lpor.201700113
10. Terekhov, P.D., Babicheva, V.E., Baryshnikova, K. V., Shalin, A.S., Karabchevsky, A., Evlyukhin, A.B.: Multipole analysis of dielectric metasurfaces composed of nonspherical nanoparticles and lattice invisibility effect. Phys Rev B. 99, (2019). https://doi.org/10.1103/PhysRevB.99.045424
11. Terekhov, P.D., Evlyukhin, A.B., Shalin, A.S., Karabchevsky, A.: Polarization-dependent asymmetric light scattering by silicon nanopyramids and their multipoles resonances. J Appl Phys. 125, 173108 (2019). https://doi.org/10.1063/1.5094162
12. Kivshar, Y., Miroshnichenko, A.: Meta-Optics with Mie Resonances. Opt Photonics News. 28, 24 (2017). https://doi.org/10.1364/opn.28.1.000024
13. Shamkhi, H.K., Baryshnikova, K. V., Sayanskiy, A., Kapitanova, P., Terekhov, P.D., Belov, P., Karabchevsky, A., Evlyukhin, A.B., Kivshar, Y., Shalin, A.S.: Transverse scattering and generalized kerker effects in all-dielectric mie-resonant metaoptics. Phys Rev Lett. 122, 193905 (2019). https://doi.org/10.1103/PhysRevLett.122.193905
14. Liu, W., Kivshar, Y.S.: Generalized Kerker effects in nanophotonics and meta-optics [Invited]. Opt Express. 26, 13085 (2018). https://doi.org/10.1364/OE.26.013085
15. Barhom, H., Machnev, A.A., Noskov, R.E., Goncharenko, A., Gurvitz, E.A., Timin, A.S., Shkoldin, V.A., Koniakhin, S. V., Koval, O.Y., Zyuzin, M. V., Shalin, A.S., Shishkin, I.I., Ginzburg, P.: Biological Kerker Effect Boosts Light Collection Efficiency in Plants. Nano Lett. 19, 7062–7071 (2019). https://doi.org/10.1021/acs.nanolett.9b02540
16. Bukharin, M.M., Pecherkin, V.Ya., Ospanova, A.K., Il'in, V.B., Vasilyak, L.M., Basharin, A.A., Luk'yanchuk, B.: Transverse Kerker effect in all-dielectric spheroidal particles. Sci Rep. 12, 7997 (2022). https://doi.org/10.1038/s41598-022-11733-4
17. Alaee, R., Filter, R., Lehr, D., Lederer, F., Rockstuhl, C.: A generalized Kerker condition for highly directive nanoantennas. Opt Lett. 40, 2645 (2015). https://doi.org/10.1364/ol.40.002645

18. Sanz-Fernández, C., Molezuelas, M., Lasa-Alonso, J., de Sousa, N., Zambrana-Puyalto, X., Olmos-Trigo, J.: Multiple Kerker anapoles in dielectric microspheres. 1–5 (2020)

19. Hesari-Shermeh, M., Abbasi-Arand, B., Yazdi, M.: Generalized Kerker's conditions under normal and oblique incidence using the polarizability tensors of nanoparticles. Opt Express. 29, 647 (2021). https://doi.org/10.1364/oe.411110

20. Ali, A., Mitra, A., Aïssa, B.: Metamaterials and Metasurfaces: A Review from the Perspectives of Materials, Mechanisms and Advanced Metadevices. Nanomaterials. 12, 1027 (2022). https://doi.org/10.3390/nano12061027

21. Chen, M., Kim, M., Wong, A.M.H., Eleftheriades, G. V.: Huygens' metasurfaces from microwaves to optics: A review. Nanophotonics. 7, 1207–1231 (2018). https://doi.org/10.1515/nanoph-2017-0117

22. Kamali, S.M., Arbabi, E., Arbabi, A., Faraon, A.: A review of dielectric optical metasurfaces for wavefront control. Nanophotonics. 7, 1041–1068 (2018). https://doi.org/10.1515/nanoph-2017-0129

23. Terekhov, P.D., Evlyukhin, A.B., Redka, D., Volkov, V.S., Shalin, A.S., Karabchevsky, A.: Magnetic Octupole Response of Dielectric Quadrumers. Laser Photon Rev. 14, 1900331 (2020). https://doi.org/10.1002/lpor.201900331

24. Geffrin, J.M., García-Cámara, B., Gómez-Medina, R., Albella, P., Froufe-Pérez, L.S., Eyraud, C., Litman, A., Vaillon, R., González, F., Nieto-Vesperinas, M., Sáenz, J.J., Moreno, F.: Magnetic and electric coherence in forward- and back-scattered electromagnetic waves by a single dielectric subwavelength sphere. Nat Commun. 3, 1171 (2012). https://doi.org/10.1038/ncomms2167

25. Ginn, J.C., Brener, I., Peters, D.W., Wendt, J.R., Stevens, J.O., Hines, P.F., Basilio, L.I., Warne, L.K., Ihlefeld, J.F., Clem, P.G., Sinclair, M.B.: Realizing optical magnetism from dielectric metamaterials. Phys Rev Lett. 108, 1–5 (2012). https://doi.org/10.1103/PhysRevLett.108.097402

26. Koshelev, K., Favraud, G., Bogdanov, A., Kivshar, Y., Fratalocchi, A.: Nonradiating photonics with resonant dielectric nanostructures. Nanophotonics. 8, 725–745 (2019). https://doi.org/10.1515/nanoph-2019-0024

27. Zanganeh, E., Song, M., Valero, A.C., Shalin, A.S., Nenasheva, E., Miroshnichenko, A., Evlyukhin, A., Kapitanova, P.: Nonradiating sources for efficient wireless power transfer. Nanophotonics. 10, 4399–4408 (2021). https://doi.org/10.1515/nanoph-2021-0378

28. Fedotov, V.A., Rogacheva, A. V., Savinov, V., Tsai, D.P., Zheludev, N.I.: Resonant transparency and non-trivial non-radiating excitations in toroidal metamaterials. Sci Rep. 3, 1–5 (2013). https://doi.org/10.1038/srep02967

29. Azzam, S.I., Kildishev, A. V.: Photonic Bound States in the Continuum: From Basics to Applications. Adv Opt Mater. 9, 16–24 (2021). https://doi.org/10.1002/adom.202001469

30. Novitsky, D. V., Shalin, A.S., Redka, D., Bobrovs, V., Novitsky, A. V.: Quasibound states in the continuum induced by PT symmetry breaking. Phys Rev B. 104, 085126 (2021). https://doi.org/10.1103/PhysRevB.104.085126

31. Canós Valero, A., Shamkhi, H.K., Kupriianov, A.S., Weiss, T., Pavlov, A.A., Redka, D., Bobrovs, V., Kivshar, Y., Shalin, A.S.: Superscattering emerging from the physics of bound states in the continuum. Nat Commun. 14, 4689 (2023). https://doi.org/10.1038/s41467-023-40382-y

32. Novitsky, D. V., Valero, A.C., Krotov, A., Salgals, T., Shalin, A.S., Novitsky, A. V.: CPA-Lasing Associated with the Quasibound States in the Continuum in Asymmetric Non-Hermitian Structures. ACS Photonics. 9, 3035–3042 (2022). https://doi.org/10.1021/acsphotonics.2c00790

33. Bonacina, L., Brevet, P.-F., Finazzi, M., Celebrano, M.: Harmonic generation at the nanoscale. J Appl Phys. 127, 230901 (2020). https://doi.org/10.1063/5.0006093

34. Grinblat, G., Li, Y., Nielsen, M.P., Oulton, R.F., Maier, S.A.: Enhanced third harmonic generation in single germanium nanodisks excited at the anapole mode. Nano Lett. 16, 4635–4640 (2016). https://doi.org/10.1021/acs.nanolett.6b01958

35. Xu, L., Rahmani, M., Zangeneh Kamali, K., Lamprianidis, A., Ghirardini, L., Sautter, J., Camacho-Morales, R., Chen, H., Parry, M., Staude, I., Zhang, G., Neshev, D., Miroshnichenko, A.E.: Boosting third-harmonic generation by a mirror-enhanced anapole resonator. Light Sci Appl. 7, 44 (2018). https://doi.org/10.1038/s41377-018-0051-8

36. Hong, J., Son, H., Kim, C., Mun, S.-E., Sung, J., Lee, B.: Absorptive metasurface color filters based on hyperbolic metamaterials for a CMOS image sensor. Opt Express. 29, 3643 (2021). https://doi.org/10.1364/oe.415874

37. La Spada, L.: Metasurfaces for Advanced Sensing and Diagnostics. Sensors. 19, 355 (2019). https://doi.org/10.3390/s19020355

38. Canós Valero, A., Kislov, D., Gurvitz, E.A., Shamkhi, H.K., Pavlov, A.A., Redka, D., Yankin, S., Zemánek, P., Shalin, A.S.: Nanovortex-Driven All-Dielectric Optical Diffusion Boosting and Sorting Concept for Lab-on-a-Chip Platforms. Advanced Science. 7, 1903049 (2020). https://doi.org/10.1002/advs.201903049

39. Zhang, Y., Li, Z., Liu, W., Li, Z., Cheng, H., Chen, S., Tian, J.: Spin-Selective and Wavelength-Selective Demultiplexing Based on Waveguide-Integrated All-Dielectric Metasurfaces. Adv Opt Mater. 7, 1–8 (2019). https://doi.org/10.1002/adom.201801273

40. Miroshnichenko, A.E., Evlyukhin, A.B., Yu, Y.F., Bakker, R.M., Chipouline, A., Kuznetsov, A.I., Luk'yanchuk, B., Chichkov, B.N., Kivshar, Y.S.: Nonradiating anapole modes in dielectric nanoparticles. Nat Commun. 6, 1–8 (2015). https://doi.org/10.1038/ncomms9069

41. Baryshnikova, K. V., Smirnova, D.A., Luk'yanchuk, B.S., Kivshar, Y.S.: Optical Anapoles: Concepts and Applications. Adv Opt Mater. 7, 1–13 (2019). https://doi.org/10.1002/adom.201801350

42. Nemkov, N.A., Basharin, A.A., Fedotov, V.A.: Nonradiating sources, dynamic anapole, and Aharonov-Bohm effect. Phys Rev B. 95, 165134 (2017). https://doi.org/10.1103/PhysRevB.95.165134

43. Baryshnikova, K. V., Smirnova, D.A., Luk'yanchuk, B.S., Kivshar, Y.S.: Optical anapoles in nanophotonics and meta-optics. Adv Opt Mater. 1801350, 1–13 (2019). https://doi.org/10.1002/adom.201801350

44. Yang, Y., Bozhevolnyi, S.I.: Nonradiating anapole states in nanophotonics: From fundamentals to applications. Nanotechnology. 30, (2019). https://doi.org/10.1088/1361-6528/ab02b0

45. Colom, R., McPhedran, R., Stout, B., Bonod, N.: Modal analysis of anapoles, internal fields, and Fano resonances in dielectric particles. Journal of the Optical Society of America B. 36, 2052 (2019). https://doi.org/10.1364/josab.36.002052

46. Wei, L., Xi, Z., Bhattacharya, N., Urbach, H.P.: Excitation of the radiationless anapole mode. Optica. 3, 799 (2016). https://doi.org/10.1364/optica.3.000799

47. Gurvitz, E.A., Ladutenko, K.S., Dergachev, P.A., Evlyukhin, A.B., Miroshnichenko, A.E., Shalin, A.S.: The High-Order Toroidal Moments and Anapole States in All-Dielectric Photonics. Laser Photon Rev. 13, 1–13 (2019). https://doi.org/10.1002/lpor.201800266

48. Zhang, T., Che, Y., Chen, K., Xu, J., Xu, Y., Wen, T., Lu, G., Liu, X., Wang, B., Xu, X., Duh, Y.-S., Tang, Y.-L., Han, J., Cao, Y., Guan, B.-O., Chu, S.-W., Li, X.: Anapole mediated giant photothermal nonlinearity in nanostructured silicon. Nat Commun. 11, 3027 (2020). https://doi.org/10.1038/s41467-020-16845-x

49. Totero Gongora, J.S., Miroshnichenko, A.E., Kivshar, Y.S., Fratalocchi, A.: Anapole nanolasers for mode-locking and ultrafast pulse generation. Nat Commun. 8, 1–9 (2017). https://doi.org/10.1038/ncomms15535

50. Luk'yanchuk, B., Paniagua-Domínguez, R., Kuznetsov, A.I., Miroshnichenko, A.E., Kivshar, Y.S.: Hybrid anapole modes of high-index dielectric nanoparticles. Phys Rev A (Coll Park). 95, 1–8 (2017). https://doi.org/10.1103/PhysRevA.95.063820

51. Canós Valero, A., Gurvitz, E.A., Benimetskiy, F.A., Pidgayko, D.A., Samusev, A., Evlyukhin, A.B., Bobrovs, V., Redka, D., Tribelsky, M.I., Rahmani, M., Kamali, K.Z., Pavlov, A.A., Miroshnichenko, A.E., Shalin, A.S.: Theory, Observation, and Ultrafast Response of the Hybrid Anapole Regime in Light Scattering. Laser Photon Rev. 15, 2100114 (2021). https://doi.org/10.1002/lpor.202100114

52. Zanganeh, E., Andrey, E., Andrey, M., Polina, K.: Magnetic and Hybrid Anapole States in Dielectric Cylindrical Particles. 368–370

53. Ospanova, A.K., Basharin, A., Miroshnichenko, A.E., Luk'yanchuk, B.: Generalized hybrid anapole modes in all-dielectric ellipsoid particles [Invited]. Opt Mater Express. 11, 23 (2021). https://doi.org/10.1364/ome.414340

54. Vennberg, F., Ravishankar, A.P., Anand, S.: Manipulating light scattering and optical confinement in vertically stacked Mie resonators. Nanophotonics. 11, 4755–4764 (2022). https://doi.org/10.1515/nanoph-2022-0605

55. Vennberg, F., Ravishankar, A.P., Anand, S.: Manipulating light scattering and optical confinement in vertically stacked Mie resonators. Nanophotonics. 11, 4755–4764 (2022). https://doi.org/10.1515/nanoph-2022-0605

56. Decker, M., Staude, I., Falkner, M., Dominguez, J., Neshev, D.N., Brener, I., Pertsch, T., Kivshar, Y.S.: High-Efficiency Dielectric Huygens' Surfaces. Adv Opt Mater. 3, 813–820 (2015). https://doi.org/10.1002/adom.201400584

57. Liu, W., Kivshar, Y.S.: Generalized Kerker effects in nanophotonics and meta-optics. ArXiv. 26, 274–284 (2017). https://doi.org/10.1364/OE.26.013085

58. Ollanik, A.J., Smith, J.A., Belue, M.J., Escarra, M.D.: High-Efficiency All-Dielectric Huygens Metasurfaces from the Ultraviolet to the Infrared. ACS Photonics. 5, 1351–1358 (2018). https://doi.org/10.1021/acsphotonics.7b01368

59. Yoon, G., Kim, K., Huh, D., Lee, H., Rho, J.: Single-step manufacturing of hierarchical dielectric metalens in the visible. Nat Commun. 11, 1–10 (2020). https://doi.org/10.1038/s41467-020-16136-5

60. Khorasaninejad, M., Capasso, F.: Metalenses: Versatile multifunctional photonic components. Science (1979). 358, (2017). https://doi.org/10.1126/science.aam8100

61. Fathnan, A.A., Liu, M., Powell, D.A.: Achromatic Huygens' Metalenses with Deeply Subwavelength Thickness. Adv Opt Mater. 8, 1–9 (2020). https://doi.org/10.1002/adom.202000754

62. Howes, A., Wang, W., Kravchenko, I., Valentine, J.: Dynamic transmission control based on all-dielectric Huygens metasurfaces. Optica. 5, 787 (2018). https://doi.org/10.1364/OPTICA.5.000787

63. Pfeiffer, C., Grbic, A.: Metamaterial Huygens' surfaces: Tailoring wave fronts with reflectionless sheets. Phys Rev Lett. 110, 1–5 (2013). https://doi.org/10.1103/PhysRevLett.110.197401

64. Asadchy, V.S., Faniayeu, I.A., Ra'di, Y., Khakhomov, S.A., Semchenko, I. V., Tretyakov, S.A.: Broadband reflectionless metasheets: Frequency-selective transmission and perfect absorption. Phys Rev X. 5, 1–10 (2015). https://doi.org/10.1103/PhysRevX.5.031005

65. Liu, W., Miroshnichenko, A.E.: Beam Steering with Dielectric Metalattices. ACS Photonics. 5, 1733–1741 (2018). https://doi.org/10.1021/acsphotonics.7b01217

66.   Overvig, A.C., Shrestha, S., Malek, S.C., Lu, M., Stein, A., Zheng, C., Yu, N.: Dielectric metasurfaces for complete and independent control of the optical amplitude and phase. Light Sci Appl. 8, (2019). https://doi.org/10.1038/s41377-019-0201-7

67.   Liu, B., Sain, B., Reineke, B., Zhao, R., Meier, C., Huang, L., Jiang, Y., Zentgraf, T.: Nonlinear Wavefront Control by Geometric-Phase Dielectric Metasurfaces: Influence of Mode Field and Rotational Symmetry. Adv Opt Mater. 8, (2020). https://doi.org/10.1002/adom.201902050

68.   Wang, B., Dong, F., Li, Q.T., Yang, D., Sun, C., Chen, J., Song, Z., Xu, L., Chu, W., Xiao, Y.F., Gong, Q., Li, Y.: Visible-Frequency Dielectric Metasurfaces for Multiwavelength Achromatic and Highly Dispersive Holograms. Nano Lett. 16, 5235–5240 (2016). https://doi.org/10.1021/acs.nanolett.6b02326

69.   Wang, L., Kruk, S., Tang, H., Li, T., Kravchenko, I., Neshev, D.N., Kivshar, Y.S.: Grayscale transparent metasurface holograms. Optica. 3, 1504 (2016). https://doi.org/10.1364/OPTICA.3.001504

70.   Jiang, Q., Cao, L., Huang, L., He, Z., Jin, G.: A complex-amplitude hologram using an ultra-thin dielectric metasurface. Nanoscale. 12, 24162–24168 (2020). https://doi.org/10.1039/d0nr06461k

71.   Vovchuk, D., Kosulnikov, S., Noskov, R.E., Ginzburg, P.: Wire resonator as a broadband Huygens superscatterer. Phys Rev B. 102, 94304 (2020). https://doi.org/10.1103/PhysRevB.102.094304

72.   Gigli, C., Li, Q., Chavel, P., Leo, G., Brongersma, M.L., Lalanne, P.: Fundamental Limitations of Huygens' Metasurfaces for Optical Beam Shaping. Laser Photon Rev. 2000448 (2021). https://doi.org/10.1002/lpor.202000448

73.   Chong, K.E., Staude, I., James, A., Dominguez, J., Liu, S., Campione, S., Subramania, G.S., Luk, T.S., Decker, M., Neshev, D.N., Brener, I., Kivshar, Y.S.: Polarization-Independent Silicon Metadevices for Efficient Optical Wavefront Control. Nano Lett. 15, 5369–5374 (2015). https://doi.org/10.1021/acs.nanolett.5b01752

74.   Zhang, X.L., Wang, S.B., Lin, Z., Sun, H.B., Chan, C.T.: Optical force on toroidal nanostructures: Toroidal dipole versus renormalized electric dipole. Phys Rev A. 92, 1–8 (2015). https://doi.org/10.1103/PhysRevA.92.043804

75.   Feng, T., Xu, Y., Zhang, W., Miroshnichenko, A.E.: Ideal Magnetic Dipole Scattering. Phys Rev Lett. 118, 173901 (2017). https://doi.org/10.1103/PhysRevLett.118.173901

76.   Baranov, D.G., Savelev, R.S., Li, S. V., Krasnok, A.E., Alù, A.: Modifying magnetic dipole spontaneous emission with nanophotonic structures. Laser Photon Rev. 11, (2017). https://doi.org/10.1002/lpor.201600268

77.   Babicheva, V.E., Evlyukhin, A.B.: Metasurfaces with Electric Quadrupole and Magnetic Dipole Resonant Coupling. ACS Photonics. 5, 2022–2033 (2018). https://doi.org/10.1021/acsphotonics.7b01520

78.   Zhang, Y., Yue, P., Liu, J.-Y., Geng, W., Bai, Y.-T., Liu, S.-D.: Ideal magnetic dipole resonances with metal-dielectric-metal hybridized nanodisks. Opt Express. 27, 16143 (2019). https://doi.org/10.1364/OE.27.016143

79.   Patoux, A., Agez, G., Girard, C., Paillard, V., Wiecha, P.R., Lecestre, A., Carcenac, F., Larrieu, G., Arbouet, A.: Challenges in nanofabrication for efficient optical metasurfaces. Sci Rep. 11, 1–12 (2021). https://doi.org/10.1038/s41598-021-84666-z

80.   Kim, Y., Yang, H., Oh, J.H.: Simple fabrication of highly sensitive capacitive pressure sensors using a porous dielectric layer with cone-shaped patterns. Mater Des. 197, 109203 (2021). https://doi.org/10.1016/j.matdes.2020.109203

81.   Toliopoulos, D., Khoury, M., Bouabdellaoui, M., Granchi, N., Claude, J.-B., Benali, A., Berbezier, I., Hannani, D., Ronda, A., Wenger, J., Bollani, M., Gurioli, M., Sanguinetti, S., Intonti, F., Abbarchi, M.: Fabrication of spectrally sharp Si-based dielectric

resonators: combining etaloning with Mie resonances. Opt Express. 28, 37734 (2020). https://doi.org/10.1364/oe.409001

82. Arfken, G.B., Weber, H.J.: Mathematical Methods for Physicists. New York: Acad. Press (1995)

83. Alaee, R., Rockstuhl, C., Fernandez-Corbaton, I.: An electromagnetic multipole expansion beyond the long-wavelength approximation. Opt Commun. 407, 17–21 (2018). https://doi.org/10.1016/j.optcom.2017.08.064

84. Pepper D. W., Heinrich J. C.: The finite element method: basic concepts and applications with MATLAB, MAPLE, and COMSOL. CRC press (2017)

85. Rajeswari, R., Jothilakshmi, R.: Modeling and Simulation of Plasmonic Nanoparticles Using Finite-Difference Time-Domain Method: A Review. Materials Science Forum. 781, 33–44 (2014). https://doi.org/10.4028/www.scientific.net/MSF.781.33

86. Raab R. E., Lange O. L.: Multipole Theory in Electromagnetism. (2005)

87. Dobrykh, D., Shakirova, D., Krasikov, S., Mikhailovskaya, A., Yusupov, I., Slobozhanyuk, A., Ladutenko, K., Filonov, D., Bogdanov, A., Ginzburg, P.: Multipole engineering for enhanced backscattering modulation. Phys Rev B. 102, 1–6 (2020). https://doi.org/10.1103/PhysRevB.102.195129

88. Mühlig, S., Menzel, C., Rockstuhl, C., Lederer, F.: Multipole analysis of meta-atoms. Metamaterials. 5, 64–73 (2011). https://doi.org/10.1016/j.metmat.2011.03.003

89. Evlyukhin, A.B., Chichkov, B.N.: Multipole decompositions for directional light scattering. Phys Rev B. 100, 125415 (2019). https://doi.org/10.1103/PhysRevB.100.125415

90. Kruk, S., Kivshar, Y.: Functional Meta-Optics and Nanophotonics Governed by Mie Resonances. ACS Photonics. 4, 2638–2649 (2017). https://doi.org/10.1021/acsphotonics.7b01038

91. Liu, T., Xu, R., Yu, P., Wang, Z., Takahara, J.: Multipole and multimode engineering in Mie resonance-based metastructures. Nanophotonics. 9, 1115–1137 (2020). https://doi.org/10.1515/nanoph-2019-0505

92. Alaee, R., Rockstuhl, C., Fernandez-Corbaton, I.: An electromagnetic multipole expansion beyond the long-wavelength approximation. Opt Commun. 407, 17–21 (2018). https://doi.org/10.1016/j.optcom.2017.08.064

93. Jackson, J.D.: Classical Electrodynamics. (1962)

94. Grahn, P., Shevchenko, A., Kaivola, M.: Electromagnetic multipole theory for optical nanomaterials. New J Phys. 14, (2012). https://doi.org/10.1088/1367-2630/14/9/093033

95. Papasimakis, N., Fedotov, V.A., Savinov, V., Raybould, T.A., Zheludev, N.I.: Electromagnetic toroidal excitations in matter and free space. Nat Mater. 15, 263–271 (2016). https://doi.org/10.1038/nmat4563

96. Fernandez-Corbaton, I., Nanz, S., Alaee, R., Rockstuhl, C.: Exact dipolar moments of a localized electric current distribution. Opt Express. 23, 33044 (2015). https://doi.org/10.1364/oe.23.033044

97. Krasnok, A., Tymchenko, M., Alù, A.: Nonlinear metasurfaces: a paradigm shift in nonlinear optics. Materials Today. 21, 8–21 (2018). https://doi.org/10.1016/j.mattod.2017.06.007

98. Lin, D., Fan, P., Hasman, E., Brongersma, M.L.: Dielectric gradient metasurface optical elements. Science (1979). 345, 298–302 (2014). https://doi.org/10.1126/science.1253213

99. Londoño, M., Sayanskiy, A., Araque-Quijano, J.L., Glybovski, S.B., Baena, J.D.: Broadband Huygens' Metasurface Based on Hybrid Resonances. Phys Rev Appl. 10, 1 (2018). https://doi.org/10.1103/PhysRevApplied.10.034026

100. Karvounis, A., Gholipour, B., MacDonald, K.F., Zheludev, N.I.: All-dielectric phase-change reconfigurable metasurface. Appl Phys Lett. 109, (2016). https://doi.org/10.1063/1.4959272

101. Zhang, X., Li, Q., Liu, F., Qiu, M., Sun, S., He, Q., Zhou, L.: Controlling angular dispersions in optical metasurfaces. Light Sci Appl. 9, 34–37 (2020). https://doi.org/10.1038/s41377-020-0313-0

102. Babicheva, V.E., Evlyukhin, A.B.: Analytical model of resonant electromagnetic dipole-quadrupole coupling in nanoparticle arrays. Phys Rev B. 99, 195444 (2019). https://doi.org/10.1103/PhysRevB.99.195444

103. Vaskin, A., Mashhadi, S., Steinert, M., Chong, K.E., Keene, D., Nanz, S., Abass, A., Rusak, E., Choi, D.-Y., Fernandez-Corbaton, I., Pertsch, T., Rockstuhl, C., Noginov, M.A., Kivshar, Y.S., Neshev, D.N., Noginova, N., Staude, I.: Manipulation of Magnetic Dipole Emission from Eu [3+] with Mie-Resonant Dielectric Metasurfaces. Nano Lett. 19, 1015–1022 (2019). https://doi.org/10.1021/acs.nanolett.8b04268

SUPPLEMENTS

[PAPER 1]: Transparent hybrid anapole metasurfaces with negligible electromagnetic coupling for phase engineering

Research Article

Alexey V. Kuznetsov*, Adrià Canós Valero, Mikhail Tarkhov, Vjaceslavs Bobrovs,
Dmitrii Redka and Alexander S. Shalin

Transparent hybrid anapole metasurfaces with negligible electromagnetic coupling for phase engineering

Abstract: All-dielectric nanophotonics has become one of the most active fields of research in modern optics, largely due to the opportunities offered by the simultaneous resonant control of electric and magnetic components of light at the nanoscale. In this rapidly evolving scenario, the possibility to design artificial Huygens sources by overlapping electric and magnetic resonances has established a new paradigm in flat optics, bringing devices closer to efficient wavefront shaping with direct phase engineering at the level of the individual meta-atoms. However, their efficiency is fundamentally limited by the near-field coupling between the constituents of the metalattice. In this work, we challenge this well-conceived notion and propose an alternative concept to achieve phase control and full transmission in metasurfaces, based on the unusual properties of the nonradiating sources known as hybrid anapoles (HAs). We analyze theoretically an array of such sources and demonstrate that HAs are characterized by negligible coupling with their neighbors. Therefore, in contrast to Huygens particles, the proposed sources can operate as individual meta-atoms even in highly compact designs, becoming robust against strong disorder and preserving its characteristics when deposited on dielectric substrates. Remarkably, the phase of the transmitted wave can be modulated with negligible reflection. To illustrate the capabilities of our platform, we also utilize a disordered HA array to implement a controlled phase modulation to an ultrafast Gaussian pulse. The results of our study represent a departure from the currently established designs and open an avenue toward the realization of new devices for flat optics with unprecedented efficiency.

Keywords: all-dielectric metasurfaces; flat optics; hybrid anapoles; nonradiating sources; resonant nanoantennas.

Alexey V. Kuznetsov and Adrià Canós Valero contributed equally to this work.

*Corresponding author: Alexey V. Kuznetsov, ITMO University, Kronverksky prospect 49, St. Petersburg 197101, Russia, E-mail: alexey.kuznetsov98@gmail.com. https://orcid.org/0000-0003-2008-9930
Adrià Canós Valero, ITMO University, Kronverksky prospect 49, St. Petersburg 197101, Russia. https://orcid.org/0000-0003-3870-6351
Mikhail Tarkhov, Institute of Nanotechnology of Microelectronics of the Russian Academy of Sciences (INME RAS), Nagatinskaya street, House 16A, building 11, Moscow, Russia
Vjaceslavs Bobrovs, Riga Technical University, Institute of Telecommunications, Azenes street 12, Riga 1048, Latvia. https://orcid.org/0000-0002-5156-5162
Dmitrii Redka, Riga Technical University, Institute of Telecommunications, Azenes street 12, Riga 1048, Latvia; and Electrotechnical University "LETI" (ETU), 5 Prof. Popova Street, Saint Petersburg 197376, Russia
Alexander S. Shalin, ITMO University, Kronverksky prospect 49, St. Petersburg 197101, Russia; Riga Technical University, Institute of Telecommunications, Azenes street 12, Riga 1048, Latvia; and Kotel'nikov Institute of Radio Engineering and Electronics of Russian Academy of Sciences (Ulyanovsk branch), Goncharova Str.48, Ulyanovsk 432000, Russia

1 Introduction

Over the past few years, all-dielectric nanophotonics has become one of the most active fields in optics [1–4]. High-index subwavelength nanostructures represent a radical departure from the field of plasmonics, paving the way toward efficient control of light at the nanoscale in the absence of dissipation losses, and offering complementary metal−oxide−semiconductor (CMOS) compatibility. Careful shape and dispersion engineering of subwavelength dielectric cavities allows exciting and tuning both electric and magnetic resonances [5–8]. Optical structures composed of such artificial elements, commonly termed 'meta-atoms', feature a plethora of exotic effects not accessible with natural materials, still being explored up to date, such as artificial magnetism [9], nonradiating sources,

supercavity modes, and bound states in the continuum, efficient second and third harmonic generation [10], or spin–orbit conversion [11].

Among all the promising phenomena uncovered in this versatile research platform, directional Huygens sources, caused by the simultaneous overlap of electric and magnetic resonances with opposite parity [12, 13], hold enormous interest in the flat optics community, since two-dimensional subwavelength arrays -metasurfaces- of dielectric Huygens nanodisks with different size can imprint varying phases to an incident field, while featuring unity transmission [14], giving birth to the vibrant field of all-dielectric 'meta-optics'. As a result of these developments, a number of applications have already been proposed, such as ultrathin metalenses [15, 16], dynamic control of transmission [17], anomalous refraction [18], beam steering [19], holograms [20–22], and broadband Huygens elements [23].

To achieve the ultimate goal of spatial wavefront control with subwavelength resolution, Huygens metasurfaces are required to overcome fundamental bottlenecks [24], usually ascribed to inter-element coupling [18, 25]. When placed on an array, there exists an important cross-talk between Huygens meta-atoms even for separations in the order of the wavelength [18], complicating the engineering of phase at the level of the individual constituents. This is a well-known problem in radio engineering when dealing with phased antenna arrays, where a number of methods have been proposed to overcome it [26, 27]. In meta-optics, several attempts have been made to minimize this issue; for instance, in Ref. [18] the authors propose the use of carefully optimized supercells, while in Ref. [28] the effect of coupling is exploited precisely in order to imprint varying phases to distinct regions of an array. These strategies have allowed pushing the performance limits of Huygens metasurfaces, but the question remains whether a direct mapping of phase to the individual meta-atom will ever be reachable. Large-scale numerical optimization of Huygens metasurfaces has indeed been shown to improve their performance, but by no means does gradient-based approaches allow to minimize interparticle interactions, rather they maximize the efficiency of the ensemble [29]. As a result, the geometrical degrees of freedom must be carefully adjusted at each stage of the design, and special care must be taken to include the influence of period, underlying substrate, and disorder in the array. Particularly the latter can drastically modify the expected transmitted phase with respect to the periodic metasurface [30, 31]. Because of the aforementioned reasons, the efficiency of such devices might be fundamentally limited [24].

Recently, an alternative to the Huygens effect allowing to realize unity transmission in a metasurface has been proposed. Specifically, the so-called 'transverse Kerker' effect characterized by out-of-phase dipoles and quadrupoles in a scatterer was shown to lead to an 'invisible' metasurface, where light traversed the array without any perturbation [32]. Thus, the rich multipolar toolbox offered by all-dielectric nanostructures still hosts a number of surprising effects that can be exploited to improve the performance of meta-devices, beyond Huygens.

In this work, we propose a novel mechanism to achieve unity transmission and phase control based on the physics of a recently observed nonradiating state, the hybrid anapole (HA) [33]. Nowadays, the so-called anapole states, originating from the destructive interference of the electric and toroidal dipole moments [34], have already revolutionized nanophotonics, demonstrating enhanced second and third harmonic generation [35, 36], giant photothermal nonlinearities [37], and 'dark' lasers [38]. HAs constitute the 'new' generation of anapoles, arising due to the simultaneous destructive interference of all dominant multipole moments with their toroidal counterparts [33]. While the possibility to overlap anapoles was first discussed in [39], only recently HAs were theoretically proposed and experimentally confirmed to occur in dielectric nanocylinders by inducing a degeneracy of two high order modes with different symmetry [33]. Unlike conventional anapoles, they have a mixed electric and magnetic nature, in some cases displaying helicity singularities [37]. Furthermore, they have been shown to outperform their counterparts both in terms of scattering suppression and stored electromagnetic energy, and retain their nonradiating character in the presence of an arbitrary dielectric substrate [33].

Here, we investigate in detail the properties of HA-based metasurfaces. We first show analytically and numerically that their ultra-weak interaction with the environment naturally leads to unity transmission. However, relaxing the constrain for complete suppression of scattering, the multiresonant nature of HAs allows one to vary the transmitted phase within a wide spectral and geometrical range. Most importantly, unlike Huygens sources, the inter-particle coupling is almost negligible. Thus, the HA particle approaches the ideal of a 'true' meta-atom. We showcase this ability by designing highly compact silicon arrays with interparticle wall-to-wall separations of 1/8th the incident wavelength in the visible range, as well as disordered HA-metasurfaces exhibiting an identical behavior to their periodic counterparts. We study the influence of a substrate and demonstrate the preservation of the transmission window when the metasurface is deposited over a broad range of dielectric materials, potentially facilitating their on-chip integration. Finally, as a proof-of-concept application, we

49

modulate the phase of an ultrafast Gaussian pulse transmitted with unity efficiency from a highly disordered HA metasurface deposited on a glass substrate, solely with the knowledge of the optical response of the periodic array.

2 Limitations of the Huygens meta-atom

The transmission characteristics of an arbitrary metasurface composed of identical resonators can be well described with the knowledge of the effective multipoles induced on a single meta-atom, taking into account their mutual interaction [40]. Then, the complex transmission coefficient $t(\omega)$ is a result of the linear addition of the complex multipole coefficients together with the direct transmission:

$$t(\omega) = 1 + \sum_i \left[t_i^e(\omega) + t_i^m(\omega) \right], \qquad (1)$$

where the superscripts e, m stem for 'electric' and 'magnetic', and the summation runs over all the multipoles having a non-negligible effect on the scattering characteristics of the isolated meta-atom ($i = 1$ dipoles, $i = 2$ quadrupoles, etc.). An expression similar to Eq. (1) can be obtained for the reflection coefficient $r(\omega)$. As we prove rigorously in the Supplementary Material S1, Eq. (1) is valid for all metasurfaces with subwavelength interparticle separations if a sufficient set of terms in the expansion are taken into account.

When the metasurface is constituted with particles much smaller than the wavelength, (i.e. $kr_{\text{eff}} \ll 1$, r_{eff} being a characteristic dimension of the particle) only the dipoles play an important role [41–43]. For clarity, from now on we omit all arguments in the expressions, and refer the interested reader to Ref. [44] and the Supplementary Material S1 for details. Considering an x-polarized plane wave propagating in the $-z$ direction with the amplitude E_0, and assuming the metasurfaces is suspended in free space, Eq. (1) takes the simplified form:

$$t = 1 + \frac{C}{S_l} \left[\tilde{p}_x + \frac{1}{c} \tilde{m}_y \right], \qquad (2)$$

where $C = ik/(2D_0)$, with $D_0 = \epsilon_0 E_0$, and S_l is the surface of the lattice unit cell. Similarly, the reflection coefficient is

$$r = \frac{C}{S_l} \left[\tilde{p}_x - \frac{1}{c} \tilde{m}_y \right]. \qquad (3)$$

The minus sign in Eq. (3) appears due to the opposite parity of the electric and magnetic dipoles and is the key-

enabling feature of Huygens metasurfaces. It gives rise to the well-known forward Kerker condition [12] implying that if the electric $\tilde{p}_x$ and magnetic $\tilde{m}_y$ dipoles are in-phase and fulfill the relation $\tilde{p}_x = \tilde{m}_y/c$, there is no reflection and therefore the transmitted amplitude $T = |t|^2 = 1 - |r|^2 = 1$ in the absence of absorption losses. Importantly, the transmitted phase can be varied with unity efficiency, as long as the phase difference between the multipoles is kept approximately constant.

One of the most attractive traits of Huygens metasurfaces is the notion of "meta-atom": a subwavelength unit cell with the individually tailored optical response, in our case designed to provide a specific phase when incorporated into an array with dissimilar characteristics, for the implementation of different types of phase gradients. In reality, it has been shown that the meta-atoms are in general highly sensitive to their surrounding [18] and therefore additional and resource-consuming optimization steps taking into account the metasurface as a whole are required to reach the desired efficiency [18, 28]. Unfortunately, during the process, the ideal notion of 'meta-atom' is lost [24], since one can no longer trace a one-to-one mapping between the response of the isolated particles and their response in the array.

The most important bottleneck is the mutual coupling between the particles in the array [18, 24]. Indeed, the effective multipoles $\tilde{\mathbf{b}} = [\tilde{p}_x, \tilde{m}_y]^T$ entering Eqs. (2–3) can only be obtained from the isolated particle response $\mathbf{b} = [p_x, m_y]^T$ after including the influence of the scattered fields from all the particles in the array. By means of the multiple scattering theory [44], one can derive a system of linear equations:

$$\tilde{\mathbf{b}} = (I - \mathcal{A}\mathcal{S})^{-1} \cdot \mathbf{b}, \qquad (4)$$

where two important physical terms can be distinguished; the *polarizability matrix* $\mathcal{A}$ is a diagonal matrix containing the electric and magnetic multipole polarizabilities of the isolated particle. The *coupling matrix* $\mathcal{S}$ quantifies the strength of the multipolar fields from each particle in the array (and its derivatives in the case of quadrupolar contributions and higher), evaluated at the center of mass of the particle (see Supplementary Material S1 and Ref. [44]). The elements of $\mathcal{S}$ are solely a function of the electromagnetic propagator in the medium evaluated at the positions of each constituent.

Customarily, in the analysis of Huygens metasurfaces, the dipolar polarizabilities entering $\mathcal{A}$ are assumed to follow a Lorentzian dispersion [14]:

$$\alpha_{p,m}(\omega) = \frac{d_0}{\omega_0^2 - \omega^2 - i\omega\gamma}. \qquad (5)$$

This formula corresponds to a phenomenological damped harmonic oscillator with amplitude d_0 resonating

50

at ω_0, driven by an external field with angular frequency ω. Here, we encounter an important limitation of the Huygens meta-atom; indeed, near resonance, $\alpha_{p,m}(\omega_0)$ is drastically enhanced, and therefore *so is the coupling* induced by the product $\mathcal{AS}$ in Eq. (4). In order to minimize coupling, a general design rule states that the period of an array l should be larger than $\sqrt{\sigma_{\text{ext}}}$, ($\sigma_{\text{ext}}$ the extinction cross-section of the single-particle), imposing clear limitations on their compactness and size of the unit cell, and complicating the design of applications. Moreover, when the metasurface is placed over a substrate, the effective multipoles must also take into account the scattered fields of their 'mirror' images [45]. Huygens metasurfaces, and in general any dielectric or plasmonic metasurface, are in consequence strongly influenced by the substrate.

3 Phase-controlling HA metasurfaces

Clearly, an unconventional approach is needed to overcome the abovementioned difficulties. If we require a *true* meta-atom, we are bound to only exploit single-particle effects, i.e., we can solely act on $\mathcal{A}$. A possible solution would then be to set $\mathcal{A} = 0$. Anapoles are promising candidates, since they allow to resonantly suppress the electric dipole polarizability beyond the Rayleigh limit [34]. However, only HAs can simultaneously cancel all the dominant electric and *magnetic* multipole moments, even leading to complete transparency [33]. Namely, if we write t up to the quadrupolar terms, we obtain

$$t = 1 + \frac{C}{S_l}\left(\tilde{p}_x + \frac{1}{c}\tilde{m}_y - \frac{ik}{6}\tilde{Q}_{xz} - \frac{ik}{2c}\tilde{M}_{yz}\right). \qquad (6)$$

$\tilde{Q}_{xz}$ and $\tilde{M}_{yz}$ in Eq. (6) are, respectively, the excited components of the electric and magnetic quadrupolar tensors. At the anapole in an isolated particle, the exact electric dipole is suppressed by the interference of the quasistatic electric dipole p_x^0 with the electric toroidal dipole T_x^p in the now classical formula $p_x = p_x^0 + ikT_x^p = 0$. Conversely, at the HA all the dominant multipoles are resonantly suppressed via the interference with their toroidal counterparts [33]. From Eq. (6), the latter implies near-unity transmission. This apparently simple realization lays the foundation of our novel proposal, *nonradiating* HA metasurfaces enabling full transmission. We must also point out that destructive interference occurs strictly outside the smallest spherical region enclosing the scatterer [46]. However, similarly to a conventional anapole, the fields within the particle remain strongly enhanced [33, 34], but are much more confined in

the high-index region due to the larger quality factors of the modes involved. As will be shown later, the combination of the two effects results in a negligible electromagnetic interaction in the near and far-field regions.

In the following subsections, we carry out a detailed investigation of both periodic and aperiodic (disordered) arrays of HA meta-particles under normally incident plane wave illumination, as schematically depicted in Figure 1(a). We demonstrate how the highly sought properties of the HA are directly inherited by the metasurface, allowing for a resonant suppression of reflection, invariance with a period, and robust protection from disorder, a unique trait of our design. Remarkably, we reveal that the transmitted phase can be varied within the region of strong scattering cancellation. We dedicate a specialized subsection to understand the influence of a dielectric substrate, demonstrating that the transmission band is preserved for a broad range of materials. In particular, we show that a glass substrate allows doubling the available phase range. Altogether, our non-Huygens metasurfaces can therefore represent a new cornerstone in Mie optics.

3.1 Near unity transmission and phase control

First, we investigate periodic square arrays of HA meta-atoms similar to the ones proposed in Ref. [33], constituted amorphous silicon, where we have also included dissipation losses (the full dispersion is provided in section S4 of the Supplementary Material). Figure 1(b) displays the calculated transmission (T) spectra for an HA metasurface with separation between walls of resonators $s = 300$ nm. λ_0 indicates the wavelength featuring an almost complete overlap of the dipole and quadrupole anapoles in a single nanoparticle (refer to the Supplementary Material S5). Confirming the theory, a broad transmission band can be observed in the vicinity of λ_0. We note that unity transmission can be achieved, if dissipation losses are neglected.

The transmitted phase is exactly 0 at λ_0 [Figure 1(c)] and experiences a gradual increase along the transmission band of approximately 40°. To gain insight into the physical origin of the phase change, we decompose the complex transmission coefficient with the help of Eq. (6) and the exact expressions for the multipole moments in Cartesian coordinates [47] (see Supplementary Material S3). We stress that, unlike the scattering cross-section, T is not the result of the direct sum of the absolute values of each individual multipole, since they interfere. Instead, T is given by the squared modulus of Eq. (6), in full agreement with the
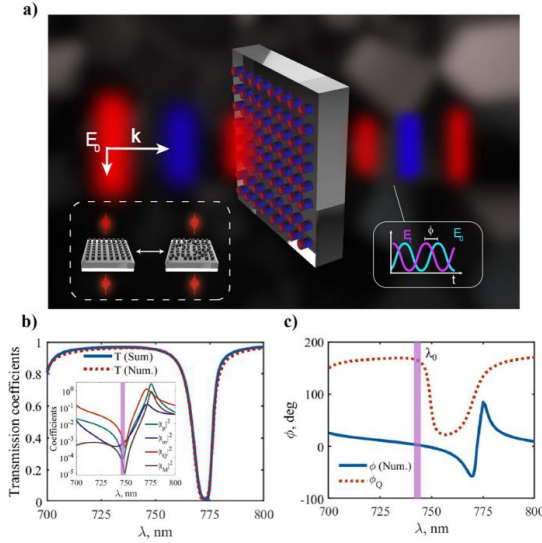
Figure 1: (a) Schematic overview of the considered Si metasurfaces composed of HA nanoparticles, illustrating its new functionalities: full transmission (left inset), phase control (right inset), and negligible electromagnetic coupling, allowing for the design of ultracompact, as well as disordered arrays retaining the single-particle response. The structure is illuminated with a normally incident plane wave with amplitude E_0. (b) Numerical and semi-analytical [Eq. (6)] transmission spectra obtained for an HA metasurface with $s = 300$ nm (inset: absolute values of the dominant multipolar contributions). The geometrical parameters of the meta-atom are height 370 nm and radius 130 nm. (c) Total transmitted phase ϕ obtained numerically, and phase variation experienced by the electric quadrupole ϕ_Q.

numerical calculations [Figure 1(b)]. We first center our attention on the absolute values of the multipolar contributions to transmission [inset of Figure 1(b)]. In direct analogy with the single-particle behavior, we observe a resonant cancellation of all the multipole moments at λ_0, in the form of dips that extend along the whole transmission band. In the Supplementary Material S6, we demonstrate that their origin is indeed due to the interference of the quasistatic moments with their toroidal counterparts.

Complete destructive interference is achieved only at λ_0 (leading to a zero-phase shift). However, the multipolar fields are still strongly suppressed in its spectral vicinity. We stress that despite its small overall contribution, the electric quadrupole moment is the dominant multipole in the spectral range of interest, exceeding the electric dipole by an order of magnitude. The latter confirms that the near-unity transmission *is not due to a generalized Kerker effect* [48] between the electric dipole and the electric quadrupole moments, but solely due to the resonant scattering suppression of the HA. Importantly, the quadrupole increases in an almost linear fashion toward shorter wavelengths, while its phase remains almost constant [Figure 1(c)]. Within the spectral region covered by the HA, despite its linear growth, the quadrupole is much smaller than unity,

and thus displays negligible reflection. Taking these observations into account, the evolution of the transmitted phase can now be understood as due to the dephasing in the forward direction of the electric quadrupole field with the incident plane wave.

We now assess one of the most distinct advantages of our novel non-Huygens metasurfaces, i.e., their robustness against changes in inter-particle separation s (Figure 2). As a comparison, we also included calculations with a less efficient non-Huygens metasurface being constituted solely of nanoparticles supporting the electric anapole [34]. Figure 2(a) shows the variation in the overall transmission as a function of period, evaluated at λ_0 (the minimum of the electric anapole has also been designed to occur at λ_0). Due to the small overall polarizabilities, both cases studied preserve unity transmission up to very small periods. HA metasurfaces, however, can successfully suppress reflection even at dramatically small separations between the constituents, i.e. in ultra-compact arrays with wall-to-wall distances reaching less than 6% the size of the incident wavelength. Furthermore, the transmitted phase is also virtually unaffected. In view of this result, we anticipate the possibility to realize ultrasmall pixels beyond what has been achieved so far with other platforms, e.g. for holography applications.
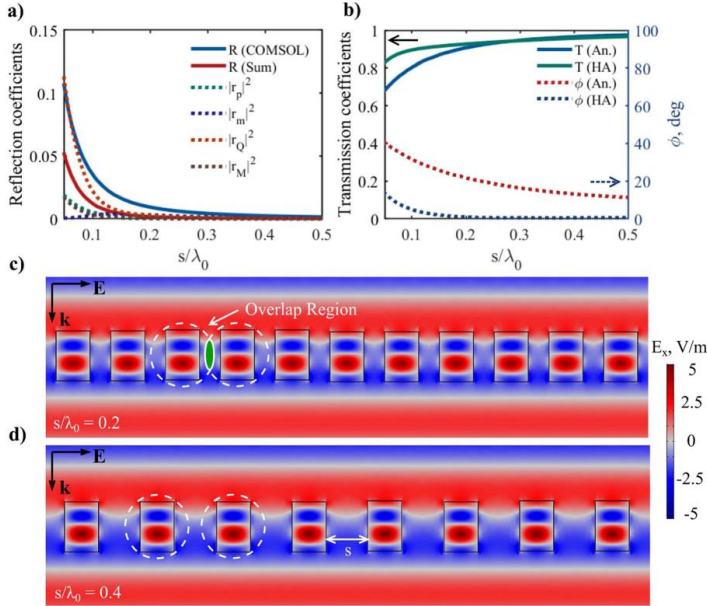
Figure 2: Optical response of the HA metasurface with particle separation s (the geometrical parameters are the same as in Figure 1). Evolution of reflection (a), and transmission (b) at λ_0. (c) and (d) x-component of the total electric field for $s/\lambda_0 = 0.2$–0.4. The dashed circles depict a section of the smallest spherical surface enclosing the scatterer. For $s/\lambda_0 = 0.2$ they overlap, demonstrating that our metasurface retains the same phase and transmission even in the extreme case when the 'equivalent' spheres would intersect. In both scenarios, the fields within the meta-atoms remain virtually identical, and the incident field is completely transmitted.

Such compact arrays cannot be analytically described with multiple scattering theory, i.e. Eq. (4) is no longer valid, since the multipole moments are not orthogonal and do not form a complete basis once neighboring particles cannot be enclosed by non-intersecting spherical surfaces [49]. However, as we proved analytically in the Supplementary Material S1, the multipole decomposition of reflection and transmission can still be performed with the effective multipole moments retrieved from numerical simulations. In Figure 2(b), we have plotted the former, given by

$$r = \frac{C}{(2a + s)^2} \left(\tilde{p}_x - \frac{1}{c}\tilde{m}_y + \frac{ik}{6}\tilde{Q}_{xz} - \frac{ik}{2c}\tilde{M}_{yz} \right). \quad (7)$$

Eq. (7) has an explicit inverse quadratic dependence with the wall-to-wall separations s, which ultimately determines the increase in reflection for small distances between the

meta-atoms. This behavior can be clearly appreciated in the absolute values of the multipolar contributions shown in Figure 2(b). We emphasize that the quadratic dependence is common to all subwavelength square arrays, not only the ones studied here, and is due to an averaging of the electric field over S_l (see Eq. (S2) in the Supplementary Material S1). A unique trait of HA metasurfaces lies in their ability to minimize this effect due to the small values of the multipolar contributions to the far-field that enter the numerator of Eq. (7), while simultaneously featuring strongly confined near fields. Most importantly, the effective multipoles are almost identical to the isolated particle (refer to Figure S4 in the Supplementary Material S7), implying that even for very small separations they are not affected by the scattered fields of the neighbors. Thus, the slight increase in reflection is not due to coupling, which remains *negligible*.

53

We illustrate this aspect further by calculating the near fields for two metasurfaces with different periods, the most compact one corresponds to an extreme case when the smallest spherical surfaces enclosing two neighboring meta-atoms intersect each other [Figure 2(c)]. For a conventional nanoantenna, the latter would usually lead to strong near-field coupling [50]. In stark contrast with this initial intuition, an inspection of the fields within the high-index regions of the two metasurfaces [Figure 2(c) and (d)], reveals an identical picture.

Motivated by these initial findings, we now aim at designing a 'map' relating a specific transmitted phase with some geometrical parameter of the meta-atom. Keeping in mind a future practical realization, we choose radius a as our degree of freedom, since radial deformations can be implemented with well-established fabrication techniques, e.g. electron beam lithography followed with reactive ion etching [14]. To this end, we calculate the transmission and

phase for the HA metasurface with small separations $s = 150$ nm for different radii and wavelengths [Figure 3(a) and (b)]. In contrast to a sphere, the behavior with a is not identical to the one with λ. This owes to the fact that the HA appears due to the overlap of Mie and Fabry–Perot modes having different dependence with a [33]. Nevertheless, we can set a wavelength of operation and observe a well-defined phase variation for a collection of radii within the HA-mediated transparency window [Figure 3(c)], which we refer to as a lookup table [14, 24]. We have calculated two lookup tables for different s, which yield almost the same results, thus once more showcasing the ability of HA nanoparticles to act as individual meta-atoms.

The lookup table allows us to select a meta-atom yielding a specific phase depending entirely on a. This behavior is shown in Figure 3(d), where we have plotted the x component of the total electric field for the points A, B, C indicated in Figure 3(c). Indeed, the transmitted wave
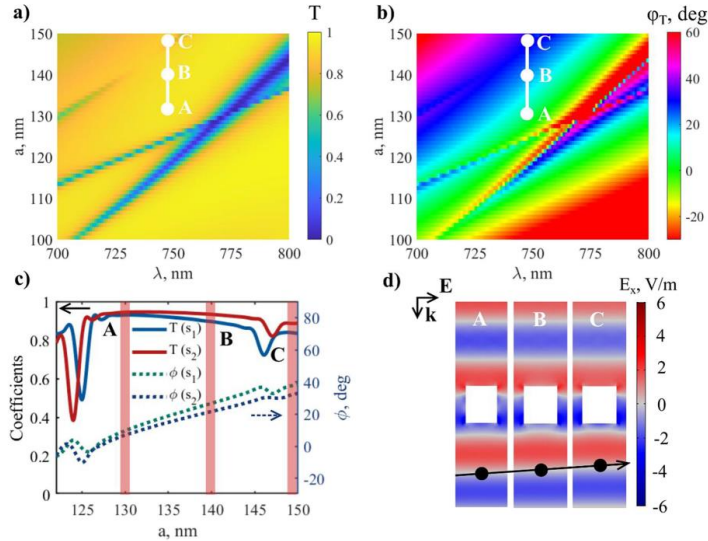

Figure 3: HA metasurfaces enabling phase control with the full transmission. (The height of the cylinders is kept constant at 370 nm) (a) Transmission as a function of wavelength and radius of the meta-atom, calculated at a fixed, (arbitrarily chosen) wall-to-wall distance between cylinders $s = 150$ nm. The chosen range corresponds to the maximum available interval of radii featuring suppressed reflection ($\lambda = 750$ nm). (b) The phase of the transmitted wave for the same parameters as in (a). (c) The lookup table of the proposed metalattice in the 0th diffractive order, calculated for two ultra-compact arrays with $s = 100, 150$ nm at $\lambda = 750$ nm. (d) From left to right: the x component of the electric field in three metasurfaces constituted, respectively, of meta-atoms with radius $a = 130, 140$, and 150 nm and transmitted phases $\phi_T = 10, 30$, and $40°$, selected from (b) (indicated with A, B, and C at $\lambda = 750$ nm).

modifies its delay with the incident field when transitioning from A to C in parameter space.

Summarizing the results, we have first designed a new kind of the transparent metasurface based on the low scattering properties of the HA and rigorously analyzed its working principle through a multipolar decomposition of reflection and transmission. The HA opens a transmission band with the possibility to alter the phase of the transmitted wave. In the case studied, the phase change occurs mainly due to an increase in the contribution of the electric quadrupole moment, whose amplitude is strongly minimized due to the electric quadrupole anapole. In accordance with our initial predictions, we have demonstrated numerically that our design truly suppresses mutual interaction between neighbors and elaborated a lookup table encoding a specific phase delay to HA nanocylinders of a given radius. In the next section, we will take a step further and unveil the true potential of our design for the fabrication of phase-controlling metasurfaces exhibiting disorder.

3.2 Disordered lattices

Despite the large bulk of literature dedicated to the study of periodic lattices, their fabrication requires the implementation of very precise nanolithography techniques. Thus, to a certain degree, all realistic metasurfaces exhibit disorder. The presence of disorder can drastically alter the optical response of a array, making the design of applications a challenging task [31]. In general, from Eq. (1), two types of randomness can be introduced [51]: (i) size disorder directly affecting the polarizability matrix $\mathcal{A}$, or (ii) positional disorder (PD), which modifies the components of the coupling matrix $\mathcal{S}$. Since we are only interested in the lattice effects, in what follows we consider solely (ii).

In conventional metasurface designs the influence of PD is essentially dependent on the mutual interaction between the meta-atoms. For instance, the collective lattice resonances of arrays of Si nanospheres were shown to be suppressed under the influence of certain types of lattice perturbations [51]. Importantly, due to their strong sensitivity to the spacing among neighboring nanoparticles [28], Huygens metasurfaces are strongly affected by disorder and exhibit spontaneous transitions at critical values of PD, featuring abrupt variations of the transmitted phase [30]. Here, once again, we encounter an important advantage offered by the HA meta-atom; indeed, disorder

effects must also be strongly suppressed due to the negligible polarizabilities entering $\mathcal{A}$.

To demonstrate the immunity to PD, we perform two sets of numerical experiments with the results displayed in Figure 4(a)–(e). In Figure 4(a) and (b), we introduce an in-plane PD in the metalattice, controlled by a normal distribution of the lattice period with mean l, and standard deviation δl. We numerically implemented the disorder when constructing a finite 4×4 lattice and then imposed periodic boundary conditions, as depicted in Figure 4(c), which also shows the displacement of each HA meta-atom with respect to the ideal array. Similarly, in Figure 4(d) and (e), the PD is induced out-of-plane, along the z-axis, as illustrated in Figure 4(f). Out-of-plane PD can be associated, e.g., with surface roughness.

Remarkably, in Figure 4(a)–(f), only small variations of the transmission spectrum and the transmitted phase can be observed in the wavelength range affected by the HA, demonstrating its striking resilience to very large deviations from the ideal periodic lattice. In stark contrast, a strong dependence on PD at the wavelengths 'unprotected' by the HA can be clearly distinguished, particularly prominent at the dip of the transmission spectra, [point P in Figure 4(a) and (d)], where a large change in the transmission amplitude takes place. These behaviors are also confirmed in the near field distributions at λ_0 and at the dip of the transmission spectrum. On the one hand, at point P, as a consequence of strong scattering, a drastic change in the fields can be appreciated when transitioning from the periodic to the disordered array, both outside and within the nanoparticles. In the rightmost panel of Figure 4(g) (disordered array illuminated at point P), strong evanescent fields appear when the particles are close to each other. On the other hand, the near fields of the disordered HA metasurfaces remain visually unaltered, even for particles that would usually exhibit large evanescent fields, such as the pair of nanorods highlighted on the second rightmost panel of Figure 4(g). In addition, it is worth mentioning that the proposed metasurface benefits from the strong field concentration characteristic of anapole-like regimes. Therefore, disordered HA metasurfaces constitute a flexible platform to enhance light–matter interactions at the nanoscale in a simple and straightforward fashion, without the need for neither complex optimization techniques nor requiring a careful arrangement of the meta-atoms.

From the results in this section, we can conclude that both phase and transmission of HA meta-atoms are 'protected' against disorder. Thus, HA-based metasurfaces might not require periodicity in order to implement a
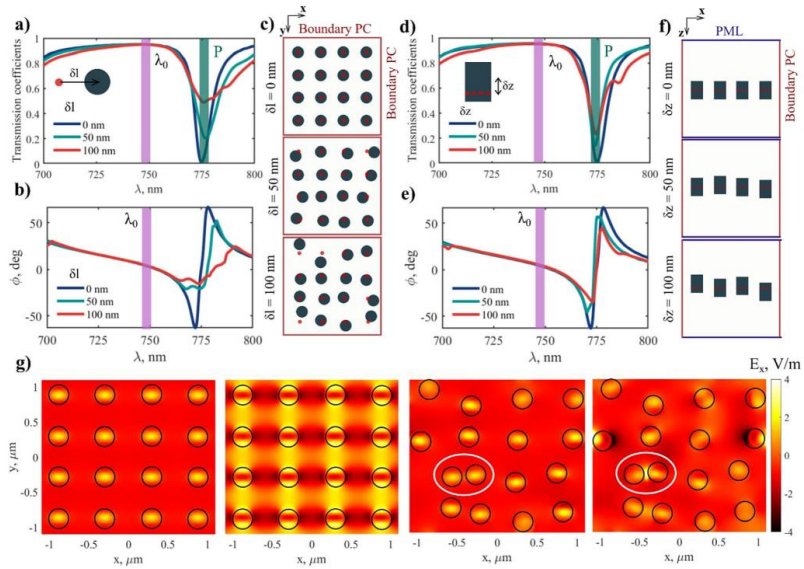
Figure 4: Numerical experiments demonstrating the resilience of HA metasurfaces to PD, paving the way toward disorder-immune meta-devices (geometrical parameters as in Figure 1). (a and b) Transmission and transmitted phase with different degrees of in-plane PD with standard deviation δl, schematically depicted in (c), where the red dots indicate the ideal periodic array. (d and e) Transmission of the array with different degrees of out-of-plane PD, with standard deviation δz, schematically depicted in (f). In the two cases studied, both transmission and phase in the HA regime are well preserved and remain almost invariant at λ_0. (g) Calculated distributions of the x-component of the electric field at λ_0 and point P indicated in (a) and (d). All fields are normalized to the same colorbar. From left to right, the first two field maps correspond to the periodic array at λ_0 and point P, respectively. The other two correspond to the same points for a PD given by $\delta l = 100$ nm. The white circles highlight two closely packed nanorods exhibiting a markedly different behavior; despite their proximity, at λ_0 no interparticle hotspot can be appreciated, while the dimer system at point P can be clearly seen to display strong near field interactions.

varying spatial phase profile, offering exciting perspectives for the realization of applications.

3.3 Influence of a dielectric substrate

A practical implementation of metasurfaces would unavoidably require the presence of a substrate. The latter can play a non-negligible role in the optical response and introduces magnetoelectric coupling [52]. In stark contrast with conventional resonances, the HA is remarkably robust when deposited over a substrate [33]. In the studied nanocylinder, the HA (differently from conventional anapoles or Huygens sources) is effectively attained through the overlap of resonant 'Mie-like' and 'Fabry–Perot-like' modes. Their field

distributions are displayed in Figure S5(b) of the Supplementary Material. The first can be associated with standing waves originating between the lateral walls of the resonator cavity, while the second is mainly formed from standing waves between the top and bottom walls (refer to the Supplementary Material S8 for further details). Therefore, variations in the substrate reflectivity affect mainly the amplitude of Fabry–Perot modes, but the Mie modes remain almost unaltered [33]. With a variation of n_{sub}, the HA gradually transforms to a conventional electric dipole anapole, still retaining a strong scattering reduction.

HA metasurfaces are expected to present similar features (Figure 5). In Figure 5(a) we have calculated transmission, reflection, and absorption at the HA regime for our metasurface deposited over a series of hypothetical
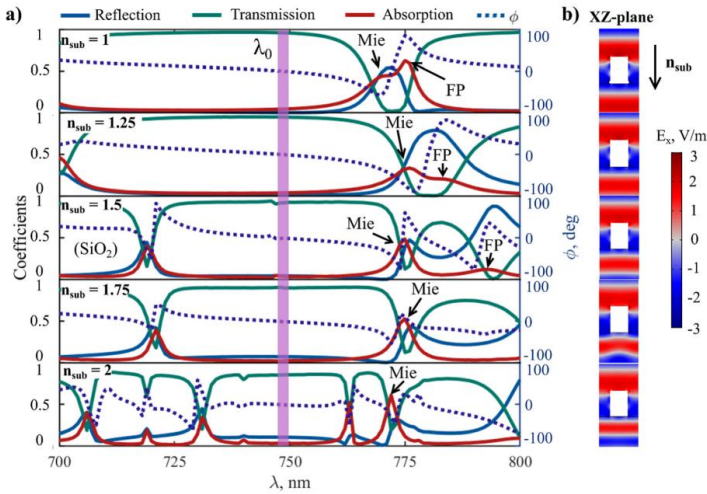
Figure 5: (a) Optical response of an HA metasurface with inter-particle separation $s = 300$ nm, and geometrical parameters as in Figure 1, deposited on hypothetical substrates with increasing refractive index. The arrows indicate the evolution of the Mie-like and Fabry–Perot (FP) modes responsible for the HA. (b) x-component of the electric field at λ_0 for the cases considered in (a).

substrates with index ranging from $n_{sub} = 1, \ldots, 2$. We observe a progressive narrowing of the transmission band mainly resulting from a redshift of high order Bloch modes. Importantly, full transmission is preserved in the vicinity of λ_0, with a decrease of only 10% for $n_{sub} = 2$. In Figure 5(b) we have calculated the E_x component of the total field, which clearly shows how the wave at λ_0 is almost fully transmitted by the metasurface even for $n_{sub} = 2$.

Unlike in the single-particle case, the Mie and Fabry–Perot modes are coupled. The drop in transmission and the change in the transmitted phase are linked to the evolution of the Fabry–Perot mode; as indicated in Figure 5(a), the substrate index influences strongly the width and spectral position of the Fabry–Perot resonance, that rapidly redshifts while the Mie-mode remains almost unaltered. As a result, the HA starts degenerating into a conventional anapole. However, the transmission band induced by the HA is very resilient to changes in the underlying substrate. Importantly, the results unambiguously show that the metasurface can be directly deposited over conventional silica (SiO$_2$) without further design steps and display full transmission as well as enabling phase control. In this case, in exchange for a small reduction of the transmission band.

Based on the prior analysis, we elaborate a lookup table for the HA metasurface deposited on a glass substrate, schematically shown in Figure 6(a). Figure 6(b) shows the results of the lookup table. The phase can now be modulated in a range of 80°, almost doubling the original design in a vacuum. The price paid is a reduction in the range of available radii, which can be tuned from 120–140 nm preserving unity transmission and negligible inter-particle coupling. The available range for phase tunability is doubled with respect to free space, suggesting there is still a large room for improvement of the effect.

4 Phase modulation of fs pulses with a disordered HA array

Next, we discuss the possibility to modulate the phase of an ultrafast Gaussian pulse in transmission mode, making use of a disordered HA array on top of a silica substrate. To illustrate the robustness of our system, we choose a strong in-plane disorder ($\delta l = 50$ nm), corresponding to 20% of the separation between nanorods ($s = 300$ nm). We then perform finite-difference time-domain simulations of an
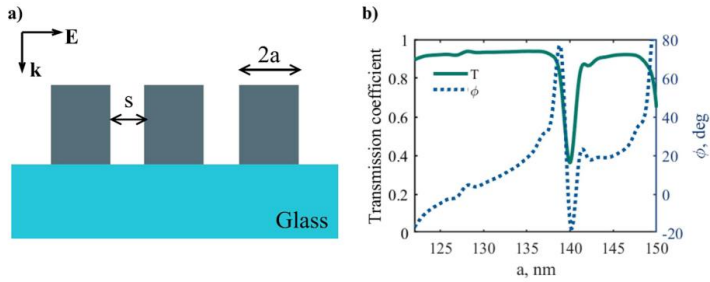
57

Figure 6: (a) Illumination scheme and geometry of the HA metasurface deposited on a semi-infinite glass substrate. (b) A lookup table of the hybrid anapole meta-atom when placed on top of a glass substrate (n_{sub} = 1.5), for s = 300 nm. The plot displays transmission (left y-axis), and transmitted phase (right y-axis) as a function of the nanorod radius a.
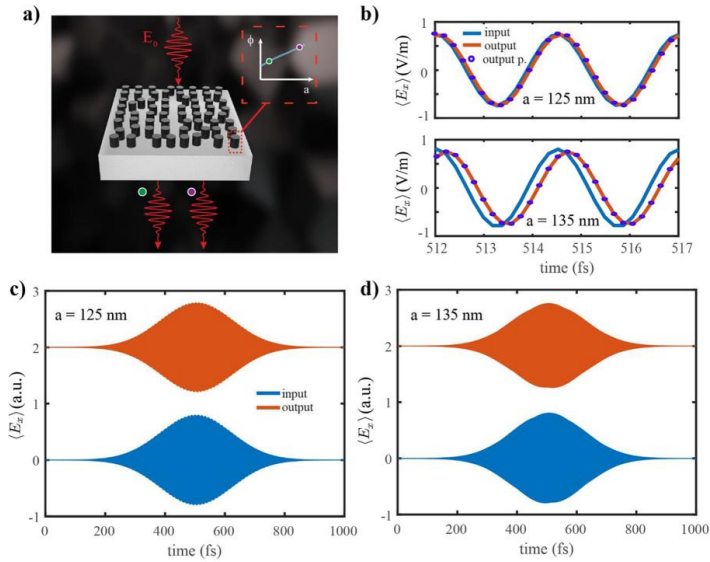

Figure 7: Manipulating the phase of an x-polarized fs Gaussian pulse with a disordered HA metasurface on a semi-infinite glass substrate. (a) Artistic representation of the concept, depicting the impinging and outgoing pulses from the disordered HA metasurface with tailored nanoparticle sizes, and a schematic of the lookup table. (b) Transparency and advanced phase of the output pulse at their maxima, for a = 125, 135 nm (top and bottom panels, respectively) in the disordered lattice, in perfect agreement with the periodic arrangement (output p.). The height of the nanorods is kept constant at 370 nm. (c and d) Temporal profiles of the incoming (input) and outgoing pulses (output), demonstrating full transmission for the two cases studied. In panels (b)–(d) the operator '⟨⟩' denotes averaging over the transverse cross-section of a single unit cell.

incoming x-polarized Gaussian pulse with 400 fs duration. The concept is depicted in Figure 7(a); the radius of the nanorods is chosen in accordance with the lookup table in Figure 6(b). With a progressive increase in a, the phase of the output pulse can be controllably tuned, as shown in Figure 7(b), where we have plotted the maxima of the output and input pulses. We have chosen a to vary between 125 and 135 nm, to be well in the range covered by the HA [Figure 6(b)]. For comparison, in Figure 7(b) we have also added the results for the periodic array.

As could be expected from our calculations in Figure 4, the phase imprinted by the periodic and the disordered metasurfaces is virtually identical, once more demonstrating that HA nanoparticles indeed operate in an almost independent fashion from their neighbors. Consequently, transmission is kept higher than 85%, as confirmed by the full temporal profiles displayed in Figure 7(c) and (d) (dissipative losses were not neglected in the simulations). Alternatively, although generally less practical, the device could also be controlled in wavelength and designed according to the results in Figure 5(a).

To summarize, we have numerically implemented an ultrafast phase modulator based on a disordered HA array, relying solely on the knowledge of the periodic lattice. The results suggest the possibility to flexibly design meta-devices without the need for time-consuming optimization steps, reaching a very high resolution. It is worth noticing that even better performances could be obtained in the mid-IR range, since our setup is easily scalable, and could be introduced in a plethora of active and passive light spatial modulation schemes.

5 Conclusions

We have proposed and investigated in detail *novel transparent HA metasurfaces* based on the unusual properties of the recently observed HA regime. Unlike recent designs exploiting, e.g., the transverse Kerker effect [32], our metasurfaces achieve not only near-unity efficiency in transmission but also allow varying the phase of the transmitted wave. Most importantly, they display negligible interparticle coupling, overcoming a critical bottleneck of conventional Huygens sources. We have demonstrated how the latter leads to a number of technological advantages, including the possibility to fabricate ultra-compact arrays retaining the single-particle response, the preservation of the transmission window when deposited on a wide range of dielectric substrates, and a robust protection against large PD, significantly relaxing the technical

requirements of the manufacturing process. As a proof-of-concept, we have numerically demonstrated an ultrafast phase modulator operating in transmission with a disordered and a periodic HA array, showing perfect agreement between the two structures. We emphasize that the HA regime is not limited by strict design constraints and can be easily implemented in (but not only) an amorphous silicon nanorod in the visible range under normally incident plane wave illumination. From the above, we can conclude that HA nanoparticles, in contrast with Huygens disks, truly approach the ideal of a 'meta-atom', i.e. a subwavelength unit cell with a unique phase imprint. The focus of this article is on resonance-based approaches to modulate phase. However, metasurfaces based on the geometric phase are also constrained by inter-element coupling. In this regard, the HA regime could help to minimize inter-element interaction (refer to section S9 of the Supplementary Material), or both mechanisms could be combined to cover a broader phase range. In the future, we believe that clever designs of HA-based metasurfaces could compete with their more established counterparts, paving the way toward new devices in meta-optics.

References

[1] Y. Kivshar, "All-dielectric meta-optics and non-linear nanophotonics," *Natl. Sci. Rev.*, vol. 5, no. 2, pp. 144–158, 2018.

[2] D. G. Baranov, D. A. Zuev, S. I. Lepeshov, et al., "All-dielectric nanophotonics: the quest for better materials and fabrication techniques," *Optica*, vol. 4, no. 7, p. 814, 2017.

[3] K. Koshelev, G. Favraud, A. Bogdanov, Y. Kivshar, and A. Fratalocchi, "Nonradiating photonics with resonant dielectric nanostructures," *Nanophotonics*, vol. 8, no. 5, pp. 725–745, 2019.

[4] P. D. Terekhov, A. B. Evlyukhin, D. Redka, V. S. Volkov, A. S. Shalin, and A. Karabchevsky, "Magnetic octupole response of dielectric quadrumers," *Laser Photon. Rev.*, vol. 1900331, p. 1900331, 2020.

[5] J. Wang and J. Du, "Plasmonic and dielectric metasurfaces: design, fabrication and applications," *Appl. Sci.*, vol. 6, no. 9, 2016. https://doi.org/10.3390/app6090239.

[6] Y. Kivshar and A. Miroshnichenko, "Meta-optics with Mie resonances," *Opt Photon. News*, vol. 28, no. 1, p. 24, 2017.

[7] T. Liu, R. Xu, P. Yu, Z. Wang, and J. Takahara, "Multipole and multimode engineering in Mie resonance-based metastructures," *Nanophotonics*, vol. 9, no. 5, pp. 1115–1137, 2020.

[8] R. E. Noskov, A. Machnev, I. I. Shishkin, et al., "Golden vaterite as a mesoscopic metamaterial for biophotonic applications," *Adv. Mater.*, vol. 33, no. 25, pp. 1–12, 2021.

[9] P. D. Terekhov, K. V. Baryshnikova, Y. Greenberg, et al., "Enhanced absorption in all-dielectric metasurfaces due to magnetic dipole excitation," *Sci. Rep.*, vol. 9, no. 1, pp. 1–9, 2019.

[10] K. Koshelev and Y. Kivshar, "Dielectric resonant metaphotonics," *ACS Photonics*, vol. 8, no. 1, pp. 102–112, 2021.

[11] A. Canós Valero, D. Kislov, E. A. Gurvitz, et al., "Nanovortex-Driven all-dielectric optical diffusion boosting and sorting concept for lab-on-a-chip platforms," *Adv. Sci.*, vol. 7, no. 11, p. 1903049, 2020.

[12] W. Liu and Y. S. Kivshar, "Generalized Kerker effects in nanophotonics and meta-optics [Invited]," *Opt. Express*, vol. 26, no. 10, p. 13085, 2018.

[13] K. M. Barhom, A. A. Machnev, R. E. Noskov, et al., "Biological Kerker effect boosts light collection efficiency in plants," *Nano Lett.*, vol. 19, no. 10, pp. 7062–7071, 2019.

[14] M. Decker, I. Staude, M. Falkner, et al., "High-Efficiency dielectric Huygens' surfaces," *Adv. Opt. Mater.*, vol. 3, no. 6, pp. 813–820, 2015.

[15] G. Yoon, K. Kim, D. Huh, H. Lee, and J. Rho, "Single-step manufacturing of hierarchical dielectric metalens in the visible," *Nat. Commun.*, vol. 11, no. 1, pp. 1–10, 2020.

[16] M. Khorasaninejad and F. Capasso, "Metalenses: versatile multifunctional photonic components," *Science*, vol. 358, no. 6367, 2017. https://doi.org/10.1126/science.aam8100.

[17] A. Howes, W. Wang, I. Kravchenko, and J. Valentine, "Dynamic transmission control based on all-dielectric Huygens metasurfaces," *Optica*, vol. 5, no. 7, p. 787, 2018.

[18] A. J. Ollanik, J. A. Smith, M. J. Belue, and M. D. Escarra, "High-efficiency all-dielectric Huygens metasurfaces from the ultraviolet to the infrared," *ACS Photonics*, vol. 5, no. 4, pp. 1351–1358, 2018.

[19] W. Liu and A. E. Miroshnichenko, "Beam steering with dielectric metalattices," *ACS Photonics*, vol. 5, no. 5, pp. 1733–1741, 2018.

[20] A. C. Overvig, S. Shrestha, S. C. Malek, et al., "Dielectric metasurfaces for complete and independent control of the optical amplitude and phase," *Light Sci. Appl.*, vol. 8, no. 1, 2019. https://doi.org/10.1038/s41377-019-0201-7.

[21] B. Liu, B. Sain, B. Reineke, et al., "Nonlinear wavefront control by geometric-phase dielectric metasurfaces: influence of mode field and rotational symmetry," *Adv. Opt. Mater.*, vol. 8, no. 9, 2020. https://doi.org/10.1002/adom.201902050.

[22] B. Wang, F. Dong, Q.-T. Li, et al., "Visible-frequency dielectric metasurfaces for multiwavelength Achromatic and highly dispersive holograms," *Nano Lett.*, vol. 16, no. 8, pp. 5235–5240, 2016.

[23] D. Vovchuk, S. Kosulnikov, R. E. Noskov, and P. Ginzburg, "Wire resonator as a broadband Huygens superscatterer," *Phys. Rev. B*, vol. 102, no. 9, p. 94304, 2020.

[24] C. Gigli, Q. Li, P. Chavel, G. Leo, M. L. Brongersma, and P. Lalanne, "Fundamental limitations of Huygens' metasurfaces for optical beam shaping," *Laser Photon. Rev.*, vol. 15, no. 8, p. 2000448, 2021.

[25] S. M. Kamali, E. Arbabi, A. Arbabi, and A. Faraon, "A review of dielectric optical metasurfaces for wavefront control," *Nanophotonics*, vol. 7, no. 6, pp. 1041–1068, 2018.

[26] H. T. Hui, "Decoupling methods for the mutual coupling effect in antenna arrays: a review," *Recent Pat. Eng.*, vol. 1, no. 2, pp. 187–193, 2008.

[27] X. Chen, H. Pei, M. Li, et al., "Revisit to mutual coupling effects on multi-antenna systems," *J. Commun. Inf. Networks*, vol. 5, no. 4, pp. 43–54, 2020.

[28] K. E. Chong, I. Staude, A. James, et al., "Polarization-independent silicon metadevices for efficient optical wavefront control," *Nano Lett.*, vol. 15, no. 8, pp. 5369–5374, 2015.

[29] J. W. Wu, Z. X. Wang, Z. Q. Fang, et al., "Full-State synthesis of electromagnetic fields using high efficiency phase-only metasurfaces," *Adv. Funct. Mater.*, vol. 30, no. 39, p. 2004144, 2020.

[30] A. Rahimzadegan, D. Arslan, R. N. S. Suryadharma, et al., "Disorder-induced phase transitions in the transmission of dielectric metasurfaces," *Phys. Rev. Lett.*, vol. 122, no. 1, 2019, Art no. 015702.

[31] K. M. Czajkowski and T. J. Antosiewicz, "Electromagnetic coupling in optical devices based on random arrays of dielectric nanoresonators," *J. Phys. Chem. C*, vol. 124, no. 1, pp. 896–905, 2020.

[32] H. K. Shamkhi, A. Sayanskiy, A. C. Valero, et al., "Transparency and perfect absorption of all-dielectric resonant metasurfaces governed by the transverse Kerker effect," *Phys. Rev. Mater.*, vol. 3, no. 8, pp. 1–10, 2019.

[33] A. Canós Valero, E. A. Gurvitz, F. A. Benimetskiy, et al., "Theory, observation, and ultrafast response of the hybrid anapole regime in light scattering," *Laser Photon. Rev.*, vol. 2100114, pp. 1–14, 2100.

[34] A. E. Miroshnichenko, A. B. Evlyukhin, Y. F. Yu, et al., "Nonradiating anapole modes in dielectric nanoparticles," *Nat. Commun.*, vol. 6, pp. 1–8, 2015.

[35] G. Grinblat, Y. Li, M. P. Nielsen, R. F. Oulton, and S. A. Maier, "Enhanced third harmonic generation in single germanium nanodisks excited at the anapole mode," *Nano Lett.*, vol. 16, no. 7, pp. 4635–4640, 2016.

[36] L. Xu, M. Rahmani, K. Zangeneh Kamali, et al., "Boosting third-harmonic generation by a mirror-enhanced anapole resonator," *Light Sci. Appl.*, vol. 7, no. 1, p. 44, 2018.

[37] T. Zhang, Y. Che, K. Chen, et al., "Anapole mediated giant photothermal nonlinearity in nanostructured silicon," *Nat. Commun.*, vol. 11, no. 1, p. 3027, 2020.

[38] J. S. Totero Gongora, A. E. Miroshnichenko, Y. S. Kivshar, and A. Fratalocchi, "Anapole nanolasers for mode-locking and ultrafast pulse generation," *Nat. Commun.*, vol. 8, no. May, pp. 1–9, 2017.

[39] B. Luk'yanchuk, R. Paniagua-Domínguez, A. I. Kuznetsov, A. E. Miroshnichenko, and Y. S. Kivshar, "Hybrid anapole modes of high-index dielectric nanoparticles," *Phys. Rev. A*, vol. 95, no. 6, pp. 1–8, 2017.

[40] P. D. Terekhov, V. E. Babicheva, K. V. Baryshnikova, A. S. Shalin, A. Karabchevsky, and A. B. Evlyukhin, "Multipole analysis of dielectric metasurfaces composed of nonspherical

60

nanoparticles and lattice invisibility effect," *Phys. Rev. B*, vol. 99, no. 4, 2019. https://doi.org/10.1103/PhysRevB.99.045424.

[41] A. S. Shalin and S. G. Moiseev, "Optical properties of nanostructured layers on the surface of an underlying medium," *Opt. Spectrosc.*, vol. 106, no. 6, pp. 916–925, 2009.

[42] A. S. Shalin, "Broadband blooming of a medium modified by an incorporated layer of nanocavities," *JETP Lett. (Engl. Transl.)*, vol. 91, no. 12, pp. 636–642, 2010.

[43] V. Kozlov, D. Filonov, A. S. Shalin, B. Z. Steinberg, and P. Ginzburg, "Asymmetric backscattering from the hybrid magneto-electric meta particle," *Appl. Phys. Lett.*, vol. 109, no. 20, 2016. https://doi.org/10.1063/1.4967238.

[44] V. E. Babicheva and A. B. Evlyukhin, "Analytical model of resonant electromagnetic dipole-quadrupole coupling in nanoparticle arrays," *Phys. Rev. B*, vol. 99, no. 19, p. 195444, 2019.

[45] A. E. Miroshnichenko, A. B. Evlyukhin, Y. S. Kivshar, and B. N. Chichkov, "Substrate-induced resonant magnetoelectric effects for dielectric nanoparticles," *ACS Photonics*, vol. 2, no. 10, pp. 1423–1428, 2015.

[46] I. Fernandez-Corbaton, S. Nanz, R. Alaee, and C. Rockstuhl, "Exact dipolar moments of a localized electric current distribution," *Opt. Express*, vol. 23, no. 26, p. 33044, 2015.

[47] R. Alaee, C. Rockstuhl, and I. Fernandez-Corbaton, "An electromagnetic multipole expansion beyond the long-wavelength approximation," *Opt. Commun.*, vol. 407, pp. 17–21, 2018.

[48] P. D. Terekhov, H. K. Shamkhi, E. A. Gurvitz, et al., "Broadband forward scattering from dielectric cubic nanoantenna in lossless media," *Opt. Express*, vol. 27, no. 8, p. 10924, 2019.

[49] J. D. Jackson, *Classical Electrodynamics*, USA, John Wiley & Sons, Inc., 1962.

[50] A. A. Dmitriev and M. V. Rybin, "Combining isolated scatterers into a dimer by strong optical coupling," *Phys. Rev. A*, vol. 99, no. 6, 2019, Art no. 063837.

[51] V. I. Zakomirnyi, S. V. Karpov, H. Ågren, and I. L. Rasskazov, "Collective lattice resonances in disordered and quasi-random all-dielectric metasurfaces," *J. Opt. Soc. Am. B*, vol. 36, no. 7, p. E21, 2019.

[52] A. E. Miroshnichenko, A. B. Evlyukhin, Y. S. Kivshar, and B. N. Chichkov, "Substrate-induced resonant magnetoelectric effects for dielectric nanoparticles," *ACS Photonics*, vol. 2, no. 10, pp. 1423–1428, 2015.

Supplementary Material for "Transparent Hybrid Anapole Metasurfaces with negligible Electromagnetic Coupling for Phase Engineering"

Alexey V. Kuznetsov[1], Adrià Canós Valero[1], Mikhail Tarkhov[4], Vjaceslavs Bobrovs[2], Dmitrii Redka[2,3], and Alexander S. Shalin[1,2,5]

[1]ITMO University, Kronverksky prospect 49, 197101, St. Petersburg, Russia

[2]Riga Technical University, Institute of Telecommunications, Latvia, Riga, Azenes street 12, post code 1048

[3]Electrotechnical University "LETI" (ETU), 5 Prof. Popova Street, Saint Petersburg 197376, Russia

[4]Institute of Nanotechnology of Microelectronics of the Russian Academy of Sciences (INME RAS), Moscow, Nagatinskaya street, house 16A, building 11

[5]Kotel'nikov Institute of Radio Engineering and Electronics of Russian Academy of Sciences (Ulyanovsk branch), Goncharova Str.48, Ulyanovsk, Russia, 432000

S1. Multipolar decomposition of reflection and transmission from a subwavelength periodic array

In Ref. [1] the exact multipolar decomposition of reflection and transmission was derived making use of multiple scattering theory. While providing with analyticity, the approach is only rigorously valid if the smallest spheres enclosing the scatterer do not intersect with each other. We now put forward a simple derivation based on more general principles that demonstrates the correctness of Eq.(6) in the main text even when multiple scattering theory cannot be applied to the system in question.

Consider an infinite periodic array located in the x-y plane, and a point located in the z-axis placed in the far field. The electric field at this point $\mathbf{r} = \begin{pmatrix} 0 & 0 & z \end{pmatrix}^T$ would correspond to the superposition of the scattered fields from all the particles in the array and the incident field $\mathbf{E}_0(\mathbf{r})$:

$$\mathbf{E}(\mathbf{r}) = \mathbf{E}_0(\mathbf{r}) + \sum \mathbf{E}_l(\mathbf{r}). \tag{S1}$$

Clearly the scattered field $\mathbf{E}_{sca}(\mathbf{r}) = \sum \mathbf{E}_l(\mathbf{r})$. Now, if the unit cell is subwavelength, we can replace the sum by an integral over the transverse area of the unit cell[2]:

$$\mathbf{E}_{sca}(\mathbf{r}) \approx \frac{1}{S_l} \int \mathbf{E}_l(\mathbf{r}) dA. \tag{S2}$$

In the far field, the multipole decomposition of $\mathbf{E}_l(\mathbf{r})$ is given by (up to the quadrupole terms):

$$\mathbf{E}_l(\mathbf{r}) \sim \frac{k_0^2}{4\pi\varepsilon_0} \frac{e^{ikr}}{r} \left([\mathbf{n} \times (\tilde{\mathbf{p}} \times \mathbf{n})] + \frac{1}{v_d}[\tilde{\mathbf{m}} \times \mathbf{n}] + \frac{ik_d}{6}[\mathbf{n} \times (\mathbf{n} \times \tilde{Q}\mathbf{n})] + \frac{ik_d}{2v_d}[\mathbf{n} \times (\tilde{M}\mathbf{n})] \right), \tag{S3}$$

where $\mathbf{n} = \mathbf{r}/r$. In our case $\mathbf{n}_\pm = \begin{pmatrix} 0 & 0 & \pm 1 \end{pmatrix}^T$. Substituting Eq.(S3) into Eq. (S2) leads to an expression for $\mathbf{E}_{sca}(\mathbf{r})$, which can then be directly used to evaluate the reflection and transmission coefficients as

$$r = \left[\mathbf{E}_{sca} / \mathbf{E}_0 \right]_{\mathbf{n}_-}, \tag{S4}$$

$$t = 1 + \left[\mathbf{E}_{sca} / \mathbf{E}_0 \right]_{\mathbf{n}_+}. \tag{S5}$$

For an x-polarized plane wave propagating in the $-z$ direction, the forward normal vector is $\mathbf{n}_+ = \left[0,0,-1 \right]$, and the backward vector is $\mathbf{n}_- = \left[0,0,1 \right]$. The angular distribution of the scattered field in any of the two directions is then:

$$
\begin{aligned}
E_{x,\pm}^{\text{sca}} \left(n_\pm \right) \sim \Bigg(& \tilde{p}_x n_\pm^2 + \frac{1}{v_d} \tilde{m}_y n_\pm - \frac{ik_d}{6} \tilde{Q}_{xz} n_\pm^3 \\
& - \frac{ik_d}{2v_d} \tilde{M}_{yz} n_\pm^2 - \frac{k_d^2}{6} \tilde{O}_{xzz} n_\pm^4 \Bigg)
\end{aligned}
\tag{S6}
$$

The reflection coefficient is [1]

$$r = \frac{ik_0}{2S_l \varepsilon_0 E_0 \left(z \right)} E_{x,-}^{sca}, \tag{S7}$$

while the transmission coefficient can be written as

$$t = 1 + \frac{ik_0}{2S_l \varepsilon_0 E_0 \left(z \right)} E_{x,+}^{sca}. \tag{S8}$$

Eqs. (S7)-(S8) are equivalent to Eqs. (6)-(7) in the main text. It is now clear that the only condition necessary for the expressions to be valid is that the *unit cell must be subwavelength*, in order to apply Eq.(S2).

S2. Multiple scattering theory

In this section we briefly summarize well-known results regarding multiple scattering theory. For simplicity in the treatment, we consider scatterers with only electric and magnetic dipolar response, and refer the interested reader to the detailed series of works [3,4] for expressions including the effective quadrupole terms.

In this simple scenario, we analyze an array of subwavelength nanoparticles which are also small with respect to their mutual separation. Then, the effective electric (magnetic) dipole moments are induced by the instantaneous electric (magnetic) fields 'seen' by each constituent, namely the incident field and the sum of all fields scattered by the other particles in the array:

$$\tilde{\mathbf{p}}_l = \alpha_p \left[\mathbf{E}_0 \left(\mathbf{r}_l \right) + \sum_{n \neq l} \mathcal{G}^0 \left(\mathbf{R}_{ln} \right) \tilde{\mathbf{p}}_n + \frac{ik_0}{c\varepsilon_0} \mathbf{g} \left(\mathbf{R}_{ln} \right) \times \tilde{\mathbf{m}}_n \right], \tag{S9}$$

$$\tilde{\mathbf{m}}_l = \alpha_m \mathbf{H}_0 \left(\mathbf{r}_l \right) + \alpha_m \sum_{n \neq l} \left[\varepsilon_0 \mathcal{G}^0 \left(\mathbf{R}_{ln} \right) \tilde{\mathbf{m}}_n - ik_0 c \mathbf{g} \left(\mathbf{R}_{ln} \right) \times \tilde{\mathbf{p}}_n \right]. \tag{S10}$$

In the previous α_p, α_m are the particle polarizabilities (inherent to a single scatterer), $\mathbf{R}_{ln} = \mathbf{r}_l - \mathbf{r}_n$, $\mathcal{G}^0 \left(\mathbf{R}_{ln} \right)$ is the free space electromagnetic propagator evaluated at $\mathbf{R}_{ln}$, and given by

$$\mathcal{G}^0 (\mathbf{r}) = \left(k^2 + \nabla \nabla \right) \frac{e^{ikr}}{r}. \tag{S11}$$

The vector $\mathbf{g} \left(\mathbf{R}_{ln} \right)$ is introduced for convenience:

$$\mathbf{g}(\mathbf{R}_{ln}) = \frac{e^{ik_0 R_{ln}}}{4\pi R_{ln}} \left(\frac{ik_0}{R_{ln}} - \frac{1}{R_{ln}^2} \right) \mathbf{R}_{ln} . \tag{S12}$$

Eqs. (S9)-(S10) form a linear system of equations for all the effective multipoles. Under normally incident x-polarized plane wave, assuming all the particles are distributed in the x-y plane, only x-polarized electric dipoles and y-polarized magnetic dipoles can be excited, and the electric and magnetic moments are not coupled (the third term in the rhs of Eqs. (S9)-(S10) vanishes). Then we can group all multipoles in a vector $\tilde{\mathbf{b}} = (\tilde{p}_1, \tilde{p}_2, ..., \tilde{p}_N, \tilde{m}_1, ..., \tilde{m}_N)^T$, and write a more compact formula:

$$[\mathcal{U} - \mathcal{A}\mathcal{S}]\tilde{\mathbf{b}} = \mathbf{b} , \tag{S13}$$

where the vector $\mathbf{b}$ contains the multipole moments induced solely by the incident field, $\mathcal{U}$ is the identity matrix, $\mathcal{A}$ is a diagonal matrix containing the single particle polarizabilities, and $\mathcal{S}$ is the coupling matrix, the elements of which in this example have the form

$$\mathcal{S}_{ln}^p = (1 - \delta_{ln})\mathcal{G}_{xx}^0(\mathbf{R}_{ln}), \tag{S14}$$

$$\mathcal{S}_{ln}^m = (1 - \delta_{ln})\varepsilon_0\mathcal{G}_{yy}^0(\mathbf{R}_{ln}) \tag{S15}$$

for the electric and magnetic parts of $\tilde{\mathbf{b}}$, respectively.

S3. Cartesian Multipole Expansion

The exact Cartesian expressions of the electromagnetic multipole moments up to the quadrupoles were recently derived in Ref. [5], and are given by the following integrals over the resonator volume:

$$\mathbf{p} = \int \mathbf{P} j_0(kr)d^3\mathbf{r} + \frac{k^2}{10}\int \left\{ [\mathbf{r} \cdot \mathbf{P}]\mathbf{r} - \frac{1}{3}r^2\mathbf{P} \right\} \frac{15 j_2(kr)}{(kr)^2}d^3\mathbf{r} , \tag{S16}$$

$$\mathbf{m} = -\frac{3i\omega}{2}\int (\mathbf{r} \times \mathbf{P})\frac{j_1(kr)}{kr}d^3\mathbf{r} , \tag{S17}$$

$$Q = \int \{3(\mathbf{r} \otimes \mathbf{P} + \mathbf{P} \otimes \mathbf{r}) - 2[\mathbf{r} \cdot \mathbf{P}]\mathcal{U}\} \times \frac{3 j_1(kr)}{kr}d^3\mathbf{r} + \\ 6k^2\int \{5\mathbf{r} \otimes \mathbf{r}[\mathbf{r} \cdot \mathbf{P}] - (\mathbf{r} \otimes \mathbf{P} + \mathbf{P} \otimes \mathbf{r})r^2 - r^2[\mathbf{r} \cdot \mathbf{P}]\mathcal{U}\} \frac{j_3(kr)}{(kr)^3}d^3\mathbf{r} , \tag{S18}$$

$$M = \frac{\omega}{3i}\int \{[\mathbf{r} \times \mathbf{P}] \otimes \mathbf{r} + \mathbf{r} \otimes [\mathbf{r} \times \mathbf{P}]\} \frac{15 j_2(kr)}{(kr)^2}d^3\mathbf{r} . \tag{S19}$$

Where $\mathbf{P}$ is the induced polarization current within the scatterer, and the $j_i(kr)$ are the ith spherical Bessel functions of the first kind. Taking the first order terms of the Taylor series of Eqs.(S16)-(S19), one recovers the quasistatic contributions having the classical expressions:

$$p_\alpha^0 = \int P_\alpha d^3\mathbf{r} , \tag{S20}$$

$$m_\alpha^0 = -\frac{i\omega}{2}\int (\mathbf{r} \times \mathbf{P})_\alpha d^3\mathbf{r} , \tag{S21}$$

$$Q_{\alpha\beta}^0 = 3\int \left[\left(r_\beta P_\alpha^\omega + r_\alpha P_\beta^\omega \right) \right] d^3\mathbf{r} , \tag{S22}$$

$$M_{\alpha\beta}^0 = -i\omega \int \left\{ r_\alpha (\mathbf{r} \times \mathbf{P})_\beta + r_\beta (\mathbf{r} \times \mathbf{P})_\alpha \right\} d^3\mathbf{r} \,. \tag{S23}$$

In Eqs. (S22)-(S23) we have omitted the diagonal terms of the tensors since they cannot be excited with conventional illumination schemes. The first toroidal terms are given by[6]

$$T_\alpha^p = -\frac{ik}{10} \int \left[-2r^2 P_\alpha + (\mathbf{r} \cdot \mathbf{P}) r_\alpha \right] d^3\mathbf{r} \,, \tag{S24}$$

$$T_\alpha^m = \frac{\omega k}{20} \int \left[(\mathbf{r} \times \mathbf{P}) r^2 \right] d^3\mathbf{r} \,, \tag{S25}$$

$$T_{\alpha\beta}^Q = -\frac{ik}{14} \int \left[4r_\alpha r_\beta (\mathbf{r} \cdot \mathbf{P}) - 5r^2 (r_\alpha P_\beta + r_\beta P_\alpha) \right] d^3\mathbf{r} \,, \tag{S26}$$

$$T_{\alpha\beta}^M = \frac{\omega k}{14} \int r^2 \left[r_\alpha (\mathbf{r} \times \mathbf{P})_\beta + r_\beta (\mathbf{r} \times \mathbf{P})_\alpha \right] d^3\mathbf{r} \,. \tag{S27}$$

The total contribution of the current multipoles to the scattered field outside the resonator can then be written as the sum of the quasistatic and the toroidal part multiplied by the prefactor 'ik'. For example, the scattered field of electric dipole type is proportional to $p_\alpha = p_\alpha^0 + ikT_\alpha^p$, where the absence of superscript indicates 'exact'. Similarly, the other 'exact' multipoles will be indicated in this fashion.
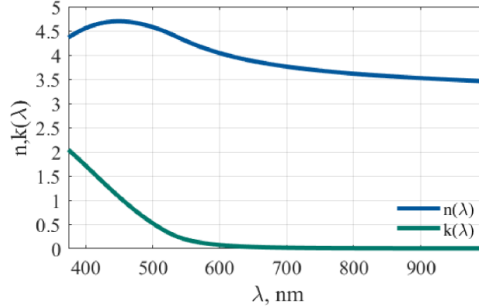
S4. Experimental Dispersion of amorphous Si

Figure S1. Real (n) and imaginary (k) parts of the experimentally measured refractive index of amorphous silicon (aSi) employed in our study, as a function of wavelength.

S5. Multipole decomposition of the scattering cross section for an isolated nanoparticle

In an homogeneous environment, the contributions to the cross section of the different 'exact' multipole moments are decoupled, and can be written as (up to the quadrupole)[7]:

$$\sigma_{sca} \simeq \frac{k_0^4}{6\pi\varepsilon_0^2|\mathbf{E}_{inc}|^2}|\mathbf{p}|^2 + \frac{k_0^4\mu_0}{6\pi\varepsilon_0|\mathbf{E}_0|^2}|\mathbf{m}|^2 +$$

$$\frac{k_0^6}{720\pi\varepsilon_0^2|\mathbf{E}_0|^2}\sum_{\alpha\beta}|Q_{\alpha\beta}|^2 + \frac{k_0^6\mu_0}{80\pi\varepsilon_0|\mathbf{E}_0|^2}\sum_{\alpha\beta}|M_{\alpha\beta}|^2 \quad . \tag{S28}$$

We plot each contribution, together with the full-wave solution in Figure S2, demonstrating perfect agreement, as well as the appearance of a dip in every dominant multipole, leading to a Hybrid Anapole state.
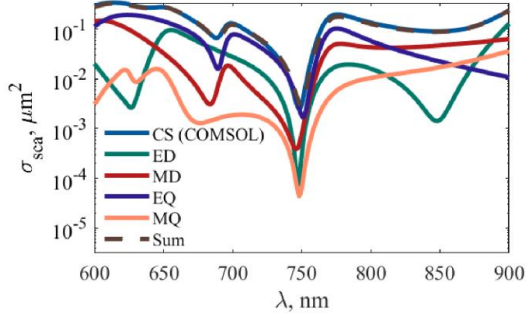
Figure S2. Calculated and reconstructed scattering cross section of an isolated aSi nanorod with height 370 nm and radius 125 nm. The abbreviations in the legend denote the electric dipole (ED), magnetic dipole (MD), electric quadrupole (EQ), and magnetic quadrupole (MQ) contributions. λ_0 is defined at the minima, corresponding to 750 nm.

S6. Alternative Cartesian Multipole decomposition separately taking into account toroidal moments

Eqs. (6) - (7) in the main text can be further decomposed into the quasistatic and toroidal contributions, simply by expanding the exact expressions for the multipoles entering each term in the reflection/transmission coefficient and utilizing Eqs. (S20)-(S27). The results of this procedure are shown in Figure S3(a)-(c) for the dominant multipole moments. The results unambiguously confirm that the resonant cancellation of reflection is produced when the partial fields of the quasistatic and toroidal contributions are equal in magnitude and interfere destructively.
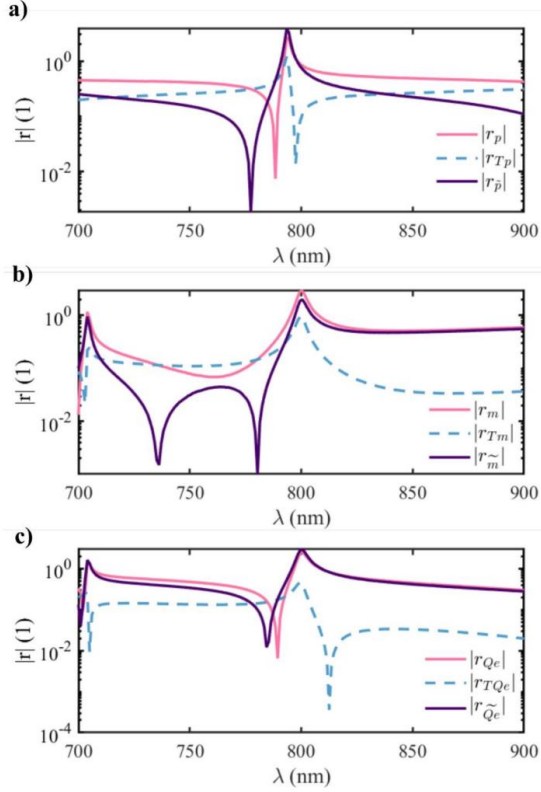
Figure S3. Quasistatic-toroidal multipole decomposition of the reflection coefficient for the three most relevant multipoles of an array of Hybrid Anapole nanorods like the ones studied in Ref. [8], with period 300 nm, under x-polarized plane wave illumination. (a) Contribution to reflection from the quasistatic electric dipole moment, the toroidal dipole moment, and the sum of both. (b)-(c) Same as (a), but for the magnetic dipole and the electric quadrupole moments.

S7. Evolution of the multipole moments with interparticle separation

In Figure S4 we have plotted the effective multipole moments of the array as a function of the normalized wall-to-wall separation at $\lambda_0 = 750$ nm . The multipoles are almost constant until very small spacings, less than 6% the incident wavelength, thus confirming that coupling effects are in general negligible.
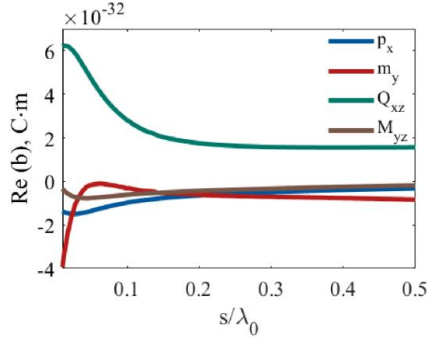
Figure S4. Real parts of the effective multipole moments in a unit cell as a function of normalized wall-to-wall separation s/λ_0, for a fixed wavelength of $\lambda_0 = 750$ nm. The notation follows the one used in the main text. It can be clearly seen that only very small distances result in a modification of their values, as explained in section 3 of the main manuscript.

S8. Modes supporting the HA effect

In this section we clarify the notions of 'Mie'-like and Fabry-Perot-like (FP) modes utilized in the main text. We refer as Mie-like to those modes that can be associated with standing waves between the lateral walls of the cavity, as depicted in Figure S8(a), leftmost panel. Most importantly, far from avoided crossings, Mie-like modes have a very small dependence with the cavity height. We call them 'Mie' in analogy with the modes supported by infinite cylinders. In contrast, the simplest FP-like mode is formed from standing waves between the top and bottom walls of the cavity, as depicted in the scheme in the rightmost panel of Figure S8(a).
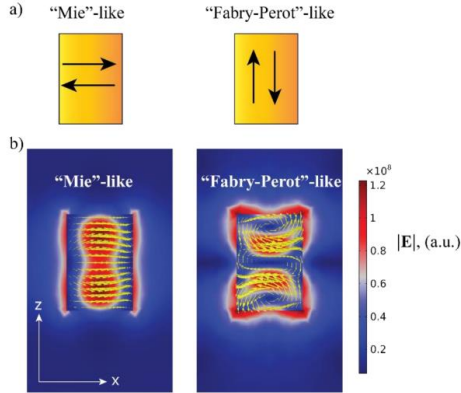

Figure S5. (a) Schematic illustration of 'Mie'-like and 'Fabry-Perot'-like (FP) modes. Black arrows indicate the propagation direction of hypothetical plane waves that interfere to generate a standing wave pattern. (b) Electric field norm in the x-z plane for the Mie (left panel) and FP (right panel) modes supporting the HA. The yellow arrows correspond to the electric field distribution. The modes have been

obtained for a metasurface with $s = 300 \, \mathrm{nm}$. Their eigenfrequencies are, from left to right, $\tilde{f}_{Mie} = 3.71e14 - i7.35e11 \,(Hz)$ and $\tilde{f}_{FP} = 3.72e14 - i1.05e12 \,(Hz)$.

In general, we refer to FP-like modes to those having a non-negligible dependence with the height of the cavity. Thus, the detuning between Mie-like and FP-like modes can be easily controlled just by playing with the cavity geometry.

Figure S8(b) shows the Mie and FP modes that, near degeneracy, give rise to the HA effect. They have been calculated for a HA metasurface in vacuum, with $s = 300 \, \mathrm{nm}$. While the Mie mode has no z-component of the electric field (it is transverse electric), the FP mode features three vortices of the electric field along the vertical axis, and two well-defined hotspots. The latter is a clear signature of standing waves formed from oscillations between the top and bottom walls of the cavity.

S9. A comparison with metasurfaces based on the Pancharatnam-Berry phase

The Pancharatnam-Berry (P-B) phase (or geometric phase) is an alternative mechanism to introduce phase jumps, which in principle does not require a resonant response [9]. In this section, we briefly analyze its working principle and point out how the latter approach suffers from similar limitations as Huygens metasurfaces. Finally, we provide a comparison with HA metasurfaces.

First of all, we note that, in order for the metasurface to induce a P-B phase, the meta-atoms must possess in-plane bianisotropy, so that incident light with opposite helicity σ will be scattered differently. This can be implemented, for instance, with elongated dielectric rods. Under normally incident plane wave illumination, the induced geometric phase emerges from the expression of the transmitted electric field [10]:

$$\mathbf{E}_T^\sigma = \mathcal{T} \cdot \mathbf{E}_I^\sigma = \frac{t_o + t_e}{2} \mathbf{E}_I^\sigma + \frac{t_o - t_e}{2} \exp(i2\sigma\alpha)\mathbf{E}_I^{-\sigma} \qquad (S29)$$

Where $\mathcal{T}$ is the Jones matrix describing the effect of the metasurface, $\mathbf{E}_I^\sigma$ is the incident circularly polarized plane wave and $\mathbf{E}_T^\sigma$ is the transmitted field. $t_{o,e}$ are the forward scattering coefficients for the ordinary and extraordinary axis of the meta-atom, respectively, and α is the rotation of the meta-atom with respect to the laboratory frame.

Eq.(S29) is the cornerstone of P-B metasurfaces; it demonstrates that a portion of the transmitted light experiences an helicity flip and acquires a phase 2α. Thus, by rotating the bianisotropic meta-atom, one should be able in principle to achieve a complete 2π phase modulation. There are, however, some limitations that can be directly inferred from Eq. (S29):

i)   In-plane bianisotropy ($t_o \neq t_e$) of the meta-atoms is an imperative requirement to recover the P-B phase, which might impose fabrication constraints.

ii)   Part of the transmitted light does not acquire a P-B phase and must usually be filtered out.

iii) Even if maximal transmission efficiency is achieved (with $t_o = -t_e$), opposite circular polarizations have opposite behavior, (due to the helicity σ entering the second term in the right-hand side of Eq.(S29)). In general, this means that a converging lens designed for right-circular polarization will be a diverging lens for left-circular polarization [11].

iv)   Strict fabrication control over the orientations of the resonators in the device is required.

Most importantly, Eq. (S29) has the same limitation as the Huygens metasurface: *it is derived for an array of periodic meta-atoms, all of them oriented in the same manner*. Moreover, the $t_{o,e}$ are in general

functions of the period. Therefore, the formula does not consider the influence of inter-element coupling in a realistic device. If the meta-atom is placed in a heterogeneous array, ideal performance would require an additional optimization step. Once again, control of the phase at the level of the individual meta-atom is not guaranteed.

The HA meta-atom does not have any of the aforementioned issues: (i) does not require bianisotropy, (ii) relies on the resonance mechanism, and transmits all light with a modulated phase, (iii) since the meta-atom has rotational symmetry, right and left circular polarizations are modulated by the same phase. Crucially, as we demonstrate in the main article, *inter-element coupling is virtually absent*, which can potentially lead to phase modulation at the level of the individual meta-atom. As we also demonstrate, (iv) *we do not require any careful arrangement of the meta-atoms, which can be disordered*. The fabrication constraints are thus significantly less stringent than those for P-B metasurfaces.

References

1. P. D. Terekhov et al., "Multipole analysis of dielectric metasurfaces composed of nonspherical nanoparticles and lattice invisibility effect," Phys. Rev. B **99**(4), 045424, American Physical Society (2019) [doi:10.1103/PhysRevB.99.045424].

2. V. Savinov, V. A. Fedotov, and N. I. Zheludev, "Toroidal dipolar excitation and macroscopic electromagnetic properties of metamaterials," Phys. Rev. B **89**(20), 205112 (2014) [doi:10.1103/PhysRevB.89.205112].

3. V. E. Babicheva and A. B. Evlyukhin, "Analytical model of resonant electromagnetic dipole-quadrupole coupling in nanoparticle arrays," Phys. Rev. B **99**(19), 195444, American Physical Society (2019) [doi:10.1103/PhysRevB.99.195444].

4. A. B. Evlyukhin, C. Reinhardt, and B. N. Chichkov, "Multipole light scattering by nonspherical nanoparticles in the discrete dipole approximation," Phys. Rev. B - Condens. Matter Mater. Phys. **84**(23), 1–8 (2011) [doi:10.1103/PhysRevB.84.235429].

5. R. Alaee, C. Rockstuhl, and I. Fernandez-Corbaton, "An electromagnetic multipole expansion beyond the long-wavelength approximation," Opt. Commun. **407**(May 2017), 17–21, Elsevier Ltd. (2018) [doi:10.1016/j.optcom.2017.08.064].

6. E. A. Gurvitz et al., "The High-Order Toroidal Moments and Anapole States in All-Dielectric Photonics," Laser Photon. Rev. **13**(5), 1800266 (2019) [doi:10.1002/lpor.201800266].

7. A. B. Evlyukhin et al., "Optical theorem and multipole scattering of light by arbitrarily shaped nanoparticles," Phys. Rev. B **94**(20), 1–7 (2016) [doi:10.1103/PhysRevB.94.205434].

8. A. Canós Valero et al., "Theory, Observation, and Ultrafast Response of the Hybrid Anapole Regime in Light Scattering," Laser Photon. Rev., 2100114 (2021) [doi:10.1002/lpor.202100114].

9. H. T. Chen, A. J. Taylor, and N. Yu, "A review of metasurfaces: Physics and applications," Reports Prog. Phys. **79**(7), IOP Publishing (2016) [doi:10.1088/0034-4885/79/7/076401].

10. M. Kang et al., "Wave front engineering from an array of thin aperture antennas," Opt. Express **20**(14), 15882 (2012) [doi:10.1364/oe.20.015882].

11. C. P. Jisha, S. Nolte, and A. Alberucci, "Geometric Phase in Optics: From Wavefront Manipulation to Waveguiding," Laser Photonics Rev. **2100003**, 1–21 (2021) [doi:10.1002/lpor.202100003].

[PAPER 2]: Special scattering regimes for conical all-dielectric nanoparticles

Kuznetsov, A.V., Canós Valero, A., Shamkhi, H.K., Terekhov P., Ni X., Bobrovs V., Rybin M.V., Shalin A.S., "*Special scattering regimes for conical all-dielectric nanoparticles*," Scientific Reports, Vol. 12, p. 21904, 18 30 November **2022**.

scientific reports

OPEN

Special scattering regimes for conical all-dielectric nanoparticles

Alexey V. Kuznetsov[1,2,3]✉, Adrià Canós Valero[3,4], Hadi K. Shamkhi[3,5], Pavel Terekhov[6], Xingjie Ni[6], Vjaceslavs Bobrovs[2], Mikhail V. Rybin[3] & Alexander S. Shalin[1,2,7,8,9]✉

All-dielectric nanophotonics opens a venue for a variety of novel phenomena and scattering regimes driven by unique optical effects in semiconductor and dielectric nanoresonators. Their peculiar optical signatures enabled by simultaneous electric and magnetic responses in the visible range pave a way for a plenty of new applications in nano-optics, biology, sensing, etc. In this work, we investigate fabrication-friendly truncated cone resonators and achieve several important scattering regimes due to the inherent property of cones—broken symmetry along the main axis without involving complex geometries or structured beams. We show how this symmetry breaking to deliver various kinds of Kerker effects (generalized and transverse Kerker effects), non-scattering hybrid anapole regime (simultaneous anapole conditions for all the multipoles in a particle leading to the nearly full scattering suppression) and, vice versa, superscattering regime. Being governed by the same straightforward geometrical paradigm, discussed effects could greatly simplify the manufacturing process of photonic devices with different functionalities. Moreover, the additional degrees of freedom driven by the conicity open new horizons to tailor light-matter interactions at the nanoscale.

Recently, ever-increasing attention has been paid to the optical properties of subwavelength dielectric and semiconductor nanoparticles. Such objects can be used to create various structures and platforms either significantly outperforming existing ones, or even belonging to a completely new class. Their undeniable advantages are low losses, high efficiency, and the ability to simultaneously tailor both the electric and magnetic components of light. Nanolasers[1], nanoantennas[2–4], ultrathin lenses[5], sensors and detectors[6–9], metamaterials and metasurfaces[10–12] and other emerging applications of the novel peculiar effects[13–18] are driven by such resonators.

A big step in high-index dielectric nanophotonics was made by implementing a flexible control over multipole excitations in subwavelength scatterers, understanding and tuning different phenomena by the means of multipole moments combinations and their interference[19,20]. For example, it became possible to implement the so-called *Kerker effect*—the cancellation of backward or forward scattering from a nanoparticle, which was originally introduced for a hypothetical sphere with equal epsilon and mu[21]. Nowadays, the Kerker effect plays a crucial role in dielectric nanophotonics, giving rise to a variety of fully transparent phase-tailoring "Huygens" metasurfaces[22–24]. As a next step, the so-called generalized Kerker effect was introduced; this effect allows one to observe an interference picture between resonantly excited electromagnetic multipoles of different orders[25–28]. Expanding the possibilities of the usual Kerker condition, it allows governing the scattering directivity via the interplay of multipolar channels. In the recent paper[29] the transverse Kerker effect was shown and verified experimentally; this effect is characterized by isotropic transverse scattering with simultaneous nearly full suppression of both forward and backward scattering. This peculiar optical signature of specially designed nanoparticles enabled fully transparent metasurfaces or even a perfect absorber[30,31].

Another intriguing possibility is an access to the so-called *anapole* (cancellation of the dipole radiation via the toroidal dipole one)[32] or *hybrid anapole* regimes (HA)[33]—simultaneous fulfillment of anapole conditions for all the main multipoles in a scatterer, giving rise to the far-field scattering suppression and strong near-field energy

[1]Center for Photonics and 2D Materials, Moscow Institute of Physics and Technology, Dolgoprudny, Russia 141700. [2]Institute of Telecommunications, Riga Technical University, Riga 1048, Latvia. [3]Faculty of Physics, ITMO University, St. Petersburg, Russia 197101. [4]Institute of Physics, University of Graz, and NAWI Graz, 8010 Graz, Austria. [5]A*STAR (Agency for Science, Technology and Research), Singapore 138634, Singapore. [6]Department of Electrical Engineering, The Pennsylvania State University, State College, Pennsylvania 16802, USA. [7]Faculty of Physics, Moscow State University, Moscow, Russia 119991. [8]School of Optical and Electronic Information, Suzhou City University, Suzhou 215104, China. [9]Kotelnikov Institute of Radio Engineering and Electronics, 432000 Ulyanovsk, Russia. ✉email: alexey.kuznetsov98@gmail.com; alexandesh@gmail.com
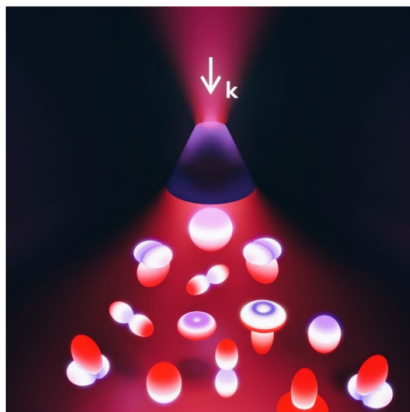
nature portfolio

1

72

Figure 1. Artistic representation of the considered silicon nanocone particles illuminated with a linearly polarized plane wave, showing the main advantage of the truncated cone geometry over the simpler shapes: the possibility of obtaining various important multipole effects within the same geometric shape.

localization regardless of a substrate. Metasurfaces based on such meta-atoms feature many useful properties such as a controlling phase shift of transmitted light, almost perfect transparency, strong nearfield enhancement useful for nonlinear and Raman applications, complex and unusual transient properties, etc., for various types of substrates and shapes[34–36].

Besides the completely non-scattering nanoobjects, researchers are also interested in the cases, when nanoparticles become anomalously strong scatterers. Such states are the opposite of an anapole, because at a certain frequency scattering maxima of several multipoles appear; this state is called *superscattering*[37]. Nanoscatterers supporting this feature can find their application in a number of areas, such as sensing, optical communication, and other emerging areas[38–40].

The cases above are usually considered for highly symmetric particles with simple geometry like spheres, cubes, or cylinders, each of them supporting a limited set of multipole interactions depending on size, material, and aspect ratio. Often, to get specific multipole configuration it is necessary to require some complications, for example multilayer structure. Breaking the symmetry enables more careful mode engineering allowing, for example, truncated conical scatterers (Fig. 1) to support all the aforementioned responses with unprecedented flexibility in scattering pattern tailoring without the use of complicated material configurations. Moreover, such geometry has many advantages in terms of fabrication, since most of the conventionally fabricated cylinders are actually cones with small side slope[41–43]. Currently, there are plenty of studies on conical particles from resonant reflectors[44], color filters[45], and nanoantennas[42] to antireflecting and light-trapping coatings for photovoltaic cells[46], and photonic nanojets[47].

Truncated cones are gaining popularity as elements of photonic structures due to their undeniable advantages. The main such advantage is the opportunity to vary the upper radius, adding an additional degree of freedom. Unlike the more popular cylinder-shaped nano-scatterers, nanocones allow one to vary the mode composition of the scatterer more precisely, which leads to a better tuning and obtaining effects that were previously unattainable[48]. For example, in[44], the authors were able to shift the reflection maximum of the metasurface by varying the geometric dimensions of the truncated nanocone meta-atom, which allowed them to move the resonance of interest through the entire visible spectrum. Additionally, in[45], the authors showed absorptive-type filters using truncated-cone hyperbolic metamaterial absorbers, where the desired operation frequency was achieved by varying the geometry and composition of the meta-atoms.

Notably, the truncated-cone geometry is still understudied compared with the "conventional" spherical, cubic, and cylindrical shapes. To bridge this gap, this work presents an extensive study of the optical properties of truncated conical scatterers. After introducing the central concepts of a multipole and a quasinormal mode, we discuss the new physics enabled by the additional degree of freedom—broken symmetry along the main axis. We demonstrate all the multipolar interference phenomena mentioned above using silicon truncated cone scatterers (experimental dispersion data for a-Si is shown in Supplementary Fig. S1) and indicate the specific parameters corresponding to these effects, for which we performed numerical simulations in Comsol Multiphysics. Based on our results, it is easy to find the desired effect in other materials and at other wavelengths with other geometric parameters, which makes the approach quite universal.

73

Modes and multipoles

Multipolar expansion. Multipole decomposition is an important tool for analyzing the interaction of light with matter. Recently new expressions for multipole moments were introduced, valid for arbitrarily sized particles of any shape. Beyond the particular case of multipolar moments induced by an incident field in a structure, these expressions can be directly applied in the many areas, where the multipole decomposition of electric current density distributions are used[20]. Exact multipole moments (1–4):

$$p_\alpha = -\frac{1}{i\omega}\left\{\int d^3\mathbf{r} J_\alpha^\omega j_0(kr) + \frac{k^2}{2}\int d^3\mathbf{r}\left[3(\mathbf{r}\cdot\mathbf{J}_\omega)r_\alpha - r^2 J_\alpha^\omega\right]\frac{j_2(kr)}{(kr)^2}\right\}, \tag{1}$$

$$m_\alpha = \frac{3}{2}\int d^3\mathbf{r}(\mathbf{r}\times\mathbf{J}_\omega)_\alpha \frac{j_1(kr)}{kr}, \tag{2}$$

$$Q_{\alpha\beta}^e = -\frac{3}{i\omega}\{\int d^3\mathbf{r}\left[3(r_\beta J_\alpha + r_\alpha J_\beta) - 2(\mathbf{r}\cdot\mathbf{J}_\omega)\delta_{\alpha\beta}\right]\frac{j_1(kr)}{kr} +$$
$$+ 2k^2\int d^3\mathbf{r}\left[5r_\alpha r_\beta(\mathbf{r}\cdot\mathbf{J}_\omega) - (r_\alpha J_\beta + r_\beta J_\alpha)r^2 - r^2(\mathbf{r}\cdot\mathbf{J}_\omega)\delta_{\alpha\beta}\right]\frac{j_3(kr)}{(kr)^3}\}, \tag{3}$$

$$Q_{\alpha\beta}^m = 15\int d^3\mathbf{r}\left\{r_\alpha(\mathbf{r}\times\mathbf{J}_\omega)_\beta + r_\beta(\mathbf{r}\times\mathbf{J}_\omega)_\alpha\right\}\frac{j_2(kr)}{(kr)^2}, \tag{4}$$

where p_α—electric dipole moment (ED), m_α—magnetic dipole moment (MD), $Q_{\alpha\beta}^e$—electric quadrupole moment (EQ) and $Q_{\alpha\beta}^m$—magnetic quadrupole moment (MQ), $\alpha, \beta = x, y, z$, $\mathbf{J}_\omega$—current density inside the particle, $j_{1,2,3}$—spherical Bessel functions of the first kind.

Hereinafter we will not consider any higher order terms [20], since they are negligible in all the cases of interest. In the far field region, the exact induced multipole moments produce an electric field given by [49]:

$$\mathbf{E} = \frac{k^2}{4\pi\varepsilon_0}\frac{e^{ikr}}{r}\left\{\mathbf{n}\times(\mathbf{p}\times\mathbf{n}) + \frac{1}{c}(\mathbf{m}\times\mathbf{n}) - \frac{ik}{6}\mathbf{n}\times\left[\mathbf{n}\times(\mathbf{Q}^e\cdot\mathbf{n})\right] - \frac{ik}{6c}\left[\mathbf{n}\times(\mathbf{Q}^m\cdot\mathbf{n})\right] + \cdots\right\} \tag{5}$$

Importantly, upon making the change $\mathbf{n}\to-\mathbf{n}$ in equation (5), the electric field produced by the ED does not change sign, while the electric field produced by the MD is reversed. For quadrupoles, the opposite happens, i.e., the MQ field is even while the EQ one is odd. The 'even–odd' character under space inversion is often referred to as the *parity* of the multipole field. This well-defined behavior under space inversion is at the core of all multipolar interference effects.

We also need to write down the following formula for the scattering cross-section (SCS)[20], to directly compare the contributions of different multipoles to the SCS:

$$C_{sca}^{total} = C_{sca}^p + C_{sca}^m + C_{sca}^{Q^e} + C_{sca}^{Q^m} + \cdots$$
$$= \frac{k^4}{6\pi\varepsilon_0^2|\mathbf{E}_{inc}|^2}\left[\sum_\alpha\left(|p_\alpha|^2 + \left|\frac{m_\alpha}{c}\right|^2\right) + \frac{1}{120}\sum_{\alpha\beta}\left(\left|kQ_{\alpha\beta}^e\right|^2 + \left|\frac{kQ_{\alpha\beta}^m}{c}\right|^2\right) + \cdots\right] \tag{6}$$

Interestingly, we note that the SCS of each multipole is decoupled from the rest. Thus, every multipole can be viewed as an independent 'scattering channel', through which the nanoparticle can exchange power with the environment[50].

Quasinormal modes. In the presence of an exciting field, dielectric nanoparticles have the ability to confine light within their volume. In other words, they act as subwavelength nanoresonators, supporting 'resonant modes'. This confinement becomes optimal near their resonant frequencies. To understand the nature of this phenomenon, one can trace an analogy with Fabry–Perot cavities. Once light enters the cavity, it bounces back and forth due to reflection from the walls until it finds a way to exit. However, for some special frequencies, a standing wave can form due to constructive interference, leading to resonant behavior. Another prominent analogy can be found in dielectric microcavities supporting whispering gallery modes, arising by total internal reflection after a roundtrip around the cavity. Resonances in dielectric nanoparticles can be visualized as a mixture between the two examples above; they can arise from standing waves along their transverse dimension (similar to whispering gallery modes), their longitudinal one (resembling Fabry Perot cavities), or a combination of both.

In an ideal system, such as a Fabry Perot resonator bounded by two perfectly conducting mirrors, light can never escape and will oscillate back and forth from the walls for an infinite time. The resonant frequencies in this context are real numbers. However, in an actual physical system, energy eventually dissipates into the environment, either by absorption or radiation. The resonant frequencies are then complex, implying that no stationary excitation can fully access them. Despite this, the system's response (e.g., scattering) is strongly affected when approaching a resonant frequency along the real axis. Thus, understanding their behavior and radiation characteristics is of great importance for the design of nanophotonic devices. Formally, resonant modes are eigensolutions of Maxwell's equations, supplemented with a set of boundary conditions. For an isolated dielectric
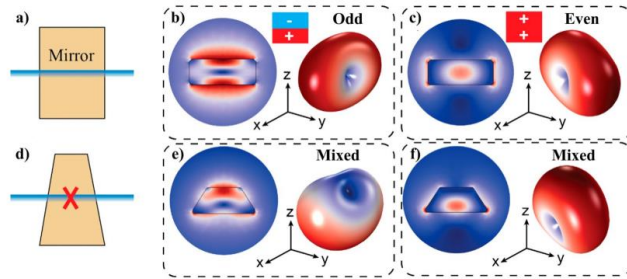
74

Figure 2. Lowest order resonant QNMs of a Si nanocylinder and a truncated Si nanocone. We consider only the QNMs that can be excited by a normally incident, x-polarized plane wave. Parameters of the nanocylinder: height 100 nm, radius 130 nm. Parameters of the nanocone: height 100 nm, bottom radius 130 nm, upper radius 65 nm. The refractive index of both nanoresonators is set to 4. (**a**) Scheme depicting the x–z cross-section of a cylinder, and it's up-down mirror symmetry. (**b**) Lowest order QNM of the nanocylinder with odd parity. It can be easily identified as the well-known MD mode. Left: near field distribution in the x–z plane, right: radiation pattern. (**c**) Lowest order QNM with even parity, corresponding to the ED mode. Left and right pictures as in (**b**). (**d**) Representation of the x–z cross-section of a nanocone, indicating the lack of up-down mirror symmetry. As a result, the QNMs are no longer even or odd. In particular, the lowest order QNMs radiate as a combination of ED and MD multipoles. (**e**–**f**) Lowest order resonant QNMs of the nanocone. Left and right pictures display the same as in (**b**) and (**c**). As a result of the mixed electric and magnetic contributions, the forward and backward directivities of a single QNM can be boosted with respect to the nanocylinder.

nanoparticle in a homogeneous environment, the boundary conditions can be replaced by a radiation condition. Assuming a dispersionless permittivity $\varepsilon(\mathbf{r})$, we write Maxwell's equations with a time dependence of the form $e^{-i\omega t}$ (we omit for brevity the spatial dependences in the fields and the permittivity):

$$\begin{pmatrix} 0 & -i\nabla\times \\ -i\nabla\times & 0 \end{pmatrix} \begin{pmatrix} \mathbf{E}_m \\ \mathbf{H}_m \end{pmatrix} = \tilde{\omega}_m \begin{pmatrix} \varepsilon & 0 \\ 0 & -\mu_0 \end{pmatrix} \begin{pmatrix} \mathbf{E}_m \\ \mathbf{H}_m \end{pmatrix}, \tag{7}$$

together with the radiation condition:

$$\lim_{r\to\infty} \hat{\mathbf{r}} \times \nabla \times \mathbf{E}_m = -i\frac{\tilde{\omega}_m}{c}\mathbf{E}_m, \tag{8}$$

where $\hat{\mathbf{r}}$ is a unit radial vector and $\tilde{\omega}_m = \omega_m - i\gamma_m$ is the resonant frequency or *eigenfrequency* associated with the eigenmode $\begin{pmatrix} \mathbf{E}_m \\ \mathbf{H}_m \end{pmatrix}$. Equation (8) essentially tells that the mode field must behave as a spherical wave at infinity, i.e. follow a dependence $\mathbf{E}_m \sim \mathbf{E}_0(\hat{\mathbf{r}})e^{i\tilde{\omega}_m r/c}/r$. Interestingly, to ensure energy decay in the time domain, γ_m is always a real, positive number. Therefore, far from the origin, the mode amplitude blows up due to a term $e^{\gamma_m r/c}/r$. In consequence, modes in open systems cannot be normalized by standard means, and often receive the name 'quasinormal' modes (QNMs). Despite this, the scattered field everywhere inside the nanoparticle can be accurately described as a linear combination of the contributions of several QNMs, i.e. $\mathbf{E}_{sca} = \sum_m \alpha_m(\omega)\mathbf{E}_m$, where $\alpha_m(\omega)$ describes the coupling of the m-th QNM to the incident field[51].

Multipolar resonances in dielectric nanoparticles are associated with a QNM. In the case of spheres, every resonant mode radiates as a specific multipole. However, this is no longer true for arbitrary shapes. In a general setting, the scattering pattern of a QNM can be described as a mixture of multipole contributions. To determine how much a QNM 'matches' a given multipole, (i.e. its multipolar content) one can define the m-th 'eigen' current $\mathbf{J}_m = -i\tilde{\omega}_m\varepsilon_0(\varepsilon_p - 1)\mathbf{E}_m$, where ε_p is the relative permittivity of the nanoparticle. Introducing $\mathbf{J}_m$ into equations (1–4), and evaluating them at the *complex* frequency $\tilde{\omega}_m$ yields the desired multipolar content of the m-th QNM[52]. At a *real* frequency ω, the QNM will radiate as a combination of its intrinsic multipole moments.

However, the particle symmetry imposes strict bounds on the multipolar contents of its QNMs. For instance, cylindrical symmetry prevents a mixture of multipoles with even and odd parity (refer to Fig. 2a–c). This has important implications, e.g., for the design of Kerker meta-atoms: since the electric and magnetic dipoles have opposite symmetry, the radiation pattern by a single mode cannot be directional. Thus, engineering a resonant Kerker effect in a dielectric nanodisk requires overlapping the resonances of two QNMs with electric and magnetic dipolar character, respectively.

Unlike cylinders, truncated nanocones lack the vertical mirror plane, as schematically depicted in Fig. 2d. As a result, the QNMs can radiate as a combination of multipoles with even and odd parity, such as the electric

75

and magnetic dipole. Consequently, the directivity of a single QNM can be enhanced in the forward or the backward direction, as can be appreciated from the radiation patterns of the two lowest order QNMs of a nanocone (Fig. 2e–f). This also immediately implies the appearance of a bianisotropic response. Thus, truncated nanocones not only hold an additional degree of freedom (conicity) with respect to more studied geometries such as cylinders: conicity provides a simple strategy to control the even–odd mixture of multipoles in a QNM, leading to new exotic effects, such as single mode directivity, strong coupling and exceptional points[53].

Kerker effects

In this section, we talk about various types of Kerker effects (generalized and transverse Kerker effects) in silicon truncated nanocones. The Kerker effect became more commonly used recently due to the explosive growth of dielectric nanophotonics. In this regard, it becomes necessary to study this type of effects considering different scatterer geometries.

The Kerker effect is a unidirectional forward or backward scattering (Generalized Kerker effects) or enhanced side scattering (transverse Kerker effect). The multipole decomposition can serve as an excellent tool to study the Kerker effect. It becomes possible to show the electric field as the sum of multipole contributions, where each term is responsible for the field of a particular multipole[20].

Generalized Kerker conditions. For the first time, the Kerker effect was discovered for spherical particles with the dielectric constant equal to the magnetic permeability. In such particles, when the electric field amplitudes of the electric and magnetic dipoles are equal, as well as at a certain phase difference of the dipoles, one can observe only forward or backward scattering[21]. There are many works that show the experimental realization of such effect in dielectric nanoparticles[54–56]. Over time, other meaningful combinations of multipoles and the phase difference between them were discovered, so the Kerker effect had to be "generalized"[25,57]. Nowadays, the term "generalized Kerker effect" is used, when it comes to pronounced forward or backward scattering.

Amplitude ratio for generalized Kerker conditions. To describe forward or backward scattering we can write the scattered field of an arbitrary shaped particle under x-polarized light[31], inserting $n = (0, 0, n_z)$ in (5), we obtain (9):

$$E_x^{sc} = \frac{k^2}{4\pi\varepsilon_0} \frac{e^{ikr}}{r} \left\{ p_x n_z^2 + \frac{1}{c} m_y n_z - \frac{ik}{6} Q_{xz}^e n_z^3 - \frac{ik}{6c} Q_{yz}^m n_z^2 + \cdots \right\}$$ (9)

The direction of forward or backward scattering can be linked to the unit vector $\boldsymbol{n}$. Let us set $\boldsymbol{n} = (0, 0, 1)$ for the forward scattering, and $\boldsymbol{n} = (0, 0, -1)$ for the backward. We consider the case of a plane wave illumination with x-polarization.

Let us assume that we do not have backscattering, and all the multipole contributions that do not participate in the Kerker effect tend to zero. In such cases, the following expressions are valid:

$$\text{ED + MD}: E_x^{bwsc} = \frac{k^2}{4\pi\varepsilon_0} \frac{e^{ikr}}{r} \left\{ p_x - \frac{1}{c} m_y \right\} = 0$$ (10)

$$\text{ED + EQ}: E_x^{bwsc} = \frac{k^2}{4\pi\varepsilon_0} \frac{e^{ikr}}{r} \left\{ p_x + \frac{ik}{6} Q_{xz}^e \right\} = 0$$ (11)

$$\text{MD + MQ}: E_x^{bwsc} = \frac{k^2}{4\pi\varepsilon_0} \frac{e^{ikr}}{r} \left\{ -\frac{1}{c} m_y - \frac{ik}{6c} Q_{yz}^m \right\} = 0$$ (12)

$$\text{EQ + MQ}: E_x^{bwsc} = \frac{k^2}{4\pi\varepsilon_0} \frac{e^{ikr}}{r} \left\{ \frac{ik}{6} Q_{xz}^e - \frac{ik}{6c} Q_{yz}^m \right\} = 0$$ (13)

$$\text{ED + MD + EQ + MQ}: E_x^{bwsc} = \frac{k^2}{4\pi\varepsilon_0} \frac{e^{ikr}}{r} \left\{ p_x - \frac{1}{c} m_y + \frac{ik}{6} Q_{xz}^e - \frac{ik}{6c} Q_{yz}^m \right\} = 0$$ (14)

It should be emphasized that the last combination (14) includes all multipoles up to quadrupoles, and therefore is a superposition of the previous cases. Also, it is worth noting that combination of four multipoles can lead not only to the generalized Kerker effect, but also to the transverse Kerker effect. Such multipole combinations will be discussed in Sect. "Conclusions on the Kerker effects".

Knowing the multipoles values for 'no backscattering' cases, we can express the forward scattering amplitudes:

$$\text{ED + MD}: E_x^{fwsc} = \frac{k^2}{4\pi\varepsilon_0} \frac{e^{ikr}}{r} \left\{ p_x + \frac{1}{c} m_y \right\} = \frac{k^2}{4\pi\varepsilon_0} \frac{e^{ikr}}{r} \left\{ \frac{2}{c} m_y \right\}$$ (15)

$$\text{ED + EQ}: E_x^{fwsc} = \frac{k^2}{4\pi\varepsilon_0} \frac{e^{ikr}}{r} \left\{ p_x - \frac{ik}{6} Q_{xz}^e \right\} = \frac{k^2}{4\pi\varepsilon_0} \frac{e^{ikr}}{r} \left\{ -\frac{ik}{3} Q_{xz}^e \right\}$$ (16)

76

$$\text{MD + MQ: } E_x^{fwsc} = \frac{k^2}{4\pi\varepsilon_0}\frac{e^{ikr}}{r}\left\{\frac{1}{c}m_y - \frac{ik}{6c}Q_{yz}^m\right\} = \frac{k^2}{4\pi\varepsilon_0}\frac{e^{ikr}}{r}\left\{-\frac{ik}{3c}Q_{yz}^m\right\} \tag{17}$$

$$\text{EQ + MQ: } E_x^{fwsc} = \frac{k^2}{4\pi\varepsilon_0}\frac{e^{ikr}}{r}\left\{-\frac{ik}{6}Q_{xz}^e - \frac{ik}{6c}Q_{yz}^m\right\} = \frac{k^2}{4\pi\varepsilon_0}\frac{e^{ikr}}{r}\left\{-\frac{ik}{3c}Q_{yz}^m\right\} \tag{18}$$

Further, considering the equations (12, 4–11), we obtain the ratios between the multipole contributions for each combination of moments leading to the Kerker effect (see Supplementary 2):

$$\text{ED + MD: } \frac{C_{sca}^{ED}}{C_{sca}^{MD}} = 1 \tag{19}$$

$$\text{ED + EQ: } \frac{C_{sca}^{ED}}{C_{sca}^{EQ}} = 1.67 \tag{20}$$

$$\text{MD + MQ: } \frac{C_{sca}^{MD}}{C_{sca}^{MQ}} = 1.67 \tag{21}$$

$$\text{EQ + MQ: } \frac{C_{sca}^{EQ}}{C_{sca}^{MQ}} = 1 \tag{22}$$

Phase difference for generalized Kerker conditions. Another important Kerker effect condition is the phase difference between the interacting multipoles. For the original problem of Mie scattering on spherical particles, it was shown that electric and magnetic multipoles of the same order have opposite parity with respect to cos θ (θ is the scattering angle with respect to the forward direction)[58]. This means that simultaneous forward scattering amplification and backscattering suppression can be achieved not only for ED and MD interference, but also for any higher-order multipoles, and scattering can be further enhanced or suppressed[59].

The fact is that the phase will directly affect the shape of the scattering diagram we obtain. For all the above combinations of multipoles, specified phase differences can be found to ensure forward scattering.

$$\text{ED + MD: } \Delta\varphi(p,m) = \arg\left(p\right) - \arg\left(m\right) = \pi \pm 2\pi n,\ n \in Z \tag{23}$$

$$\text{ED + EQ: } \Delta\varphi(p,Q^e) = \arg\left(p\right) - \arg\left(Q^e\right) = \pi \pm 2\pi n, n \in Z \tag{24}$$

$$\text{MD + MQ: } \Delta\varphi(m,Q^m) = \arg\left(m\right) - \arg\left(Q^m\right) = \pi \pm 2\pi n,\ n \in Z \tag{25}$$

$$\text{EQ + MQ: } \Delta\varphi(Q^e,Q^m) = \arg\left(Q^e\right) - \arg\left(Q^m\right) = \pi \pm 2\pi n, n \in Z \tag{26}$$

In our work, all the generalized Kerker conditions with forward direction were obtained for truncated conical nanoscatterers (Fig. 3).

Figure 3 shows the Kerker effects calculated numerically, using Comsol Multiphysics, and analytically, using equation (5). With the help of this equation, it is possible to construct the far field distribution by varying the values of the multipole moments in such a way as to obtain the Kerker effect. The dependence of the multipole contributions to the scattering cross-section on the radiation wavelength is shown in Fig. 3(a–e). The points of the Kerker effect are marked in red, following the equations (19–22). To confirm this, the analytical (f–j) and numerical (k–o) far-field patterns are shown for each case. The scattering shape is similar but not completely the same due to the minor contributions of other multipoles in the numerical calculations.

Thus, various kinds of Kerker effects, and necessary far field and scattering cross-section conditions are shown for real silicon truncated cones. The resulting shapes of radiation patterns for cones, obtained in COMSOL Multiphysics, are in a good agreement with the expected Kerker-type shapes for an ideal point calculations. In real systems, it is impossible to obtain the ideal combination of the necessary multipoles, and therefore weak discrepancies are observed. The absence of the need to use higher-order multipoles is also evidenced by good coincidence of the sum of scattering cross-section of multipoles with calculation of scattering cross-section, using the integration of the Pointing vector over a closed surface in the far-field zone and the normalization to the incident field intensity (Fig. 3a–e, gray and orange lines).

Transverse Kerker conditions. Another equally important scattering feature is the transverse Kerker effect, which was first described in[29,60]. The main cause of the transverse Kerker effect is the combination of multipoles featuring scattering to the sides only leaving the small portion of forward scattering according to optical theorem[61]. Such effect can be obtained both through simple combinations of two multipoles[62] and through more complex configurations[30].
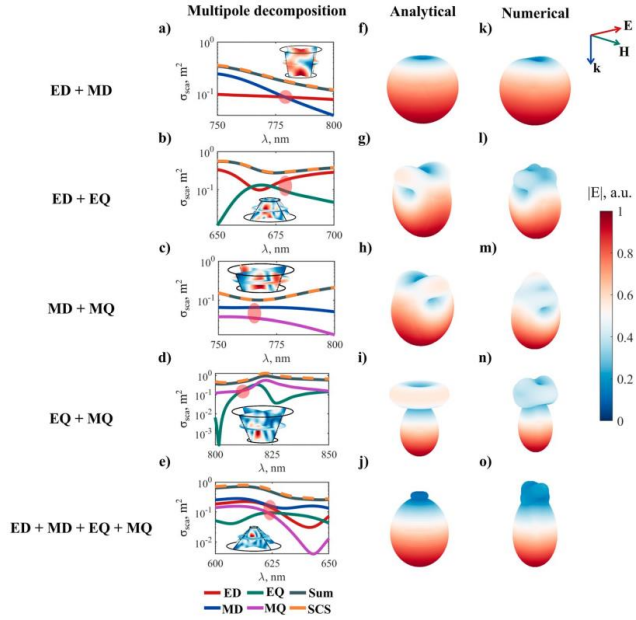
6

77

Figure 3. Generalized Kerker effects for truncated conical nanoparticles with different shapes. (**a**–**e**)—multipolar decomposition, (**f**–**j**)—far-field sum of multipoles for a point particle, calculated analytically, (**k**–**o**)—far-field distribution for conical nanoparticles with different geometries calculated numerically for real particles at the spectral points shown in (**a**–**e**). Conditions of the illumination—incident plane wave from the top of the page. The geometrical parameters for every case can be found in section S3 of the Supplementary Information. The experimental dispersion data for a-Si is shown in Supplementary Fig. S1.

Let us assume that both backward and forward scattering are suppressed, and all the multipole contributions not participating in the transverse Kerker effect tend to zero. Then, the following system of equations is valid for possible ways to obtain transverse Kerker effect (4 multipoles and 2 multipoles):

$$\text{ED} + \text{MQ: } E_x^{bwsc} = E_x^{fwsc} = \frac{k^2}{4\pi\varepsilon_0} \frac{e^{ikr}}{r} \left\{ p_x - \frac{ik}{6c} Q_{yz}^m \right\} = 0 \tag{27}$$

$$\text{MD} + \text{EQ: } \begin{cases} E_x^{bwsc} = \frac{k^2}{4\pi\varepsilon_0} \frac{e^{ikr}}{r} \left\{ -\frac{1}{c} m_y + \frac{ik}{6} Q_{xz}^e \right\} = 0 \\ E_x^{fwsc} = \frac{k^2}{4\pi\varepsilon_0} \frac{e^{ikr}}{r} \left\{ \frac{1}{c} m_y - \frac{ik}{6} Q_{xz}^e \right\} = 0 \end{cases} \tag{28}$$

$$\text{ED} + \text{MD} + \text{EQ} + \text{MQ: } \begin{cases} E_x^{bwsc} = \frac{k^2}{4\pi\varepsilon_0} \frac{e^{ikr}}{r} \left\{ p_x - \frac{1}{c} m_y + \frac{ik}{6} Q_{xz}^e - \frac{ik}{6c} Q_{yz}^m \right\} = 0 \\ E_x^{fwsc} = \frac{k^2}{4\pi\varepsilon_0} \frac{e^{ikr}}{r} \left\{ p_x + \frac{1}{c} m_y - \frac{ik}{6} Q_{xz}^e - \frac{ik}{6c} Q_{yz}^m \right\} = 0 \end{cases} \tag{29}$$

After some simple algebra, one can obtain the following conditions for the multipole amplitudes:

$$\text{ED} + \text{MQ: } p_x = \frac{ik}{6c} Q_{yz}^m \tag{30}$$

78

$$\text{MD} \; + \; \text{EQ:} \; \frac{1}{c} m_y = \frac{ik}{6} Q_{xz}^e \tag{31}$$

$$\text{ED} \; + \; \text{MD} \; + \; \text{EQ} \; + \; \text{MQ:} \begin{cases} p_x = \dfrac{ik}{6c} Q_{yz}^m \\ \dfrac{1}{c} m_y = \dfrac{ik}{6} Q_{xz}^e \end{cases} \tag{32}$$

Further, taking into account the equations (27–29), we obtain the ratios between the multipole contributions for each of their combinations (see Supplementary S2):

$$\text{ED} \; + \; \text{MQ:} \; \frac{C_{sca}^{ED}}{C_{sca}^{MQ}} = 1.67 \tag{33}$$

$$\text{MD} \; + \; \text{EQ:} \; \frac{C_{sca}^{MD}}{C_{sca}^{EQ}} = 1.67 \tag{34}$$

$$\text{ED} \; + \; \text{MD} \; + \; \text{EQ} \; + \; \text{MQ:} \begin{cases} \dfrac{C_{sca}^{ED}}{C_{sca}^{MQ}} = 1.67 \\ \dfrac{C_{sca}^{MD}}{C_{sca}^{EQ}} = 1.67 \end{cases} \tag{35}$$

For all the above combinations, phase differences between multipoles can be obtained. Transverse phase conditions are:

$$\text{ED} \; + \; \text{MQ:} \; \Delta\varphi(p, Q^m) = \arg(p) - \arg(Q^m) = \pi \pm 2\pi n, \, n \in Z \tag{36}$$

$$\text{MD} \; + \; \text{EQ:} \; \Delta\varphi(m, Q^e) = \arg(m) - \arg(Q^e) = \pi \pm 2\pi n, \, n \in Z \tag{37}$$

$$\text{ED} \; + \; \text{MD} \; + \; \text{EQ} \; + \; \text{MQ:} \begin{cases} \Delta\varphi(p, Q^m) = \arg(p) - \arg(Q^m) = \pi \pm 2\pi n, \, n \in Z \\ \Delta\varphi(m, Q^e) = \arg(m) - \arg(Q^e) = \pi \pm 2\pi n, \, n \in Z \end{cases} \tag{38}$$

In our work, all the transverse Kerker conditions are shown for truncated conical nano-scatterers (Fig. 4). Figure 4 shows the different transverse Kerker effects obtained both numerically and analytically, calculated in the same way as in Fig. 3. Scattering patterns shape is an obvious reason why this effect is called "transverse". By the proper choice of the multipole phases and amplitudes, it is possible to achieve side scattering together with forward and backward scattering suppression.

Conclusions on the Kerker effects. Kerker effects are indeed unique phenomena, which are key to a range of novel photonic devices. Prior to our work, each one of these had previously been only shown for completely different shapes and materials of nano-scatterers. The following are some examples demonstrating various Kerker-type effects (Table 1).

In this section, we have demonstrated for the first time all known Kerker effects for single nanoscatterers within the same geometry. Thus, nanocones represent a versatile, fabrication-friendly platform for the implementation of new photonic devices benefitting from a comprehensive toolbox of multipolar interference effects including flexible tailoring of scattering patterns.

Non-scattering regimes: anapole and hybrid anapole

In the past few years, the emergent field of 'anapole electrodynamics' is experiencing exponential growth[69]. Anapoles are semi-nonradiating sources that arise due to the destructive interference of the quasistatic electric dipole moment and the toroidal dipole in the far field. Alternatively, in a more general picture, they can be understood as being originated by the destructive interference of symmetry-compatible quasinormal modes[33]. However, the energy stored by the quasinormal modes within the nanoparticle is nonzero, leading to counterintuitive light-matter interaction processes in the absence of elastic scattering. Until very recently, the suppression of scattering in these states was limited to the electric dipole contribution to radiation. The experimental demonstration of *hybrid anapoles* (HA) following the pioneering theoretical proposal[70], has evidenced the possibility to simultaneously overlap the zeros of all the dominant multipolar channels through a careful design of the nanoparticle geometry. These novel states are much more promising than their dipolar counterparts for a number of reasons[33,34]; despite the larger volume of the nanoresonator required to obtain them, the scattering suppression is improved by more than 20 times, while the excited quasinormal modes store approximately 10 times more energy. Such values exceed by far the performance of anapoles and 2nd order anapoles[71] arising in homogeneous disk nanoresonators.

In nanocylinders pertaining to the cylindrical symmetry, it was shown in[33] how the anapoles from different multipolar orders but equal parity were connected. Counterintuitively, such connection allows to simultaneously
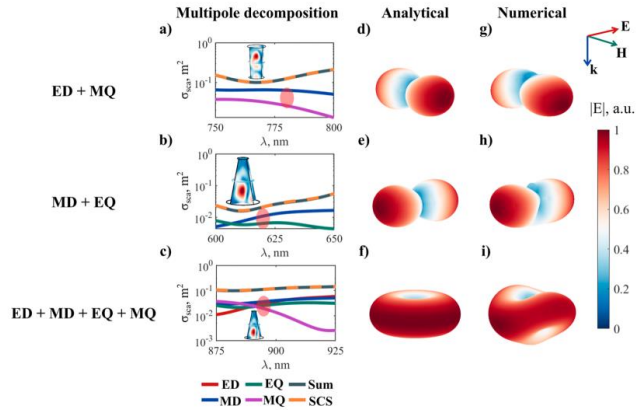
79

Figure 4. Transverse Kerker effects for truncated conical nanoparticles with different shapes. (**a–c**)—multipolar decomposition, (**d–f**)—far-field sum of multipoles for a point particle, calculated analytically, (**g–i**)–far-field distribution for conical nanoparticles with different geometries calculated numerically for real particles at the spectral points shown in (**a–c**). Conditions of the illumination—incident plane wave from the top of the page. The geometrical parameters for every case can be found in section S3 of the Supplementary Information. The experimental dispersion data for a-Si is shown in Supplementary Fig. S1.

	Generalized	Transverse
ED + MD	Silicon spherical nanoparticles[55,63]	–
ED + EQ	Plasmonic gold nanoring nanoantenna[25]	–
ED + MQ	–	Ceramic spheroidal particle[64] Silicon square nanoplate[62]
MD + EQ	–	Core–shell SiO2@InSb and Si@InSb in a one-dimensional (1D) metalattice geometry in the Terahertz range[65]
MD + MQ	Ceramic core–shell[66]	–
EQ + MQ	Both isolated and periodically arranged homogeneous cross dielectric structure[67]	–
ED + MD + EQ + MQ	Individual core–shell nanoparticles[68]	Silicon cube[29] Ceramic cube and cylinder[30]

Table 1. Examples demonstrating various Kerker-type effects for different shapes and material of scatterers.

overlap four anapoles with just the two geometrical degrees of freedom of the nanoparticle. As mentioned earlier, however, the even and odd multipoles are no longer necessarily coupled once the reflection symmetry in z is broken. In this section, we aim at investigating the effect of z-symmetry breaking on a HA nanocylinder, by introducing a small geometrical perturbation on the upper radius. Such a situation occurs quite often, (unintentionally) during a sample fabrication process. It is rarely possible to obtain particles of an ideal shape, and samples with small defects can often be found. In practice, the manufactured nanocylinders are most likely truncated cones[72,73].

Figure 5a displays the exact multipole decomposition of the HA regimes of the silicon cylinder studied in[33,34]. The simultaneous suppression of the ED, MD, EQ, and MQ channels at the same spectral position can be appreciated. The inset depicts the norm of the electric field at the spectral point with the lowest scattering, hereafter referred to as the 'HA wavelength (λ_{HA})'. The field can be seen to be strongly concentrated within the nanoparticle, (where two hotspots appear), with the exception of a few hotspots at the surface with a size of the order of $\lambda_{HA}/40$. Thus, even in the near field outside the particle, the incident wave is barely distorted by scattering. We now keep the height of the resonator constant and progressively increase conicity ($1 - R_{top}/R_{bottom}$). The multipole decompositions for three selected conicities are shown in Fig. 5a–c In all cases, illumination from the top is considered. A log scale is used to enhance the contrast of the zeros in the spectrum.

Firstly, we observe a spectral blue-shift of all resonant features. This is expected, due to the overall size reduction of the lateral dimensions of the resonator. Secondly, the original MQ and ED anapoles blue-shift faster
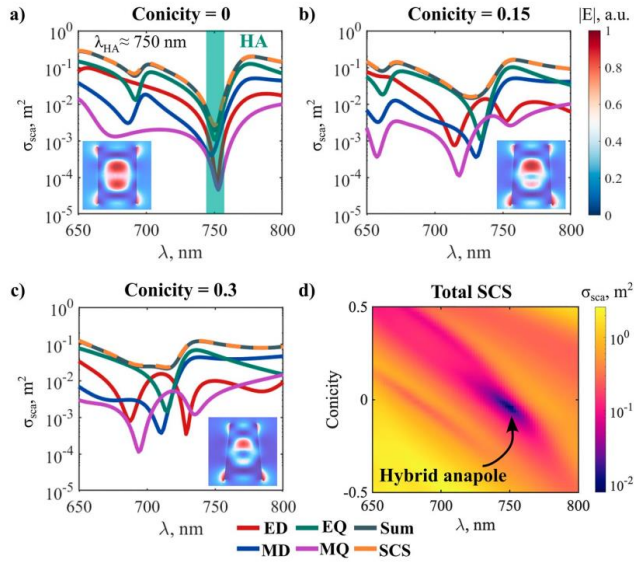
80

Figure 5. Evolution of the HA as a function of conicity and wavelength. (**a–c**): Multipole decompositions of the SCS (semilogarithmic scale) for selected conicities (see geometric parameters of HA in section S3 of the Supplementary Information). In all calculations, the height of the nanoparticle was kept constant. Insets: distribution of the electric field norm at λ_{HA} (**d**): Total SCS as a function of conicity and wavelength. The experimental dispersion data for a-Si is shown in Supplementary Fig. S1.

than the EQ and MD. As a result, the four anapoles are no longer superposed in the spectrum, and the scatterer becomes less 'transparent' to the incident illumination. This is demonstrated by calculations of the total SCS as a function of conicity (Fig. 5d).

However, we also observe a progressive emergence of *new anapoles* in the ED and the MQ SCSs (red and purple solid lines, respectively), coinciding with the maxima in the EQ and MD SCSs near the HA. These new features become more pronounced with increasing conicity. Interestingly, their formation is acompanied by a 'split' (two separated anapoles close to each other, see Fig. 5c) in the unperturbed ED and MQ resonances.

We evaluate quantitatively this effect by calculating the wavelength shifts of the multipolar anapoles as a function of conicity (Fig. 6). The white-dashed lines show the paths followed in parameter space (only the anapoles involved in the vicinity of the HA regime are investigated). The unperturbed anapoles in the ED and MQ channels are labeled as A_1 and B_1, respectively (Fig. 6a, d). As could be anticipated from the results in Ref.[33], the latter follow the same path in parameter space. This is because they are both associated to the same resonant QNM. The same occurs with the MD and EQ anapoles (Fig. 6b, c).

For values of $1 - R_{top}/R_{bottom} > 0$, we confirm the appearance of new anapoles in both the ED and MQ channels, manifesting as pronounced dips in their contributions to the SCS (Fig. 6a, d). For convenience, we denote them as A_2 and B_2. Importantly, we notice that they both follow a similar path in parameter space. What's more, there seems to be a connection between the paths of A_2 and B_2 and those followed by the original EQ and MD anapoles; after their appearance, the former spectrally overlap with the latter. In contrast, no appreciable new features can be seen when $1 - R_{top}/R_{bottom} < 0$. In a first regard, this observation seems contradictory, since symmetry is analogically broken. However, later the physical reason for it will become clear. It is necessary to mention that in the calculations of the conicity we keep R_{bottom} constant and increase R_{top}, then the volume of the $1 - R_{top}/R_{bottom} < 0$ is larger than $1 - R_{top}/R_{bottom} > 0$.

To gain more insight, we briefly revisit the origin of anapoles, from the QNM perspective[74,75]. As an example, consider a scatterer supporting one resonant QNM radiating to the ED channel. The SCS would then be well approximated by the first term in equation (6), i.e.:

$$\sigma_{sca} \propto |\mathbf{p}|^2 = |\mathbf{p}_{bg} + \mathbf{p}_1|^2 \qquad (39)$$

81
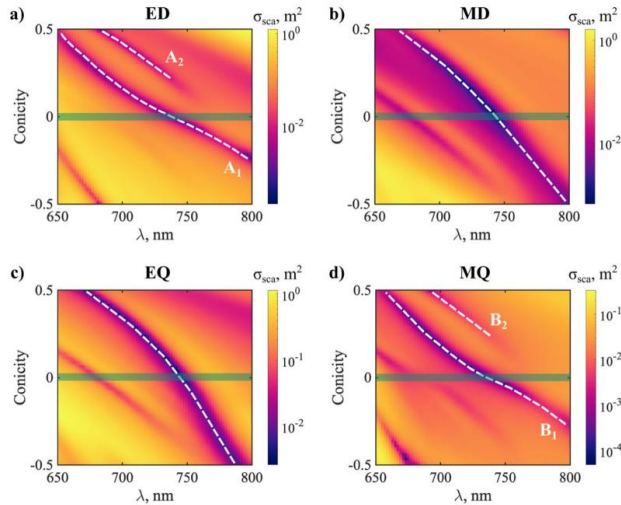
Figure 6. Evolution of the SCS of each multipole (in log scale), as a function of wavelength and conicity. White dashed lines are a guide to the eye, and indicate the paths traced by anapoles in parameter space. The shaded green lines highlight the unperturbed cylinder (with conicity = 0). (**a**) ED. A_1 labels the original ED anapole in the unperturbed cylinder, and A_2 is the new ED anapole induced by symmetry breaking. (**b**) MD, (**c**) EQ, (**d**) MQ. B_1 labels the original MQ anapole in the unperturbed cylinder, and B_2 is the new MQ anapole induced by symmetry breaking. The experimental dispersion data for a-Si is shown in Supplementary Fig. S1.

Here, $\mathbf{p}_1$ is the induced ED moment by the resonant QNM, and $\mathbf{p}_{bg}$ corresponds to a non-resonant contribution stemming from QNMs outside the spectral range of interest, as well as direct scattering from the object's shape[76]. A zero (anapole), takes place when $|\mathbf{p}|^2 = 0$, so that the resonant contribution cancels out with the background:

$$\mathbf{p}_1 = -\mathbf{p}_{bg} \qquad (40)$$

We note that, in general, $\mathbf{p}_{bg}$ is a smooth function of frequency that cannot, a priori, be controlled by design, while $\mathbf{p}_1$ becomes non-negligible only near the resonance frequency. In particular, one can model $\mathbf{p}_1$ as a Lorentzian function centered at the resonance frequency. In the presence of a second resonant QNM, equation (40) can be expressed as:

$$\mathbf{p}_1 + \mathbf{p}_2 = -\mathbf{p}_{bg} \qquad (41)$$

Equation (41) provides one more degree of freedom to reach the anapole condition. In principle, it is possible to tune $\mathbf{p}_1$ so that $\mathbf{p}_1 = -\mathbf{p}_{bg} - \mathbf{p}_2$, or change $\mathbf{p}_2$ so that $\mathbf{p}_2 = -\mathbf{p}_{bg} - \mathbf{p}_1$. Since $\mathbf{p}_{1,2}$ vary naturally in amplitude and phase near the resonance frequencies of the associated QNMs, a new anapole should emerge for every new QNM contributing to the ED cross-section[77]. This conclusion can be readily generalized to any multipole.

From the above discussion, it follows that anapole formation is intrinsically related to modal evolution. In particular, the emergence of a new anapole in the ED and the MQ SCSs must be directly connected to an additional QNM contribution to these multipoles. With this idea in mind, we calculate the resonant QNMs in the vicinity of the HA as a function of the conicity (Fig. 7a). Three QNMs were considered: the two QNMs primarily responsible for the HA effect (M1 and M2 in Fig. 7a) and, for completeness, a third QNM lying within the visible range (M3 in Fig. 7a).

In Ref.[33], it was shown that M1 was associated with the formation of both the ED and MQ anapoles (A_1 and B_1), while M2 was responsible for the MD and EQ ones. This is further confirmed here by comparing the paths of the anapoles in Fig. 6 with the evolution of the resonant wavelengths in Fig. 7a. The role of M3 can be safely neglected in the discussion (or considered part of the background), since it is spectrally isolated from M1 and M2 in the range of parameters considered.

82
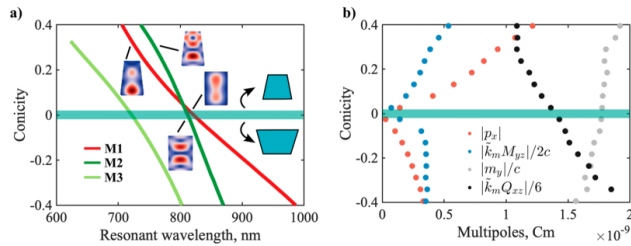
Figure 7. (**a**) Resonant wavelength shifts of the QNMs in the vicinity of the HA, as a function of conicity. In an unperturbed cylinder, QNMs M1 and M2 correspond to TE_{120} and TM_{113} discussed in Ref.[33]. M3 is associated with TM_{111}. Insets depict the internal fields of the QNMs for selected values of conicity (red–more intense field, blue–less intense field). In all the calculations we neglected the dispersion of Si, and fixed its value to an average in the spectral range under consideration, $n \approx 3.45$. (**b**) Intrinsic multipole moments of M2 as a function of conicity. To allow a proper visualization, all moments are normalized in ED units, i.e. C.m. $\bar{k}_m = \bar{\omega}_m/c$ is the (complex) wavevector associated with the m-th QNM.

We now focus our attention on the multipolar character of QNM M2 (Fig. 7b). We calculate the intrinsic multipole moments as explained in Sect. "Quasinormal modes". This indicates us whether a QNM will contribute or not to the SCS of a given multipole. For our purposes, if the contribution of a specific QNM is zero, it cannot play a role in the formation of an anapole in that multipole SCS.

The results reveal a surprising fact: for an unperturbed cylinder, the contributions of M2 to the ED and MQ are zero, while the MD and EQ are not, as expected since it interferes in those two channels to form anapoles. However, when $1 - R_{top}/R_{bottom} \neq 0$, M2 starts contributing to the ED and MQ SCSs. The MQ and ED contents of M2 grow as a function of the perturbation. It immediately follows from the discussion above that a new anapole can emerge in the two multipoles under consideration. Furthermore, the contributions to the MD and EQ SCS also change: for $1 - R_{top}/R_{bottom} < 0$ the QNM is better matched to the EQ. Conversely, for $1 - R_{top}/R_{bottom} > 0$, the MD becomes dominant.

The fact that M2 couples to multipoles with opposite parities when symmetry is broken can be understood from Fig. 2 and the discussion in Sect. "Quasinormal modes". In a truncated cone, the modes are no longer eigenstates of parity, and therefore can scatter light as a mixture of even and odd multipoles.

In brief, the emergence of anapoles A_2 and B_2 is due to mode M2 being able to contribute to the ED and MQ SCS, once cylindrical symmetry is broken. This also explains the apparent connection between the paths followed by the EQ and MD anapoles (associated with M2) and the new emerging anapoles. The reason why A_2 and B_2 appear only for $1 - R_{top}/R_{bottom} > 0$ can be elucidated from the behavior of the resonant wavelengths in Fig. 7a. It can be seen that M1 and M2 remain spectrally close when increasing $1 - R_{top}/R_{bottom}$. In contrast, for the range of parameters considered, M1 rapidly redshifts towards the near IR when decreasing $1 - R_{top}/R_{bottom}$, while M2 remains in the visible. In consequence, M1 is spectrally isolated from M2, and the latter does not play an important role anymore. Thus, no new anapoles are formed.

Regarding the robustness of the HA regime under small perturbations, extensive numerical tests demonstrate that it is still possible to recover the spectral overlap of the four anapoles up to perturbations in the range of $1 - R_{top}/R_{bottom} = \{0.2, -0.2\}$ by varying the resonator height (not shown). Interestingly, the lower limit appears to coincide with the region where A_2 and B_2 become more pronounced (Fig. 7a,b). This suggests that, once the MQ and ED content of M2 becomes significant, the MQ and ED anapoles can no longer be tuned independently from the EQ and MD ones, which constituted the general strategy to design HA in nanocylinders.

Next, we study the possibility to realize HA in truncated cones for conicity close to 1 (Fig. 8). Keeping the bottom radius and the height constant, we perform calculations of the total SCS for conicities in the range between 1 (perfect cone) and 0.5 (Fig. 8a). Our simulations reveal the existence of regions with strongly suppressed SCS (white square in Fig. 8a). Figure 8b displays the multipole decomposition for a nanocone with conicity 0.88. A HA can be seen to form due to the overlap between the ED and EQ anapoles, and the spectral proximity of MD and MQ anapoles. For the example at hand, scattering is suppressed by approximately 8 times the average SCS in the visible range. In the wavelength featuring the lowest SCS the scatterer is virtually transparent to the incident plane wave, as demonstrated in the field profile shown in Fig. 8c. The incident plane wave is seen to propagate undistorted by the cone. Although significant, the result leaves room for improvement. More intensive multiparameter searches can lead to a closer overlap between the four anapoles, and an even more pronounced scattering suppression.

The study in this section reveals the strong effect that small perturbations in conicity can have in the resonances responsible for the HA, since they effectively break the underlying symmetry, and render previously closed channels open, which leads to additional interactions between the modes. The knowledge of these can be important for future applications that benefit from the exotic properties of HA, for instance, metasurface engineering, sensing, etc. Furthermore, we have demonstrated, for the first time, the possibility to achieve HA in
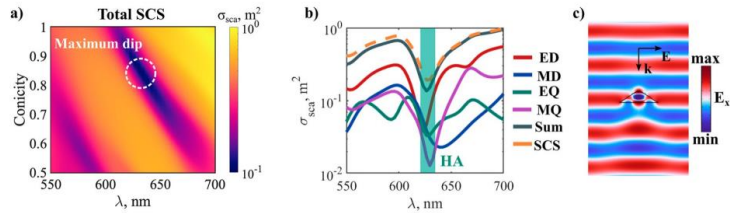
Figure 8. (**a**) Evolution of the total SCS near the HA for cone. The white-dashed circle highlights the region with the strongest scattering suppression in the parameter range considered. (**b**) Multipole decomposition of the SCS for a truncated nanocone with conicity 0.88, lying within the region of maximum scattering suppression shown in (**a**). The green-shaded area indicates the spectral range with the maximum scattering suppression (approximately 8 times less than the average SCS in the visible). (**c**) x-component of the electric field when illuminating the nanocone with an x-polarized plane wave at a wavelength of 625 nm, corresponding to the HA. The geometrical parameters can be found in section S3 of the Supplementary Information. The experimental dispersion data for a-Si is shown in Supplementary Fig. S1.

nanocones. In this way, we have expanded the library of all-dielectric nanostructures that support HA, beyond cylinders[33] and ellipsoids[36]. Once again, cones present themselves as a simple, fabrication-friendly platform for the implementation of multipolar interference effects.

Superscattering regime

In the last section, we introduce the superscattering effect. In contrast to the hybrid anapole this effect concerns scattering enhancement from a subwavelength particle. This unique regime has already found a plethora of emerging applications, such as, e.g. sensing[78], energy harvesting[79], radar deception[80], etc. To enhance scattering, it is generally believed that one needs to spectrally overlap the resonant frequencies of several QNMs scattering to different multipoles[37]. It follows from a simple geometry tuning where the thicknesses of core–shell structures were optimized to precisely bring modes together. Since the structure retains spherical symmetry, no multipole mixing is allowed, and thus there is no interaction between the different QNMs. Several other works followed on the same foot-steps; the superscattering regime has been investigated in a variety of structures retaining spherical symmetry[39,58,81–83] and was recently confirmed experimentally in the microwave frequency range[84].

The generally accepted definition of superscattering is as follows[37]: the total scattering cross-section of a resonator must exceed (by far) the maximum scattering cross-section of a dipolar particle with spherical symmetry[37]. The maximum contribution of a multipolar channel to the scattering for the specified resonator can be formulated as [37,85],

$$C_{max}^l = \frac{2l+1}{2\pi}\lambda^2,$$ (42)

where l is the total angular momentum and λ is the wavelength. Thus, for the first order multipoles (electric and magnetic dipoles) the maximum cross-section reduces to

$$C_{max}^p = \frac{3}{2\pi}\lambda^2,$$ (43)

Hereafter we refer to this limitation as the dipolar maximum for the spherically symmetric scatterer or the DM as an abbreviation. Hence, superscattering corresponds to the condition $C_{max} >> C_{max}^p$.

Recently, it has been noticed that departing from the spherical scatterer to a scatterer lacking a rotation and/or a reflection symmetry, this bound no longer holds[85]. Therefore, the scattering maxima of the multipoles are no longer limited by equation (42). In fact, to our knowledge, in a scatterer of arbitrary size and shape, the contribution of a multipole to the scattering cross-section is not bounded[50]. In the literature, however, the scattering limitations defined for spherical scatterers remain as a benchmark for the superscattering occurrence. Henceforth, we are normalizing the scattering by the dipolar channel maxima defined in equation (43) to establish consistent comparisons for the scattering enhancement in different setups.

In our recent work[85], we have suggested and experimentally demonstrated a new paradigm to achieve superscattering. It benefits from the vastly growing fields of non-Hermitian physics. Indeed, it has been established that subwavelength open-cavity resonators support QNMs that may interact and collectively lead to a plethora of light-matter interactions effects such as enhanced directionality or broadband scattering.

We have shown[85] starting from a spherical resonator supporting two QNMs that radiate independently to two multipolar channels of different order but equal parity, a fine tuning of the vertical and/or the horizontal radius (i.e., deforming the sphere into a spheroid) results in increasing scattering on a certain multipole so that it exceeds the limitation introduced in equation (42). It also proves that breaking the fully symmetric structure, in this case defined by the sphere, into an axisymmetric structure such as the ellipsoid may lead to strong coupling
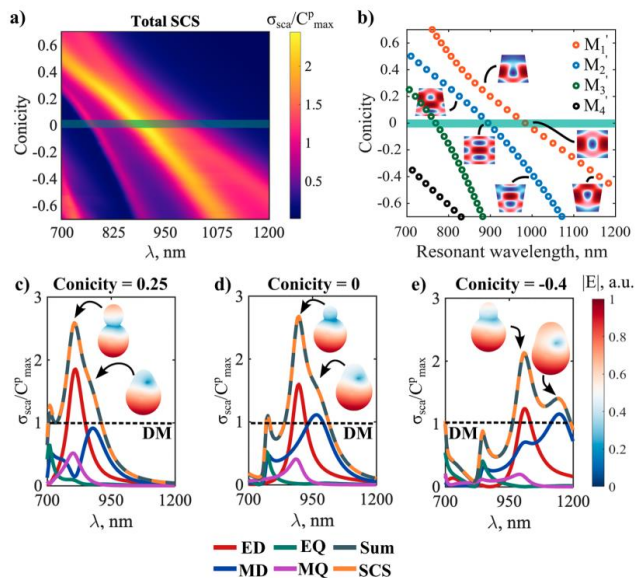
13

84

Figure 9. Evolution of the superscattering features as a function of conicity and wavelength. (**a**) Normalized total scattering cross-section of the perturbed cone under normal incidence plane wave excitation. (**b**) Resonant wavelengths of the QNMs (M_1'–M_4') as a function of the conicity. Insets define modes inner fields at three selected conicities (red—more intense field, blue—less intense field). Cones height and bottom radius considered constant with values (500 nm) and (100 nm), respectively. The cones top radius was modified with constant step size in the range (30–170 nm), while the material is considered dispersionless ($n = 3.45$) for calculations simplicity reasons. (**c**–**e**) Multipole decomposition of the normalized total scattering cross-section for the three selected conicities in (**a**). Scattering patterns at the peaks of the electric and magnetic dipoles resonances are inserted for each case. The dashed lines point to the dipolar channel scattering maxima in the case of spherical symmetric resonator (DM). Multipolar channels that contribute more than the DM are superscattering.

between two QNMs and furthermore allows controlling the multipolar character of the scattered wave (i.e. its far field characteristics). Thus, for the first time the concept of super multipoles was introduced. This newly suggested pathway to superscattering opens uncharted territories for designing resonators that capture incident photons in an unusually large area. Compared to core–shell particles where superscattering can be achieved only through the accidental overlapping of modes, scattering of reduced symmetry resonators can be enhanced both accidentally (spectrally tuning the resonance frequencies of two noninteracting QNMs) or by carefully tailoring the interference of coupled QNMs.

As emphasized in the previous sections, the tuning of the conicity offers more degrees of freedom in controlling the radiation patterns of the QNMs that are unavailable for scatterers with cylindrical symmetry. Lack of the reflection symmetry in conical geometries allows for interference between modes with unequal parities. This additional degree of freedom has an important consequence on realizing super multipoles as we later explain.

Figure 9a displays the total scattering cross-section (Eq. (43)) as a function of the conicity and the wavelength. To reduce the computational complexity, we again assume dispersionless Si materials similarly to the setup described in the previous section. Cone's geometrical parameters are enlisted in the figure caption, we here selected a subwavelength cone in the visible and near-infrared region as a practical low-loss superscatterer structure. It is apparent that the normalized scattering exceeds by more than double the DM in the specified range. One can also observe that the now presented "superscattering" broadens while tuning conicity with multiple appreciable superscattering peaks. Noteworthily, the normalization factor (the DM) is not a function of the geometry, therefore, one can assume that the value of superscattering can be readily increased by considering factors of geometry along with the operating wavelength range and the material composition of the resonator.

85
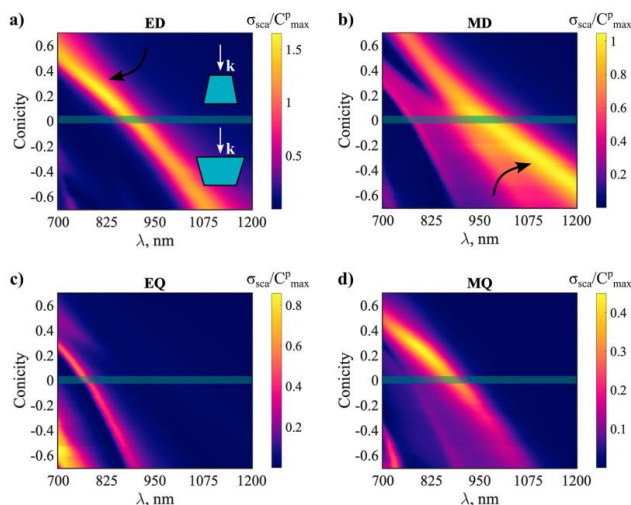
Figure 10. The multipole contributions to total scattering of the cone setup presented in Fig. 9 with ED (**a**), MD (**b**), EQ (**c**), and MQ (**d**). The shaded green line corresponds to the unperturbed cylinder (conicity = 0). The two black arrows point to the regions of maximum of electric dipole and magnetic dipole contributions in the lower and upper branches of modes M_1' and M_2' interference. Material is considered dispersionless ($n = 3.45$) for calculations simplicity reasons.

The resonance frequencies of the QNMs in the spectral range of interest are shown in Fig. 9b as a function of conicity. The QNMs are labeled as M_1'–M_4'. It can be noticed that the cylinder (conicity = 0, marked by the shaded green line) supports the conventional magnetic dipole mode M_1' at the resonant wavelength 983 nm and a super-ED mode M_2' at resonant wavelength 895 nm[85]. The insets in Fig. 9b show the internal field distribution of the two modes, (detailed field profiles inside and in the vicinity of the cylinder are shown in supplementary figure S2). M_1' and M_2' avoid the crossing, and redshift as the cone volume increases (for an increased conicity). We consider these two QNMs as the focus of our investigation to alter and potentially enhance scattering.

From Fig. 9d, it can be appreciated that the two even multipolar channels, the electric dipole and the magnetic quadrupole, contribute to the scattering at spectral points coinciding with the resonant wavelength of M_2'. We notice that the electric dipole is showing superscattering where it exceeds the DM by about 1.5 times. The latter are closely related to the super dipole resonances studied in Ref[85]. Similarly, M_1' and M_3' appear to radiate on the odd multipolar channels, the magnetic dipole and the electric quadrupole, respectively. The magnetic dipole displays a scattering cross-section with values slightly above the DM. Summarizing, mode M_2' is even and scatters as a combination of electric dipole and magnetic quadrupole moments, while odd QNMs M_1' and M_3' are odd and scatter as a combination of magnetic dipole and electric quadrupole moments.

We show in Fig. 9c and d cases for conicity 0.25 and −0.4, respectively. In the first, the electric dipole cross-section is now almost double the DM, while the magnetic dipole is reduced below that level. When decreasing the upper radius of the cavity, the resonant wavelengths of QNMs M_1' and M_2' are blueshifted [Fig. 9b]. As a result, the multipole resonances are also blueshifted [Fig. 9c]. The opposite occurs when increasing the upper radius, [Fig. 9e]. However, a second magnetic dipole scattering peak is now observable, overlapping with the electric dipole and magnetic quadrupole peaks. Meanwhile, we show for all the three cases the scattering patterns at the distinguished dipolar scattering peaks. The scattering is more directive when both dipoles are present and comparable in values, and it takes obviously a dipolar scattering signature when either of the dipoles is dominant. To have a clearer picture of the mechanism at play that controls the position and amplitudes of the superscattering multipolar channels, we show in Fig. 10 the scattering evolution of the first four multipoles as a function of the conicity and the wavelength.

When compared to the QNMs' dispersion in Fig. 9b, we notice that the power scattered by the electric dipole is mainly attributed to mode M_2' while it appears that modes M_1'–M_3' are able to scatter through the magnetic dipole channel. For this reason, we see that the magnetic dipole appears with two peaks on the scattering spectrum where it is especially noticeable for negative higher conicities (conicity < − 0.2). Modes M_3' and M_4' across

86

the parametric space are radiating on the electric quadrupole channel. One can notice also that the magnetic quadrupole channel is mostly apparent aligning with the electric dipole peak scattering. Although the quadrupolar channels are not superscattering within themselves in the current design, they have important contributions to the total scattering cross-section.

It can be concluded that modes M_1' and M_2' of the cylinder are allowed to interfere with each other after breaking the vertical mirror symmetry i.e., with conicity $\neq 0$. This implies that both modes are now able to radiate on the even and odd parity multipolar channels. One important result of this interference is an increase of the electric dipolar superscattering with almost doubling the DM at small conicities. We can also appreciate that M_2' start to scatter on the magnetic dipolar channel in the bigger conicities region of the parametric figure. Considering this mode is originally even parity in the cylinder, it becomes hybrid when tuning conicity in the sense that it scatters as a mixture of electric and magnetic dipole moments. Therefore, a single QNM in the conical geometry is able to drive opposite parity multipolar channels to superscattering regime. This type of superscattering cannot be obtained in cylindrical resonators without spectrally overlapping the resonant wavelengths of at least two QNMs. Such hybridization of superscattering channels is particularly important for the superscattering effect since it also decisively impacts the directivity of the overall scattering. This means, that it can be utilized to enhance forward or the backward scattering upon prerequisites. Another important consequence of M_1'/M_2' interference is the broadening of the superscattering. This can be seen in both the lower and upper regions of the interference.

The above systematic exploration of the superscattering achievable through designing conical geometry has revealed a new approach to obtain desired outcomes in superscattering features. We focused on tuning two modes (M_1' and M_2') of a cylinder that are in spectral proximity, sufficiently confined within the resonator domain, and with an unequal parity. This strategy can be sufficient but is not necessary to achieve superscattering in the geometry under consideration. However, the investigated mechanism highlights important features of superscattering in a cone, namely, (i) the possibility to exceed the DM with the help of the novel supermultipoles and (ii) the mixed character of the involved QNMs, which scatter as a combination of even and odd multipoles, unlike in spheres or cylinders. Alternatively, other strategies remain possible as well, however with optimized conical structure in this work we believe that several important aspects of the superscattering conical geometry have been revealed.

Thus far we have shown a remarkable control over scattering, due to the design flexibility and symmetry rules governing the conical geometry. Tuning a single geometrical parameter (in this case—the conicity) can result in strong coupling between two QNMs of opposite parity, as was previously shown very recently[53]. Remarkably, this mechanism can be utilized to enhance scattering and manipulate the radiation pattern at the resonance to render it more directive. It indeed provides a plethora of opportunities to optimize truncated cones for applications in optics.

Conclusion

In this work, we have proposed the conical geometry as a universal platform for obtaining many important optical effects that are of interest in nanophotonics. For the first time, all known Kerker effects were obtained on one scatterer shape for a real dispersion of the refractive index of silicon. It was found that the recently discovered non-scattering hybrid anapole regime can also be obtained in conical nanoparticles, in addition to elliptical and cylindrical ones. It is shown how, by changing the geometric parameters, it is possible to adjust the anapole regime of different multipoles and obtain a hybrid anapole regime. We also studied the possibility of obtaining superscattering, the effect inverse to the anapole regime, in conical particles, showing the dependence on the geometry of the scatterer. This research takes a step towards nanophotonics of more complex shapes with the ability to fine-tune the effects that can be obtained on a single shape of a nano-scatterer. This research significantly reduces the cost of developing photonic devices and opens up new horizons for the practical application of the next-generation photonics. This work can find its application in various fields of research, for example, to create various dielectric nanoantennas in the form of a chain of resonators in comparison with chains of spheres or cylinders, or for metasurfaces based on which it will be possible to obtain a number of optical effects that were previously inaccessible.

Data availability

All data generated or analysed during this study are included in this published article [and its supplementary information files].

References

1. Xu, K., Fang, M. & Huang, Z. Compact unidirectional laser based on all-dielectric metasurface with high quality factor. *IEEE Photonics J.* **13**, 1–9 (2021).
2. Sain, B., Meier, C. & Zentgraf, T. Nonlinear optics at all-dielectric nanoantennas and metasurfaces. *ArXiv* **1**, 1–14 (2020).
3. Krasnok, A. E., Miroshnichenko, A. E., Belov, P. A. & Kivshar, Y. S. All-dielectric optical nanoantennas. *Opt. Express* **20**, 20599 (2012).
4. Zouros, G. P., Kolezas, G. D., Fikioris, G. & Tsitsas, N. L. End-fire all-anisotropic transition metal dichalcogenide nanoantennas. *Phys. Rev. B* **104**, 245432 (2021).
5. Tian, Y., Li, Z., Xu, Z., Wei, Y. & Wu, F. High transmission focusing lenses based on ultrathin all-dielectric Huygens' metasurfaces. *Opt. Mater. (Amst)* **109**, 110358 (2020).
6. Mitrofanov, O. *et al.* Terahertz detectors based on all-dielectric photoconductive metasurfaces. In *Terahertz Emitters, Receivers, and Applications X* Vol. 36 (eds Razeghi, M. *et al.*) (2019).

87

7. Terekhov, P. D. *et al*. Broadband forward scattering from dielectric cubic nanoantenna in lossless media. *Opt. Express* **27**, 10924 (2019).
8. Terekhov, P. D. *et al*. Magnetic octupole response of dielectric quadrumers. *Laser Photon. Rev.* **14**, 1900331 (2020).
9. Gueddida, A. *et al*. Tubular phononic crystal sensor. *J. Appl. Phys.* **130**, 10 (2021).
10. Chebykin, A. V., Orlov, A. A., Shalin, A. S., Poddubny, A. N. & Belov, P. A. Strong purcell effect in anisotropic ε-near-zero metamaterials. *Phys. Rev. B* **91**, 205126 (2015).
11. Kozlov, V., Filonov, D., Shalin, A. S., Steinberg, B. Z. & Ginzburg, P. Asymmetric backscattering from the hybrid magneto-electric meta particle. *Appl. Phys. Lett.* **109**, 203503 (2016).
12. Terekhov, P. D. *et al*. Enhanced absorption in all-dielectric metasurfaces due to magnetic dipole excitation. *Sci. Rep.* **9**, 1–9 (2019).
13. Kostina, N. *et al*. Optical binding via surface plasmon polariton interference. *Phys. Rev. B* **99**, 1–11 (2019).
14. Canós Valero, A. *et al*. Nanovortex-driven all-dielectric optical diffusion boosting and sorting concept for lab-on-a-chip platforms. *Adv. Sci.* **7**, 1903049 (2020).
15. Novitsky, D. V., Karabchevsky, A., Lavrinenko, A. V., Shalin, A. S. & Novitsky, A. V. PT symmetry breaking in multilayers with resonant loss and gain locks light propagation direction. *Phys. Rev. B* **98**, 125102 (2018).
16. Vestler, D. *et al*. Circular dichroism enhancement in plasmonic nanorod metamaterials. *Opt. Express* **26**, 17841 (2018).
17. Konoplev, G. *et al*. Label-free physical techniques and methodologies for proteins detection in microfluidic biosensor structures. *Biomedicines* **10**, 1–60 (2022).
18. Ermolovich, E. A., Ivannikov, A. L., Khayrutdinov, M. M., Kongar-Syuryun, C. B. & Tyulyaeva, Y. S. Creation of a nanomodified backfill based on the waste from enrichment of water-soluble ores. *Materials* **15**, 3689 (2022).
19. Evlyukhin, A. B. & Chichkov, B. N. Multipole decompositions for directional light scattering. *Phys. Rev. B* **100**, 125415 (2019).
20. Alaee, R., Rockstuhl, C. & Fernandez-Corbaton, I. An electromagnetic multipole expansion beyond the long-wavelength approximation. *Opt. Commun.* **407**, 17–21 (2018).
21. Kerker, M., Wang, D. S. & Giles, C. L. Electromagnetic scattering by magnetic spheres. *J. Opt. Soc. Am.* **73**, 765–767 (1983).
22. Zhang, X., Li, J., Donegan, J. F. & Bradley, A. L. Constructive and destructive interference of kerker-type scattering in an ultrathin silicon Huygens metasurface. *Phys. Rev. Mater.* **4**, 1–6 (2020).
23. Fan, K., Shadrivov, I. V., Miroshnichenko, A. E. & Padilla, W. J. Infrared all-dielectric kerker metasurfaces. *Opt. Express* **29**, 10518 (2021).
24. Chen, M., Kim, M., Wong, A. M. H. & Eleftheriades, G. V. Huygens' metasurfaces from microwaves to optics: A review. *Nanophotonics* **7**, 1207–1231 (2018).
25. Alaee, R., Filter, R., Lehr, D., Lederer, F. & Rockstuhl, C. A generalized kerker condition for highly directive nanoantennas. *Opt. Lett.* **40**, 2645 (2015).
26. Liu, W. & Kivshar, Y. S. Generalized kerker effects in nanophotonics and meta-optics. *ArXiv* **26**, 274–284 (2017).
27. Hesari-Shermeh, M., Abbasi-Arand, B. & Yazdi, M. Generalized kerker's conditions under normal and oblique incidence using the polarizability tensors of nanoparticles. *Opt. Express* **29**, 647 (2021).
28. Barhom, H. *et al*. Biological kerker effect boosts light collection efficiency in plants. *Nano Lett.* **19**, 7062–7071 (2019).
29. Shamkhi, H. K. *et al*. Transverse scattering and generalized kerker effects in all-dielectric mie-resonant metaoptics. *Phys. Rev. Lett.* **122**, 193905 (2019).
30. Shamkhi, H. K. *et al*. Transparency and perfect absorption of all-dielectric resonant metasurfaces governed by the transverse kerker effect. *Phys. Rev. Mater.* **3**, 1–10 (2019).
31. Terekhov, P. D. *et al*. Multipole analysis of dielectric metasurfaces composed of nonspherical nanoparticles and lattice invisibility effect. *Phys. Rev. B* **99**, 4 (2019).
32. Miroshnichenko, A. E. *et al*. Nonradiating anapole modes in dielectric nanoparticles. *Nat. Commun.* **6**, 1–8 (2015).
33. Canós Valero, A. *et al*. Theory, observation, and ultrafast response of the hybrid anapole regime in light scattering. *Laser Photon. Rev.* **15**, 2100114 (2021).
34. Kuznetsov, A. V. *et al*. Transparent hybrid anapole metasurfaces with negligible electromagnetic coupling for phase engineering. *Nanophotonics* **10**, 4385–4398 (2021).
35. Zanganeh, E. *et al*. Nonradiating sources for efficient wireless power transfer. *Nanophotonics* **10**, 4399–4408 (2021).
36. Ospanova, A. K., Basharin, A., Miroshnichenko, A. E. & Luk'yanchuk, B. Generalized hybrid anapole modes in all-dielectric ellipsoid particles [Invited]. *Opt. Mater. Express* **11**(1), 23 (2021).
37. Ruan, Z. & Fan, S. Superscattering of light from subwavelength nanostructures. *Phys. Rev. Lett.* **105**, 1–4 (2010).
38. Krasikov, S. D. *et al*. Superscattering for non-spherical objects. *J. Phys. Conf. Ser.* **2015**, 012073 (2021).
39. Liu, W., Lei, B., Shi, J. & Hu, H. Unidirectional superscattering by multilayered cavities of effective radial anisotropy. *Sci. Rep.* **6**, 1–9 (2016).
40. Shcherbinin, V. I., Fesenko, V. I., Tkachova, T. I. & Tuz, V. R. Superscattering from subwavelength corrugated cylinders. *Phys. Rev. Appl* **13**, 024081 (2020).
41. Patoux, A. *et al*. Challenges in nanofabrication for efficient optical metasurfaces. *Sci. Rep.* **11**, 1–12 (2021).
42. Kim, Y., Yang, H. & Oh, J. H. Simple fabrication of highly sensitive capacitive pressure sensors using a porous dielectric layer with cone-shaped patterns. *Mater. Des.* **197**, 109203 (2021).
43. Toliopoulos, D. *et al*. Fabrication of spectrally sharp Si-based dielectric resonators: Combining etaloning with Mie resonances. *Opt. Express* **28**, 37734 (2020).
44. Zhu, T. *et al*. All-dielectric colored truncated cone metasurfaces with silicon Mie magnetic resonators. *Appl. Opt.* **58**, 6742 (2019).
45. Hong, J. *et al*. Absorptive metasurface color filters based on hyperbolic metamaterials for a CMOS image sensor. *Opt. Express* **29**, 3643 (2021).
46. Milichko, V. A. *et al*. Solar photovoltaics: Current state and trends. *Phys. Usp.* **59**, 727–772 (2016).
47. Geintz, Y. E., Zemlyanov, A. A. & Panina, E. K. Optics and spectroscopy: Photonic nanonanojets from nonspherical dielectric microparticles. *Russ. Phys. J.* **58**, 904–910 (2015).
48. Gladishev, S., Frizyuk, K. & Bogdanov, A. Symmetry analysis and multipole classification of eigenmodes in electromagnetic resonators for engineering their optical properties. *Phys. Rev. B* **102**(7), 075103 (2020).
49. Jackson, J. D. (1962) Classical electrodynamics.
50. Krasikov, S. *et al*. Multipolar engineering of subwavelength dielectric particles for scattering enhancement. *Phys. Rev. Appl.* **15**, 1 (2021).
51. Lalanne, P., Yan, W., Vynck, K., Sauvan, C. & Hugonin, J. P. Light interaction with photonic and plasmonic resonances. *Laser Photon. Rev.* **12**, 1–38 (2018).
52. Wu, T., Baron, A., Lalanne, P. & Vynck, K. Intrinsic multipolar contents of nanoresonators for tailored scattering. *Phys. Rev. A (Coll Park)* **101**, 1–5 (2020).
53. Canós Valero, A., Bobrovs, V., Redka, D., Shalin, A. S. & Kivshar, Y. (2022) Magnetoelectric exceptional points in isolated all-dielectric nanoparticles. *ArXiv*
54. Luk'yanchuk, B. S., Voshchinnikov, N. V., Paniagua-Domínguez, R. & Kuznetsov, A. I. Optimum forward light scattering by spherical and spheroidal dielectric nanoparticles with high refractive index. *ACS Photonics* **2**, 993–999 (2015).
55. Fu, Y. H., Kuznetsov, A. I., Miroshnichenko, A. E., Yu, Y. F. & Luk'yanchuk, B. Directional visible light scattering by silicon nanoparticles. *Nat. Commun.* **4**, 1–6 (2013).

88

56. Person, S. *et al.* Demonstration of zero optical backscattering from single nanoparticles. *Nano Lett.* **13**, 1806–1809 (2013).
57. Liu, W. & Kivshar, Y. S. Generalized kerker effects in nanophotonics and meta-optics [Invited]. *Opt. Express* **26**, 13085 (2018).
58. Liu, W. Ultra-directional super-scattering of homogenous spherical particles with radial anisotropy. *Opt. Express* **23**, 14734 (2015).
59. Liu, W. & Kivshar, Y. S. Multipolar interference effects in nanophotonics. *Philos. Trans. Royal Soc. A: Math. Phys. Eng. Sci.* **375**(2090), 20160317 (2017).
60. Terekhov, P. D. *et al.* Multipolar response of nonspherical silicon nanoparticles in the visible and near-infrared spectral ranges. *Phys. Rev. B* **96**, 1–8 (2017).
61. Evlyukhin, A. B., Fischer, T., Reinhardt, C. & Chichkov, B. N. Optical theorem and multipole scattering of light by arbitrarily shaped nanoparticles. *Phys. Rev. B* **94**, 1–7 (2016).
62. Zhang, X. & Bradley, A. L. Wide-angle invisible dielectric metasurface driven by transverse kerker scattering. *Phys. Rev. B* **103**, 1–8 (2021).
63. Geffrin, J. M. *et al.* Magnetic and electric coherence in forward- and back-scattered electromagnetic waves by a single dielectric subwavelength sphere. *Nat. Commun.* **3**, 1171 (2012).
64. Bukharin, M. M. *et al.* Transverse kerker effect in all-dielectric spheroidal particles. *Sci. Rep.* **12**, 7997 (2022).
65. Liu, M. Q. & Zhao, C. Y. Lattice invisibility effect based on transverse Kerker scattering in 1D metalattices. *J. Phys. D Appl. Phys.* **52**(49), 495107 (2019).
66. Dobrykh, D. *et al.* Multipole engineering for enhanced backscattering modulation. *Phys. Rev. B* **102**, 1–6 (2020).
67. Liu, C. *et al.* Characteristics of electric quadrupole and magnetic quadrupole coupling in a symmetric silicon structure. *New J. Phys.* **22**(2), 023018 (2020).
68. Liu, W. *et al.* Ultra-directional forward scattering by individual core-shell nanoparticles. *Opt. Express* **22**, 16178 (2014).
69. Baryshnikova, K. V., Smirnova, D. A. & Luk'yanchukKivshar, B. S. Y. S. Optical anapoles in nanophotonics and meta-optics. *Adv. Opt. Mater.* **1801350**, 1–13 (2019).
70. Luk'yanchuk, B., Paniagua-Domínguez, R., Kuznetsov, A. I., Miroshnichenko, A. E. & Kivshar, Y. S. Hybrid anapole modes of high-index dielectric nanoparticles. *Phys. Rev. A (Coll Park)* **95**, 1–8 (2017).
71. Grinblat, G., Li, Y., Nielsen, M. P., Oulton, R. F. & Maier, S. A. Enhanced third harmonic generation in single germanium nanodisks excited at the anapole mode. *Nano Lett.* **16**, 4635–4640 (2016).
72. Wang, J. & Du, J. Plasmonic and dielectric metasurfaces: Design fabrication and applications. *Appl. Sci.* **6**, 239 (2016).
73. Su, V.-C., Chu, C. H., Sun, G. & Tsai, D. P. Advances in optical metasurfaces: Fabrication and applications [Invited]. *Opt. Express* **26**, 13148 (2018).
74. Powell, D. A. Interference between the modes of an all-dielectric meta-atom. *Phys. Rev. Appl.* **7**, 1–13 (2017).
75. Colom, R., McPhedran, R., Stout, B. & Bonod, N. Modal analysis of anapoles, internal fields, and Fano resonances in dielectric particles. *J. Opt. Soc. Am. B* **36**, 2052 (2019).
76. Zhang, H. & Miller, O. D. (2020) Quasinormal coupled mode theory.
77. Hsu, C. W., Delacy, B. G., Johnson, S. G., Joannopoulos, J. D. & Soljačić, M. Theoretical criteria for scattering dark states in nano-structured particles. *Nano Lett.* **14**, 2783–2788 (2014).
78. Xu, W., Xie, L. & Ying, Y. Mechanisms and applications of terahertz metamaterial sensing: A review. *Nanoscale* **9**, 13864–13878. https://doi.org/10.1039/c7nr03824k (2017).
79. Green, M. A. & Pillai, S. Harnessing plasmonics for solar cells. *Nat. Photonics* **6**, 130–132 (2012).
80. Kozlov, V., Vovchuk, D. & Ginzburg, P. Broadband radar invisibility with time-dependent metasurfaces. *Sci. Rep.* **11**, 14187 (2021).
81. Ruan, Z. & Fan, S. Design of subwavelength superscattering nanospheres. *Appl. Phys. Lett.* **98**, 96–99 (2011).
82. Huang, Y. & Gao, L. Superscattering of light from core-shell nonlocal plasmonic nanoparticles. *J. Phys. Chem. C* **118**, 30170–30178 (2014).
83. Lepeshov, S., Krasnok, A. & Alù, A. Nonscattering-to-superscattering switch with phase-change materials. *ACS Photonics* **6**, 2126–2132 (2019).
84. Qian, C. *et al.* Experimental observation of superscattering. *Phys. Rev. Lett.* **122**, 63901 (2019).
85. Valero, A. C. *et al.* (2021).Superscattering empowered by bound states in the continuum. *ArXiv*

Acknowledgements

Author contributions

A.K. wrote the main manuscript text and prepared figures. A.C.V. wrote the chapter "Quasinormal Modes", made a significant contribution to the chapter "Non-scattering regimes: anapole and hybrid anapole". A.C.V. and H.S. made a significant contribution to the chapter "Superscattering regime". All authors reviewed the manuscript.

Competing interests

The authors declare no competing interests.

Additional information

Supplementary Information The online version contains supplementary material available at https://doi.org/10.1038/s41598-022-25542-2.

Correspondence and requests for materials should be addressed to A.V.K. or A.S.S.

Reprints and permissions information is available at www.nature.com/reprints.

Publisher's note Springer Nature remains neutral with regard to jurisdictional claims in published maps and institutional affiliations.

nature portfolio

18

89

90

Special scattering regimes for conical all-dielectric nanoparticles

Alexey V. Kuznetsov[1,2,3,*], Adrià Canós Valero[3,4], Hadi K. Shamkhi[3,5], Pavel Terekhov[6], Xingjie Ni[6], Vjaceslavs Bobrovs[2], Mikhail V. Rybin[3], Alexander S. Shalin[1,2,7,8,9*]

[1]Moscow Institute of Physics and Technology, Center for Photonics and 2D Materials, Dolgoprudny, 141700, Russia

[2]Riga Technical University, Institute of Telecommunications, Riga, 1048, Latvia

[3]ITMO University, Faculty of Physics, St. Petersburg, 197101, Russia

[4]University of Graz, and NAWI Graz, Institute of Physics, Graz, 8010, Austria

[5]A*STAR (Agency for Science, Technology and Research), Institute of Materials Research and Engineering, 138634, Singapore

[6]The Pennsylvania State University, Department of Electrical Engineering, Pennsylvania, 16802, United States

[7]Moscow State University, Faculty of Physics, Moscow, 119991, Russia

[8]Suzhou City University, School of Optical and Electronic Information, Suzhou, 215104, China

[9]Kotelnikov Institute of Radio Engineering and Electronics, Ulyanovsk, 432000, Russia

*alexey.kuznetsov98@gmail.com

*alexandesh@gmail.com

S1. Experimental Dispersion of amorphous Si
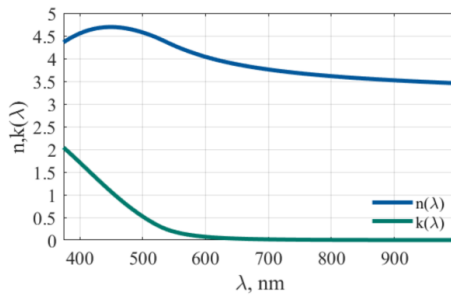
Supplementary Figure S1. Real (n) and imaginary (k) parts of the experimentally measured refractive index of amorphous silicon (aSi) employed in our study, as a function of wavelength.

S2. Conditions for Generalized Kerker effects

In the main part of the article the conditions for the forward Kerker effect were obtained. We used formula (6) in main part of manuscript and vanished the terms that do not participate in the effect.

ED + MD:
$$C_{sca}^{total} = C_{sca}^{p} + C_{sca}^{m} = \frac{k^4}{6\pi\varepsilon_0^2 |\mathbf{E}_{inc}|^2}\left[|p_x|^2 + \left|\frac{m_y}{c}\right|^2\right] \qquad (S1)$$

ED + EQ:
$$C_{sca}^{total} = C_{sca}^{p} + C_{sca}^{Q^e} = \frac{k^4}{6\pi\varepsilon_0^2 |\mathbf{E}_{inc}|^2}\left[|p_x|^2 + \frac{1}{120}\left(\left|kQ_{xz}^e\right|^2 + \left|kQ_{zx}^e\right|^2\right)\right] \qquad (S2)$$

MD + MQ:
$$C_{sca}^{total} = C_{sca}^{m} + C_{sca}^{Q^m} = \frac{k^4}{6\pi\varepsilon_0^2 |\mathbf{E}_{inc}|^2}\left[\left|\frac{m_y}{c}\right|^2 + \frac{1}{120}\left(\left|\frac{kQ_{yz}^m}{c}\right|^2 + \left|\frac{kQ_{zy}^m}{c}\right|^2\right)\right] \qquad (S3)$$

EQ + MQ:
$$C_{sca}^{total} = C_{sca}^{Q^e} + C_{sca}^{Q^m} = \frac{k^4}{6\pi\varepsilon_0^2 |\mathbf{E}_{inc}|^2}\left[\frac{1}{120}\left(\left|kQ_{xz}^e\right|^2 + \left|kQ_{zx}^e\right|^2 + \left|\frac{kQ_{yz}^m}{c}\right|^2 + \left|\frac{kQ_{zy}^m}{c}\right|^2\right)\right] \qquad (S4)$$

We proceed in a similar way with the formula (9) in main part of manuscript for the scattering cross-section of multipoles ($n_z = -1$, $E_x^{bwsc} = 0$, because forward scattering only).

ED + MD:
$$E_x^{bwsc} = \frac{k^2}{4\pi\varepsilon_0}\frac{e^{ikr}}{r}\left\{p_x - \frac{1}{c}m_y\right\} = 0 \qquad (S5)$$

ED + EQ:
$$E_x^{bwsc} = \frac{k^2}{4\pi\varepsilon_0}\frac{e^{ikr}}{r}\left\{p_x + \frac{ik}{6}Q_{xz}^e\right\} = 0 \qquad (S6)$$

MD + MQ:
$$E_x^{bwsc} = \frac{k^2}{4\pi\varepsilon_0}\frac{e^{ikr}}{r}\left\{-\frac{1}{c}m_y - \frac{ik}{6c}Q_{yz}^m\right\} = 0 \qquad (S7)$$

EQ + MQ:
$$E_x^{bwsc} = \frac{k^2}{4\pi\varepsilon_0}\frac{e^{ikr}}{r}\left\{\frac{ik}{6}Q_{xz}^e - \frac{ik}{6c}Q_{yz}^m\right\} = 0 \qquad (S8)$$

Now we can take the multipoles moments from the formulas and substitute them into the formulas for the scattering cross-section to obtain conditions in the absence of backscattering.

ED + MD:
$$C_{sca}^{total} = C_{sca}^{p} + C_{sca}^{m} = \frac{k^4}{6\pi\varepsilon_0^2 |\mathbf{E}_{inc}|^2}\left[\left|\frac{m_y}{c}\right|^2 + \left|\frac{m_y}{c}\right|^2\right] \qquad (S9)$$

ED + EQ:
$$C_{sca}^{total} = C_{sca}^{p} + C_{sca}^{Q^e} = \frac{k^4}{6\pi\varepsilon_0^2 |\mathbf{E}_{inc}|^2}\left[\frac{1}{36}\left|-ikQ_{xz}^e\right|^2 + \frac{1}{60}\left(\left|kQ_{xz}^e\right|^2\right)\right] \qquad (S10)$$

2

MD + MQ: $\quad C_{sca}^{total} = C_{sca}^{m} + C_{sca}^{Q^m} = \dfrac{k^4}{6\pi\varepsilon_0^2 |\mathbf{E}_{inc}|^2} \left[\dfrac{1}{36} \left| -\dfrac{ikQ_{yz}^m}{c} \right|^2 + \dfrac{1}{60} \left(\left| \dfrac{kQ_{yz}^m}{c} \right|^2 \right) \right] \qquad$ (S11)

EQ + MQ: $\quad C_{sca}^{total} = C_{sca}^{Q^e} + C_{sca}^{Q^m} = \dfrac{k^4}{6\pi\varepsilon_0^2 |\mathbf{E}_{inc}|^2} \left[\dfrac{1}{60} \left(\left| \dfrac{kQ_{yz}^m}{c} \right|^2 + \left| \dfrac{kQ_{yz}^m}{c} \right|^2 \right) \right] \qquad$ (S12)

This shows how the scattering cross-sections of different multipoles must be related to each other to fulfill the conditions for the absence of backscattering. Similar calculations can be used to obtain the same values for the absence of forward scattering.

ED + MD: $\qquad\qquad\qquad \dfrac{C_{sca}^{ED}}{C_{sca}^{MD}} = 1 \qquad$ (S13)

ED + EQ: $\qquad\qquad\qquad \dfrac{C_{sca}^{ED}}{C_{sca}^{EQ}} = 1.67 \qquad$ (S14)

MD + MQ: $\qquad\qquad\qquad \dfrac{C_{sca}^{MD}}{C_{sca}^{MQ}} = 1.67 \qquad$ (S15)

EQ + MQ: $\qquad\qquad\qquad \dfrac{C_{sca}^{EQ}}{C_{sca}^{MQ}} = 1 \qquad$ (S16)

Following the same logic as for the Generalized Kerker effect, we obtain the conditions for the Transverse Kerker effect.

ED + MQ: $\qquad E_x^{bwsc} = E_x^{fwsc} = \dfrac{k^2}{4\pi\varepsilon_0} \dfrac{e^{ikr}}{r} \left\{ p_x - \dfrac{ik}{6c} Q_{yz}^m \right\} = 0 \qquad$ (S17)

MD + EQ: $\qquad \begin{cases} E_x^{bwsc} = \dfrac{k^2}{4\pi\varepsilon_0} \dfrac{e^{ikr}}{r} \left\{ -\dfrac{1}{c} m_y + \dfrac{ik}{6} Q_{xz}^e \right\} = 0 \\[3mm] E_x^{fwsc} = \dfrac{k^2}{4\pi\varepsilon_0} \dfrac{e^{ikr}}{r} \left\{ \dfrac{1}{c} m_y - \dfrac{ik}{6} Q_{xz}^e \right\} = 0 \end{cases} \qquad$ (S18)

Then

ED + MQ: $\quad C_{sca}^{total} = C_{sca}^{p} + C_{sca}^{Q^m} = \dfrac{k^4}{6\pi\varepsilon_0^2 |\mathbf{E}_{inc}|^2} \left[\dfrac{1}{36} \left| \dfrac{ikQ_{yz}^m}{c} \right|^2 + \dfrac{1}{60} \left(\left| \dfrac{kQ_{yz}^m}{c} \right|^2 \right) \right] \qquad$ (S19)

3

MD + EQ: $$C_{sca}^{total} = C_{sca}^m + C_{sca}^{Q^e} = \frac{k^4}{6\pi\varepsilon_0^2 \left|\mathbf{E}_{inc}\right|^2}\left[\frac{1}{36}\left|-ikQ_{xz}^e\right|^2 + \frac{1}{60}\left(\left|kQ_{xz}^e\right|^2\right)\right]$$ (S20)

Whence it follows that:

ED + MQ: $$\frac{C_{sca}^{ED}}{C_{sca}^{MQ}} = 1.67$$ (S21)

MD + EQ: $$\frac{C_{sca}^{MD}}{C_{sca}^{EQ}} = 1.67$$ (S22)

S3. Specific parameters of the considered effects for truncated silicon nanocones.

These data will make it easy to get any listed effect at the desired wavelength using the following simple relationships, provided that the refractive indices at these wavelengths are approximately equal:

$$\begin{cases} \dfrac{R_{top}}{R_{bottom}}n \approx \dfrac{R_{top}^*}{R_{bottom}^*}n^* \approx const \\[3mm] \dfrac{H}{\lambda}n \approx \dfrac{H^*}{\lambda^*}n^* \approx const \\[3mm] \dfrac{R}{\lambda}n \approx \dfrac{R^*}{\lambda^*}n^* \approx const \end{cases}$$ (S23)

, where the parameters without an asterisk are the parameters below and the parameters with an asterisk are the parameters to be retrieved.

	Generalized	Transverse
ED + MD	H = 140 nm R_{top} = 120 nm R_{bottom} = 90 nm λ = 779 nm	-
ED + EQ	H = 160 nm R_{top} = 100 nm R_{bottom} = 250 nm λ = 675 nm	-
ED + MQ	-	H = 420 nm

4

		$R_{top} = 130$ nm
		$R_{bottom} = 110$ nm
		$\lambda = 779$ nm
MD + EQ	-	$H = 300$ nm
		$R_{top} = 40$ nm
		$R_{bottom} = 120$ nm
		$\lambda = 617$ nm
MD + MQ	$H = 100$ nm	-
	$R_{top} = 190$ nm	
	$R_{bottom} = 140$ nm	
	$\lambda = 767$ nm	
EQ + MQ	$H = 320$ nm	-
	$R_{top} = 360$ nm	
	$R_{bottom} = 180$ nm	
	$\lambda = 815$ nm	
ED + MD + EQ + MQ	$H = 220$ nm	$H = 520$ nm
	$R_{top} = 50$ nm	$R_{top} = 55$ nm
	$R_{bottom} = 330$ nm	$R_{bottom} = 195$ nm
	$\lambda = 625$ nm	$\lambda = 900$ nm

Supplementary Table S1. Specific parameters of nano-scatterers for obtaining Kerker effects for truncated silicon nanocones.

Hybrid Anapole regime

$H = 200$ nm, $R_{top} = 40$ nm, $R_{bottom} = 340$ nm, $\lambda = 625$ nm (truncated cone)

$H = 369$ nm, $R = 127$ nm, $\lambda = 748$ nm (cylinder)

5
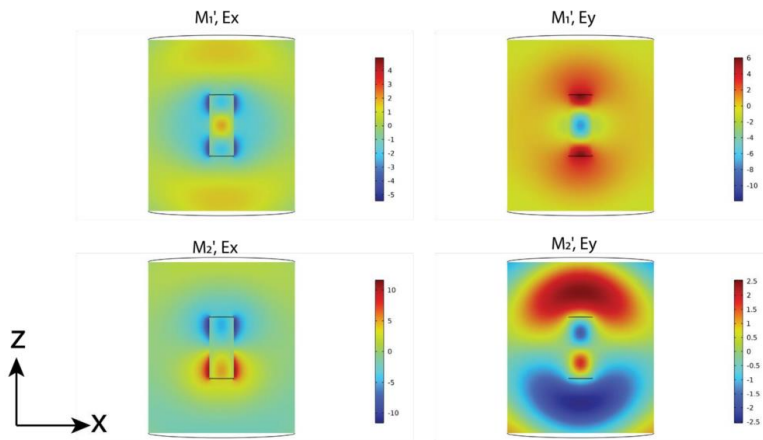
Supplementary Figure S2. QNMs M_1' and M_2' field distributions for the cylinder presented in figure 10 in the main text. The field distributions show M_1' is an even-parity mode while M_2' is an odd-parity mode.

[PAPER 3]: Optical properties of a metasurface based on silicon nanocylinders in a hybrid anapole state

Optical properties of a metasurface based on silicon nanocylinders in a hybrid Anapole state

Alexey V. Kuznetsov, Adrià Canós Valero, and Alexander S. Shalin

View Online   Export Citation

Optical Properties of a Metasurface Based on Silicon Nanocylinders in a Hybrid Anapole State

Alexey V. Kuznetsov, Adrià Canós Valero and Alexander S. Shalin

ITMO University, Lomonosova street, 9, St. Petersburg, 191002, Russia

Corresponding author: alexey.kuznetsov@metalab.ifmo.ru

Abstract. In this work, using the numerical simulation in the COMSOL Multiphysic package, we studied the optical properties of the hybrid anapole state in silicon nanocylinders and their metasurfaces. Our investigations show the possibility of creating invisible metasurfaces consisting of silicon cylinders based on the novel state. These results can be used in various fields of nanophotonics and may have important outcome in the development of various sensors and other photonic devices.

INTRODUCTION

In recent years, studies in the field of dielectric nanophotonics are gaining more and more popularity. A huge number of works are devoted to discoveries in this field [1-7]. This interest is due in part to the emerging possibilities of applying the anapole state of dielectric nanoparticles in practice [8,9]. Due to the fact that the anapole states in dielectric nanoparticles are practically invisible at a certain wavelength [10], they, for example, can be used to hide objects, making them invisible [11].

Anapole particles have found applications in many branches of nanophotonics, in particular, ideas about their use for the development of metasurfaces in order to solve various optical problems are beginning to emerge [12]. Metasurfaces of anapole particles can be useful for developing new coded metasurface architectures and holographic structures [13].

Great prospects in this direction appeared after a detailed examination of high-order toroidal moments, with the help of which it is possible to obtain interference of the far fields of basic multipole moments and their toroidal analogues. To date, Cartesian multipoles up to 16-pole magnetic and 32-pole electric, as well as toroidal moments to magnetic quadrupole and electric octupole members have been explicitly derived [14].

In the future, the anapole state of nanoparticles makes it possible to control light, which will contribute to the creation of new photonic elements, and the anapole state also finds its application in radiation generation, sounding, and nonlinear optics [15].

RESULTS AND DISCUSSION

In this work, using the numerical simulation in the COMSOL Multiphysics package, we studied the optical properties of the anapole hybrid state in silicon nanocylinders and their metasurfaces.

First of all, the anapole state for a silicon nanocylinder was found by optimizing its geometric dimensions to obtain a minimum scattering cross section at a specific wavelength (fig. 1). For this, the radius and height of the cylinder were changed with a fixed step at fixed incident wavelength. Then the scattering cross section was considered for each geometric configuration. From the obtained data array, the minimum value was selected.
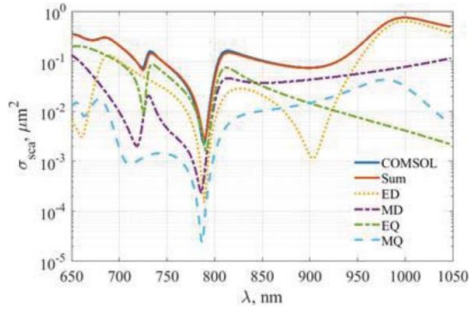
020075-1

99

FIGURE 1. Graphs of the dependence of the scattering cross section on the length of the exciting radiation for a silicon nanocylinder with a radius R = 128 nm and a height H = 369 nm.

The graphs show that the scattering minimum for the optimized nanocylinder is at a wavelength of λ = 789 nm. This point corresponds to the hybrid anapole state of a silicon nanocylinder. For this state, a multipole decomposition was performed, represented by dashed lines. The graph shows that the electric dipole (ED), magnetic dipole (MD), electric quadrupole (EQ) and magnetic quadrupole (MQ) contribute to the overall picture of the scattering cross section, which describes the data obtained by numerical simulation with sufficient accuracy. Thus, due to the destructive interference of multipoles in the far zone, this cylinder will be practically invisible at a wavelength of λ = 789 nm.

Then, a metasurface consisting of these nanocylinders having an anapole state at a wavelength of λ = 789 nm was developed, and its optical properties depending on the wavelength of the incident radiation were considered (fig. 2).
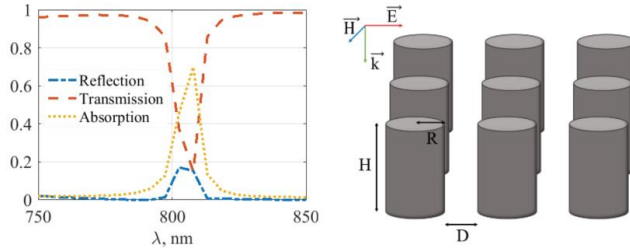
FIGURE 2. Graphs of the dependence of the transmission, reflection and absorption of radiation with a wavelength of λ = 789 nm metasurface consisting of silicon nanocylinders with a radius of R = 128 nm and a height of H = 369 nm, on the wavelength of the incident radiation (a), artistic representation of the considered silicon metasurface composed of nanocylinders (infinite nanostructure illuminated with the linearly polarized plane wave). (b).

The graphs show that such a metasurface has a high transmittance and low reflection coefficient, which makes it practically invisible at the wavelength of the anapole state. The cylinders of the metasurface are located quite far from each other, so their mutual interaction minimal. We designed a metasurface where each element is practically invisible at a specific wavelength, which means that the metasurface itself is also practically invisible.

Thus, in this work, the anapole state for silicon nanocylinders was found by optimizing their geometric dimensions and finding the minimum value of the scattering cross section. From these nanocylinders, a metasurface model was

developed which is practically invisible at a wavelength of $\lambda = 789$ nm at a fixed distance between the cylinders D = 244 nm. The results of our study demonstrate the possibility of creating invisible metasurfaces consisting of silicon cylinders in the hybrid anapole state. Thus, our design can be used in various fields of nanophotonics, and may play an important role in the development of future sensors and other photonic devices.

ACKNOWLEDGMENTS

REFERENCES

1. Pavel M. Voroshilov, Constantin R. Simovski, Pavel A. Belov and Alexander S. Shalin, "Light-trapping and antireflective coatings for amorphous Si-based thin film solar cells" in J. Appl. Phys., vol. 117, pp. 203101, 2015.
2. Kseniia V. Baryshnikova, Andrey Novitsky, Andrey B. Evlyukhin and Alexander S. Shalin, "Magnetic field concentration with coaxial silicon nanocylinders in optical spectral range" in JOSA B, Vol. 34, No. 7, July 2017, P. D36 - D41.
3. Liyang Yue, Oleg Minin, Zengbo Wang, James Monks, Alexander Shalin, Igor Minin "Photonic hook: A new curved light beam" in Optics Letters, Vol. 43, No. 4, 15 February 2018.
4. Aliaksandra Ivinskaya, Natalia Kostina, Alexey Proskurin, Mihail I. Petrov, Andrey A. Bogdanov, Sergey Sukhov, Alexey V. Krasavin, Alina Karabchevsky, Alexander S. Shalin, and Pavel Ginzburg, "Optomechanical Manipulation with Hyperbolic Metasurfaces" in ACS Photonics, 2018, 5 (11), pp 4371–4377.
5. Natalia Kostina, Mihail Petrov, Aliaksandra Ivinskaya, Sergey Sukhov, Andrey Bogdanov, Ivan Toftul, Manuel Nieto-Vesperinas, Pavel Ginzburg, and Alexander S. Shalin, "Optical binding via surface plasmon polariton interference" in Phys. Rev. B, B 99, 125416 2019.
6. Kseniia Baryshnikova, Dmitriy Filonov, Constantin Simovski, Andrey Evlyukhin, Alexey Kadochkin, Elizaveta Nenasheva, Pavel Ginzburg, and Alexander S. Shalin, "Giant magnetoelectric field separation via anapole-type states in high-index dielectric structures" in Phys. Rev. B 98, 165419, 2018.
7. Angeleene S. Ang, Alina Karabchevsky, Igor V. Minin, Oleg V. Minin, Sergey V. Sukhov & Alexander S. Shalin, 'Photonic Hook' based optomechanical nanoparticle manipulator // Scientific Reports, 8:2029, (2018).
8. Kseniia V. Baryshnikova, Daria A. Smirnova, Boris S. Luk'yanchuk, and Yuri S. Kivshar, "Optical Anapoles: Concepts and Applications," in Advanced optical materials. 2019.
9. Denis Zhigunov, Andrey B. Evlyukhin, Alexander Sergeevich Shalin, Urs Zywietz, and Boris N. Chichkov, "Femtosecond laser printing of single Ge and SiGe nanoparticles with electric and magnetic optical resonances" in ACS Photonics, 2018, 5 (3), pp 977–983.
10. Andrey E. Miroshnichenko, Andrey B. Evlyukhin, Ye Feng Yu, Reuben M. Bakker, Arkadi Chipouline, Arseniy I. Kuznetsov, Boris Luk'yanchuk, Boris N. Chichkov & Yuri S. Kivshar, "Nonradiating anapole modes in dielectric nanoparticles," in Nature Communications, 2015.
11. Anar K. Ospanova, Giuseppe Labate, Ladislau Matekovits & Alexey A. Basharin. "Multipolar passive cloaking by nonradiating anapole excitation" in Scientific Reports volume, 2018.
12. Pavel D. Terekhov, Viktoriia E. Babicheva, Kseniia V. Baryshnikova, Alexander S. Shalin, Alina Karabchevsky, and Andrey B. Evlyukhin, "Multipole analysis of dielectric metasurfaces composed of nonspherical nanoparticles and lattice invisibility effect," in Physical review, 2019.
13. Shamkhi Hadi K, Belov Pavel, Kivshar Yuri, Shalin Alexander, Baryshnikova Kseniia, Sayanskiy Andrey, Terekhov Pavel, Gurvitz Egor, Canós Valero Adrià, Karabchevsky Alina, Kapitanova Polina, Evlyukhin Andrey, "Non-Huygens Invisible Metasurfaces", 2019.
14. Gurvitz E.A., Ladutenko K.S., Dergachev P.A., Evlyukhin A.B., Miroshnichenko A.E., Shalin A.S, "The High-Order Toroidal Moments and Anapole States in All-Dielectric Photonics," in Laser & Photonics Reviews, 2019.
15. Yuanqing Yang, Sergey I Bozhevolny, "Nonradiating anapole states in nanophotonics: from fundamentals to applications" in Nanotechnology, 2019.

[PAPER 4]: Non-Huygens transparent metasurfaces based on the novel Hybrid anapole state

Kuznetsov, A.V., Canos Valero, A., "*Non-Huygens transparent metasurfaces based on the novel Hybrid anapole state*," Proceedings of the 6th International conference on metamaterials and nanophotonics «METANANO 2021», Vol. 2015, No. 1, p. 012079, online, November **2021**.

Non-Huygens transparent metasurfaces based on the novel Hybrid anapole state

To cite this article: A V Kuznetsov and A Canós Valero 2021 *J. Phys.: Conf. Ser.* **2015** 012079

View the article online for updates and enhancements.

Non-Huygens transparent metasurfaces based on the novel Hybrid anapole state

A V Kuznetsov[1,2], A Canós Valero[1]

[1]ITMO University, Lomonosova street, 9, St. Petersburg, 191002, Russia
[2]Riga Technical University, Riga, Azenes street 12, post code 1048, Latvia

Corresponding author: alexey.kuznetsov@metalab.ifmo.ru

Abstract. In this work we studied the optical properties of the metasurfaces based on silicon nanocylinders experincing hybrid anapole. Our investigation shows the possibility of creating fully invisible metasurfaces consisting of silicon nanocylinders based on the novel state which in their properties can compete with the Huygens' metasurfaces. These results can be used in various fields of nanophotonics and may have important outcome in the development of various photonic devices.

1. Introduction

In the recent years, dielectric nanophotonics has become ubiquitous in numerous scientific and technological disciplines [1–6]. Enabling the ability to control the electric and magnetic components of light at the subwavelength scale with negligible losses, this fast-developing field holds the key to the design and fabrication of ultrasmall optical devices for flat optics. Dielectric metasurfaces have allowed the manufacturing of ultraflat lenses [7,8], hologram displays [9–12], light-managing devices [13–15], and dispersion control applications [16]. To a large extent, these developments were facilitated by Huygens metasurfaces, featuring the possibility to vary the transmitted phase with unity transmission, namely due to spectrally overlapping electric and magnetic dipole resonances of almost equal strength [17]. However, their efficiency is fundamentally limited by the near field coupling between the constituents of the metalattice [18], which has motivated the search for alternative means to achieve the desired 2π phase variation [19].

The recently observed hybrid anapole states [20] are nonradiating sources that, unlike conventional anapoles, simultaneously suppress electric and magnetic contributions to radiation (figure 1). This unique peculiarity can be exploited to suppress both far and near field coupling from the structure, unlike Huygens' sources. In this work, we explore this promising alternative to the Huygens's effect and design a fully transmissive metasurface that can control the phase, based on the hybrid anapole state of the individual metaatoms.

2. Results and discussion

Figure 1 shows the dependence of the reflection of the metasurface depending on the distance between the surfaces of the meta-atoms (a) and the distribution of the electric field norm in the particles at different distances (b). A model of a non-Huygens' metasurface consisting of silicon nanocylinders in a hybrid anapole state is schematically shown in (c).
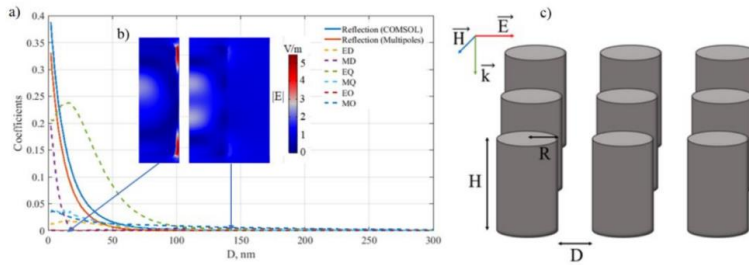
Figure 1. Dependence of the reflection of radiation with a wavelength of hybrid anapole state λ = 789 nm metasurface consisting of silicon nanocylinders with radius R = 128 nm and height H = 369 nm, on the distance between cylinders (a), fragments of the spatial electric field norm distribution in the xz-plane for distance between surfaces of metaatoms D = 20 nm, 144 nm show that near field coupling occurs only at very small periods (b) and artistic representation of the considered silicon metasurface composed of nanocylinders (c)

It is seen from the figure that even highly compact metasurfaces display minimal reflection until the near field of the metaatoms begins to influence the field inside neighboring scatterers. In addition, contrarily to other recently proposed effects inducing zero transmission, the hybrid anapole is preserved when deposited over substrates having almost any refractive index contrast. This reduces the requirements for the technical production process, allowing more design flexibility in terms of the material of the underlying substrate.

3. Conclusion

Thus, in this work, a metasurface model was developed, which, in terms of its optical properties, can become a worthy alternative to Huygens' metasurfaces. The developed non-Huygens' metsurface model based on nanocylinders in a hybrid anapole state has a number of indisputable advantages, such as full transmission of incident radiation, zero phase shift when radiation passes through it, and the possibility of deposition on various types of substrates without significant changes in the optical properties of the metasurface. All of the above properties make it possible to largely unlock the potential for creating various devices based on metasurfaces, for example, various metal lenses, sensors, holographic devices, and so on.

4. Acknowledgment

References

[1]   Kivshar Y 2018 All-dielectric meta-optics and non-linear nanophotonics *Natl. Sci. Rev.* **5** 144–58
[2]   Yan J, Liu X, Ma C, Huang Y and Yang G 2020 All-dielectric materials and related nanophotonic applications *Mater. Sci. Eng. R Reports* **141** 100563
[3]   Chebykin A V., Orlov A A, Shalin A S, Poddubny A N and Belov P A 2015 Strong Purcell effect in anisotropic ε-near-zero metamaterials *Phys. Rev. B - Condens. Matter Mater. Phys.* **91**
[4]   Kostina N, Petrov M, Ivinskaya A, Sukhov S, Bogdanov A, Toftul I, Nieto-Vesperinas M, Ginzburg P and Shalin A 2019 Optical binding via surface plasmon polariton interference *Phys. Rev. B* **99** 1–11

[5]   Canós Valero A, Kislov D, Gurvitz E A, Shamkhi H K, Pavlov A A, Redka D, Yankin S, Zemánek P and Shalin A S 2020 Nanovortex-Driven All-Dielectric Optical Diffusion Boosting and Sorting Concept for Lab-on-a-Chip Platforms *Adv. Sci.* **7**

[6]   Barhom H, Machnev A A, Noskov R E, Goncharenko A, Gurvitz E A, Timin A S, Shkoldin V A, Koniakhin S V., Koval O Y, Zyuzin M V., Shalin A S, Shishkin I I and Ginzburg P 2019 Biological Kerker Effect Boosts Light Collection Efficiency in Plants *Nano Lett.* **19** 7062–71

[7]   Fathnan A A, Liu M and Powell D A 2020 Achromatic Huygens' Metalenses with Deeply Subwavelength Thickness *Adv. Opt. Mater.* **8** 1–9

[8]   Chen X, Zhang X, Koten M A, Chen H, Xiao Z, Zhang L, Shield J E, Dowben P A and Hong X 2017 Interfacial Charge Engineering in Ferroelectric-Controlled Mott Transistors *Adv. Mater.* **29** 1–8

[9]   Chong K E, Wang L, Staude I, James A R, Dominguez J, Liu S, Subramania G S, Decker M, Neshev D N, Brener I and Kivshar Y S 2016 Efficient Polarization-Insensitive Complex Wavefront Control Using Huygens' Metasurfaces Based on Dielectric Resonant Meta-atoms *ACS Photonics* **3** 514–9

[10]   Wang L, Kruk S, Tang H, Li T, Kravchenko I, Neshev D N and Kivshar Y S 2016 Grayscale transparent metasurface holograms *Optica* **3** 1504

[11]   Overvig A C, Shrestha S, Malek S C, Lu M, Stein A, Zheng C and Yu N 2019 Dielectric metasurfaces for complete and independent control of the optical amplitude and phase *Light Sci. Appl.* **8**

[12]   Kozlov V, Filonov D, Shalin A S, Steinberg B Z and Ginzburg P 2016 Asymmetric backscattering from the hybrid magneto-electric meta particle *Appl. Phys. Lett.* **109**

[13]   Kruk S and Kivshar Y 2017 Functional Meta-Optics and Nanophotonics Govern by Mie Resonances *ACS Photonics* **4** 2638–49

[14]   Aoni R A, Rahmani M, Xu L, Zangeneh Kamali K, Komar A, Yan J, Neshev D and Miroshnichenko A E 2019 High-Efficiency Visible Light Manipulation Using Dielectric Metasurfaces *Sci. Rep.* **9** 1–9

[15]   Terekhov P D, Shamkhi H K, Gurvitz E A, Baryshnikova K V., Evlyukhin A B, Shalin A S and Karabchevsky A 2019 Broadband forward scattering from dielectric cubic nanoantenna in lossless media *Opt. Express* **27** 10924

[16]   Zhang X, Li Q, Liu F, Qiu M, Sun S, He Q and Zhou L 2020 Controlling angular dispersions in optical metasurfaces *Light Sci. Appl.* **9** 34–7

[17]   Decker M, Staude I, Falkner M, Dominguez J, Neshev D N, Brener I, Pertsch T and Kivshar Y S 2015 High-Efficiency Dielectric Huygens' Surfaces *Adv. Opt. Mater.* **3** 813–20

[18]   Olk A E and Powell D A 2019 Accurate Metasurface Synthesis Incorporating Near-Field Coupling Effects *Phys. Rev. Appl.* **11** 1

[19]   Rahimzadegan A, Arslan D, Dams D, Groner A, Garcia-Santiago X, Alaee R, Fernandez-Corbaton I, Pertsch T, Staude I and Rockstuhl C 2020 Beyond dipolar Huygens' metasurfaces for full-phase coverage and unity transmittance *Nanophotonics* **9** 75–82

[20]   Canos Valero A, Gurvitz E, Evlyukhin A and Redka D 2020 Theory, observation and ultrafast response of novel hybrid anapole states *arXiv*

106

[PAPER 5]: Various multipole combinations for conical Si particles

Kuznetsov, A.V., Canos Valero, A., Terekhov, P. D., Shamkhi, H. K., "*Various multipole combinations for conical Si particles*," Proceedings of the 6th International conference on metamaterials and nanophotonics «METANANO 2021», Vol. 2015, No. 1, p. 012080, online, November **2021**.

Various multipole combinations for conical Si particles

To cite this article: A V Kuznetsov *et al* 2021 *J. Phys.: Conf. Ser.* **2015** 012080

View the article online for updates and enhancements.

Various multipole combinations for conical Si particles

A V Kuznetsov[1,2], A Canós Valero[1], P D Terekhov[3], H K Shamkhi[1]

[1]ITMO University, Lomonosova street, 9, St. Petersburg, 191002, Russia
[2]Riga Technical University, Riga, Azenes street 12, post code 1048, Latvia
[3]Duke University, Durham, NC, United States

Corresponding author: alexey.kuznetsov@metalab.ifmo.ru

Abstract. In this work, we investigated the possibility of creating various multipole combinations in conical silicon nanoparticles. It was found that in conical silicon particles it seems possible to create key effects for nanophotonics, such as various kinds of Kerker effects (Generalized Kerker, Transverse Kerker), Hybrid anapole state, Bound states in the continuum. This greatly simplifies the manufacturing process of photonic devices due to the easier production of nanocones in practice. Also, conical particles allow an additional degree of freedom, which opens up new horizons for obtaining previously unknown effects.

1. Introduction

In recent years, an increasing number of scientific studies have been devoted to areas in which subwavelength dielectric nanoparticles are used. The fact is that such particles can be used to create various kinds of devices, the characteristics of which either significantly exceed the characteristics of existing ones, or even open up the possibility of creating a new class of devices. Their undeniable advantage lies in their high efficiency and relatively easy production. There are a lot of examples of the use of devices based on dielectric nanoparticles: nanolasers [1], nanoantennas [2], metamaterials [3] and metasurfaces [4], ultrathin lenses [5], detectors [6] and other equally interesting applications [7,8].

A huge impetus to the development of high-index dielectric nanophotonics was made by opening the possibility of separate control of multipole excitations in scatterers and, as a consequence, combining multipole moments to obtain various effects [9–12].

Thanks to this possibility, it became possible to obtain the Kerker effect, which was originally introduced for a hypothetical magnetic sphere and did not attract the attention of researchers [13]. Now, the Kerker effect has been significantly expanded thanks to the capabilities of dielectric nanophotonics, where it became possible to obtain a magnetic moment in small particles. An excellent example for this is the generalized Kerker effect, which allows one to obtain resonant excitation and interference of various electromagnetic multipoles [14–18] or transverse Kerker, characterized by transverse isotropic scattering by subwavelength nanoparticles with simultaneous suppression of both forward and backward scattered fields [19].

Another important discovery related to multipole combinations is the possibility of obtaining a hybrid anapole state (HAS) of nanoobjects. It is possible to create a metasurface from such nano-objects, which will have many useful properties, for example, a zero phase shift of a light wave when passing through a metasurface, almost complete light transmittance, the ability to apply such a metasurface on various types of substrates [20]. This opens up incredible opportunities for creating various kinds of devices for flat optics.

Devices using bound states in the continuum (BIC) also play an important role in the development of dielectric nanophotonics. The flexibility that quasi-BICs has brought to the design and implementation of high Q resonances in nanophotonic systems has made them very useful to the nonlinear photonics community. BICs have so far been used to amplify a variety of nonlinear effects, including optical Kerr effect, laser action, second and third harmonic generation, and four-wave mixing. Thanks to BIC, lasers, harmonic generating devices, optical fibers, beamforming devices, etc. can be created [21].

All of the above cases were presented for particles with elementary geometry, for example, on spheres or cylinders, but, for example, frustoconical scatterers are currently poorly studied, although this geometry has many advantages.

Due to the additional degree of freedom in the form of the upper radius, unpredictable new effects may appear that have not been investigated before.

Another important advantage of the geometry of the cones is that the practical production of elements for photonic devices has not yet been perfected. For example, in the process of fabricating such scatterers, it is practically impossible to obtain a perfectly flat nanocylinder with the given parameters. It is much easier in practice to create a truncated cone.

Thus, this work is devoted to the study of the optical properties of the scatterer in the form of a truncated cone, the search for cases that are inaccessible to standard geometries, and testing the obtained results.

2. Results and discussion

Figure 1 shows a schematic drawing of the model for which mathematical modeling was carried out. As a scatterer, a silicon nanocylinder was taken from which, by changing the upper and lower radii, height and wavelength, various combinations of multipoles were obtained (a). Distributions for the far-field were plotted (c,e) for conical silicon particles, which were confirmed by theoretical combinations of multipoles for a point (b,d).
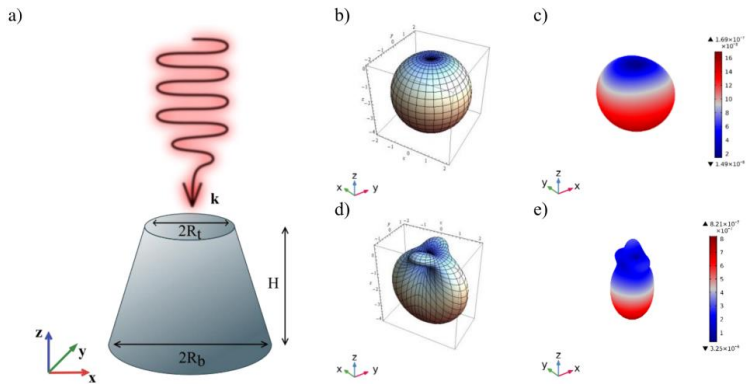

Figure 1. Artistic representation of the considered silicon particle composed of nanocylinders (infinite nanostructure illuminated with the linearly polarized plane wave) (a), theoretically far-field distributions of different combinations of multipoles for point (b,d) and simulated far-field distributions of different combinations of multipoles for conical silicon particles

It can be seen that by varying the parameters of conical silicon particles, we managed to obtain various combinations of multipoles, for example, the usual Kerker (c) and generalized Kerker effect (e). In the report we will show other possible combinations and unusual effects enabled by the truncated cone shape via separate tailoring of different multipoles.

3. Conclusion

Thus, this work is devoted to the extensive tutorial study of the optical properties of truncated conical nanoscatterers. In this work, various optical effects are obtained by tuning the parameters of the fabrication-friendly resonators - conical silicon scatterers. This opens up new possibilities for the production of photonic devices based on such shape of nanoscatterers. Also, conical particles allow an additional degree of freedom, which opens up new horizons for obtaining previously unknown effects.

4. Acknowledgement

References

[1]   Xu K, Fang M and Huang Z 2020 Compact unidirectional laser based on all-dielectric metasurface with high quality factor *IEEE Photonics J.* **13**
[2]   Sain B, Meier C and Zentgraf T 2020 Nonlinear optics at all-dielectric nanoantennas and metasurfaces *arXiv* **1** 1–14
[3]   Kozlov V, Filonov D, Shalin A S, Steinberg B Z and Ginzburg P 2016 Asymmetric backscattering from the hybrid magneto-electric meta particle *Appl. Phys. Lett.* **109**
[4]   Overvig A C, Shrestha S, Malek S C, Lu M, Stein A, Zheng C and Yu N 2019 Dielectric metasurfaces for complete and independent control of the optical amplitude and phase *Light Sci. Appl.* **8**
[5]   Tian Y, Li Z, Xu Z, Wei Y and Wu F 2020 High transmission focusing lenses based on ultrathin all-dielectric Huygens' metasurfaces *Opt. Mater. (Amst).* **109** 110358
[6]   Mitrofanov O, Siday T, Vabishchevich P, Hale L, Harris T, Luk T S, Reno J L and Brener I 2019 Terahertz detectors based on all-dielectric photoconductive metasurfaces 36
[7]   Yan J, Liu X, Ma C, Huang Y and Yang G 2020 All-dielectric materials and related nanophotonic applications *Mater. Sci. Eng. R Reports* **141** 100563
[8]   Chebykin A V., Orlov A A, Shalin A S, Poddubny A N and Belov P A 2015 Strong Purcell effect in anisotropic ε-near-zero metamaterials *Phys. Rev. B - Condens. Matter Mater. Phys.* **91**
[9]   Evlyukhin A B and Chichkov B N 2019 Multipole decompositions for directional light scattering *Phys. Rev. B* **100** 125415
[10]   Alaee R, Rockstuhl C and Fernandez-Corbaton I 2018 An electromagnetic multipole expansion beyond the long-wavelength approximation *Opt. Commun.* **407** 17–21
[11]   Kostina N, Petrov M, Ivinskaya A, Sukhov S, Bogdanov A, Toftul I, Nieto-Vesperinas M, Ginzburg P and Shalin A 2019 Optical binding via surface plasmon polariton interference *Phys. Rev. B* **99** 1–11
[12]   Canós Valero A, Kislov D, Gurvitz E A, Shamkhi H K, Pavlov A A, Redka D, Yankin S, Zemánek P and Shalin A S 2020 Nanovortex-Driven All-Dielectric Optical Diffusion Boosting and Sorting Concept for Lab-on-a-Chip Platforms *Adv. Sci.* **7**
[13]   Kerker M, Wang D S and Giles C L 1983 Electromagnetic Scattering By Magnetic Spheres. *J. Opt. Soc. Am.* **73** 765–7
[14]   Alaee R, Filter R, Lehr D, Lederer F and Rockstuhl C 2015 A generalized Kerker condition for highly directive nanoantennas *Opt. Lett.* **40** 2645
[15]   Liu W and Kivshar Y S 2017 Generalized Kerker effects in nanophotonics and meta-optics *arXiv* **26** 274–84
[16]   Hesari-Shermeh M, Abbasi-Arand B and Yazdi M 2021 Generalized Kerker's conditions under normal and oblique incidence using the polarizability tensors of nanoparticles *Opt.*

Express **29** 647

[17]   Terekhov P D, Shamkhi H K, Gurvitz E A, Baryshnikova K V., Evlyukhin A B, Shalin A S and Karabchevsky A 2019 Broadband forward scattering from dielectric cubic nanoantenna in lossless media *Opt. Express* **27** 10924

[18]   Barhom H, Machnev A A, Noskov R E, Goncharenko A, Gurvitz E A, Timin A S, Shkoldin V A, Koniakhin S V., Koval O Y, Zyuzin M V., Shalin A S, Shishkin I I and Ginzburg P 2019 Biological Kerker Effect Boosts Light Collection Efficiency in Plants *Nano Lett.* **19** 7062–71

[19]   Shamkhi H K, Baryshnikova K V., Sayanskiy A, Kapitanova P, Terekhov P D, Belov P, Karabchevsky A, Evlyukhin A B, Kivshar Y and Shalin A S 2019 Transverse scattering and generalized kerker effects in all-dielectric mie-resonant metaoptics *Phys. Rev. Lett.* **122** 193905

[20]   Canos Valero A, Gurvitz E, Evlyukhin A and Redka D 2020 Theory, observation and ultrafast response of novel hybrid anapole states *arXiv*

[21]   Azzam S I and Kildishev A V. 2021 Photonic Bound States in the Continuum: From Basics to Applications *Adv. Opt. Mater.* **9** 16–24

[PAPER 6]: Novel Hybrid anapole state and non-Huygens' transparent metasurfaces

Shalin, A.S., **Kuznetsov, A.V.,** Bobrovs, V., Valero, A.C., "*Novel Hybrid anapole state and non-Huygens' transparent metasurfaces*," Proceedings of the 4th International Smart NanoMaterials Conference 2021: Advances, Innovation and Applications «SNAIA 2021», Vol. 2172, No. 1, p. 012001, Paris, France, February **2022**.

PAPER • OPEN ACCESS

Novel Hybrid anapole state and non-Huygens' transparent metasurfaces

To cite this article: A S Shalin *et al* 2022 *J. Phys.: Conf. Ser.* **2172** 012001

View the article online for updates and enhancements.

Novel Hybrid anapole state and non-Huygens' transparent metasurfaces

A S Shalin[1,2,3], A V Kuznetsov[1,2], V Bobrovs[2], A Canós Valero[1]

[1]ITMO University, Russia
[2]Riga Technical University
[3]Kotel'nikov Institute of Radio Engineering and Electronics of RAS (Ulyanovsk branch)

alexandesh@gmail.com

Abstract. The purpose of this work is to study of the optical properties of metasurfaces consisting of cylindrical metaatoms in the recently discovered hybrid anapole state. With the help of such metasurfaces, it was possible to obtain completely invisible metasurfaces based on new principles that is an alternative branch of development to the already known Huygens' metasurfaces. This research might be helpful for the development of modern ultra-compact photonic devices based on new effects.

1. Introduction

To date, all-dielectric nanophotonics is developing extremely rapidly, in particular, precisely because of its practical significance in many fields of science and technology [1–4]. Due to the possibility of lossless control of the components of electromagnetic radiation on a subwavelength scale, it becomes possible to produce super-thin optical devices. All-dielectric metasurfaces give the opportunity to create hologram displays [5,6], flat lenses [7,8], dispersion control applications [9] and light-managing devices [10–13]. A huge contribution to this area was made by the Huygens' metasurfaces, which provide complete transparency and at the same time make it possible to change the phase of the radiation passing through them [14,15]. But such metasurfaces have a fundamental limitation - the connection of near fields between the elements of the metalattice [16]. This limitation motivates the search for new concepts to obtain 2π phase variation [17].

Newly discovered hybrid anapole states [18] are nonradiating sources that, unlike anapoles, jointly quenches the electrical and magnetic contributions to the scattering (Figure 1). This effect can be used to suppress coupling in the far and near fields between meta-atoms, which is difficult to implement for Huygens' sources. In this work, we propose a metasurface model composed of silicon nanocylinders in a hybrid anapole state, which will have complete transparency and the capability to regulate the phase of the transmitted signal [19].
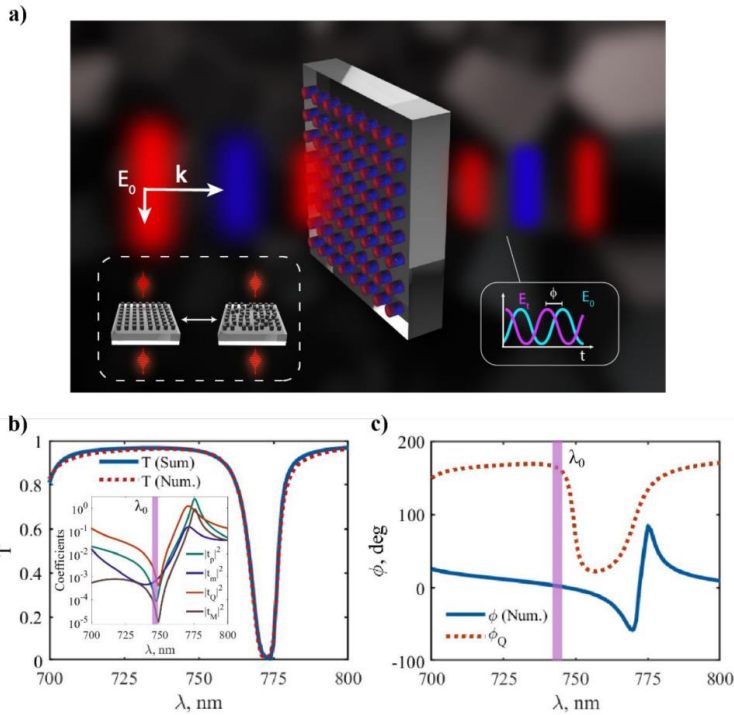
Figure 1. Schematic representation of the introduced metasurface, consisting of silicon nanocylinders, which shows the main advantages: unity transmission, the capability to adjust the phase and almost complete independence of optical properties from the position of nanocylinders (a), relation of the transmission of radiation with fixed separation between meta-atoms s = 300 nm (inset: absolute values of the dominant multipolar contributions) (b), total phase of transmitted radiation ϕ and phase variation of the electric quadrupole ϕ_Q (c) obtained numerically.

Figure 1 presents the relation of the transmission of radiation through a metasurface, consisting of silicon nanocylinders (b) and the phase shift of radiation transmitted through such a metasurface (c), depending on the wavelength, the separation between the surfaces of the nanocylinders was constant. In the figure, you can see the so-called "transparency window" which appears due to the hybrid anapole state and remains even with a dense arrangement of meta-atoms. An indisputable advantage of such a metasurface is the possibility of applying it to various substrates with almost zero contrast of the refractive index while maintaining unit transmission, which greatly simplifies the choice of the substrate material and opens new possibilities for practical implementation.

2. Conclusion

As a result, in this work, unique models of metasurfaces were developed, the meta-atoms of which are in the recently discovered hybrid anapole state. Such metasurfaces have full optical transparency, thereby competing with the already known Huygens' metasurfaces while working on other principles. Such metasurfaces have many advantages, for example, the absence of interaction of meta-atoms with the substrate and with neighboring meta-atoms. Due to this, it becomes possible to choose practically any dielectric substrate for experiments, as well as the ability to create a disordered metasurfaces by varying the optical properties directly at the level of individual meta-atoms. Thus, all these features contribute to the development of the direction of creating different photonic devices based on hybrid anapole metasurfaces, for example, sensors, various lenses, holographic devices, and much more useful devises.

References

[1]   Kivshar Y 2018 All-dielectric meta-optics and non-linear nanophotonics *Natl. Sci. Rev.* **5** 144–58
[2]   Kozlov V, Filonov D, Shalin A S, Steinberg B Z and Ginzburg P 2016 Asymmetric backscattering from the hybrid magneto-electric meta particle *Appl. Phys. Lett.* **109** 203503
[3]   Canós Valero A, Kislov D, Gurvitz E A, Shamkhi H K, Pavlov A A, Redka D, Yankin S, Zemánek P and Shalin A S 2020 Nanovortex-Driven All-Dielectric Optical Diffusion Boosting and Sorting Concept for Lab-on-a-Chip Platforms *Adv. Sci.* **7** 1903049
[4]   Novitsky D V., Karabchevsky A, Lavrinenko A V., Shalin A S and Novitsky A V. 2018 PT symmetry breaking in multilayers with resonant loss and gain locks light propagation direction *Phys. Rev. B* **98** 125102
[5]   Chong K E, Wang L, Staude I, James A R, Dominguez J, Liu S, Subramania G S, Decker M, Neshev D N, Brener I and Kivshar Y S 2016 Efficient Polarization-Insensitive Complex Wavefront Control Using Huygens' Metasurfaces Based on Dielectric Resonant Meta-atoms *ACS Photonics* **3** 514–9
[6]   Wang L, Kruk S, Tang H, Li T, Kravchenko I, Neshev D N and Kivshar Y S 2016 Grayscale transparent metasurface holograms *Optica* **3** 1504
[7]   Chen X, Zhang X, Koten M A, Chen H, Xiao Z, Zhang L, Shield J E, Dowben P A and Hong X 2017 Interfacial Charge Engineering in Ferroelectric-Controlled Mott Transistors *Adv. Mater.* **29** 1701385
[8]   Fathnan A A, Liu M and Powell D A 2020 Achromatic Huygens' Metalenses with Deeply Subwavelength Thickness *Adv. Opt. Mater.* **8** 1–9
[9]   Zhang X, Li Q, Liu F, Qiu M, Sun S, He Q and Zhou L 2020 Controlling angular dispersions in optical metasurfaces *Light Sci. Appl.* **9** 34–7
[10]   Kruk S and Kivshar Y 2017 Functional Meta-Optics and Nanophotonics Govern by Mie Resonances *ACS Photonics* **4** 2638–49
[11]   Terekhov P D, Baryshnikova K V., Greenberg Y, Fu Y H, Evlyukhin A B, Shalin A S and Karabchevsky A 2019 Enhanced absorption in all-dielectric metasurfaces due to magnetic dipole excitation *Sci. Rep.* **9** 1–9
[12]   Barhom H, Machnev A A, Noskov R E, Goncharenko A, Gurvitz E A, Timin A S, Shkoldin V A, Koniakhin S V., Koval O Y, Zyuzin M V., Shalin A S, Shishkin I I and Ginzburg P 2019 Biological Kerker Effect Boosts Light Collection Efficiency in Plants *Nano Lett.* **19** 7062–71

3

117

[13]   Terekhov P D, Evlyukhin A B, Redka D, Volkov V S, Shalin A S and Karabchevsky A 2020
       Magnetic Octupole Response of Dielectric Quadrumers *Laser Photon. Rev.* **14** 1900331
[14]   Decker M, Staude I, Falkner M, Dominguez J, Neshev D N, Brener I, Pertsch T and Kivshar Y
       S 2015 High-Efficiency Dielectric Huygens' Surfaces *Adv. Opt. Mater.* **3** 813–20
[15]   Shamkhi H K, Sayanskiy A, Valero A C, Kupriianov A S, Kapitanova P, Kivshar Y S, Shalin
       A S and Tuz V R 2019 Transparency and perfect absorption of all-dielectric resonant
       metasurfaces governed by the transverse Kerker effect *Phys. Rev. Mater.* **3** 1–10
[16]   Olk A E and Powell D A 2019 Accurate Metasurface Synthesis Incorporating Near-Field
       Coupling Effects *Phys. Rev. Appl.* **11** 1
[17]   Rahimzadegan A, Arslan D, Dams D, Groner A, Garcia-Santiago X, Alaee R, Fernandez-
       Corbaton I, Pertsch T, Staude I and Rockstuhl C 2020 Beyond dipolar Huygens' metasurfaces
       for full-phase coverage and unity transmittance *Nanophotonics* **9** 75–82
[18]   Canós Valero A, Gurvitz E A, Benimetskiy F A, Pidgayko D A, Samusev A, Evlyukhin A B,
       Bobrovs V, Redka D, Tribelsky M I, Rahmani M, Kamali K Z, Pavlov A A, Miroshnichenko A
       E and Shalin A S 2021 Theory, Observation, and Ultrafast Response of the Hybrid Anapole
       Regime in Light Scattering *Laser Photonics Rev.* **15** 2100114
[19]   Kuznetsov A V., Canós Valero A, Tarkhov M, Bobrovs V, Redka D and Shalin A S 2021
       Transparent hybrid anapole metasurfaces with negligible electromagnetic coupling for phase
       engineering *Nanophotonics* **10** 4385–98

118

[PAPER 7]: Various Scattering Regimes of Truncated Cone Particles

Terekhov, P.D., **Kuznetsov, A.V.,** Canos Valero, A., Shamkhi, H.K., Ni X., Bobrovs V., Rybin M.V., Shalin A.S., "*Various Scattering Regimes of Truncated Cone Particles*," Proceedings of the CLEO: Applications and Technology 2023, San Jose, USA, 7-12 May **2023**.

Various Scattering Regimes of Truncated Cone Particles

Pavel Terekhov[1, *], Alexey Kuznetsov[2,3,4], Adrià Canós Valero[4], Hadi K. Shamkhi[4], Xingjie Ni[1], Vjaceslavs Bobrovs[3], Mikhail Rybin[4], Alexander S. Shalin[2,3, *]

[1]*Department of Electrical Engineering, The Pennsylvania State University, University Park, PA 16802, USA*
[2]*Moscow Institute of Physics and Technology, Center for Photonics and 2D Materials, Dolgoprudny, 141700, Russia*
[3]*Riga Technical University, Institute of Telecommunications, Riga, 1048, Latvia*
[4]*ITMO University, Faculty of Physics, St. Petersburg, 197101, Russia*
*pdt5109@psu.edu
*alexandesh@gmail.com

Abstract: Here, we show how to use out-of-plane symmetry breaking using easy-to-fabricate truncated nanocones. Using the same shape, it is possible to achieve various types of Kerker effects, hybrid anapole regime and other peculiar effects. © 2023 The Authors

1. Introduction

Dielectric nanophotonics opens a lot of possibilities to control light at the nanoscale. Emerging devices include nanolasers, nanoantennas, ultrathin lenses, sensors and detectors, and other peculiar approaches to manipulate electromagnetic field. [1-7]

Research groups are constantly looking for new opportunities to tune optical response of nanostructures, such as metasurfaces and nanoantennas. Usually, fabrication restrictions impose the requirement of out-of-plane symmetry, thus prohibiting the use of this degree of freedom. Here, we present the way to overcome this restriction by easy to fabricate truncated cones. We numerically show that a few peculiar properties can be achieved, making an example of hybrid anapole effect for truncated cones with large conicity.

2. Results and Discussion

Anapole physics at the nanoscale gained a lot of attention recently, and truncated cone shape is a good candidate to add more freedom to the anapole effects optimization. Multipole decomposition and the use of high-order multipole moments [8-10] are essential for analyzing anapole conditions. Conventionally, dielectric nanodisks were used for anapole demonstrations, [11] but perfect cylindrical shape is not usually easy to achieve due to fabrication limits. However, hybrid anapole can be achieved and effectively optimized when particle conicity is considered. [12]
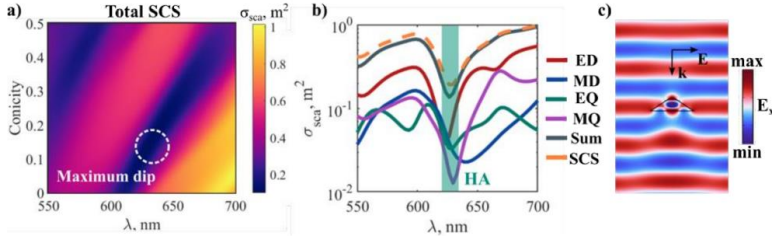

Figure 1. [Adapted from [12]] (a) Evolution of the total SCS near the HA for large conicities. The white-dashed circle highlights the region with the strongest scattering suppression in the parameter range considered. (b) Multipole decomposition of the SCS for a truncated nanocone with conicity 0.12, lying within the region of maximum scattering suppression shown in (a). The green-shaded area indicates the spectral range with the maximum scattering suppression (approximately 8 times less than the average SCS in the visible). (c) x-component of the electric field when illuminating the nanocone with an x-polarized plane wave at a wavelength of 625 nm, corresponding to the HA

Figure 1 shows the scattering cross section analysis for nanoparticles with high conicity. The considered particles are silicon truncated (refractive index n is obtained experimentally [11]). Particle conicity is calculated as a ratio between top and bottom edge diameters, while bottom diameter is fixed as D = 254 nm. Particle height is H = 369 nm. Figure 1 (a) shows the evolution of total scattering cross-section for such particles, and the maximum scattering dip is marked with white dashed line. One can see that hybrid anapole position can be spectrally tuned by particle conicity. Figure 1 (b) illustrates the multipole decomposition for conicity 0.12, where the maximum scattering dip was observed. The total scattering is at least 8 times lower than average scattering in this frequency range due to the variety of multipole moments under suppression. Figure 1 (c) additionally illustrates the emerged hybrid anapole by showing the x-component of electric field interacting with the considered nanoparticle. One can see that field almost does not sense the truncated cone; however, field is concentrated inside the particle.

3. Conclusion

In this work, we showed the hybrid anapole in truncated cone nanoparticles. Such nanoparticles can be also used to achieve various Kerker-type effects [12-14], superscattering regime, conventional anapole, and other peculiar effects. Our investigation paves the way for wider usage of currently underrated truncated cone shape at the nanoscale.

Acknowledgements

References

[1] Barhom, Hani, et al. "Biological Kerker effect boosts light collection efficiency in plants." Nano Letters 19.10 (2019): 7062-7071.

[2] Shankhwar, Nishant, et al. "High-quality laser cavity based on all-dielectric metasurfaces." Photonics and Nanostructures-Fundamentals and Applications 24 (2017): 18-23.

[3] Shen, Kunhong, et al. "On-chip optical levitation with a metalens in vacuum." Optica 8.11 (2021): 1359-1362.

[4] Canós Valero, Adrià, et al. "Nanovortex-Driven all-dielectric optical diffusion boosting and sorting concept for lab-on-a-chip platforms." Advanced Science 7.11 (2020): 1903049.

[5] Kuznetsov, Alexey V., et al. "Transparent hybrid anapole metasurfaces with negligible electromagnetic coupling for phase engineering." Nanophotonics 10.17 (2021): 4385-4398.

[6] Kivshar, Yuri. "All-dielectric meta-optics and non-linear nanophotonics." National Science Review 5.2 (2018): 144-158.

[7] Meng, Yuan, et al. "Optical meta-waveguides for integrated photonics and beyond." Light: Science & Applications 10.1 (2021): 1-44.

[8] Evlyukhin, Andrey B., and Boris N. Chichkov. "Multipole decompositions for directional light scattering." Physical Review B 100.12 (2019): 125415.

[9] Terekhov, Pavel D., et al. "Multipole analysis of dielectric metasurfaces composed of nonspherical nanoparticles and lattice invisibility effect." Physical Review B 99.4 (2019): 045424.

[10] Terekhov, Pavel D., et al. "Magnetic octupole response of dielectric quadrumers." Laser & Photonics Reviews 14.4 (2020): 1900331.

[11] Miroshnichenko, Andrey E., et al. "Nonradiating anapole modes in dielectric nanoparticles." Nature communications 6.1 (2015): 1-8.

[12] Kuznetsov, Alexey V., et al. "Special scattering regimes for conical all-dielectric nanoparticles," arXiv preprint arXiv:2209.06736 (2022).

[13] Shamkhi, Hadi K., et al. "Transverse scattering and generalized Kerker effects in all-dielectric Mie-resonant metaoptics." Physical Review Letters 122.19 (2019): 193905.

[PAPER 8]: Existence of the Hybrid Anapole for Si Conical Nanoparticles

Kuznetsov, A.V., Bobrovs, V., "*Existence of the Hybrid Anapole for Si Conical Nanoparticles*," Proceedings of 12th International Conference on Computer Science Online Conference «CSOC 2023», Lecture Notes in Networks and Systems, Vol. 772, pp 397 – 401, online, 3-5 April **2023**.

Existence of the Hybrid Anapole for Si Conical Nanoparticles

Alexey V. Kuznetsov[1,2] and Vjaceslavs Bobrovs[2(✉)]

[1] Moscow Institute of Physics and Technology, Dolgoprudny, Russia
[2] Riga Technical University, Riga, Latvia
vjaceslavs.bobrovs@rtu.lv

Abstract. All-dielectric nanophotonics opens up new possibilities for obtaining a large number of useful optical effect. Here, we investigate fabrication-friendly truncated-cone nanoresonators and achieve non-scattering regimes due to the inherent property of cones - broken symmetry along the main axis without involving complex geometry or structured beams. In this study, we demonstrate the anapole regime in conical silicon particles, which is achieved due to symmetry breaking along the main axis. Additional degrees of freedom due to the conicity allow for more fine-tuning of the optical properties at the nanoscale.

Keywords: Anapole · Non-Scattering Regime · Truncated Cone

1 Introduction

Due to the possibility of controlling the electromagnetic components of the field, studies of the interaction of light with dielectric nanoparticles are becoming increasingly popular. Light control devices [1, 2], color filters [3], nanolasers [4], nanoantennas [5], optomechanical manipulation [6], sensors [7–10], metamaterials and metasurfaces [11–14] and many other interesting applications are driven by such resonators. To date, research is being actively conducted in nanophotonics aimed at studying the different geometry shapes of metaatoms to obtain different unexpected effects.

As a result, using the unusual shapes of nanoscatterers, it is possible to obtain new effects and more finely tune the optical properties of structures by controlling the multipole components. In particular, truncated conical particles are promising, which have an additional variable radius in contrast to cylinders, which is its undeniable advantage. Also, this geometry has many advantages in practice, because most cylinders in practice turn out to be truncated cones for the reason that imperfections in fabrication [15, 16].

Newly obtained anapole (cancellation of the dipole radiation via the toroidal dipole one due to their destructive interference) [17] or hybrid anapole regimes (HA) [12] – simultaneous fulfillment of anapole conditions for all the main multipoles (up to the magnetic quadrupole) in a scatterer, giving rise to the far-field scattering suppression and strong near-field localization regardless of a substrate. Such properties open up new possibilities for creating various devices. Based on such metaatoms, it is possible to

create almost perfectly transparent metasurfaces to tune the phase shift of transmitted light with a strong near-field enhancement, useful for nonlinear and Raman applications for various materials of substrates and shapes of scatterers [13, 18].

In this study, we investigate the influence of symmetry breaking along the main axis of the cylinder in the Hybrid anapole regime on the conservation of the effect. Quite often, due to the non-ideal fabrication process, it is not possible to obtain ideally shaped cylinders, which makes it necessary to understand the tolerance. In practice, samples are most often obtained in the form of a truncated cone [19, 20]. Please note that the first paragraph of a section or subsection is not indented. The first paragraphs that follows a table, figure, equation etc. does not have an indent, either.

2   Non-scattering Regime in Cone Silicon Particles

Anapole electrodynamics has recently gained a lot of popularity [21]. Anapoles are semi-nonradiating sources that arise due to the destructive interference of the electric dipole moment and the toroidal dipole in the far field. Alternatively, in a more general picture, they can be understood as being due to the destructive interference of symmetry-compatible quasinormal modes [12].

The nonzero stored energy of quasi-normal modes inside a particle leads to unexpected processes of interaction of light with matter in the absence of elastic scattering. Initially, the suppression of scattering in these states was limited to the electric dipole contribution to radiation.

Recently, after a theoretical description, the experimental possibility of obtaining a Hybrid anapole was demonstrated by overlapping multipole channels up to a magnetic quadrupole by carefully selecting the geometric parameters of the particle [22]. Such states are the next step in anapole electrodynamics for a number of reasons [12, 13]. In such particles, scattering is suppressed approximately 20 times more strongly, and the energy stored by quasi-normal modes increases by about 10 times. These values exceed by far the performance of anapoles, and 2nd order anapoles [23] arising in homogeneous disk nanoresonators.

For a cylindrical silicon particle in the Hybrid anapole regime, a multipole decomposition was demonstrated in Fig. 1a studied in [12, 13].

The 'Hybrid anapole wavelength (λHA)' will be the point with the least scattering on the spectrum, the image in the inset demonstrates the distribution of the electric field norm at this point. The field for particles in the Hybrid anapole regime is concentrated inside the particle, which can be seen from the inserts (two hot spots appear inside the cylinder). The evolution of the distribution of the electric field norm in a nanoparticle with a change in the conicity parameter can be traced in the insets. Areas where the electric field norm reaches its maximum are marked in red. Due to this, particles become insensitive to the environment and to neighboring meta-atoms, which opens up new possibilities for designing metasurfaces.

As a result, the scatterer practically does not distort the field incident on it, even in the near zone. Keeping the height of the particle, we change its conicity Rtop/Rbottom. The multipole decompositions for three selected conicities are shown in Fig. 1a-c. All figures show spectra for illumination from top side of particles shown in the insets in Fig. 1. A log scale is used to enhance the contrast of the zeros in the spectrum.

First, we see a shift of all resonances to the shortwave region of the spectrum shown in Fig. 1. This is expected, due to the overall size reduction of the lateral dimensions of the resonator. Secondly, the original electric quadrupole (EQ) and magnetic dipole (MD) anapoles blue-shift slower than the magnetic quadrupole (MQ) and electric dipole (ED). As a result, all resonances are shifted relative to each other, and, due to this, the total value of the particle scattering cross section increases. This is demonstrated by calculations of the total scattering cross-section (SCS) as a function of conicity (Fig. 1d).
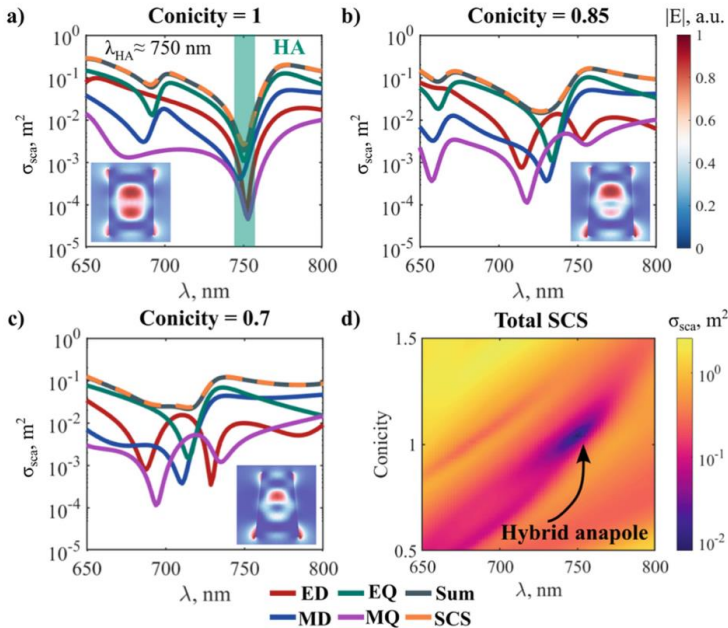
Fig. 1. Evolution of the Hybrid anapole regime as a function of conicity and wavelength. (a-c): Multipole decompositions of the scattering cross-section (semilogarithmic scale) for selected conicities. In all calculations, the height (H) of the nanoparticle was kept constant. Insets: distribution of the electric field norm at Hybrid anapole wavelength (λ_{HA}) (d): Total scattering cross-section as a function of conicity and wavelength (λ). Geometric parameters for all cases: H = 369 nm, R = 127 nm, λ = 748 nm

In practice, it is important to take into account the multipole shifts shown in the Fig. 1. The fact is that due to the imperfection of fabrication (etching usually goes from top to bottom), it is very difficult to obtain ideal cylinders. Various defects can also appear on the edges of the cylinder, which can unexpectedly affect the final effect, since we are dealing with resonances. Therefore, it is very important to study "non-ideal" cylindrical

shapes of nanoscatterers, namely, truncated nanocones, which are demonstrated in this work.

3   Conclusion

The results in this study show that changes in the conicity of the particle significantly affect its resonant properties, which entails the destruction of the Hybrid anapole regime. We have shown how, using the fine tuning of geometric parameters, it is possible to improve the effect obtained and how the imperfection of technological processes can affect the Hybrid anapole regime.

This knowledge can be useful when designing devices for different photonic applications based on a Hybrid anapole regime, such a metasurface engineering for sensing, holographic applications, warless transfer power etc.

References

1. Barhom, H., et al.: Biological kerker effect boosts light collection efficiency in plants. Nano Lett. **19**, 7062–7071 (2019)
2. Shamkhi, H.K., et al.: Transparency and perfect absorption of all-dielectric resonant metasurfaces governed by the transverse Kerker effect. Phys. Rev. Mater. **3**, 1–10 (2019)
3. Hong, J., Son, H., Kim, C., Mun, S.-E., Sung, J., Lee, B.: Absorptive metasurface color filters based on hyperbolic metamaterials for a CMOS image sensor. Opt. Express **29**, 3643 (2021)
4. Xu, K., Fang, M., Huang, Z.: Compact unidirectional laser based on all-dielectric metasurface with high quality factor. IEEE Photon. J. **13**, 1–9 (2021)
5. Sain, B., Meier, C., Zentgraf, T.: Nonlinear optics at all-dielectric nanoantennas and metasurfaces. ArXiv. **1**, 1–14 (2020)
6. Canós Valero, A., et al.: Nanovortex-driven all-dielectric optical diffusion boosting and sorting concept for lab-on-a-chip platforms. Adv. Sci. **7**, 1903049 (2020)
7. Novitsky, D.V., Karabchevsky, A., Lavrinenko, A.V., Shalin, A.S., Novitsky, A.V.: PT symmetry breaking in multilayers with resonant loss and gain locks light propagation direction. Phys. Rev. B. **98**, 125102 (2018)
8. Terekhov, P.D., Evlyukhin, A.B., Redka, D., Volkov, V.S., Shalin, A.S., Karabchevsky, A.: Magnetic octupole response of dielectric quadrumers. Laser Photon. Rev. **14**, 1900331 (2020)
9. Vestler, D., et al.: Circular dichroism enhancement in plasmonic nanorod metamaterials. Opt. Express **26**, 17841 (2018)
10. Novitsky, D.V., Shalin, A.S., Redka, D., Bobrovs, V., Novitsky, A.V.: Quasibound states in the continuum induced by PT symmetry breaking. Phys. Rev. B. **104**, 085126 (2021)
11. Terekhov, P.D., et al.: Enhanced absorption in all-dielectric metasurfaces due to magnetic dipole excitation. Sci. Rep. **9**, 1–9 (2019)
12. Canós Valero, A., et al.: Theory, observation, and ultrafast response of the hybrid anapole regime in light scattering. Laser Photon. Rev. **15**, 2100114 (2021)

13. Kuznetsov, A.V., Canós Valero, A., Tarkhov, M., Bobrovs, V., Redka, D., Shalin, A.S.: Transparent hybrid anapole metasurfaces with negligible electromagnetic coupling for phase engineering. Nanophotonics **10**, 4385–4398 (2021)

14. Kostina, N.A., et al.: Nanoscale tunable optical binding mediated by hyperbolic metamaterials. ACS Photon. **7**, 425–433 (2020)

15. Patoux, A., et al.: Challenges in nanofabrication for efficient optical metasurfaces. Sci. Rep. **11**, 1–12 (2021)

16. Toliopoulos, D., et al.: Fabrication of spectrally sharp Si-based dielectric resonators: combining etaloning with Mie resonances. Opt. Express **28**, 37734 (2020)

17. Miroshnichenko, A.E., et al.: Nonradiating anapole modes in dielectric nanoparticles. Nat. Commun. **6**, 1–8 (2015)

18. Ospanova, A.K., Basharin, A., Miroshnichenko, A.E., Luk'yanchuk, B.: Generalized hybrid anapole modes in all-dielectric ellipsoid particles [Invited]. Opt. Mater Express **11**, 23 (2021)

19. Wang, J., Du, J.: Plasmonic and dielectric metasurfaces: design, fabrication and applications. Appl. Sci. **6**, 239 (2016)

20. Su, V.-C., Chu, C.H., Sun, G., Tsai, D.P.: Advances in optical metasurfaces: fabrication and applications [Invited]. Opt. Express **26**, 13148 (2018)

21. Baryshnikova, K.V., Smirnova, D.A., Luk'yanchuk, B.S., Kivshar, Y.S.: Optical anapoles in nanophotonics and meta-optics. Adv. Opt. Mater **1801350**, 1–13 (2019)

22. Luk'yanchuk, B., Paniagua-Domínguez, R., Kuznetsov, A.I., Miroshnichenko, A.E., Kivshar, Y.S.: Hybrid anapole modes of high-index dielectric nanoparticles. Phys. Rev. A (Coll Park). **95**, 1–8 (2017)

23. Grinblat, G., Li, Y., Nielsen, M.P., Oulton, R.F., Maier, S.A.: Enhanced third harmonic generation in single germanium nanodisks excited at the anapole mode. Nano Lett. **16**, 4635–4640 (2016)

[PAPER 9]: Superscattering Regime for Si Conical Nanoparticles for the Different Directions of Excitation

Kuznetsov, A.V., Bobrovs, V., "*Superscattering Regime for Si Conical Nanoparticles for the Different Directions of Excitation*," Proceedings of 12th International Conference on Computer Science Online Conference «CSOC 2023», Lecture Notes in Networks and Systems, Vol. 723, pp. 254 – 258, online, 3-5 April **2023**.

Superscattering Regime for Si Conical Nanoparticles for the Different Directions of Excitation

Alexey V. Kuznetsov[1,2]([⊠]) [iD] and Vjaceslavs Bobrovs[2] [iD]

[1] Moscow Institute of Physics and Technology, Dolgoprudny, Russia
alexey.kuznetsov98@gmail.com
[2] Riga Technical University, Riga, Latvia

Abstract. Through all-dielectric nanophotonics, it becomes possible to obtain a huge variety of new optical phenomena based on semiconductor dielectric nanoresonators. In this study, we investigate easy-to-make truncated-cone resonators and achieve superscattering regime due to the inherent property of cones – broken symmetry along the main axis without involving complex geometry or structured beams. Additional degrees of freedom due to the conicity allow for more fine-tuning of the interaction of light with matter at the nanoscale. #CSOC1120.

Keywords: Superscattering · All-Dielectric Nanophotonics · Truncated Cone

1   Introduction

In recent years, more and more relevant to the optical properties of subwavelength dielectric nanoparticles. With the help of such elements, it is possible to create platforms that exceed existing analogues in their properties, and sometimes even belong to a new class of devices. The undeniable advantages of such elements include high efficiency, low losses and the ability to control light at the nanolevel. Light control devices [1, 2], nanolasers [3, 5], nanoantennas [6, 8], optomechanical manipulation [9, 10], sensors [11, 14], metamaterials and metasurfaces [15–19] are driven by such resonators for different photonic application.

Interest in this direction grew significantly when it became possible to spectrally overlap resonances, which leads to various nanophotonic effects. Besides the completely non-scattering nanoobjects, researchers are also interested in the cases, when nanoparticles become anomalously strong scatterers. Such states are the opposite of an anapole [17, 18], because at a certain frequency scattering maxima of several multipoles appear; this state is called superscattering [20]. Nanoscatterers supporting this feature can find their application in a number of applications, such as sensing, optical communication, and other emerging areas [21, 22].

2   Superscattering Regime in Cone Silicon Particles

The study of various shapes of nanoscatterers has become increasingly popular in recent years due to the possibility of obtaining new effects and more precise tuning of multipole contributions to scattering pattern.

The most convenient in manufacturing geometry shape of scatterer with a large number of degrees of freedom is a truncated cone. Due to directed etching, a truncated cone is most likely to be obtained during sample production; therefore, the study of this shape of nanoresonators is important for optimizing the fabrication process and getting new effects [23, 24].

It is because of the symmetry breaking in the case of truncated nanocones along the z axis, it is important to study the multipole content of nanoscatterers depending on the direction of radiation (Fig. 1). By changing the direction, the multipole content of the nanoscatterer changes, while the total cross-section does not change.
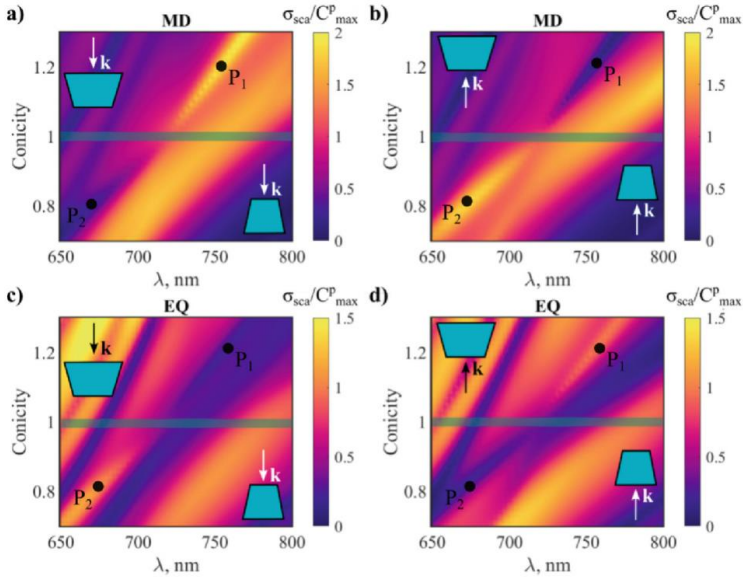
Fig. 1. Magnetic dipole and electric quadrupole contributions to the total scattering cross-section of the truncated cone. (a), (b) Multipole contributions for normally-incident plane wave for propagating along the z-direction (forward). (c), (d) Multipole contributions of the scattering for the opposite (backward) excitation. Geometric parameters: P_1: H = 415 nm, R_{top} = 216 nm, R_{bottom} = 180 nm, λ = 760 nm, P_2: H = 415 nm, R_{top} = 144 nm, R_{bottom} = 180 nm, λ = 673 nm

As depicted in Fig. 1, radiation occurs through the magnetic dipole (MD) and electric quadrupole (EQ) channels depending on the direction of the incident radiation. Interestingly, if the propagation of the light has a different direction the magnetic dipole channel displays strong superscattering in the lower branch of the interference (see Fig. 1(a), (b)).

A similar but opposite statement can be made for the electric quadrupole channel (see Fig. 1(c), (d)). Considering the structure is assumed to be lossless then the total scattering is conserved upon a reversed excitation direction. Notably, the two odd multipolar channels offset the difference in the scattering whereas their summed contribution to scattering and the overall bandwidth is nearly identical for both the forward and backward incident light propagation.

In Fig. 2 the near-field and far-field scattering signatures are shown for the two points P_1 and P_2 of the scattering maxima. The figure shows how a particle in the superscattering regime can significantly change the field around it. By carefully tuning the geometry of the nanoresonator, it is possible to obtain the necessary radiation patterns, which makes such particles a promising platform for devices capable of controlling light at the nanoscale.
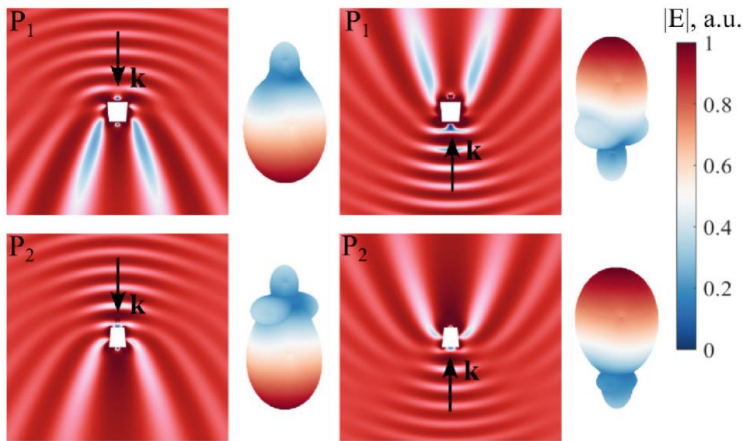

Fig. 2. Strong near-field distribution and the correspondent scattering pattern for the points (P_1 and P_2 (see Fig. 1)) of maximum scattering. Scattering patterns and distribution of the near field are shown depending on the direction of the incident radiation on the truncated cone particle. A plane wave was used as the incident radiation.

Although the total scattering remains identical upon reversed excitation direction there are noticeable differences in scattering patterns. While the presence of the scattering side lobes evidences a strong presence of electric quadrupole radiation the overall directivity at P_2 is higher compared to P_1. This can be noticed by the scaled backscattering-caused shadow at P_1 for the case of the backward excitation. However, when the magnetic

dipole dominates the scattering, the situation is reversed where the scattering is more directive under the forward excitation.

In such way, by changing the direction of the incident light onto a cone particle, one can obtain different radiation patterns in the particle superscattering regime. This opens up new horizons for designing various structures with the ability to control optical properties depending on the direction of radiation.

3   Conclusion

Thus, we have demonstrated a remarkable control over scattering afforded by the conical geometry. We have demonstrated that conicity can be utilized to enhance scattering strongly and to control scattering linewidth in a broad range.

We showed that the behavior of different multipoles, which can be controlled by conicity, influences certain outcome in scattering for instance. It indeed leaves plethora of opportunities to optimize "the practical" cone geometry for intended applications.

References

1. Barhom, H., et al.: Biological Kerker effect boosts light collection efficiency in plants. Nano Lett. **19**, 7062–7071 (2019)
2. Shamkhi, H.K., et al.: Transparency and perfect absorption of all-dielectric resonant metasurfaces governed by the transverse Kerker effect. Phys. Rev. Mater. **3**, 1–10 (2019)
3. Xu, K., Fang, M., Huang, Z.: Compact unidirectional laser based on all-dielectric metasurface with high quality factor. IEEE Photon. J. **13**, 1–9 (2021)
4. Shankhwar, N., Sinha, R.K., Kalra, Y., Makarov, S., Krasnok, A., Belov, P.: High-quality laser cavity based on all-dielectric metasurfaces. Photon. Nanostruct. **24**, 18–23 (2017)
5. Totero Gongora, J.S., Miroshnichenko, A.E., Kivshar, Y.S., Fratalocchi, A.: Anapole nanolasers for mode-locking and ultrafast pulse generation. Nat Commun. **8**, 1–9 (2017)
6. Sain, B., Meier, C., Zentgraf, T.: Nonlinear optics at all-dielectric nanoantennas and metasurfaces. ArXiv. **1**, 1–14 (2020)
7. Krasnok, A.E., Miroshnichenko, A.E., Belov, P.A., Kivshar, Y.S.: All-dielectric optical nanoantennas. Opt. Express. **20**, 20599 (2012)
8. Li, N., Lai, Y., Lam, S.H., Bai, H., Shao, L., Wang, J.: Directional control of light with nanoantennas. Adv. Opt. Mater. **9**, 1–32 (2021)
9. Canós Valero, A., et al.: Nanovortex-driven all-dielectric optical diffusion boosting and sorting concept for lab-on-a-chip platforms. Adv. Sci. **7**, 1903049 (2020)
10. Dienerowitz, M., Mazilu, M., Dholakia, K.: Optical manipulation of nanoparticles: a review. J. Nanophoton. **2**, 021875 (2008)
11. Novitsky, D.V., Karabchevsky, A., Lavrinenko, A.V., Shalin, A.S., Novitsky, A.V.: PT symmetry breaking in multilayers with resonant loss and gain locks light propagation direction. Phys. Rev. B. **98**, 125102 (2018)

12. Terekhov, P.D., Evlyukhin, A.B., Redka, D., Volkov, V.S., Shalin, A.S., Karabchevsky, A.: Magnetic octupole response of dielectric quadrumers. Laser Photon. Rev. **14**, 1900331 (2020)
13. Vestler, D., et al.: Circular dichroism enhancement in plasmonic nanorod metamaterials. Opt. Express. **26**, 17841 (2018)
14. Novitsky, D.V., Shalin, A.S., Redka, D., Bobrovs, V., Novitsky, A.V.: Quasibound states in the continuum induced by PT symmetry breaking. Phys. Rev. B. **104**, 085126 (2021)
15. Kozlov, V., Filonov, D., Shalin, A.S., Steinberg, B.Z., Ginzburg, P.: Asymmetric backscattering from the hybrid magneto-electric meta particle. Appl. Phys. Lett. **109**, 203503 (2016)
16. Terekhov, P.D., et al.: Enhanced absorption in all-dielectric metasurfaces due to magnetic dipole excitation. Sci. Rep. **9**, 1–9 (2019)
17. Canós Valero, A., et al.: Theory, observation, and ultrafast response of the hybrid anapole regime in light scattering. Laser Photon. Rev. **15**, 2100114 (2021)
18. Kuznetsov, A.V., Canós Valero, A., Tarkhov, M., Bobrovs, V., Redka, D., Shalin, A.S.: Transparent hybrid anapole metasurfaces with negligible electromagnetic coupling for phase engineering. Nanophotonics **10**, 4385–4398 (2021)
19. Kostina, N.A., et al.: Nanoscale tunable optical binding mediated by hyperbolic metamaterials. ACS Photon. **7**, 425–433 (2020)
20. Ruan, Z., Fan, S.: Superscattering of light from subwavelength nanostructures. Phys. Rev. Lett. **105**, 1–4 (2010)
21. Krasikov, S.D., et al.: Superscattering for non-spherical objects. J. Phys. Conf. Ser. **2015**, 012073 (2021)
22. Liu, W., Lei, B., Shi, J., Hu, H.: Unidirectional superscattering by multilayered cavities of effective radial anisotropy. Sci. Rep. **6**, 1–9 (2016)
23. Wang, J., Du, J.: Plasmonic and dielectric metasurfaces: design, fabrication and applications. Appl. Sci. **6**, 239 (2016)
24. Su, V.-C., Chu, C.H., Sun, G., Tsai, D.P.: Advances in optical metasurfaces: fabrication and applications [Invited]. Opt. Express. **26**, 13148 (2018)

[PAPER 10]: Optomechanical Manipulation of Nanoparticles in Hybrid Anapole State

Babich N., **Kuznetsov, A.**, Bobrovs V., Kislov D., "*Optomechanical Manipulation of Nanoparticles in Hybrid Anapole State*," Proceedings of 12th International Conference on Computer Science Online Conference «CSOC 2023», Lecture Notes in Networks and Systems, Vol. 723, pp. 237 – 243, online, 3-5 April **2023**.

Optomechanical Manipulation of Nanoparticles in Hybrid Anapole State

Nikita Babich[1], Alexey Kuznetsov[1,2,3] , Vjaceslavs Bobrovs[2(✉)] ,
and Denis Kislov[2,3]

[1] ITMO University, St. Petersburg 197101, Russia
[2] Institute of Telecommunications, Riga Technical University, Riga 1048, Latvia
vjaceslavs.bobrovs@rtu.lv
[3] Center for Photonics and 2D Materials, Moscow Institute of Physics and Technology,
Dolgoprudny 141700, Russia

Abstract. The report analyzes the optomechanical interaction of a Gaussian beam and a silicon nanoparticle in a hybrid anapole state. To study the particle scattering in the Gaussian beam waist, as well as to confirm the appearance of a hybrid anapole state, a multipole decomposition was carried out. We made calculations of the optical forces acting on the particle along different directions depending on the relative position of the light beam and the particle. The pressure and gradient components of force were analyzed separately. In addition, the torque acting on the anapole and scattering particles at the center of the beam waist was calculated. It is shown that the torque can change sign if the particle is at anapole. #CSOC1120.

Keywords: Anapole · Optical Force · Multipole Decomposition

1 Introduction

The phenomenon of the mechanical action of light on various objects [1] has been widely used in science and technology [2–5]. On its basis, an optical tweezer was created, which revolutionized biology [6–8]. With its help, cells and proteins are manipulated, which is impossible with mechanical tools. This technology allows us to study cells and bacteria at a qualitatively new level, as well as to study intracellular processes. In addition to biology, optical tweezers have been widely used in physics [9–11] and chemistry [12–16]. The adaptation of this technology made it possible to obtain a Bose condensate, which greatly advanced the study of quantum effects.

Turning to the nature of the phenomenon, we should note that when a wave interacts with a particle, two components of forces of different nature can be distinguished. The pressure component of the force is caused by the transmission of the wave momentum to the object, and the gradient component arising from the inhomogeneous distribution of the amplitude of the light intensity along the wave profile draws the particle into the region of maximum intensity [4]. In this paper, we wondered whether the hybrid anapole state [17–21] has advantages in terms of optical force [22–28]. The purpose of this report

was to investigate how the ratio of the components of the pressure and gradient forces acting on a particle in a hybrid anapole state [29–32] will change.

In the course of the work, a hypothesis was put forward about the existence of the hybrid anapole state for a cylindrical silicon nanoparticle in a linearly polarized Gaussian beam. The goal of the report was to study the optical forces and torque arising in a focused Gaussian beam for various configurations of the system.

2 Methods

We For the numerical experiment, simulations were carried out in the COMSOL Multiphysics package. To calculate the components of the forces $\boldsymbol{F}$, a time-averaged Maxwell stress-tensor $\overset{\leftrightarrow}{\mathbf{M}}$ is integrated over a surface around the nanoparticle. The similar way was to calculate the torque $\boldsymbol{T}$ arising in the system relative to the origin – integrating the cross product of the radius-vector and Maxwell stress-tensor. Integrating nanoparticles by volume, electric and magnetic dipole and quadrupole moments were obtained, using them, the scattering coefficients of each component were calculated, that are necessary to determine the existence of a hybrid anapole state. Here and further by forces and torques meant time-averaged forces and torques:

$$\langle \mathbf{F} \rangle = \int_S \left\langle \overset{\leftrightarrow}{\mathbf{M}} \right\rangle \cdot \mathbf{n} \, d\sigma \tag{1}$$

$$\langle \mathbf{T} \rangle = -\int_S \mathbf{n} \cdot \left[\left\langle \overset{\leftrightarrow}{\mathbf{M}} \right\rangle \times \mathbf{r} \right] d\sigma \tag{2}$$

where $\left\langle \overset{\leftrightarrow}{\mathbf{M}} \right\rangle = \frac{1}{2}\mathrm{Re}\left[\varepsilon_0 \mathbf{E} \otimes \mathbf{E}^* + \mu_0 \mathbf{H} \otimes \mathbf{H}^* - \frac{1}{2}\left(\varepsilon_0 |\mathbf{E}|^2 + \mu_0 |\mathbf{H}|^2 \right) \overset{\leftrightarrow}{\mathbf{I}} \right]$.

The system we are exploring is the cylindrical silicon resonator with special size parameters. The height of the cylinder is h = 369 nm, the radius is r = 127 nm. These parameters have been chosen to have a resonance wavelength of 750 nm where hybrid anapole state is observed with linearly polarized plane wave. The cylinder is placed in a Gaussian beam, and its center of mass is in the waist plane of the beam as it can be mentioned from Fig. 1. The default beam's waist radius was $w_0 = \lambda$.
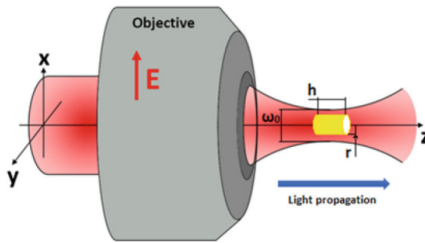

Fig. 1. The geometry of the problem.

3   Results

To confirm the existence of the hybrid anapole state (HAS) the linearly polarized wave was simulated. The scattering coefficient from the wavelength was calculated. Hybridity at $\lambda \sim 750$ nm was clearly confirmed, which allowed us to proceed to a further solution of the problem.

Then during the numerical experiment, the hypothesis of the existence of a HAS for a cylindrical nanoparticle in a Gaussian beam was tested, and the properties of a HAS were analyzed. The primary conclusion of the experiment is the fact of the destruction of the HAS as the nanoparticle moves away from the optical axis, which can be seen in Fig. 2.
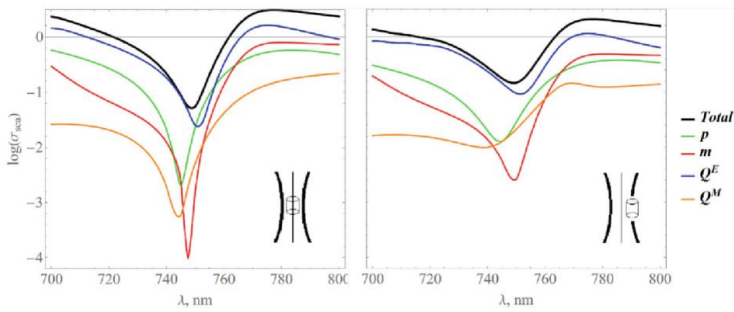
Fig. 2. Logarithm of scattering cross-section from the wavelength. HAS destruction demonstration with moving nanoparticle from the optical axis of the Gaussian beam.

Total is the sum of every multipole component of the coefficient (p – electric dipole, m – magnetic dipole, Q^E – electric quadrupole, Q^M – magnetic quadrupole). The minima of multipoles cease to be at the same wavelength. This is explained by the fact that at a distance from the optical axis, even in the focal plane of the beam, the wave front is curved and it cannot be approximated as a plane wave.

To obtain a gradient force comparable to the pressure force, a large curvature of the beam is required. This can be achieved by reducing the waist w_0 to values comparable to half the wavelength. During the simulation, an additional factor was revealed that strongly affects the optical forces in the system. The minimum waist radius is comparable to the radius of the cylinder itself. Therefore, the profiles of forces in our experiment for differently focused, will be different, which can be seen in Fig. 3.
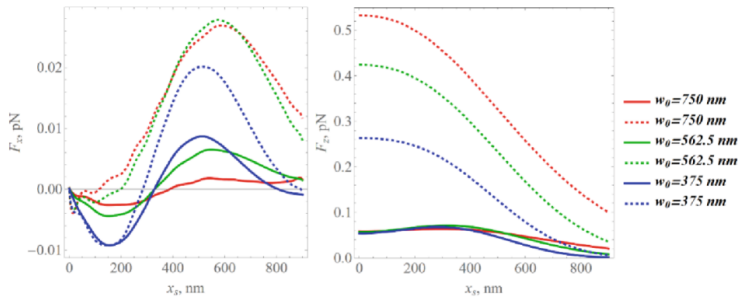
Fig. 3. The forces dependence on the position of nanoparticle. Dotted lines – non-anapole state ($\lambda_1 = 770$ nm). Solid graphs – anapole state ($\lambda_2 = 750$ nm).

During the experiment, three configurations of a Gaussian beam ($w_1 = 375$ nm, $w_2 = 562.5$ nm, $w_3 = 750$ nm) were considered at two wavelengths – anapole $\lambda_1 = 750$ nm and non-anapole $\lambda_2 = 770$ nm. Since the forces are symmetric with respect to the optical beam, they were considered only for a one-way shift – $x_s \in [0, 0.9]$ µm.

It is clearly proved that in the anapole state, the pressure force on the particle is an order of magnitude smaller. Let us consider separately the case of the waist radius equal to the wavelength ($w_0 = \lambda = 750$ nm). When the hybrid anapole state exists the pressure force on the cylinder placed on the optical axis of the beam $F_{z,\text{anap.}}(0) \sim 0.08$ pN. If HAS do not exists ($\lambda = 770$ nm, $w_0 = 750$ nm) the pressure force is maximum $F_{z,\text{no anap.}}(0) \sim 0.53$ pN. The relation of these forces exactly repeats relation of the scattering coefficients.

4   Discussions

In this report we also explore the rotation of the nanoparticle around the y-axis and torques arising in this system. It was important to understand how the hybrid anapole state behaves during the rotation of the cylinder in the Gaussian beam. It was clearly shown that HAS destructs and the scattering properties of the particle aims to non-anapole.

If the cylinder is coaxial to the optical beam, apparently there are no moments and there is only one component of the optical power (F_z is pressure). In our case, there is only one moment component (T_y), with T_x, $T_z = 0$. As expected, in the non-anapole system, there is one equilibrium position when the cylinder axis coincides with the beam axis (Fig. 4, dotted curve).

In the case when a hybrid anapole state is formed in the particle, there is one-point $\alpha = 40°$, when the torque changes sign. Thus, it was obtained that there are two equilibrium positions $0°$ and $90°$ in HAS. This is not a typical behavior compared to "ordinary" particles.
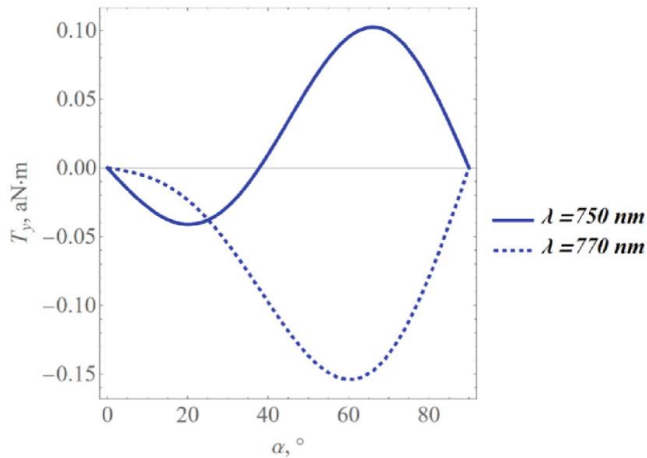
Fig. 4. Torque arising in the system out of rotating the cylinder in the Gaussian beam.

5 Conclusion

Summing up the results of the work, we can first of all highlight the fact of confirmation of the hypothesis of a decrease in the pressure force in the hybrid anapole state for a Gaussian beam. Some nontrivial features of the HAS were also discovered. The first of them is the fact of the destruction of the hybrid anapole state in the particle as it moves away from the optical axis. This is explained by the curvature of the beam front. Another fact highlights the dependence of the pressure force on the waist radius of the beam. This phenomenon is due to the fact that the waist radius of the beam is comparable with the radius of the cylinder. The beam intensity is distributed non-linearly at the end of the cylinder.

Moreover, torques arising when cylinder is tilted relative to the optical axis of the Gaussian beam were studied. There is a balance in the general case if the particle is not coaxial to the optical axis. However, for the anapole particles there is an angle ($\alpha = 40°$) when $\mathbf{T} = 0$ and torque changes sign.

References

1. Ashkin, A., Dziedzic, J.M., Bjorkholm, J.E., Chu, S.: Observation of a single-beam gradient force optical trap for dielectric particles. Opt Lett. **11**(5), 288 (1986)
2. Tkachenko, G., Brasselet, E.: Optofluidic sorting of material chirality by chiral light. Nat. Commun. **5**, 3577 (2014)
3. Canós Valero, A., Kislov, D., Gurvitz, E.A., et al.: Nanovortex-driven all-dielectric optical diffusion boosting and sorting concept for lab-on-a-chip platforms. Adv. Sci. **7**(11), 1903049 (2020)
4. Kislov, D., Novitsky, D., Kadochkin, A., Redka, D., Shalin, A.S., Ginzburg, P.: Diffusion-inspired time-varying phosphorescent decay in a nanostructured environment. Phys. Rev. B **101**, 035420 (2020)
5. Kucherenko, M.G., Kislov, D.A.: Plasmon-activated intermolecular nonradiative energy transfer in spherical nanoreactors. The J. Photochem. Photobiol. A: Chem. **354**, 25 (2018)
6. Favre-Bulle, I.A., et al.: Optical trapping in vivo: theory, practice, and applications. Nanophotonics **8**, 1023 (2019)
7. Liu, X., et al.: All-optical targeted drug delivery and real-time detection of a single cancer cell. Nanophotonics **9**, 611 (2020)
8. Izmodenova, S.V., Kislov, D.A., Kucherenko, M.G.: Accelerated nonradiative electron-excitation energy transfer between molecules in aqueous pools of reverse micelles containing encapsulated silver nanoparticles. Colloid J. **76**(6), 683–693 (2014). https://doi.org/10.1134/S1061933X14060088
9. Kostina, N., et al.: Optical binding via surface plasmon polariton interference. Phys. Rev. B **99**, 125416 (2019)
10. Kislov, D.: Effect of plasmonic silver nanoparticles on the photovoltaic properties of Graetzel solar cells. Phys. Procedia **73**, 114 (2015)
11. Vestler, D., Shishkin, I., Gurvitz, E.A., et al.: Circular dichroism enhancement in plasmonic nanorod metamaterials. Opt Express **26**(14), 17841–17848 (2018)
12. Kostina, N.A., Kislov, D.A., Ivinskaya, A.N., et al.: Nanoscale tunable optical binding mediated by hyperbolic metamaterials. ACS Photonics **7**(2), 425–433 (2020)
13. Ivinskaya, A., et al.: Optomechanical manipulation with hyperbolic metasurfaces. ACS Photonics **5**, 4371 (2018)
14. Ivinskaya, A., Petrov, M.I., Bogdanov, A.A., Shishkin, I., Ginzburg, P., Shalin, A.S.: Plasmon-assisted optical trapping and anti-trapping. Light Sci. Appl. **6**, e16258 (2017)
15. Novitsky, D., Karabchevsky, A., Lavrinenko, A., Shalin, A., Novitsky, A.: PT symmetry breaking in multilayers with resonant loss and gain locks light propagation direction. Phys Rev B **98**, 125102 (2018)
16. Novitsky, D.V., Shalin, A.S., Redka, D., Bobrovs, V., Novitsky, A.V.: Quasibound states in the continuum induced by PT symmetry breaking. Phys Rev B **104**(8), 85126 (2021)
17. Baryshnikova, K., et al.: Giant magnetoelectric field separation via anapole-type states in high-index dielectric structures. Phys. Rev. B **98**, 165419 (2018)
18. Barhom, H., et al.: Biological kerker effect boosts light collection efficiency in plants. Nano Lett. **19**(10), 7062 (2019)
19. Terekhov, P.D., Baryshnikova, K.V., Greenberg, Y., et al.: Enhanced absorption in all-dielectric metasurfaces due to magnetic dipole excitation. Sci. Rep. **9**, 3438 (2019)
20. Kozlov, V., Filonov, D., Shalin, A.S., Steinberg, B.Z., Ginzburg, P.: Asymmetric backscattering from the hybrid magneto-electric meta particle. Appl. Phys. Lett. **109**, 203503 (2016)
21. Terekhov, P.D., et al.: Broadband forward scattering from dielectric cubic nanoantenna in lossless media. Opt. Express **27**(8), 10924 (2019)

22. Xu, X., et al.: Kerker-type intensity-gradient force of light. Laser Photonics Rev. **14**, 1 (2020)
23. Länk, N.O., Johansson, P., Käll, M.: Directional scattering and multipolar contributions to optical forces on silicon nanoparticles in focused laser beams. Opt. Express **26**(22), 29074 (2018)
24. Liu, H., Panmai, M., Peng, Y., Lan, S.: Optical pulling and pushing forces exerted on silicon nanospheres with strong coherent interaction between electric and magnetic resonances. Opt. Express **25**(11), 12357 (2017)
25. Salandrino, A., Fardad, S., Christodoulides, D.N.: Generalized Mie theory of optical forces. J. Opt. Soc. Am. B **29**(4), 855 (2012)
26. Duan, X.Y., Wang, Z.G.: Fano resonances in the optical scattering force upon a high-index dielectric nanoparticle. Phys. Rev. A **96**(5), 053811 (2017)
27. Chen, J., Ng, J., Lin, Z., Chan, C.T.: Optical pulling force. Nat. Photonics **5**, 531 (2011)
28. Nieto-Vesperinas, M., Sáenz, J.J., Gómez-Medina, R., Chantada, L.: Optical forces on small magnetodielectric particles. Opt. Express **18**(11), 11428 (2010)
29. Terekhov, P.D., Evlyukhin, A.B., Redka, D., Volkov, V.S., Shalin, A.S., Karabchevsky, A.: Magnetic octupole response of dielectric quadrumers. Laser Photon Rev **14**(4), 1900331 (2020)
30. Shamkhi, H.K., Sayanskiy, A., Valero, A.C., et al.: Transparency and perfect absorption of all-dielectric resonant metasurfaces governed by the transverse Kerker effect. Phys. Rev. Mater. **3**(8), 85201 (2019)
31. Canós Valero, A., Gurvitz, E.A., Benimetskiy, F.A., et al.: Theory, observation, and ultrafast response of the hybrid anapole regime in light scattering. Laser Photon. Rev. **15**(10), 2100114 (2021)
32. Kuznetsov, A.V., Canós Valero, A., Tarkhov, M., Bobrovs, V., Redka, D., Shalin, A.S.: Transparent hybrid anapole metasurfaces with negligible electromagnetic coupling for phase engineering. Nanophotonics **10**(17), 4385–4398 (2021)

[PAPER 11]: Transverse Kerker Effects in All-Dielectric Conical Nanoparticles

Transverse Kerker Effects in All-Dielectric Conical Nanoparticles

Alexey V. Kuznetsov[1,2]([envelope]) [ORCID] and Vjaceslavs Bobrovs[2] [ORCID]

[1] Moscow Institute of Physics and Technology, Dolgoprudny, Russia
alexey.kuznetsov98@gmail.com
[2] Riga Technical University, Riga, Latvia

Abstract. A lot of new effects and phenomena based on dielectric nanoscatterers are becoming possible through research in the field of dielectric nanophotonics. These resonators show exceptional optical characteristics, encompassing both electric and magnetic responses within the visible spectrum. The conical shape introduces additional degrees of freedom, paving the way for fresh opportunities to tailor light-matter interactions at the nanoscale. In this research, we study truncated cone resonators, which demonstrate transverse Kerker effects.

Keywords: Transverse Kerker effects · Truncated Cone · All-dielectric nanophotonics

1 Introduction

In recent years, interest in studying the optical properties of subwavelength dielectric nanoparticles has been constantly growing. These nanoparticles represent a promising basis for creating photonic devices that outperform their counterparts. They suggest several undeniable advantages [1], such as minimal losses, high efficiency [2–4], and the capability to manipulate both the electric and magnetic components of light simultaneously [5]. As a result of these remarkable properties, nanolasers [6], nanoantennas [7], ultrathin lenses [8], sensors, detectors, metamaterials [9], metasurfaces [10], and numerous other emerging applications have been developed to harness the distinctive effects facilitated by these resonators [11–13].

Remarkable progress in high-index dielectric nanophotonics has been achieved through the efficient use of versatile manipulation of multipole excitations in subwavelength scatterers [14, 15]. This contributed to a deeper understanding and effective control of various phenomena through the integration and interaction of multipole moments. An important result of this achievement is the transverse Kerker effect, which entails the suppression of both backward and forward scattering of nanoparticles. Originally conceived for a hypothetical sphere with equal epsilon and mu [16], the Kerker effect now holds great significance in dielectric nanophotonics. It has paved the way for the development of fully transparent phase-tailoring "Huygens" metasurfaces, offering a wide range of possibilities in this field [8, 17].

Truncated cones are increasingly preferred as components in photonic structures due to their numerous advantages [18]. An important benefit lies in their capacity to adjust one of the radii, introducing an additional level of flexibility. Unlike the more commonly used cylindrical nanoscatterers, nanocones provide precise control over the modal composition of the scatterer. This advanced control allows for improved customization options and effects that were previously unavailable.

This research primarily focuses on the transverse Kerker effects exhibited in silicon truncated nanocones. With the increasing importance of the transverse Kerker effect in the rapidly developing field of dielectric nanophotonics, there is a need to investigate and conceptualize these effects in the context of different scatterer geometries.

2   Transverse Kerker Effects in Cone Silicon Particles

As the Kerker effect has been studied, various combinations of multipole moments and phase differences have been discovered, leading to a broader understanding of the Kerker effect. In addition to the generalized Kerker effect, another crucial scattering phenomenon is the transverse Kerker effect, which was first described in [19, 20]. The transverse Kerker effect primarily arises from the interplay of multipole interactions, leading to scattering that predominantly occurs sideways, with only a minor portion involving forward scattering, in line with the optical theorem. This effect can be realized through straightforward combinations of two multipoles, as well as through more complex configurations (see Fig. 1).

Figure 1 shows the transverse Kerker effects achieved through a combination of numerical and analytical approaches. The term 'transverse' is derived from the shape of the scattering patterns. By adjusting the phases and amplitudes of the multipole components, it is possible to induce lateral scattering while minimizing forward and backward scattering.

This work shows various manifestations of the transverse Kerker effects. The radiation patterns of these cones generated using COMSOL Multiphysics closely resemble the expected Kerker-type patterns obtained from ideal point calculations. However, minor differences arise due to practical limitations in implementing the ideal combination of required multipoles in real systems.

In addition, the results highlight that higher order multipoles are redundant, as evidenced by the good agreement between summation of multipole scattering cross sections and calculations obtained from integration of the Poynting vector over a closed surface within the long range. This agreement is evident from the gray and orange lines shown in Fig. 1a–e.
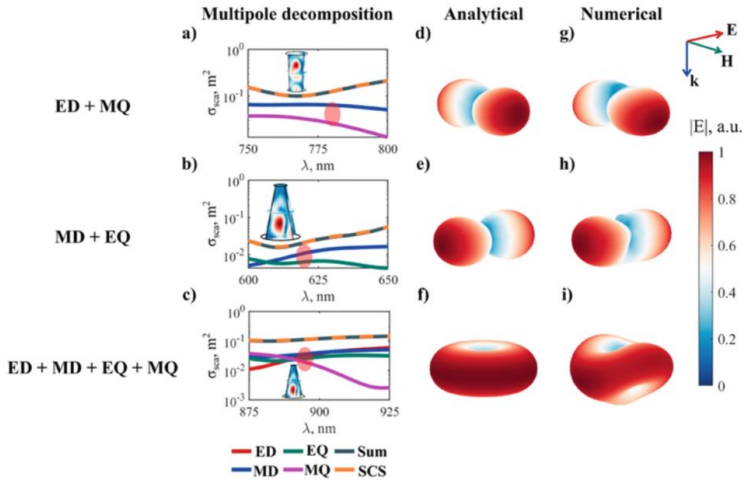
Fig. 1. Transverse Kerker effects in truncated conical nanoparticles with different geometries. Figures (a–c) provide a visual representation of the multipolar decomposition, while figures (d–f) display the far-field sum of multipoles calculated analytically for a point. Figures (g–i) illustrate the numerically calculated far-field distribution for conical nanoparticles of different sizes at the spectral points indicated in (a–c).

3   Conclusion

In this study, we have demonstrated transverse Kerker effects within individual nanoscatterers of the same geometry shape. This makes nanocones a versatile and easy-to-fabricate platform for realizing new photonic devices that use a wide range of effects. This platform provides the flexibility to customize the scattering pattern.

Moreover, our study reveals conical geometry as a versatile platform for achieving numerous important optical effects in the field of nanophotonics. We achieved transverse Kerker effects on a single scatterer shape while accounting for realistic refractive index dispersion of silicon. This research represents a significant advance in the field of nanophotonics, especially in the context of more complex shapes, offering the ability to precisely control the effects achievable with a single nanoscatterer shape. Such advances significantly reduce the costs associated with developing photonic devices and open new opportunities for practical applications in next-generation photonics.

The results of this study have wide implications in various fields of research. In addition, the proposed approach can be used in the development of metasurfaces, opening a number of optical effects that were previously unattainable.

References

1. Shalin, A.S., Sukhov, S.V.: Plasmonic nanostructures as accelerators for nanoparticles: optical nanocannon. Plasmonics **8**, 625–629 (2013)
2. Simovski, C.R., Shalin, A.S., Voroshilov, P.M., Belov, P.A.: Photovoltaic absorption enhancement in thin-film solar cells by non-resonant beam collimation by submicron dielectric particles. J. Appl. Phys. **114** (2013)
3. Shalin, A.S.: Broadband blooming of a medium modified by an incorporated layer of nanocavities. JETP Lett. **91**, 636–642 (2010)
4. Shalin, A.S., Moiseev, S.G.: Optical properties of nanostructured layers on the surface of an underlying medium. Opt. Spectrosc. **106**, 916–925 (2009)
5. Canós Valero, A., et al.: Theory, observation, and ultrafast response of the hybrid anapole regime in light scattering. Laser Photon Rev. **15**, 2100114 (2021)
6. Novitsky, D.V., Valero, A.C., Krotov, A., Salgals, T., Shalin, A.S., Novitsky, A.V.: CPA-lasing associated with the quasibound states in the continuum in asymmetric non-hermitian structures. ACS Photonics **9**, 3035–3042 (2022)
7. Kucherik, A., et al.: Nano-antennas based on silicon-gold nanostructures. Sci. Rep. **9**, 338 (2019)
8. Tian, Y., Li, Z., Xu, Z., Wei, Y., Wu, F.: High transmission focusing lenses based on ultrathin all-dielectric Huygens' metasurfaces. Opt. Mater. (Amst.) **109**, 110358 (2020)
9. Vestler, D., et al.: Circular dichroism enhancement in plasmonic nanorod metamaterials. Opt. Express **26**, 17841 (2018)
10. Kuznetsov, A.V., Canós Valero, A., Tarkhov, M., Bobrovs, V., Redka, D., Shalin, A.S.: Transparent hybrid anapole metasurfaces with negligible electromagnetic coupling for phase engineering. Nanophotonics. **10**, 4385–4398 (2021)
11. Canós Valero, A., et al.: Nanovortex-driven all-dielectric optical diffusion boosting and sorting concept for lab-on-a-chip platforms. Adv. Sci. **7**, 1903049 (2020)
12. Novitsky, D.V., Karabchevsky, A., Lavrinenko, A.V., Shalin, A.S., Novitsky, A.V.: PT symmetry breaking in multilayers with resonant loss and gain locks light propagation direction. Phys. Rev. B **98**, 125102 (2018)
13. Kostina, N.A., et al.: Nanoscale tunable optical binding mediated by hyperbolic metamaterials. ACS Photonics **7**, 425–433 (2020)
14. Terekhov, P.D., Evlyukhin, A.B., Redka, D., Volkov, V.S., Shalin, A.S., Karabchevsky, A.: Magnetic octupole response of dielectric quadrumers. Laser Photon Rev. **14**, 1900331 (2020)
15. Terekhov, P.D., Evlyukhin, A.B., Shalin, A.S., Karabchevsky, A.: Polarization-dependent asymmetric light scattering by silicon nanopyramids and their multipoles resonances. J. Appl. Phys. **125**, 173108 (2019)
16. Kerker, M., Wang, D.S., Giles, C.L.: Electromagnetic scattering by magnetic spheres. J. Opt. Soc. Am. **73**, 765–767 (1983). https://doi.org/10.1364/JOSA.73.000765
17. Pfeiffer, C., Grbic, A.: Metamaterial Huygens' surfaces: Tailoring wave fronts with reflectionless sheets. Phys. Rev. Lett. **110**, 1–5 (2013)
18. Kuznetsov, A.V., et al.: Special scattering regimes for conical all-dielectric nanoparticles. Sci. Rep. **12**, 21904 (2022)

19. Shamkhi, H.K., et al.: Transparency and perfect absorption of all-dielectric resonant metasurfaces governed by the transverse Kerker effect. Phys Rev Mater. **3**, 1–10 (2019)
20. Shamkhi, H.K., et al.: Transverse scattering and generalized kerker effects in all-dielectric mie-resonant metaoptics. Phys. Rev. Lett. **122**, 193905 (2019)

[PAPER 12]: Generalized Kerker Effects in All-Dielectric Conical Nanoparticles

Generalized Kerker Effects in All-Dielectric Conical Nanoparticles

Alexey V. Kuznetsov[1,2] and Vjaceslavs Bobrovs[2(✉)]

[1] Moscow Institute of Physics and Technology, Dolgoprudny, Russia
[2] Riga Technical University, Riga, Latvia
vjaceslavs.bobrovs@rtu.lv

Abstract. All-dielectric nanophotonics allows the study of new optical phenomena and different scattering characteristics from dielectric nanoparticles. These resonators have unique optical properties spanning both electrical and magnetic responses in the visible spectrum, offering promising applications in nano-optics, biology, sensing, and various other fields. Our research focuses on truncated cone resonators, which demonstrate the full range of generalized Kerker effects. This achievement is attributed to an inherent characteristic of cones—their asymmetry along the primary axis. Through a simple geometric approach, these effects enable the optimization of the fabrication of photonic devices with diverse functionalities.

Keywords: Generalized Kerker effects · Truncated Cone · All-dielectric nanophotonics

1 Introduction

Recently, there has been significant interest in studying the optical properties of subwavelength dielectric and semiconductor nanoparticles. These particles hold significant promise, potentially surpassing current technologies and even creating entirely new classes of devices. They offer several undeniable advantages [1], including low losses, high efficiency [2–4], and the ability to manipulate both the electric and magnetic components of light simultaneously [5]. These properties allow to develop of nanolasers [6], nanoantennas [7], ultrathin lenses [8], sensors [9], metamaterials [10, 11], metasurfaces [12], and other emerging applications that harness the unique effects enabled by these resonators [13, 14].

Significant progress has been made in high-index dielectric nanophotonics by successfully achieving flexible control over multipole excitations in subwavelength scatterers [15]. This achievement has enabled a deeper understanding and effective manipulation of various phenomena by combining multipole moments. One notable outcome of this advancement is the realization of the Kerker effect, which allows for the suppression of backward or forward scattering from a nanoparticle [16]. Kerker effect now holds immense importance in the field of dielectric nanophotonics. It has paved the way for the development of fully transparent Huygens metasurfaces that can precisely tailor the phase of light, offering a wide range of possibilities in this area of research [17, 18].

Truncated cones are becoming increasingly popular as components of photonic structures due to their undeniable advantages [19]. A key benefit is that one of the radii can be adjusted, providing an additional level of flexibility. Unlike the frequently employed cylindrical nano-scattering structures, nanocones provide finer control over the mode of the scatterer. This increased level of control results in improved customization capabilities, allowing you to achieve effects that were previously unattainable.

Notably, the truncated-cone geometry is still relatively underexplored when compared to more 'conventional' shapes like spheres, cubes, and cylinders [20, 21]. In this study, we explore the generalized Kerker effects displayed by truncated silicon nanocones. The Kerker effect has found wide application in the rapidly developing field of dielectric nanophotonics. Therefore, it is critical to delve deeper and understand these effects in the context of different scatterer geometries.

2   Generalized Kerker Effects in Cone Silicon Particles

The Kerker effect was originally discovered in spherical particles characterized by identical electrical permeabilities and magnetic permeabilities. In such particles, when the electric and magnetic dipoles have identical field amplitudes and a certain phase shift, only forward or backward scattering is observed. Numerous studies have experimentally confirmed the manifestation of this phenomenon in dielectric nanoparticles. As research progressed, additional important combinations of multipole moments and phase differences were discovered, leading to the broader concept of the Kerker effect. Currently, the term "generalized Kerker effect" is used to characterize situations where there is significant forward or backward scattering. (see Fig. 1).

Figure 1 presents a study of the Kerker effects using both numerical (Comsol Multiphysics) and analytical calculations. Figure 1(a-e) shows the dependence of the multipole contributions to the scattering cross section.

The Kerker effect points are highlighted in red. Corresponding analytical representations (f-j) and numerical simulations (k-o) of the far-field patterns are provided for each case. Although the scattering shapes are similar, small deviations occur in the numerical calculations due to the small contributions of other multipoles. The strong agreement between the summation of scattering cross-sections from the multipoles and the calculations derived by integrating the Pointing vector over a closed surface in the far-field region, normalized to the incident field intensity, further supports the notion that higher-order multipoles are not required. This agreement is showed by the gray and orange lines in Fig. 1(a-e).
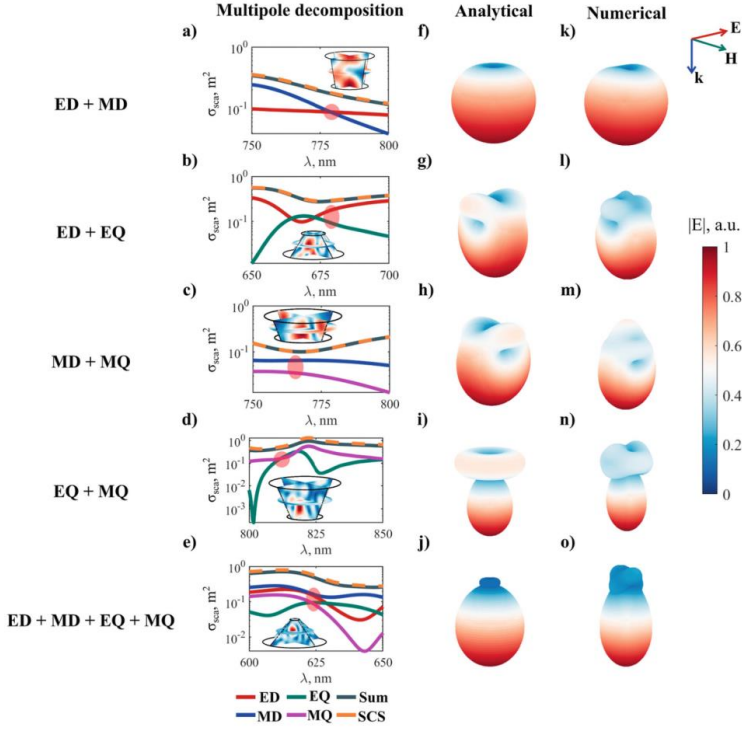
Fig. 1. Generalized Kerker effects in truncated conical nanoparticles. Figures (a-e) illustrate the decomposition of multipolar contributions, while figures (f-j) present the analytical summation of multipoles in the far field for a point. Figures (k-o) show the numerically computed far-field distributions for conical nanoparticles with varying geometries at the spectral points indicated red dots in (a-e). The incident plane wave illuminates the nanoparticles from the top of cone.

3 Conclusion

In this study, we have showed the complete range of established generalized Kerker effects for individual nanoscatterers with the same geometric shapes, representing a pioneering achievement. This underscores the adaptability associated with nanocones as a foundation for introducing novel photonic devices that demonstrate a broad spectrum of multipolar interference phenomena. These effects provide versatile control over scattering patterns.

Furthermore, we propose the conical geometry as a universal platform for achieving all known generalized Kerker effects within a single scatterer shape, while considering the realistic dispersion of the refractive index of silicon. This research marks particularly

advantages concerning more intricate shapes. The use of nanoscatterers of the same shape significantly reduces the cost of developing photonic devices and paves the way for fresh prospects in the next generation of photonics.

References

1. Shalin, A.S., Sukhov, S.V.: Plasmonic nanostructures as accelerators for nanoparticles: optical nanocannon. Plasmonics **8**, 625–629 (2013)
2. Simovski, C.R., Shalin, A.S., Voroshilov, P.M., Belov, P.A.: Photovoltaic absorption enhancement in thin-film solar cells by non-resonant beam collimation by submicron dielectric particles. J. Appl. Phys. **114** (2013)
3. Shalin, A.S.: Broadband blooming of a medium modified by an incorporated layer of nanocavities. JETP Lett. **91**, 636–642 (2010)
4. Shalin, A.S., Moiseev, S.G.: Optical properties of nanostructured layers on the surface of an underlying medium. Opt. Spectrosc. **106**, 916–925 (2009)
5. Terekhov, P.D., Babicheva, V.E., Baryshnikova, K.V., Shalin, A.S., Karabchevsky, A., Evlyukhin, A.B.: Multipole analysis of dielectric metasurfaces composed of nonspherical nanoparticles and lattice invisibility effect. Phys. Rev. B. **99** (2019)
6. Novitsky, D.V., Valero, A.C., Krotov, A., Salgals, T., Shalin, A.S., Novitsky, A.V.: CPA-lasing associated with the quasibound states in the continuum in asymmetric non-hermitian structures. ACS Photonics **9**, 3035–3042 (2022)
7. Kucherik, A., et al.: Nano-antennas based on silicon-gold nanostructures. Sci. Rep. **9**, 338 (2019). https://doi.org/10.1038/s41598-018-36851-w
8. Tian, Y., Li, Z., Xu, Z., Wei, Y., Wu, F.: High transmission focusing lenses based on ultrathin all-dielectric Huygens' metasurfaces. Opt. Mater. (Amst). **109**, 110358 (2020)
9. Kuznetsov, A.V., Canós Valero, A., Tarkhov, M., Bobrovs, V., Redka, D., Shalin, A.S.: Transparent hybrid anapole metasurfaces with negligible electromagnetic coupling for phase engineering. Nanophotonics. **10**, 4385–4398 (2021)
10. Vestler, D., et al.: Circular dichroism enhancement in plasmonic nanorod metamaterials. Opt. Express **26**, 17841 (2018)
11. Kostina, N.A., et al.: Nanoscale tunable optical binding mediated by hyperbolic metamaterials. ACS Photonics **7**, 425–433 (2020)
12. Canós Valero, A., et al.: Theory, observation, and ultrafast response of the hybrid anapole regime in light scattering. Laser Photon Rev. **15**, 2100114 (2021)
13. Canós Valero, A., et al.: Nanovortex-driven all-dielectric optical diffusion boosting and sorting concept for lab-on-a-chip platforms. Adv. Sci. **7**, 1903049 (2020)
14. Novitsky, D.V., Karabchevsky, A., Lavrinenko, A.V., Shalin, A.S., Novitsky, A.V.: PT symmetry breaking in multilayers with resonant loss and gain locks light propagation direction. Phys. Rev. B **98**, 125102 (2018)
15. Terekhov, P.D., Evlyukhin, A.B., Redka, D., Volkov, V.S., Shalin, A.S., Karabchevsky, A.: Magnetic octupole response of dielectric quadrumers. Laser Photon Rev. **14**, 1900331 (2020)
16. Kerker, M., Wang, D.S., Giles, C.L.: Electromagnetic scattering by magnetic spheres. J. Opt. Soc. Am. **73**, 765–767 (1983)

17. Rahimzadegan, A., et al.: Beyond dipolar Huygens' metasurfaces for full-phase coverage and unity transmittance. Nanophotonics. **9**, 75–82 (2020)
18. Chen, M., Kim, M., Wong, A.M.H., Eleftheriades, G.V.: Huygens' metasurfaces from microwaves to optics: a review. Nanophotonics. **7**, 1207–1231 (2018)
19. Kuznetsov, A.V., et al.: Special scattering regimes for conical all-dielectric nanoparticles. Sci. Rep. **12**, 21904 (2022)
20. Terekhov, P.D., Evlyukhin, A.B., Shalin, A.S., Karabchevsky, A.: Polarization-dependent asymmetric light scattering by silicon nanopyramids and their multipoles resonances. J. Appl. Phys. **125**, 173108 (2019)
21. Terekhov, P.D., et al.: Broadband forward scattering from dielectric cubic nanoantenna in lossless media. Opt. Express **27**, 10924 (2019)

Aleksei Kuznetsov was born in 1998, in Irkutsk. He received a Master's degree in Laser Equipment and Laser Technologies from ITMO University in Saint Petersburg in 2021. He is currently a researcher at the Institute of Photonics, Electronics and Telecommunications of RTU Faculty of Computer Science, Information Technology and Energy.